Catalytic Asymmetric Transformation of Chiral Amines by Crystallisation with In-*Situ* Racemisation of Conglomerates

Peter Baldwin

Submitted in accordance with the requirements for the degree of Doctor of Philosophy

University of Leeds

School of Chemical and Process Engineering

Institute of Particle Science and Engineering (IPSE), Institute of Process Research and Development (iPRD)

November 2014

The candidate confirms that the work submitted is his own and that appropriate credit has been given where reference has been made to the work of others.

Peter Baldwin

Acknowledgements

I would like to thank my supervisors Xiaojun Lai, John Blacker and Antonia Borissova for their ongoing guidance, support and encouragement.

I would also like to thank my colleagues in the Engineering and Chemistry Departments for their invaluable contributions. In particular: John Cooksey, Qassim Hussain, Toshiko Izumi, Zhipeng Lan, James Tunstall, and Phillip Winkworth.

Finally I would like to acknowledge Martin Huscroft for his continued assistance with HPLC analysis.

Abstract

Optically pure chiral molecules account for an increasing number of active pharmaceutical ingredients (API's); yet despite giving high enantiomeric excesses, existing techniques for obtaining pure enantiomers are hindered by low yields, high complexities, large waste streams, and hence high operational costs. Diastereomic crystallisation is the most commonly used resolution method and is capable of giving high enantiomeric excesses yet many additional processing stages are required to recover the desired enantiomer. If a racemate exists as a conglomerate, i.e. a mechanical mixture of discreet homochiral crystals, preferential crystallisation may be employed. However, both techniques are limited to a theoretical maximum yield of 50%. Coupling resolution by preferential crystallisation with organometallic catalysed racemisation in a crystallisation induced asymmetric transformation (CIAT) process may overcome these problems potentially giving a theoretical quantitative yield of a chosen enantiomer from an initially racemic solution in a single, efficient crystallisation step.

CIAT was attempted under isothermal and polythermal conditions using the conglomerate diol hydrobenzoin and the organometallic catalyst chloro(indenyl)-bis-(triphenylphosphine)-ruthenium(II) for solution phase racemisation. Optically pure product crystals were obtained with chemical purities of up to 99.71% when isothermal temperature programmes were employed in short process runs yet only relatively low yields could be recovered. Under polythermal conditions, crystal yields were improved significantly whilst increases of up to 61.57% were observed in the total quantity of the desired (*S*,*S*)-hydrobenzoin enantiomer present in both the solid and solution phases at the end of the process indicating that CIAT had occurred. However, in all of the polythermal runs trialled, nucleation of the undesired counter enantiomer and meso forms of hydrobenzoin could not be avoided. This was found to be a result of the catalysts being completely consumed in a side reaction leading to racemisation ceasing to progress after approximately 1-2 h. Hence, as the seeded enantiomer continued to be crystallised, the concentrations of the undesired

species were not reduced through transformation leading to them reaching their metastable solubility limits.

CIAT of hydrobenzoin was also attempted using chloromonocarbonyltriphenylphosphine-(1,2,3,4,5-pentaphenylcyclopentadienyl)-ruthenium(II) which was shown to remain active for up to 5 days. However, over the course of the CIAT experiments which exceeded 2 h, hydrobenzoin in solution was converted to benzaldehyde via C-C bond cleavage which resulted in the seed crystals being completely dissolved.

Contents

i. Nomenclature

a	Activity	
B	Nucleation rate	# crystals m^{-3} s^{-1}
b	Cooling rate	K s^{-1}
C	Heat capacity	J K^{-1}
C	Number of components	
c	Molar concentration	mol m^{-3}
*c**	Equilibrium concentration	mol m^{-3}
D	Dextrorotatory	
D	Diffusion coefficient	m^2 s^{-1}
ee	Enantiomeric excess	%
F	Face-centred lattice (unless stated otherwide)	
G	Free energy	J
G	Linear growth rate	m s^{-1}
ΔG_{crit}	Critical free energy for nuclei formation	J
H	Enthalpy	J
ΔH^f	Molar enthalpy of fusion	J mol^{-1}
J	Mass change rate	kg m^{-3} s^{-1}
k	Boltzmann constant	W m^{-2} K^{-4}
k_n	Nucleation rate constant	s^{-1}
k_v	Geometric shape factor	
L	Levorotatory	
L	Characteristic crystal size	m
M	Mass	kg
M_w	Molecular weight	kg mol^{-1}
m	Nucleation order (unless stated otherwise)	
n	Crystal number density distribution	# crystals m^{-3}
P	Number of phases	
R	Rectus	
	note in this report, using the CIP rules, subscript $_A$ denotes either enantiomer, *R* or *S* e.g. $\Delta H_A^f = \Delta H_R^f = \Delta H_S^f$ and $T_A^f = T_R^f = T_S^f$	
R	Universal gas constant	8.314 J mol^{-1} K^{-1}
r	Radius	m
r_c	Critical radius	m
S	Relative supersaturation	
S	Sinister	
ΔS^m	Entropy of mixing	J mol^{-1} K^{-1}
T	Temperature	K or ˚C
T^f	Melting (fusion) Temperature	K or ˚C

$t_{1/2}$	Racemisation half-life	s
t_{ind}	Induction time	s
V	Volume (unless stated otherwise)	m^{-3}
v	Molar volume	mol m^{-3}
x	Mole fraction	
α	Optical rotation (unless stated otherwise)	°
γ	Interfacial tension (unless stated otherwise)	J m^{-2}
μ	Chemical potential	J mol^{-1}
ϕ	Proportionality factor	

Subscripts

A	Enantiomer *R* or *S*
R	Racemate (unless stated otherwise)
c	Conglomerate

Superscripts

f	Fusion
l	Liquid phase
m	Mixing
Rac	Racemisation
s	Solid phase

Abbreviations

API	Active Pharmaceutical Ingredient	
CIAT	Crystallisation-Induced Asymmetric Transformation	
CSD	Crystal Size Distribution	
DKR	Dynamic Kinetic Resolution	
DSC	Differential Scanning Calorimetry	
GC	Gas Chromatography	
HPLC	High Performance Liquid Chromatography	
IR	Infra-Red Spectroscopy	
MSZW	Metastable Zone Width	
NMR	Nuclear Magnetic Resonance	
ssNMR	Solid State Nuclear Magnetic Resonance	
PXRD	Powder X-Ray Diffraction	
SCRAM™	Pentamethylcyclopentadienyl iridium dichloride dimer or $[Cp^*IrCl_2]_2$	
SCXRD	Single Crystal X-Ray Diffraction	
SHG	Second Harmonic Generation	

ii. List of Figures

iii. List of Tables

1 Introduction

Chirality is a geometric phenomenon whereby an object cannot be superposed upon its mirror image. A left hand, for example, cannot be superposed upon its mirror image, a right hand. Molecules exhibit chirality when their three dimensional spatial configuration lacks any reflectional symmetry [1] due to the presence of a central atom bound asymmetrically to several different groups (Figure 1.1). Consequently, an interchange of any two groups about the stereogenic centre will produce two stereoisomers[2]. The resulting pair, known as *enantiomers*, share the same chemical and physical properties in an achiral environment; one possessing no chiral species. However, varying degrees of activity are seen between enantiomers of the same molecule when other chiral species are present, and additionally, each enantiomer is able to rotate plane-polarised light in opposite directions giving rise to the expression *optical isomers.*

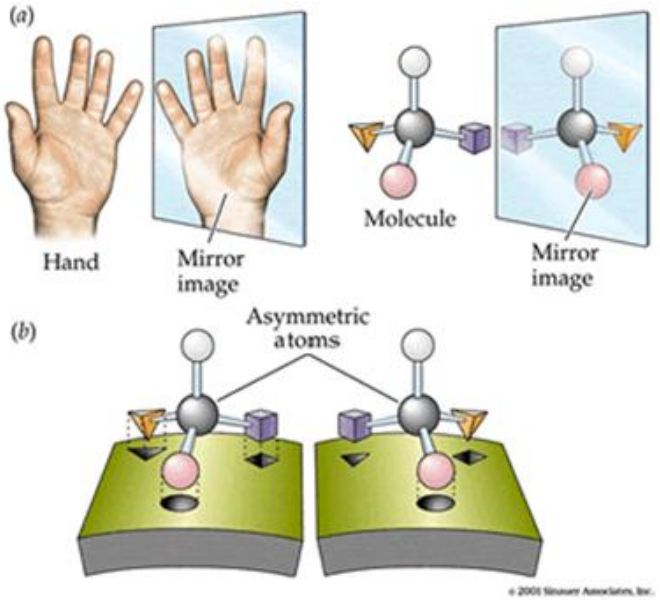

Figure 1.1a) Non-superimposable mirror images, b) two enantiomers [3].

When more than one asymmetric centre is present in a molecule *diastereomers* are possible. These are stereoisomers that are not mirror images of each other due to different orientations of groups about the corresponding asymmetric centres in each molecule. Ephedrine, for example, contains two stereogenic

carbon centres resulting in four different molecular configurations (Figure 1.2 - Note the two possible orientations about the stereo centres are assigned either *R* (rectus), or *S* (sinister), using the Cahn-Ingold-Prelog notation system which is recommended by IUPAC[4]. DL and +/- nomenclature are also used throughout this report where necessary). In this case the prefix '*pseudo'* is used to denote the stereoisomers with opposite configurations around their chiral carbon atoms. Each of these has one molecule which is a mirror image of itself and two that are not therefore they are either enantiomers or diastereomers depending on which corresponding stereoisomer is considered. Diastereomers are unlike enantiomers in that they have different chemical and physical properties allowing them to be separated from each other by conventional techniques e.g. crystallisation. Consequently enantiomers are often converted to diastereomers using a suitable resolving agent allowing for their physical separation.

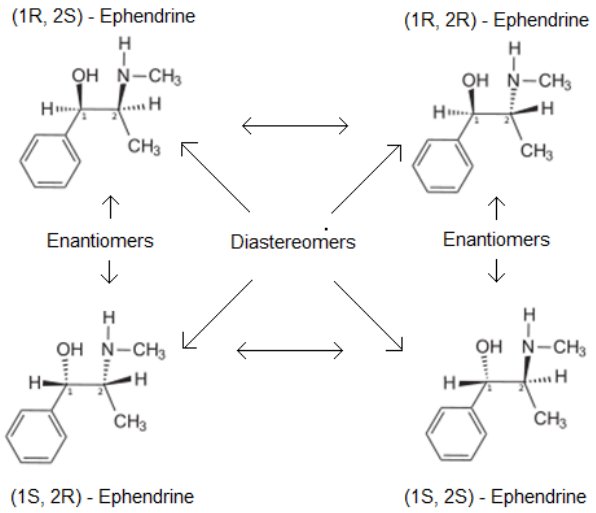

Figure 1.2 Enantiomers and diastereomers of ephedrine

The building blocks of life, amino acids, are all chiral (with the exception of glycine) as a result of the variation of their side groups and the tetravalency displayed by carbon, the most prevalent asymmetric central atom. Interestingly, all biological organisms are comprised predominantly of levorotatory or L-amino acid, and dextrorotatory, or D-carbohydrate, enantiomers. Biological organisms therefore interact selectively with chiral molecules showing varying degrees of activity as a result of the chiral recognition process[5]. Cushny [6] was the first to

identify this phenomenon when he noticed a difference in the pharmacological effects of pure hyoscyamine enantiomers administered to frogs. As enzyme and receptor binding is enantio-specific [7, 8], different enantiomers of the same molecule often have different effects on biological organisms.

In recent years this discovery has had a profound impact on the pharmaceuticals and agricultural industries where traditionally, many enantiomeric compounds were produced as a racemate i.e. an equimolar mixture of two enantiomers [9]. Although the enantiomers in racemic active pharmaceutical ingredients (APIs) do at times show the same desired effect, such as ibuprofren whose enantiomers are both anti-inflammatory agents [10], more frequently, markedly different effects can be seen in their pharmacological activities. Often one enantiomer is simply less active yet there have been many cases where one of the administered enantiomers has induced an unexpected side-effect. Arguably the worst occurrence of this was with thalidomide which was marketed as a racemate during the 1960s. The (*R*)-enantiomer, an effective sedative, was administered to pregnant patients to remedy morning sickness; however, unknown at the time was that (*S*)-thalidomide was a teratogen[11] and consequently thousands of children were born with birth defects.

1.1 Methods of Obtaining Enantiopure Compounds

Since the tragic thalidomide case, great emphasis has been placed on obtaining only the active enantiomer for chiral APIs. Several techniques exist although each is attributed with its own limitations:

- Asymmetric synthesis
- Diastereomic crystallisation
- Preferential crystallisation
- Kinetic resolution/Dynamic kinetic resolution
- Crystallisation induced asymmetric transformation (CIAT)/ crystallisation induced diastereomic transformation (CIDT)

The success of these processes is based less so on the obtainable yields and instead, more importance is placed on achieving high enantiomeric purities. The

relative amounts of enantiomer present in a mixture can be expressed as the enantiomeric excess, *ee*, with respect to the major enantiomer (Equation 1.1[12]). For [R] > [S]:

$$enantiomeric\ excess, ee = \frac{[R] - [S]}{[R] + [S]}$$ Equation 1.1

Thus a pure enantiomer has an enantiomeric excess of 100% whereas that of a 50:50 mixture or *racemate* is 0%.

The existing techniques for obtaining pure enantiomers are able to give high ***ee***'s yet they are hindered by low yields, high complexities, large waste streams, and hence high operational costs. Asymmetric hydrogenations and functional group interchange from optically active alcohol to amine are capable of giving high yields, however, development and operation of these processes is often complex requiring many different reagents and processing stages [13]. Biocatalysts such as hydrolases and transaminases used in kinetic resolutions have been shown to be very enantioselective giving high ***ee***'s [14-20] . However, these are often chemoselective, limiting their application, and require reactions in water which is an unsuitable process solvent for most organic compounds. Due to its relative simplicity, diastereomic crystallisation is by far the most commonly used resolution method being responsible the manufacture of many common pharmaceutical APIs. However, without recycling the unwanted enantiomer using racemisation, the maximum theoretical yield obtainable is 50%, and consequently, large volumes of waste are associated with this process. Preferential crystallisation also suffers from the same problems.

Several processes exist in which the desired enantiomer is crystallised inducing the racemisation of the counter enantiomer in-*situ* giving a theoretical maximum yield of 100%. Crystallisation Induced Diastereomic Transformations (CIDT) are possible, yet these all rely on chiral centres that are easily racemised[21, 22]. Crystallisation Induced Asymmetric Transformations (CIAT) of enantiomers have been shown to give high yields and enantiomeric excesses[23-31], but these all rely on complex racemisation mechanisms which are specific to the compounds used. To resolve these problems, a more general racemisation

method must be employed which can be applied to molecules baring the same functional groups without the need for chiral protons with low pKa's.

1.2 Objectives

The aim of this research is to investigate the possibility of coupling seeded isothermal and polythermal programmed preferential crystallisation of conglomerates (SIPC and S3PC respectively) with in-*situ* solution phase racemisation using organometallic catalysts. Establishing dynamic equilibrium between enantiomers using a suitable organometallic catalyst, and subsequently seeding the metastable solution with enantiopure crystals of the desired stereoisomer should initiate its selective crystallisation which, in turn, should induce racemisation of the counter-enantiomer in solution (Figure 1.3). Unwanted spontaneous nucleation of the antipode should be avoided if the rate of racemisation exceeds that of crystallisation since a racemic or near-racemic solution will be maintained and therefore its magnitude of supersaturation will be equivalent to that of the desired enantiomer. This method could potentially lead to a quantitative yield of a chosen enantiomer from an equilibrated solution in a single, efficient process step, whilst the use of organometallic catalysts capable of racemising functionally related compounds could increase the applicability of this technique by eliminating the requirement of low pKa chiral protons seen in existing CIAT processes.

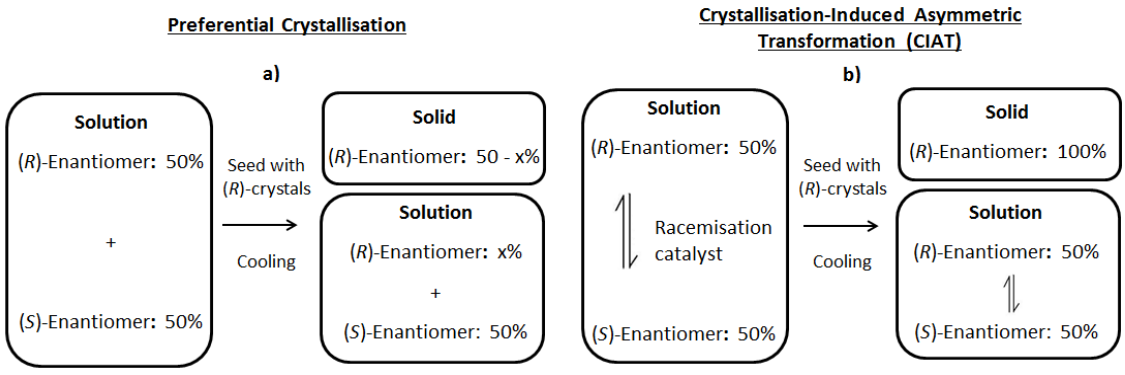

Figure 1.3 Preferential Crystallisation and b) proposed Crystallisation-Induced Asymmetric Transformation (CIAT) process using organometallic racemisation catalysts, with maximum theoretical yields of 50% and 100% respectively.

1.3 Thesis overview

Chapter 1: Introduction and research objectives

Chapter 2: Discussion of the underlying fundamentals of crystallisation, racemate phase behaviour and conglomerates.

Chapter 3: Review of chiral amine and alcohol organometallic catalysts, existing crystallisation-induced asymmetric transformation techniques and attrition-enhanced de-racemisation

Chapter 4: Selection and characterisation of suitable conglomerates for use as model compounds in the CIAT process

Chapter 5: Selection of organometallic catalysts for racemisation of the model conglomerates identified in chapter 4

Chapter 6: Identification of the CIAT conditions through characterisation of the conglomerate solubility, preparation of enantiopure seed crystals

Chapter 7: Presentation of results for CIAT using the conglomerates identified in chapter 4, the racemisation catalysts selected in chapter 5, and the CIAT conditions determined in chapter 6

Chapter 8: Study conclusions

Chapter 9: Recommended work based on the findings of the investigations

2 Crystallisation

2.1 Solubility

Solubility describes the maximum amount of a substance that can be dissolved in a solvent in order to achieve a saturated solution. This is an equilibrium process and a function of temperature therefore solubility can be more precisely referred to as equilibrium solubility. Generally solubility increases with temperature allowing for more solute to be dissolved. The opposite occurs with a reduction in temperature in which the solution becomes supersaturated causing a certain amount of solute to precipitate in order to re-establish equilibrium

A solute-solvent system can be considered as ideal if the molecular interactions between the solute and solvent are identical to those between the solute molecules and solvent molecules themselves[32] or thermodynamically speaking, the enthalpy of mixing is zero. Using this approximation the equilibrium solubility of a given compound can be predicted using the van't Hoff equation:

$$\ln x = \frac{\Delta H^f}{\mathrm{R}}\left[\frac{1}{T^f} - \frac{1}{T}\right] \qquad \text{Equation 2.1}$$

where *x* is the mole fraction of solution in solution, ΔH^f is the molar enthalpy of fusion of the solute (J mol^{-1}), T^f is the solute melting temperature (*K*), *T* is the solution temperature (*K*), and R is the universal gas constant (8.314 J mol^{-1} K^{-1}). Equation 2.1 gives solubility as a function of the physical properties of the solute and the system temperature; however, it does not take into account the presence of any solvent molecules and any interactions that may result. To account for the deviation from ideality displayed by most solutions, the degree of non-ideality must be quantified. This can be approximated by considering the Gibbs free energy change of dissolution,ΔG^{Diss}, at a constant temperature:

$$\Delta G^{Diss} = \Delta H^m - T\Delta S^m \qquad \text{Equation 2.2}$$

where ΔH^m is the enthalpy of mixing (J mol^{-1} K^{-1}) and ΔS^m is the entropy of mixing (J mol^{-1} K^{-1}). For the formation of an ideal solution the Gibbs free energy may also be expressed as:

$$\Delta G^{Diss} = \mathrm{R}T \ln x \qquad \text{Equation 2.3}$$

where x represents the mole faction of one of the components being mixed in solution, in this case the solute. As the solution is considered ideal, the enthalpy of mixing, ΔH^m = 0, therefore from Equation 2.2:

$$\Delta S^m = -\mathrm{R} \ln x \qquad \text{Equation 2.4}$$

If the overall free energy change is expressed in terms of activity, *a*, i.e. the degree of deviation from ideality, Equation 2.1 can be approximated for a non-ideal system by way of an activity coefficient, γ. Therefore Equation 2.3 becomes:

$$\Delta G^{Diss} = \mathrm{R}T \ln a \qquad \text{Equation 2.5}$$

For an ideal solution:

$$a = x \ (i.e. \gamma = 1) \qquad \text{Equation 2.6}$$

For a non-ideal solution:

$$a = \gamma x \qquad \text{Equation 2.7}$$

where the activity coefficient, γ, is less than one for non-ideal systems. Thus Equation 2.1becomes:

$$\ln(\gamma x) = \frac{\Delta H^f}{\mathrm{R}} \left[\frac{1}{T^f} - \frac{1}{T}\right] \qquad \text{Equation 2.8}$$

2.2 Supersaturation

If the solubility of a compound in a given solvent is known over a range of temperatures, an equilibrium solubility curve can be constructed. Consequently, the solubility curve for a solute-solvent system can be used to describe the process of crystallisation from solution by cooling. Figure 2.1 shows a typically solubility curve in which the solubility of the solute in question, is reduced with cooling. At point A, the solution is homogeneous as the temperature of the system is greater than the equilibrium temperature for that particular concentration so the solute remains in solution. It is therefore said to be unsaturated as it is possible to dissolve more solute in the solution at this temperature. With regards to a crystallisation process, this would represent the feed or initial state where the concentration of the solute in solution is at its highest point before any mass transfer to the solid phase has occurred.

A reduction in temperature takes the system to point B. At this stage the kinetic motion of the molecules within the homogeneous solution is reduced and the thermodynamic equilibrium solubility is achieved therefore the solution becomes saturated as no more solute can in theory be dissolved without precipitation occurring. As the temperature is reduced further the system enters a region known as the metastable zone. At this stage the solution has more dissolved solute than the equilibrium concentration and is therefore supersaturated. However, the solute remains in solution and does not crystallise as result of a kinetic barrier preventing the formation of stable nuclei from which crystals are grown. The width of this metastable zone i.e. the temperature range in which the system remains supersaturated and does not crystallise, is influenced considerably by factors such as the rate at which supersaturation is generated, the intensity of agitation, and the presence of foreign particles which can act as nuclei[32]. This means that the width of the metastable zone can vary considerably if the crystallisation conditions are not kept constant. In practice this can be difficult to achieve. However, if the system can be held within a metastable, supersaturated state, crystal ‘seeds’ can be introduced to act as sites for crystal growth as the solute molecules will leave the liquid phase to allow for equilibration. Supersaturation is the driving force for crystallisation and the degree of which can be given by the concentration driving force, Δc:

$$\Delta c = c - c^*$$ Equation 2.9

where c is the solution concentration and c^* is the equilibrium concentration. Supersaturation can also be expressed as the ratio of solution concentration to equilibrium concentration, S, or the relative supersaturation, σ[32].

$$\mathrm{S} = \frac{c}{c^*}$$ Equation 2.10

In the absence of seed, at point C, crystallisation, or more precisely nucleation, begins to take place instantaneously. This is the formation of very small nuclei of the solute which is a very complex process which has yet to be fully understood. Nucleation occurs after an induction time, t_{ind} (section 2.3.4), which is the time taken to form the first nuclei to form after saturation has been achieved. Once stable nuclei are formed, the crystals begin to grow and take shape. In its simplest form, crystal growth may be considered a two-step process involving mass transport, either by diffusion or convection from the bulk solution to the crystal face, followed by a surface reaction in which the growth units are integrated into the crystal lattice. Either step may control the overall growth process, although convective mass transport is unimportant for crystals smaller than ca. 10 μm because these crystals are scarcely affected by turbulent eddies and diffusional mass transport predominates[32].

Alternatively, supersaturation may also be described in terms of chemical potentials. The difference in chemical potential between a solute in the solution, μ_1, and in the crystalline state, μ_2 i.e:

$$\Delta\mu = \mu_1 - \mu_1$$ Equation 2.11

and:

$$\mu = \mu_0 - RTlna$$ Equation 2.12

An expression for supersaturation can thus be obtained:

$$\ln S = ln\left(\frac{a}{a^*}\right) = \frac{\Delta\mu}{\mathrm{R}T}$$ Equation 2.13

$$S = exp\left(\frac{\Delta\mu}{RT}\right)$$ Equation 2.14

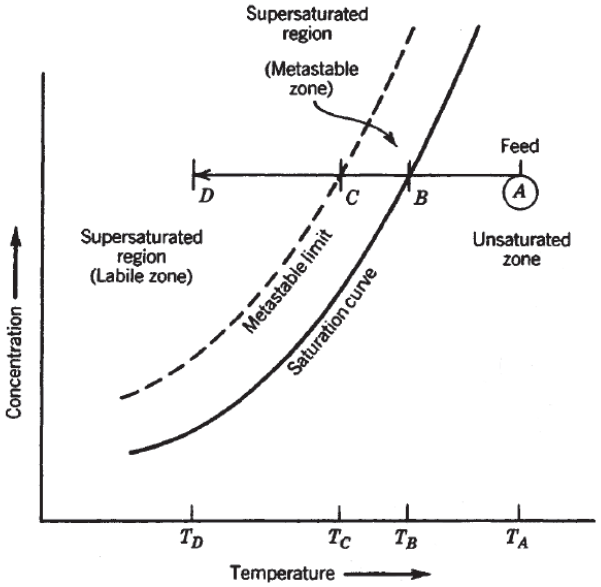

Figure 2.1 General solubility curve showing A) unsaturated zone, B) saturation point, C) metastable limit/supersaturation point, D) supersaturated region[33]

2.3 Nucleation

Two modes of nucleation are possible; primary, in the absence of crystals, and secondary, in the presence of crystals (Figure 2.2).

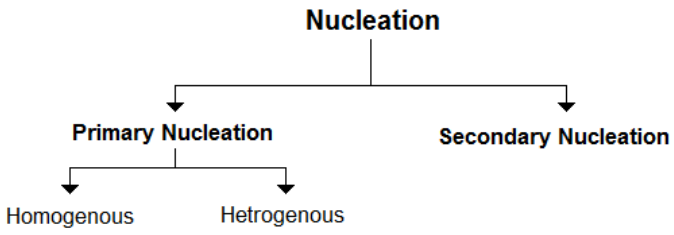

Figure 2.2 Nucleation modes

2.3.1 Primary Nucleation

2.3.1.1 Homogeneous Nucleation

The formation of crystals from a homogeneous, supersaturated solution (i.e. completely free of any crystalline matter or foreign particles) requires the solute molecules to first form thermodynamically stable nuclei to act as centres on which subsequent crystallisation can occur. The exact mechanism behind nuclei formation is yet to be fully understood, however; it is thought that localised concentration fluctuations in the liquid phase give rise to ordered clusters of solute molecules[34], with subsequent bimolecular collisions and interactions resulting in the formation of crystalline, lattice structures[35].

To form the new distinct solid phase, the nuclei must become thermodynamically stable by achieving a critical size. Particles not reaching the critical size will re-dissolve, whilst those larger than this are able to grow to form macroscopic crystals. For a spherical particle of radius *r*, the overall excess free energy change, ΔG, between the particle and the solute in solution is equal to the sum of the surface excess free energy, ΔG_S, and the volume excess free energy, ΔG_V, i.e. the excess free energy between a particle with a radius, r = ∞, and the solute in solution[32] or

$$\Delta G = \Delta G_S + \Delta G_V \qquad \text{Equation 2.15}$$

Since for a spherical particle the magnitude of ΔG_S is proportional to r^2 and that of ΔG_V is proportional to r^3, Equation 2.15 becomes:

$$\Delta G = 4\pi r^2 \gamma + \frac{4}{3}\pi r^3 \Delta G_V \qquad \text{Equation 2.16}$$

where ΔG_V is the free energy change of the transformation per unit volume and γ is the interfacial tension between the developing crystal surface and its corresponding supersaturated solution[32]. ΔG_S and ΔG_V are positive and negative quantities respectively, and Equation 2.16 shows that they each share a different relationship with *r*, therefore; ΔG has a maximum value corresponding to a nuclei of critical radius, r_c,. This can be found when $d\Delta G/dr = 0$ *and* ΔG is at its maximum value or:

$$\frac{d\Delta G}{dr} = 8\pi r\gamma + 4\pi r^2 \Delta G_V = 0 \qquad \text{Equation 2.17}$$

Therefore:

$$r_c = \frac{-2\gamma}{\Delta G_V} \qquad \text{Equation 2.18}$$

The critical free energy, ΔG_{crit}, can be found by substituting for ΔG_V from Equation 2.17 and Equation 2.18 giving:

$$\Delta G_{crit} = \frac{16\pi\gamma^3}{3(\Delta G_V)^2} = \frac{4\pi\gamma r_c^2}{3} \qquad \text{Equation 2.19}$$

Equation 2.16 is reproduced graphically in Figure 2.3 to illustrate the concept of the critical nuclei radius with regards to the overall free energy change of the particle. For all vales of *r* less than r_c, the nuclei dissolves as the free energy of the particle must decrease. Similarly, for all values of *r* greater than r_c, the free energy is reduced and the nuclei continue grow.

Smaller particles have greater surface energies as a result of their increased surface to volume ratios therefore solubility is reduced with particle size. The Gibbs-Thomson equation governs the growth of the nuclei based on their size, surface energies and the magnitude of supersaturation displayed by the solution:

$$ln\frac{c}{c^*} = \ln \mathrm{S} = \frac{2\gamma v}{kTr} \qquad \text{Equation 2.20}$$

where *S* is the magnitude of supersaturation, *c* is the concentration of solute clusters of radius *r, k* is the Boltzmann constant and *v* is the molecular volume. Therefore:

$$-\Delta G_V = \frac{2\gamma}{r} = \frac{kT\ ln\ \mathrm{S}}{v} \qquad \text{Equation 2.21}$$

and Equation 2.19 becomes:

$$\Delta G_{crit} = \frac{16\pi\gamma^3 v^2}{3(kT\ ln\ \mathrm{S})^2} \qquad \text{Equation 2.22}$$

The rate of nucleation, *J*, i.e. the number of nuclei formed per unit time per unit volume can be expressed as:

$$J = Aexp(-\Delta G/kT)$$ Equation 2.23

Therefore from Equation 2.22 and Equation 2.23 the nucleation rate can be given as follows:

$$J = Aexp\left[-\frac{16\pi\gamma^3 v^2}{3k^3T^3\ (ln\ \mathrm{S})^2}\right]$$ Equation 2.24

Nucleation has considerable influence on the mean crystal size and Crystal Size Distribution (CSD) resulting at the end of a crystallisation process. Fast rates of nucleation give rise fine crystals with a narrow CSD (and vice versa) as little time is allowed for crystal growth. It can be seen from Equation 2.24 that the magnitude of supersaturation is one of the primary influences on the rate of nucleation along with the temperature and interfacial tension. When the magnitude of supersaturation, *S*, reaches some critical value, nucleation proceeds at a very fast rate therefore the degree of sub-cooling is of paramount importance if it is necessary to control the final CSD. Form this equation it would be expected that the rate of nucleation would increase exponentially and indefinitely with supersaturation, however, a maximum value is achieved after which the nucleation rate decreases.

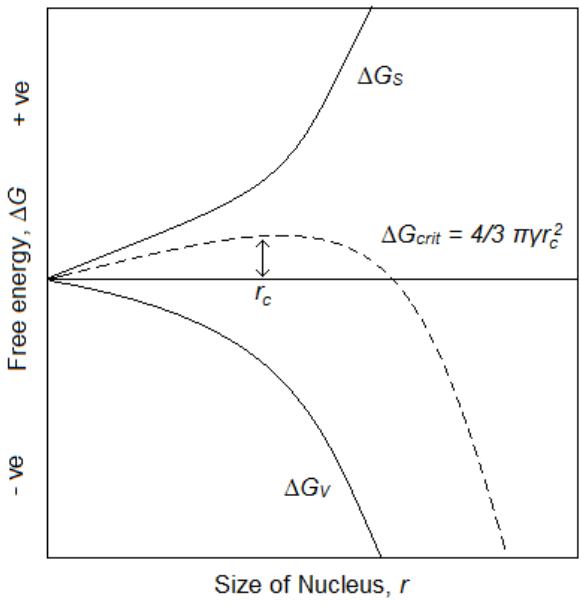

Figure 2.3 Free energy change for nuclei formation

2.3.1.2 Heterogeneous Nucleation

To keep a solution completely homogenous is practically impossible, especially during industrial crystallizations. Foreign substances or heteronuclei e.g. dust particles are naturally found in process solutions and act to reduce the energy required for nucleation by providing a surface onto which molecules can adhere and grow to form crystals. It is suggested that the most active heteronuclei in liquid solutions lie in the range 0.1-1 μm[32]. In addition to this, the physical attributes of process equipment such as crystalliser walls, stirrers and baffles can also act as nucleation surfaces. Consequently, heterogeneous nucleation will occur at a reduced magnitude of supersaturation than homogeneous supersaturation therefore the overall free energy change associated with critical nucleus formation under heterogeneous conditions, $\Delta G'_{crit}$ will be less than the corresponding homogeneous nucleation free energy change, ΔG_{crit}[32]. This can be expressed as:

$$\Delta G'_{crit} = \phi \Delta G_{crit} \qquad \text{Equation 2.25}$$

$$\phi = \frac{(2 + \cos\theta)(1 - \cos\theta)^2}{4} \qquad \text{Equation 2.26}$$

where the proportionality factor ϕ is less than unity. The reduction in free energy was shown by Volmer (1939)[36] to be dependent on the contact angle or wetting of the solid phase by the solution as a result of the relative affinities for each phase. Thus a contact angle of 180° corresponds to complete non-affinity between the foreign substance and the crystalline solid therefore the overall free energy change is equivalent to that exhibited during homogeneous nucleation (i.e. ϕ = 1). It follows then that contact angles less than 180 ° represent a partial-affinity between the solid and solution therefore the free energy change for the heterogeneous process is lower than that for homogeneous nucleation. The system corresponds to a seeded solution i.e. no nucleation occurs, when θ and ϕ = 0 and thus $\Delta G_{crit} = 0$ [32].

2.3.2 Secondary Nucleation

Secondary nucleation results from the addition of seed crystals to a supersaturated solution. The presence of seed provides a surface onto which molecules from the solution can adhere to build up the crystalline structure. This lowers the overall free energy change (relative to homogenous nucleation) allowing crystallisation to occur at lower degrees of supersaturation. Several secondary nucleation mechanisms have been suggested (Figure 2.4) based either on the phase from which the nuclei are derived i.e. from the solid seed crystals or from the solute molecules in solution.

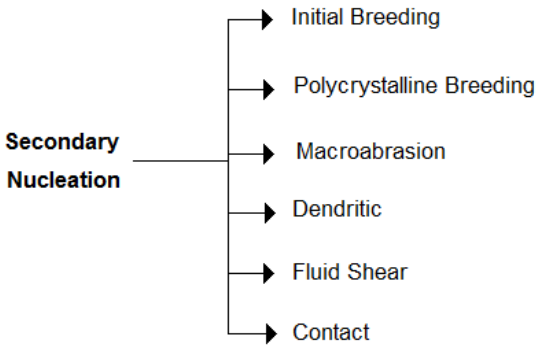

Figure 2.4 Secondary nucleation mechanisms[34]

Initial breeding occurs when small “crystallites”, formed on the surface of seed crystals during crystal growth and greater than r_c, act as nucleation sites[37, 38] therefore supersaturation has no effect on nucleation. This problem can be eliminated by washing seed crystals with a suitable solvent to remove crystallites and smooth out the crystal surface.

When the magnitude of supersaturation is very large, dendritic or needle-like structures can be formed, which act as nucleation sites upon fragmentation in the solution. Similarly, at even greater degrees of supersaturation, polycrystalline aggregates can form which produce nucleation sites upon fragmentation; however, these mechanisms are unlikely to occur during industrial crystallisation[34].

It is possible to form fragments greater than r_c when high stirrer speeds result in macroabrasion of crystal seeds. Similarly, microabrasion by collision or attrition can both lead to the formation of fragments which act as nucleation sites in which case the rate of nucleation is dependent on the crystal hardness, the concentration of the suspension and the retention time[34]. Additionally, the stirrer speed and hardness has been shown to have an influence on the rate of secondary nucleation by enhancing macro and microabrasion[39].

2.3.3 Metastable Zone Width

As previously described, when more solute is dissolved in a solvent than the equilibrium composition at prescribed operating conditions (i.e. its solubility), the solution is supersaturated and is said to be in a metastable state. With regards to cooling crystallisation, the metastable sate is achieved when the system is sub-cooled below the equilibrium solubility for a given concentration and no crystallisation results (see Figure 2.1). It is expected that at this stage, spontaneous nucleation will occur; however, it is first necessary form molecular clusters of critical radius, r_c, and thus the solution will remain supersaturated until this condition is met. The size of r_c is dependent on the extent of sub-cooling i.e. the magnitude of supersaturation achieved. Combining Equation 2.18 and Equation 2.21 gives the critical radius taking into account the effect of supersaturation[32]:

$$r_c = \frac{2\gamma v}{kT\ ln\ S}$$ Equation 2.27

As the magnitude of supersaturation is increased, the size of the critical radius necessary for crystallisation to ensue is reduced and, as a consequence, the time taken for nucleation to occur, $t_{ind,}$ is also reduced. The rate of nucleation can therefore be controlled by the extent and rate of sub-cooling employed and hence the solution becomes less and less stable as supersaturation is increased[34]. Eventually the solution will become unstable resulting in crystallisation as it reaches its maximum non-equilibrium solute capacity. This is known as the metastable limit, or the spinodal, which is the absolute limit of the metastable zone at which phase separation must occur[34].

Many different factors influence the width of the metastable zone (MSZW) for example[32, 40, 41]:

- The cooling rate (rate at which supersaturation is generated)
- Saturation temperature
- Intensity of agitation
- The presence of crystalline material, impurities or other foreign particles such as dust
- Solution thermal history i.e. the extent of heating above the saturation temperature prior to cooling
- Solubility
- Viscosity
- Type of solvent

It is therefore difficult to accurately define the MSZW and in practice, crystallisation processes relying on crystal seeding operate well within the metastable zone to minimise the potential for spontaneous nucleation.

Using the empirical method proposed by Nyvlt[42, 43], measurement of the MSZW allows the nucleation kinetics to be determined. The nucleation rate, J, can be defined as being a function of the maximum supersaturation possible, Δc_{max}, giving the empirical relationship:

$$J = k_n \Delta c_{max}^m$$ Equation 2.28

$$\Delta c_{max} = c - c^*$$ Equation 2.29

where k_n is the nucleation rate constant and m is the order of nucleation. Δc_{max} can be expressed as a function of the MSZW which is equivalent the maximum possible sub-cooling, ΔT_{max}:

$$\Delta c_{max} = \left(\frac{dc^*}{dT}\right) \Delta T_{max}$$ Equation 2.30

$$\Delta T_{max} = T_{sat} - T_{cryst}$$ Equation 2.31

where dc^*/dT is the dependence of solubility on the solution temperature, T, and T_{sat} and T_{cryst} are the saturation and crystallisation temperatures respectively.

The rate of nucleation at the metastable limit can be expressed as[34]:

$$J = \left(\frac{dc^*}{dT}\right) b$$ Equation 2.32

where b is the cooling rate. Combining Equation 2.28, Equation 2.30 and Equation 2.32, simplifying and taking logarithms results in an expression which relates the MSZW to the maximum supersaturation temperature:

$$\log b = (m-1) \log \frac{dc^*}{dt} \log k_n + m \log \Delta T_{max}$$ Equation 2.33

A plot of log b against log ΔT_{max} will result in a straight line, the slope of which being equal to the order of nucleation, m, with the constant, k_n, being obtained at the intercept[43].

2.3.4 Induction Time

The time delay between the onset of supersaturation and the formation of the first crystals of detectable size is known as the induction time, $t_{ind.}$ This takes into consideration the time taken to achieve steady-state nucleation, t_r, the time taken to form of stable nuclei, t_n, and the time required for the nuclei to grow to a detectable size, t_g, therefore t_{ind} can be expressed as[32]:

$$t_{ind} = t_r + t_n + t_g \qquad \text{Equation 2.34}$$

2.4 Crystal Growth

The formation of crystals involves the growth of stable nuclei by molecular surface addition. Molecules in the bulk solution are transported either by diffusion or convection to the surface of the crystal and subsequently integrated into the crystal lattice in a surface reaction with either step controlling the rate of the overall process[44]. For a non-ionic crystal, the theoretical linear diffusion-controlled growth rate, G, can be expressed as:

$$\mathrm{G} = \frac{Dv\Delta c}{L} \qquad \text{Equation 2.35}$$

where D is the diffusion coefficient, v is the molar volume and L is the crystal size. Convection-controlled crystal growth is less important as crystals with a size, L, less than 10 μm only slightly affected by turbulent eddies.

Integration of molecules onto the crystal surface has a considerable influence on the overall rate of crystal growth. Two mechanisms dominate this process; polynuclear or birth and spread, and BCF or spiral growth. In the former, two-dimensional nuclei form on the surface on the crystal which subsequently grow and spread forming a new monolayer (Figure 2.5). This process is analogous to three-dimensional nucleation in that it is necessary to form stable surface nuclei for growth of each new monolayer to ensue. The critical two-dimensional radius can therefore be similarly expressed in terms of supersaturation, S, and the step edge free energy, α, as[45]:

$$r_c = \frac{v\alpha}{kTln(1+S)}$$ Equation 2.36

Polynuclear growth is favoured by high supersaturations as the nuclei are only required to reach a small size to become stable. As the magnitude of supersaturation is decreased, many more molecules are required to form r_c the and BCF growth begins to dominate[45]. This mechanism occurs due the existence of screw dislocations which result in the formation of a step on the crystal surface (Figure 2.5a). Molecules are incorporated into the kinks associated with the formation of these step resulting in their growth in a spiral manner. It is therefore not necessary to form surface nuclei as sites for molecular addition are constantly provided as long as a screw dislocation is present hence growth by this mechanism can occur at low supersaturations. If the crystal surface becomes completely flat, growth can occur only by the polynuclear mechanism.

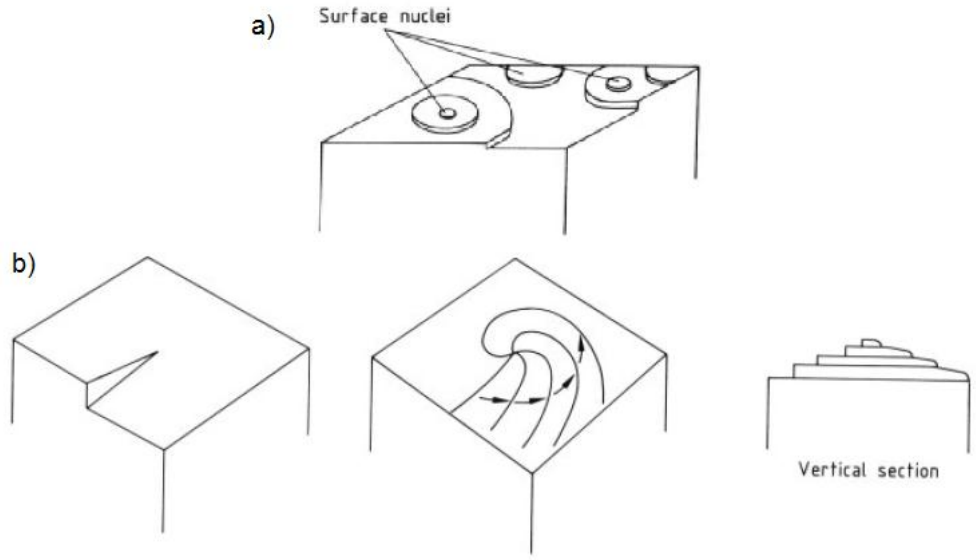

Figure 2.5 Crystal growth mechanisms a) polynuclear 2D nucleation b) spiral/BCF

The rate of crystal growth can be determined by considering either the linear growth rate of a chosen face or the indirect estimation of the overall linear growth rate, incorporating all crystal faces, by measuring the change in mass of an individual or group of crystals during crystallisation. Consequently three methods of expressing crystal growth rate exist[32]: mass deposition rate, B,

(kg/m^2.s), mean linear growth velocity, $\bar{v}$ = *dr/dt* (m/s), and overall linear growth rate G_{cryst} = *dL/dt* (m/s). These are related as:

$$B = K_g \Delta c^g = \frac{1}{A}\frac{dm}{dt} = \frac{3\alpha\rho G_{cryst}}{\beta} = \frac{6\alpha\rho}{\beta}\frac{dr}{dt} = \frac{6\alpha\rho\bar{v}}{\beta}$$

Equation 2.37

where L is the characteristic crystal dimension, r is the radius of the equivalent sphere, g is the crystal growth order and α and β are volume and surface shape factors respectively which are related to the particle mass, m, and surface area, A, by[32]:

$$m = \alpha\beta L^3$$

Equation 2.38

$$A = \beta L^2$$

Equation 2.39

2.5 Enantiomers

2.5.1 Racemates

Equimolar mixtures of two enantiomers whose physical sate is unspecified are referred to as racemates [9]. In the crystalline sate, enantiomers of a given molecule are able to assume three different structures; racemic compound, conglomerate, or solid solutions (Figure 2.6).

Racemic compounds are the most prevalent accounting for approximately 90% of all crystalline racemates according to literature sources[1] yet no comprehensive investigation to date has confirmed this figure. These are co-crystals that are comprised of a 1:1 mixture of each enantiomer, alternating within the crystal lattice in an ordered array. Conglomerates are mechanical mixtures of discrete, homochiral crystals which account for approximately 10% of all racemates yet their occurrence may be underestimated as chemists rarely characterise both racemic and pure enantiomer crystal structures. Conglomerates are of particular interest since an optically active compound can be obtained directly by resolution rather than requiring multiple, time-consuming

(and therefore expensive) processing steps as is required with diastereomic crystallisation. Moreover, they are separable by physical methods such as manual sorting, as performed in Pasteur's experiment. Solid solutions are much less common than the former and are rarely encountered therefore these will not be discussed any further. Analogous to polymorphism, the same racemate may exist as either a racemic compound or a conglomerate depending on their formation conditions i.e. solvent and temperature, with either being the most stable phase (for example 2-chromomandelic acid can exist as a stable racemic compound or a metastable conglomerate when the crystallisation conditions are varied [46]).

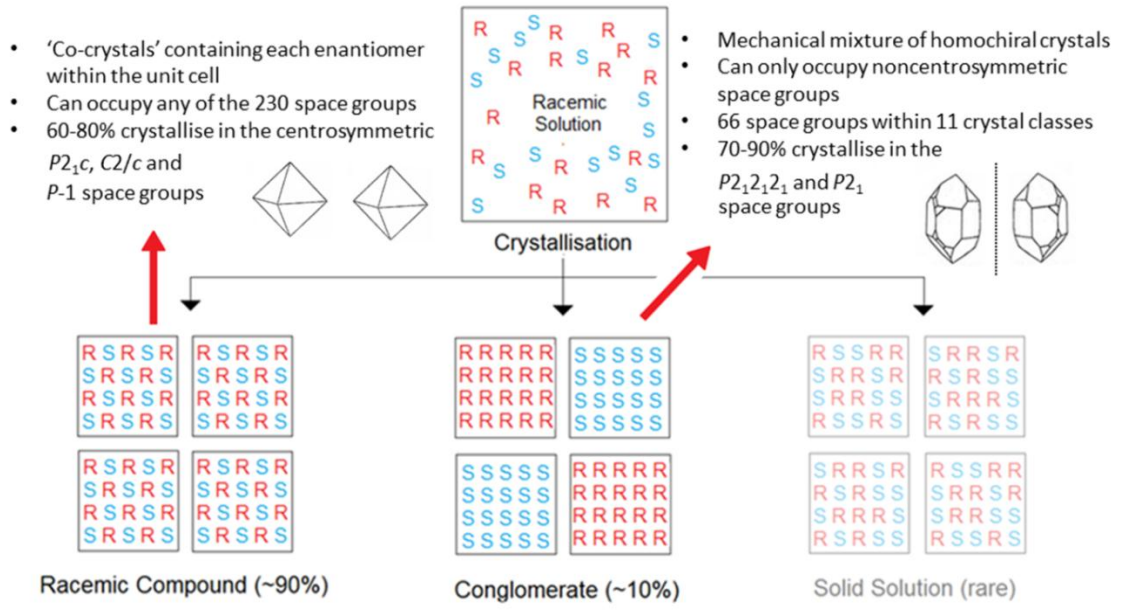

Figure 2.6 Crystalline racemates

2.5.2 Binary Phase Equilibria

Phase diagrams describe the equilibrium relationships between distinct, mechanically separable portions of a system comprised of one or more components, as a function of temperature, pressure or concentration. These can therefore be used to distinguish between different types of racemate as they each exhibit characteristic melting behaviours as a result of their differing racemic crystal structures. If both enantiomers are available, it is possible to construct a binary phase diagram using DSC by measuring the melting points of a range of different enantiomeric compositions. Roozeboom[47] was the first to

characterise binary systems of crystalline racemates based on their melting points (Figure 2.7). In each case, the horizontal line represents the solidus below which only the solid phase exists. Above this, the solid and liquid phases can coexist until the liquidus line is reached, after which only the liquid phase is present.

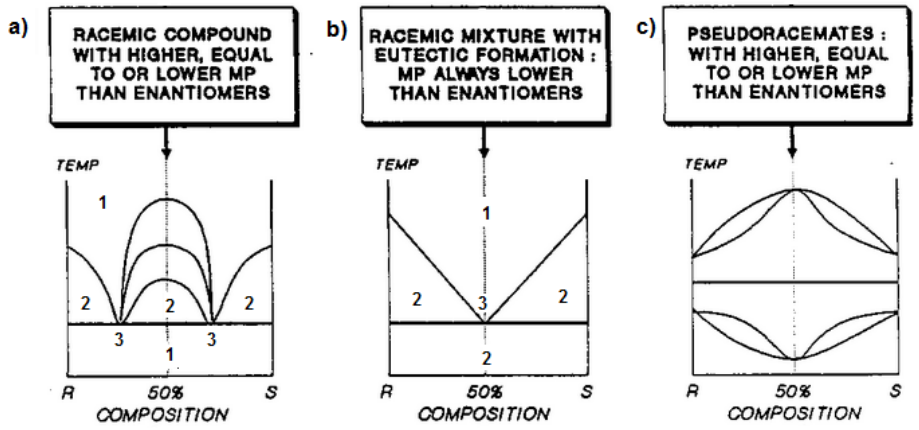

Figure 2.7 Characteristic binary phase diagrams for crystalline racemates: a) racemic compound b) conglomerate c) solid solution [48] (numbers indicate the number of phases present)

The Gibb's phase rule can be used to better understand the different regions of the phase diagrams with regards to their dependence on the system conditions. This describes the number of intensive variables in a system i.e. temperature pressure and component fraction, that can be altered without a change in the phases present, and is known as the degrees of freedom. For a given system consisting of a number of components, C, and phases, *P*, the degrees of freedom can be given by[32] :

$$F = \mathrm{C} - P + 2$$

Equation 2.40

For condensed systems i.e. those with no gases present, pressure has little effect on phase equilibrium therefore Equation 2.40 can be reduced to:

$$F = \mathrm{C} - P + 1$$

Equation 2.41

2.5.2.1 Conglomerates

Conglomerates are the primary focus of this study due to their ability to be resolved directly from the melt or solution by seeding. Conglomerates are characterised by the existence of only a single eutectic point which occurs only when the enantiomers are present in a 50:50 mixture. At the eutectic point the system is invariant since C = 2 (each enantiomer is a single component), and *P* = 3, therefore *F* = 0 and any change in temperature (or concentration) will result in a change in the number of phases present. Two phase regions are present either side of the eutectic point which consist of a pure enantiomer, *R* or *S,* and a liquid phase, saturated with respect to the excess enantiomer, whose composition is given by the corresponding point on the liquidus curve. Below the solidus line, both enantiomers are present as discreet crystals this is a bi-phasic region, and above the liquidus line, both enantiomers are present in the liquid phase. The melting point of the pure enantiomers is always higher than that of the racemate. As the conglomerate consists of physically distinct crystals of each enantiomer, it would be expected that they share the same melting points. However, this is not the case and in fact, a difference in temperature between the enantiomers of > 25˚C is usually an indicator for the presence of a conglomerate [9] (section 2.6.2 melting behaviour).

Consider the binary phase diagram for a conglomerate forming mixture of enantiomers, *Q* (Figure 2.8). In this case *R*, the more abundant enantiomer, has a mole fraction represented by point *x*; the mole fraction of *S* is therefore (1-*x*). In the solidus region, a mechanical mixture of *R* and *S* are present. Heating the mixture to the eutectic line initiates the melting of all of the *S* crystal and an identical mass of *R* crystals (i.e. 2(1-*x*)) as the number of degrees of freedom, *F* = 1. At this point, only *R* exists in crystalline form whilst the liquid phase has a eutectic, i.e. 50:50 composition represented by point *E*. On further heating, the *R* crystals continue to melt in the two-phase region and the liquid phase follows the liquidus curve ET^f_A until the temperature reaches T^f. All of the remaining *R* crystals melt at this point and the liquid phase has the composition *m* resembling the starting solid phase composition.

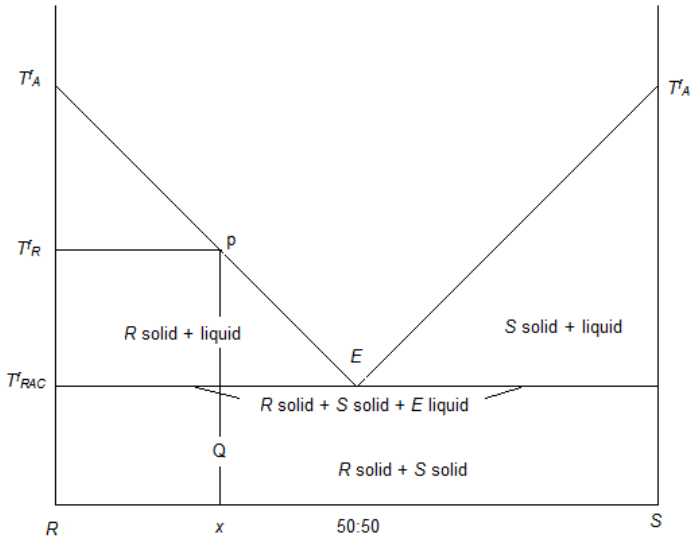

Figure 2.8 Binary phase diagram for a conglomerate forming racemate. x is the mole fraction of the excess enantiomer, *R*, in a mixture, *Q*.

Enantiomers of conglomerate forming chiral systems are miscible in the liquid phase whilst being, by definition, immiscible in the solid phase. Assuming that in the liquid phase, the enantiomers behave ideally (i.e. there are no molecular interactions between the antipodes thus the enthalpy of mixing, $\Delta H_l^m = 0$), and that the difference between the enantiopure liquid and solid phase specific heat capacities, C^l and C^s (cal mol^{-1} K^{-1}), remains constant with respect to temperature (for a conglomerate $C^l = C_A{}^l = C_R{}^l$ and $C^s = C_A{}^s = C_R{}^s$), the melting point, T^f, of a given mixture of enantiomers can be determined using the Schröder van-Laar equation[49, 50]:

$$ln\, x = \frac{\Delta H_A^f}{\mathrm{R}}\left(\frac{1}{T_A^f} - \frac{1}{T^f}\right) - \frac{C^l - C^s}{\mathrm{R}}\left(ln\frac{T_A^f}{T^f} + 1 - \frac{T_A^f}{T^f}\right) \qquad \text{Equation 2.42}$$

where x is the mole fraction of the excess enantiomer, ΔH_A^f(cal mol^{-1}) and T_A^f are the enthalpy of fusion and melting point of the pure enantiomers respectively, R is the universal gas constant (cal mol^{-1} K^{-1}), and subscript $_A$ denotes either enantiomer. Equation 2.42 is seldom used as the effect of specific heat capacities on fusion temperature is negligible; instead the

simplified form is sufficient to calculate the binary phase diagram using the experimentally determined pure enantiomer heat of fusion and melting point:

$$ln\, x = \frac{\Delta H_A^f}{R}\left(\frac{1}{T_A^f} - \frac{1}{T^f}\right)$$ Equation 2.43

2.5.2.2 Racemic Compounds

Racemic compounds are characterised by the presence of two eutectic points i.e. where the three phases; solid *R*, solid *S*, and a liquid phase mixture of *R* and *S*, all coexist at equilibrium. 50:50 mixtures of enantiomers can exhibit a melting point either lower or higher than the pure enantiomers with the latter being exclusive to racemic compounds. Below the solidus line (Figure 2.7) only a single phase exists as both enantiomers are mechanically indistinct. A two-phase region exists at the far left and right hand sides of the diagram consisting of a pure enantiomer and a liquid phase, saturated with respect to the excess enantiomer, whose composition is given by the corresponding point on the liquidus curve, with a third two-phase region located at the centre of the diagram where the racemic crystals and the liquid phase coexist. Only the liquid phase consisting of the two miscible enantiomers is present above the liquidus curve.

Assuming ideality, it is possible to construct a binary phase diagram for racemic compounds using the Prigogine-Defay equation which relates the melting point, T_f (subscript $_f$ denotes the end of fusion) of the major enantiomer, *x*, to the enthalpy of fusion, ΔH_R^f, and melting point, T_R^f, of the racemate [9]:

$$ln\, 4x(1-x) = \frac{2\Delta H_R^f}{R}\left(\frac{1}{T_R^f} - \frac{1}{T^f}\right)$$ Equation 2.44

2.5.3 Ternary Phase Equilibria

Ternary phase diagrams describe the equilibrium relationship between three different components under prescribed conditions of temperature, pressure, or concentration. The aim of this study is to preferentially crystallise one enantiomer from solution, and as a mixture of two enantiomers and a solvent

are a three-phase thermodynamic system, it is essential to understand the stable and metastable equilibrium relationships between them.

Taking into account the presence of solvent, the planar binary phase diagrams described in the previous sections become three dimensional. For simplicity, however, the ternary phase diagram is generally presented as a 2D isothermal slice, with a collection of these isotherms allowing for the construction of the 3D representation. Both will be considered in the following discussion.

The isotherm for a ternary conglomerate-solvent system consisting of enantiomers *R* and *S*, and solvent, *V*, is presented in Figure 2.9a[51]. Each vertex represents the pure components with the mole fraction of *R*, *S* and *V* following the lines *SR*, *RV* and *SV* respectively. DE and DE' are the equilibrium solubility curves for *R* and *S* respectively, and the eutectic point is given by point E. The extensions of the solubility curves (dotted lines) are the metastable solubility curves for each enantiomer. The region A represents an undersaturated solution of *R* and *S* in the solvent, *V*. B and B' are the bi-phasic regions consisting of pure *R* crystals + a solution saturated in *R*, and *S* crystals + a solution saturated in *S,* respectively. Discreet crystals of *R* and *S* + a solution saturated in *R* and *S* exist in the region C. As enantiomers share the same physical properties in a non-chiral environment, the phase diagram is symmetrical

Consider a binary mixture of enantiomers with an excess of *R* whose composition is given by v. If a small amount of solvent is added, the system moves point w. Recrystallisation of the system, e.g. by cooling, gives crystals exhibiting a new composition, U, and a racemic solution whose composition is represented by point E. When more solvent is added, the system moves to x, where recrystallisation gives pure crystals of and a racemic solution *R* therefore *S* is entirely in solution, which itself is racemic. Continuing to add solvent, the system moves to y where the pure *R* crystals are in equilibrium with a solution saturated in *R* whose composition is given by m. At z, recrystallisation results in a homogeneous yet saturated solution with a composition mirroring that at the start (v). Beyond z the solution remains undersaturated.

Collecting a series of ternary isotherms allows the 3D polythermic phase relationship for the *R-S-V* system to be depicted (Figure 2.9b). As the temperature is increased, the undersaturated 1 phase region grows larger corresponding to the increasing solubility of the enantiomers. The solubility curve for racemic mixture can therefore be deduced by following the eutectic curve Eε, with the solubility for varying enantiomeric compositions given by the shaded surfaces (Figure 2.9c). T^f_R is the melting point of the racemate, E, and it can be seen that the plane T^f_A-*R*-*S*-T^f_R represents the binary phase relationship for the two enantiomers.

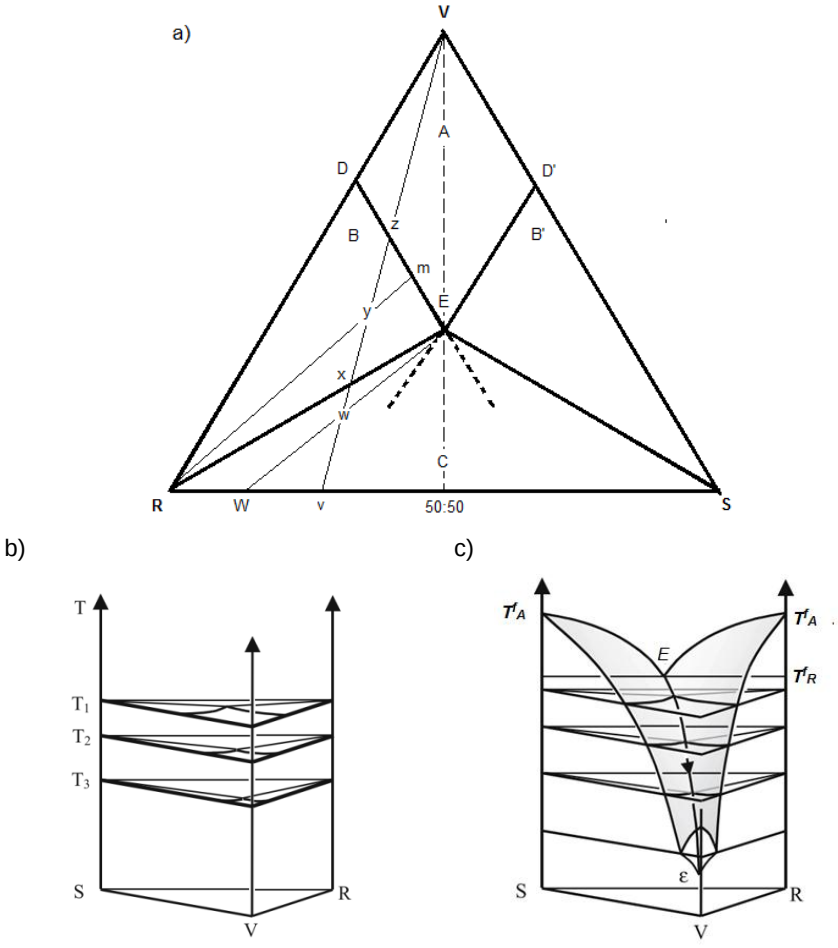

Figure 2.9 Isothermal section of a ternary phase diagram for a conglomerate forming system R-S-V, showing the different regions A: undersaturated solution, B and B': R solid + solution saturated in R and S solid + solution saturated in S respectively, C: R solid + S solid + solution saturates in S, b) Polythermal 3D representation of the R-S-V system constructed using three isotherms, c) symmetrical surface od solubility for the R-S-V surface[51]

Figure 2.10a-c illustrates the isoplethal plane R-Y-T for a ternary system forming crystalline conglomerates[51]. Throughout this section of the phase diagram, the solute-solvent ratio is constant which is of significant importance to the crystallisation process, as, in the figure displayed, only *R* crystals are produced if the system does not deviated from this plane. These diagrams are used to describe preferential crystallisation and will be considered more detail in section 2.6.5

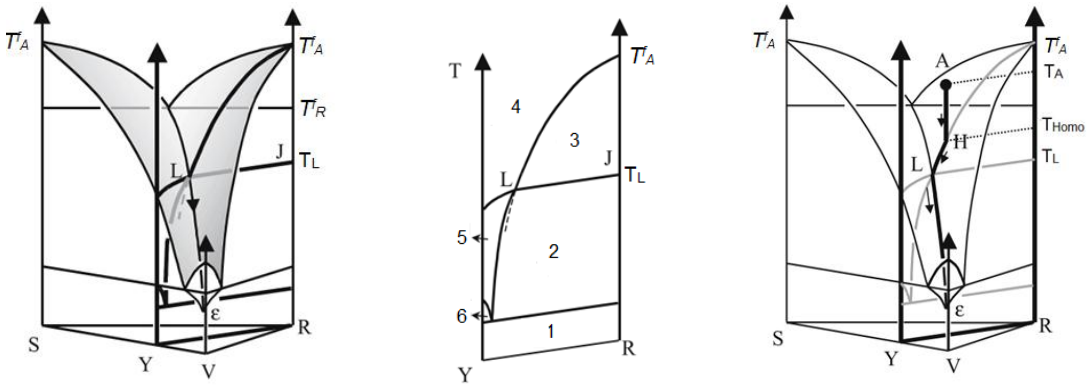

Figure 2.10 R-Y-T isoplethal plane in a ternary phase diagram, for the conglomerate crystal system, in which the ratio S:V is constant, b) isolated isopleth illustrating the various regions 1: R solid + S solid + V solvent, 2: S solid + solution saturated in R and S, 3: R solid + solution saturated in R, 4: undersaturated solution, 5: S solid + solution saturated in S, 6: S solid + V solvent + solution saturated in R and S, c) trajectory of solution phase composition on cooling for the T-R-Y isopleth in which the system remains equilibrated throughout the process[51]

2.5.4 Phase Diagram Construction

If the racemate and at least one of the pure enantiomers are available, it is possible to construct a binary phase diagram by simply measuring the melting points of enantiomer mixtures with a range of compositions. Differential Scanning Calorimetry (DSC) is an effective and accurate technique that can be employed[52-54]. The samples must firstly be prepared by mixing a known amount of racemate and pure enantiomer and either crystallising form the melt or by solvent evaporation. It is essential that the crystalline sample is as homogeneous as possible which can be achieved by crushing or grinding[9]. For accuracy, it is useful to determine the *ee* for each sample, for example by chiral

chromatography, eliminating any experimental error associated with sample weighing.

Due to the symmetrical nature of enantiomeric binary (and ternary) phase relationships, only a single enantiomer and the racemate are required to construct half of the phase diagram with the other half being safely assumed as identical. Additionally, it may only be necessary to identify several melting temperatures for the different compositions as coincidence with the calculated equilibrium lines, signifying ideality, would allow for the remainder of the diagram to be determined numerically.

Construction of ternary phase diagrams require the identification of the solubility curves at a constant temperature for the pure enantiomer and racemate, and a range of mixtures, in a chosen solvent system. Generally five or six mixtures of enantiomers, the pure and racemic forms are required, covering the range 0-100% *ee* in equal increments[9]. Sufficient time should be allowed to ensure that equilibrium is achieved between the solid and liquid phases. Thus identifying the saturated solution phase enantiomeric composition e.g. by chiral GC/HPLC gives a single point of the solubility curve. Figure 2.11 illustrates this process. Allowing a mixture of enantiomers, *R* and *S*, and solvent, *V*, of composition, b, to reach equilibrium results in a saturated solution whose composition is given by c. The composition of the crystal phase, A, can be estimated by drawing the tie line ca. Repeating the process for different compositions allows the solubility curve PEP' to be constructed, and drawing tie lines from the eutectic point, E, segregates the bi and tri-phasic regions.

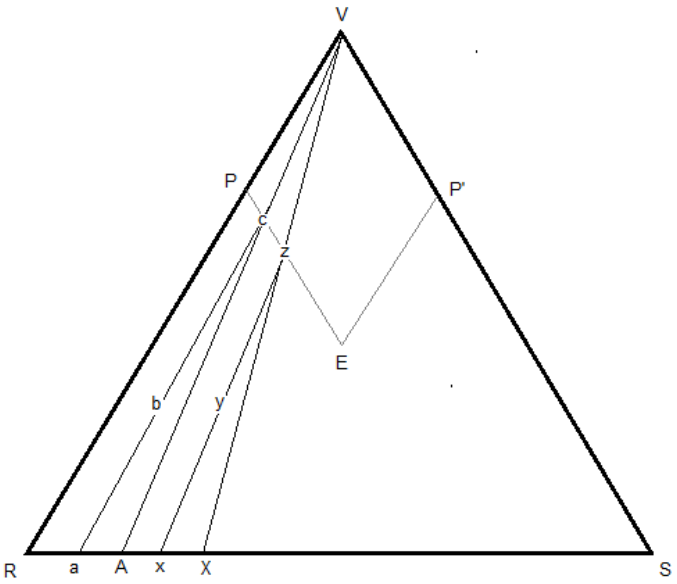

Figure 2.11 Construction of a conglomerate ternary phase diagram

2.6 Conglomerates

2.6.1 Formation

Chiral molecules are by definition unsymmetrical. It follows then that homochiral crystals must occupy only chiral crystallographic space groups i.e. those with no inverse elements of symmetry i.e. a centre of inversion (one-fold rotary inversion) or a mirror plane (two-fold rotary inversion)[55]. Of the 32 point groups, 11 are void of inverse symmetry elements therefore only 65 space groups are possible for enantiomers crystallising as conglomerates with the most frequently encountered being $P2_12_12_1$ (~58%) and $P2_1$ (~30%) [9]. Conversely, racemic compounds can occur in all crystal configurations; however, these are generally limited to the 164 space groups exhibiting inverse symmetry elements[9]. This may be a contributing factor towards the infrequent occurrence of enantiomers crystallising as conglomerates.

Conglomerates are highly desirable as they possess the unique characteristic of being resolvable by crystallisation rather than comparably more complex processes. Consequently, much research has been concerned with investigating the factors influencing their formation[56-64]. The most comprehensive study to date, performed by Kinbara *et al*[65], involved X-ray

crystallographic studies on a range of chiral primary amine salts with achiral carboxylic acids. Previous studies[66, 67] had suggested a link between the occurrence of a conglomerate and the characteristic columnar hydrogen bond networks observed in the crystals of chiral 1° amine-carboxylic acid salts therefore an assortment of different crystals were examined to provide some statistical evidence for this observation; seven conglomerates, seventeen racemic compounds and four pure enantiomers. Each of the enantiopure salts and those crystallising as a conglomerate displayed characteristic hydrogen bond networks between the molecules, and as a consequence, the space groups $P2_1$ and $P2_12_12_1$ were always encountered. In each case, hydrogen bonding was observed between adjacent enantiomers, and also between translation units resulting in a columnar assembly about a two-fold screw axis along the shortest cell axis, *b* or *c*[65] (Figure 2.12a). Formation of the macroscopic crystal structure occurs due to van der Waals interactions between the 2_1-columns resulting in either parallel ($P2_1$) or antiparallel ($P2_12_12_1$) packing of homochiral columns (Figure 2.12b). Racemic compounds of these salts were found to crystallise in both chiral and achiral space groups ($P2_1$and $P\bar{1}$) with equal probability. In the former, homochiral supramolecular 2_1-columns were packed alternatively, either parallel or anti parallel, by van der Waals interactions to form the macroscopic crystal structure. An achiral inversion column ($P\bar{1}$) was also formed due to the existence of an inversion centre between the ammonium cations and carboxylate anions within the unit cell.

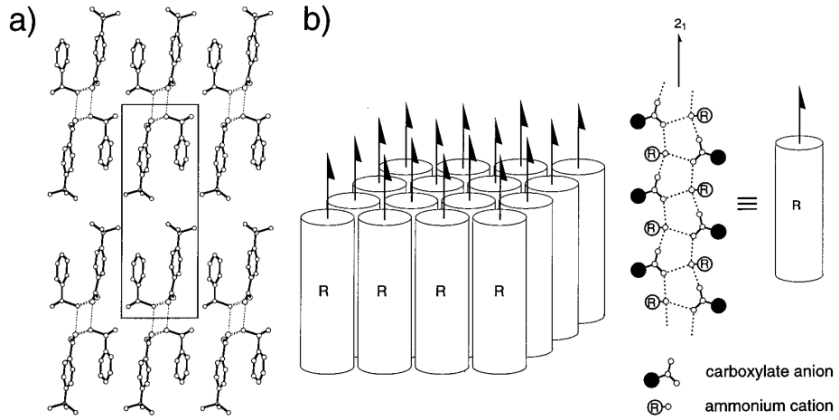

Figure 2.12 Conglomerate crystal structure of a primary chiral amine-achiral carboxylic salt forming a 2_1-column a) viewed down the axis of the 2_1 column (b axis) with the unit cell outlined (solid line) and the hydrogen bonds shown (dotted lines), b) schematic illustration of 2_1-column packing

In another study into the formation of homochiral salt crystals, Kinbara *et al*[68] considered the role of the derivatising agent in influencing the resultant crystal structure. The investigation focused on chiral amines and chiral carboxylic acids, normally used in conjunction during diastereomeric crystallisation, rather than chiral amine-achiral acid systems previously investigated with direct crystallisation in mind. Previous studies[69] into diastereomic crystallisation showed that high resolution efficiencies could be achieved when the chiral resolving agent exhibited a similar molecular length to the racemate, and the crystal produced occupied the $P2_1$ space groups. From these findings, it was postulated that the prevalence of conglomerates resolvable by preferential crystallisation could therefore be increased by using high performance diastereomic resolving agents as derivatising agents. Their results suggested that the probability of obtaining a conglomerate can be increased from ~10% to over 50% when the chiral derivatising agent used is also an effective resolving agent in diastereomic crystallisations. Generally speaking, the probability of obtaining a conglomerate can be increased by forming a salt using any derivatising agent that has a similar molecular length and/or shape as the racemate and forms helical 2_1-columns resulting from supramolecular hydrogen networks[65].

2.6.2 Melting Behaviour

When a crystalline substance is at its melting point the solid and liquid phases are in equilibrium i.e.

$$\Delta G^f = \Delta H^f - T^f \Delta S^f \qquad \text{Equation 2.45}$$

where the superscript ^{f} denotes fusion. Therefore when enantiopure crystals melt, they are in equilibrium with a single liquid phase whereas racemates are in equilibrium with a binary liquid mixture.

The Shröder Van Laar relationship (Equation 2.42) assumes that a mixture of liquid phase enantiomers behaves ideally i.e. its enthalpy of mixing is zero, whilst its entropy of mixing can be given by[9]:

$$\Delta S_l^m = -\mathrm{R}(x_R \, ln x_R + x_S ln x_S) \qquad \text{Equation 2.46}$$

For a racemate, $x_R = x_S$ (where $_R$ and $_S$ denote each enantiomer) = 0.5 therefore ΔS_l^m = R ln 2 = 5.78 J/mol K.

Racemic compounds have zero mixing entropy in the solid state, or more specifically zero configuration entropy. The configuration entropy for conglomerates, ΔS_c^m, given by[70],

$$\Delta S_c^m = \left(\frac{N_{c/m}}{N_0}\right) \mathrm{R} \; ln \; 2 \qquad \text{Equation 2.47}$$

where $N_{c/m}$ is the number of crystals per mole of material and N_0 is Avogadro's number, is greater than zero; however, it is negligibly small and can only be measured in systems that are disordered at the molecular level[70]. The entropy of mixing associated with the melting of a binary mixture of enantiomers is therefore Rln2 greater than that of the pure enantiomer which, as a consequence, has a higher melting point due to the lower free energy of the liquid phase. A conglomerate has the same enthalpy and, in effect, the same entropy as the pure enantiomers. The difference in melting point between

racemic conglomerates and their corresponding crystalline enantiomers is thus determined only by the liquid with which it is in equilibrium.

Figure 2.13 illustrates this graphically. The free energy of the “racemic” liquid RTln2 is less than the enantiopure “chiral” liquid. For chiral crystals i.e. enantiopure crystals, the melting point is located at the intersection of the liquid free energy curve for the enantiopure liquid. Similarly, the conglomerate and racemic compound melting points can be obtained at the corresponding intersects of the binary liquid phase free energy curve. Figure 2.13 also shows that the racemic compound an conglomerate are in equilibrium with the same liquid i.e. there relative stabilities are only governed by their differences in enthalpy. In the diagram shown, the racemic compound has the higher melting point; however, the conglomerate is the more stable of the two. This therefore shows that the racemic compound is not always the most stable crystalline form for chiral molecules[70] contradictory to Wallach’s rule[71]: racemic compounds are denser than homochiral crystals and are, hence, more stable due to the tighter packing within the unit cell.

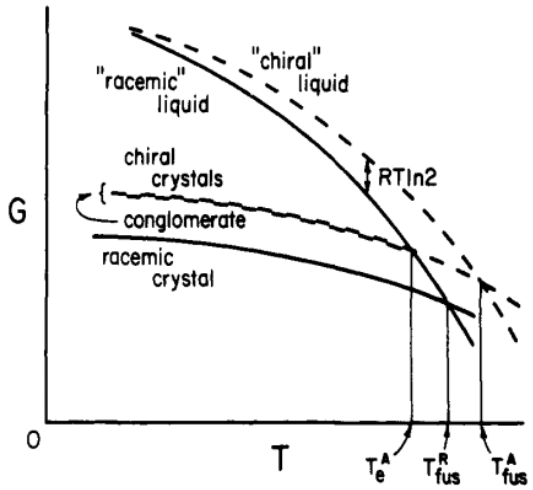

Figure 2.13 Free energy diagram for the solid and liquid phases illustrating the difference in melting temperatures between chiral crystals i.e. enantiopure, conglomerates, and racemic crystals i.e. racemic compounds, as a consequence of the entropy of mixing associated with melting binary racemates[70].

The enthalpy and entropy changes associated with the melting of conglomerates can be described using thermodynamic cycles shown in Scheme 2.1[9]. Consider a pair of solid phase enantiomers, R_s + S_s, at the melting point of the pure enantiomer, T^f_A. Melting yields the liquid phase R_l + S_l which upon mixing gives the racemic liquid, RS_l. A reduction in the liquid phase heat capacity, C^l, occurs as the racemic liquid is cooled to the melting point of the racemate, T^f_R (note: for conglomerates there is no difference between the pure enantiomer and racemic solid phase heat capacities, and those for the corresponding liquid i.e. $C^s_A = C^s_R = C_s$, and $C^l_A = C^l_R = C_s$). Solidification of the racemic liquid to form RS_s is accompanied by a change in the fusion enthalpy/entropy for the racemate, ΔH^f_R / Δs^f_R, and the enthalpy/entropy of mixing of the solid phase, ΔH^f_R / Δs^f_S.

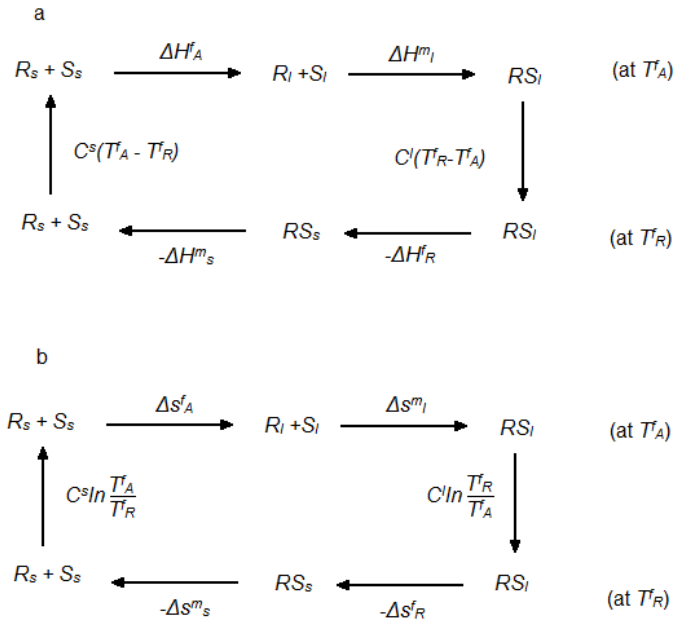

Scheme 2.1 Thermodynamic cycles for the a) enthalpy and b) entropy changes associated with the melting of a conglomerate (subscripts $_s$ and $_l$ denote solid and liquid phases respectively).

The Shröder Van Laar expression (Equation 2.43) for ideal conglomerates postulates that the enantiomers are perfectly miscible in the solid phase and are ideal in the liquid phase i.e. $\Delta H^m_s = \Delta H^m_l = 0$. Therefore using Scheme 2.1 the following expressions can be obtained:

$$\Delta H_s^m = C^s\left(T_A^f - T_R^f\right) + \Delta H_A^f + C^l\left(T_R^f - T_A^f\right) - \Delta H_R^f = 0 \qquad \text{Equation 2.48}$$

$$\Delta H_A^f - \Delta H_R^f = (C^l - C^s)(T_A^f - T_R^f) \qquad \text{Equation 2.49}$$

As $C^s > C^l$ and has a magnitude of 84–168 J mol^{-1} [9] and T^f_A-T^f_R for conglomerates is typically 20-30°C, $\Delta H^f_A > \Delta H^f_R$ with the difference for ideal systems lying between 1.7-5.0 kJ mol^{-1}.

Considering entropy changes, a mechanical mixture of two separate phases, R_s and S_s, constitute the conglomerate, RS_s, therefore no entropy change is associated with the mixing of R_s and S_s i.e. $\Delta s^m_s = 0$. However, for the liquid phase enantiomers, R_l and S_l, interactions between them result in the entropy of mixing, Δs^m_l, being equal to Rln2 = 5.78 J mol^{-1} if they behave ideally (see Equation 2.46). Using Scheme 2.1, in a similar manner as shown above for enthalpy, the following expressions can be obtained which permits calculate of Δs^m_l for a given system using the experimentally determined melting points and enthalpies of fusion of the racemate and pure enantiomer:

$$\Delta s_s^m = C^s ln\frac{T_A^f}{T_R^f} + \Delta s_A^f + \Delta s_l^m + C^l ln\frac{T_R^f}{T_A^f} - \Delta s_R^f = 0 \qquad \text{Equation 2.50}$$

$$-\Delta s_l^m = \frac{\Delta H_A^f}{T_A^f} - \frac{\Delta H_R^f}{T_R^f} - \frac{\Delta H_A^f - \Delta H_R^f}{T_A^f - T_R^f} ln\frac{T_A^f}{T_R^f} \qquad \text{Equation 2.51}$$

2.6.3 Solubility

Since enantiomers share the same physical and chemical properties, their solubilities are identical. Assuming ideal behaviour, each enantiomer exhibits its solubility independently when present as a mixture of crystalline enantiomers in equilibrium with a saturated solution. As a consequence, a 50:50 mixture will

have a solubility twice that of the pure enantiomers. This is known as the "Meyerhoffer double solubility rule"[72].

Using crystals of the conglomerate forming imine 2-methyl-benzaldehyde and phenylglycinamide in equilibrium with a saturated racemic solution, Izumi (2009)[73] showed that this is also true for enantiomers racemising in solution. The compound undergoes rapid base-catalysed racemisation in methanol when small amounts of 1,8-diazabucycloundec-7ene (DBU) are added. Little variation was seen between the solution concentrations of non-racemising and racemising systems. It must follow then that for slower rates of racemisation, whereby the solution can be observed to be non-racemic, the solid-liquid equilibrium position changes throughout the duration of the process as the solution phase *ee* evolves. At the end of crystallisation, dissolution of an equal amount of homochiral crystals should be observed for an equilibrated slurry with and initial crystalline enantiomeric excess undergoing slow racemisation. This is a result of the entropy of mixing increasing as the solution becomes racemic i.e. the solid phase is in equilibrium with a solution that has a different enantiomeric composition hence some solid dissolves to re-establish solid-liquid equilibrium . This may need to be addressed during this study if the racemisation rate is found to be too slow to maintain a racemic solution yet fast enough to prevent nucleation of the counter enantiomer. The product crystals can simply be filtered from the process solution at the end of crystallisation and before solution phase racemisation is achieved.

2.6.4 Detection

The first successful detection of a conglomerate was by Pasteur in 1848[74]. The sodium ammonium tartrate tetrahydrate crystals which he was using displayed hemihedral <111> faces which allowed each homochiral crystal to be distinguished under a microscope. This technique is applicable to chiral compounds crystallising the same space group $P2_12_12_1$ as these display hemihedrism; however, visibility of the faces is dependent on the crystal habit. Additionally, this method of manual sorting is very inefficient and becomes unfeasible beyond laboratory scales.

When both the racemate and pure enantiomers are present, characterisation of the racemate type can be achieved using modern spectroscopic techniques that are capable of distinguishing differences in solid state structure; powder X-ray diffraction (PXRD), single crystal X-ray diffraction (SCXRD), infrared (IR), Raman spectroscopy and solid-state nuclear magnetic resonance (ssNMR). Since the molecular arrangements seen in opposing homochiral crystals are identical yet opposing, and conglomerates are mechanical mixtures of these, the resultant spectra for the racemate and corresponding pure enantiomers will be superimposable. SCXRD is particularly useful as this allows for characterisation of the crystal structure.

When sufficient quantities of both the racemate and one of the enantiomers are available, the characteristic binary phase diagram can be constructed. This can be achieved by mixing varying amounts of the racemate and pure enantiomer to give a desired enantiomeric excess, and measuring the resultant melting point using a thermal analytic technique such as DSC (for systems in which thermal decomposition is not observed below the melting point of the pure enantiomers). Using only one of the enantiomers and the racemate, several samples of different *ee* are all that is required to construct the diagram. If the melting point of any of the mixtures is lower than that of the racemate, a racemic compound must be present as the eutectic points are always at compositions other that 50:50. Samples with an *ee* close to 0% must therefore be prepared to account for systems forming a racemic compound whose eutectic points are close the racemic composition. If the racemate is a conglomerate, the melting points of the mixtures will always decrease from the pure enantiomers to the racemate. Additionally, the experimental data can be compared with the values obtained using the Shröder Van Laar and Prigogine-Defay expressions whereby coincidence with the calculated curve indicates the presence of a conglomerate or racemic compound respectively.

Another simple yet effective characterisation technique requiring both a single enantiomer and the racemate is the solubility test. Addition of the pure enantiomer to a saturated racemic solution will result in no dissolution or partial/complete dissolution if the racemate is a conglomerate or racemic compound respectively. This is analogous to construction of the binary phase

diagram in which the racemic compound has a lower stability as its enantiomeric composition deviates from racemic up until the eutectic points, upon which the stability subsequently increases.

The number of characterisation techniques becomes limited when only the racemate is available. Analysis of a single crystal using chiral chromatography (GC and HPLC) can give an indication to which form of racemate is present. For a racemic compound, both enantiomers are present in the unit cell therefore two peaks will appear on the resultant plot when a single crystal of the racemate is analysed. Conversely, only a single component will be identified if the racemate is a conglomerate as each crystal is homochiral. Polarimetry can be used in a similar manner whereby a single crystal of a racemate dissolved in a solvent will rotate plane polarised light if it is a conglomerate and hence enantiomerically pure.

It has recently been shown by Coquerel *et al*[75] that it is possible to efficiently identify conglomerates using Second Harmonic Generation (SHG) which requires only a small amount of the crystalline racemate. When light of wavelength, λ, is beamed on a sample of the racemate, a new beam of wavelength $\lambda/2$ is generated for crystals occupying non-centrosymmetric space groups, whose intensity is given by the second order susceptibility tensor, $X^{(2)}$. Conversely, the elements of the second order susceptibility tensor, $X^{(2)}$, are zero for crystals occupying centrosymmetric space groups[51]. Conglomerates can therefore be quickly detected as, by definition, they can only occupy non-centrosymmetric space groups whereas the vast majority of racemic compounds crystallise in those that are centrosymmetric. Despite this, there are several limitations associated with its use[51]. Some racemic compounds are able to crystallise in chiral space groups giving a positive yet false SHG response. Additionally, it is possible that the incident or emitted electromagnetic radiation is absorbed by the crystal, or that $X^{(2)}$ is too small to observed meaning that the conglomerate remains undetected. These drawbacks, despite being relatively infrequent, have limited the use of SHG as the sole method of characterising conglomerates; however, its use in preliminary analysis, as a complementary tool to traditional methods, is becoming more prevalent.

2.6.5 Preferential Crystallisation of Conglomerates

If a racemic system can exist as a conglomerate, it may be possible to resolve the mixture using preferential crystallisation. Also referred to as *resolution by entrainment*, this technique involves the selective crystallisation of only a single enantiomer by seeding a supersaturated solution that is slightly enriched with the enantiomer being crystallised (although this is not a necessity). Preferential crystallisation is an attractive technique for resolving enantiomers since it gives high *ee*s (> 99%), is relatively inexpensive and requires no auxiliaries or reagents; only solvents are required. Despite this, as with all chiral resolution methods, preferential crystallisation is limited to a maximum theoretical yield of 50%.

The process of preferential crystallisation was first identified by Gernez in 1866[76]. He noticed that no crystallisation occurred when a supersaturated solution of levorotatory sodium ammonium tartrate was seeded with crystals of its antipode. The procedure was repeated using a saturated racemic solution. Crystallisation of only the seeded enantiomer occurred, and as a consequence, the composition of the resultant mother liquor had an excess of the levorotatory enantiomer which was subsequently crystallised upon seeding.

Despite being confirmed as an effective resolution procedure[77], the use of preferential crystallisation for enantiomer resolution on an industrial scale has been limited primarily as only ~ 10% of compounds have been shown to crystallise as conglomerates[9]. However, several compounds exist which are resolved on an industrial scale by the entrainment process for example α-methyldopa[78]. Development of the technique has led to three different methods of resolving enantiomers by entrainment[51]:

- Seeded Isothermal Preferential Crystallisation (SIPC)
- Seeded Programmed Polythermic Preferential Crystallisation (S3PC)
- Auto-Seeded Programmed Polythermic Preferential Crystallisation (AS3PC)
- Evaporative Preferential Crystallisation

The general procedure for Seeded Isothermal Preferential Crystallisation (SIPC) is best described using a ternary phase diagram for a racemate that forms a

conglomerate crystal system (Figure 2.14)[79]. Note for each of the preferential crystallisation techniques described, ideality is assumed therefore the following conditions apply:

- No solid solution exists between the enantiomers
- No stable or metastable solvate exists
- No unstable or metastable racemic compound exists
- The effect of the heat of crystallisation on temperature is neglected

Firstly consider a system where no homochiral seed crystals are used and crystallisation of both enantiomers is allowed to occur. Initially, the system is undersaturated at the temperature T_1 and has a composition represented by point *a* showing there is a slight excess of the (-)-enantiomer. Although this does increase the rate of the resolution process, it is not a necessary condition therefore it is possible to start with a racemic composition. However, an initial enantiomeric excess can be achieved by simply dissolving a known amount of the pure enantiomer in an undersaturated racemic mixture to produce an optically active solution. If the system reaches the reduced temperature, T_2, in the absence of seed crystals, the system will be supersaturated and the phase composition will move from *a* to *c* to achieve equilibrium. At this point, simultaneous crystallisation of both enantiomers would occur and the eutectic composition consists of an equimolar mixture of both enantiomers in solution, and a solid composition represented by point d i.e. there is an excess of the (-)-enantiomer crystals.

Alternatively, if homochiral seeds are added to the supersaturated system, in this case the (-)-enantiomer, the change in system composition follows a different route. As there is an initial excess of one enantiomer in solution, this experiences a greater degree of supersaturation at T_2 than that of the minor enantiomer. Consequently, when the seed crystals are added, the (-)-enantiomer molecules in solution are deposited on the surface of the crystals due to chiral recognition and the greater mass transfer driving force. Hence the system composition follows the trajectory *abc*. Nucleation of the undesired (+)-enantiomer crystals occurs at the point where the curved path *abc* leaves the line *aa'* (which represents the change in system composition when only the (-)-

enantiomer is crystallised with no nucleation of its antipode). Nucleation of the minor enantiomer must of course be avoided therefore the most favourable resolution conditions will remain close to the line *aa'* for the maximum possible time which corresponds to the greatest difference in crystallisation rates of the two enantiomers[9].

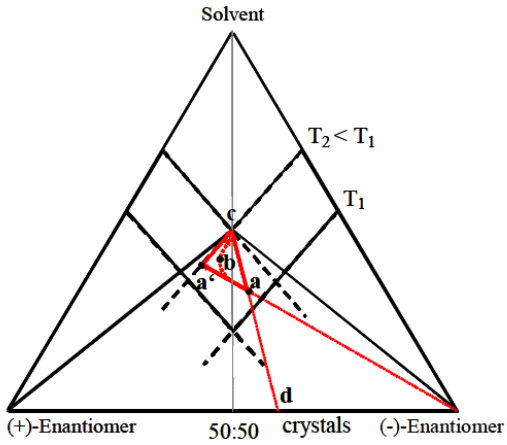

Figure 2.14 Ternary phase diagram for a conglomerate system illustrating the process of preferential crystallisation[79]

It is clear that the method described for the preferential crystallisation of a single enantiomer is poorly productive as the theoretical maximum yield obtainable of the desired enantiomer is limited to the duration of time it takes for the counter enantiomer in solution to reach its supersaturation limit. Elsner *et al*[80] suggested a 'quasi-continuous' operational mode whereby each enantiomer is preferentially crystallised sequentially in a cyclic process eliminating these problems (Figure 2.15)[79]. As before, the system composition is represented by point *a*; an optically active solution. Seeding with the (-)-enantiomer whilst the system is supersaturated results in the growth of the seed crystals due to mass transfer from the solution phase to the solid surface in an attempt to reach equilibrium, and the system composition moves along the line *ab*. At *b* there is now an excess of the (+)-enantiomer in solution. The newly formed (-)-enantiomer crystals are removed from the system (e.g. by filtration) and a mass of racemate equivalent to that of the crystals produced are added. The system now exhibits a composition represented by point *c* mirroring the starting conditions in which there is an excess of the (+)-enantiomer. The procedure is then repeated using seeds of the (+)-enantiomer therefore the complete cycle *abcd* is capable of producing a single batch of each enantiomer.

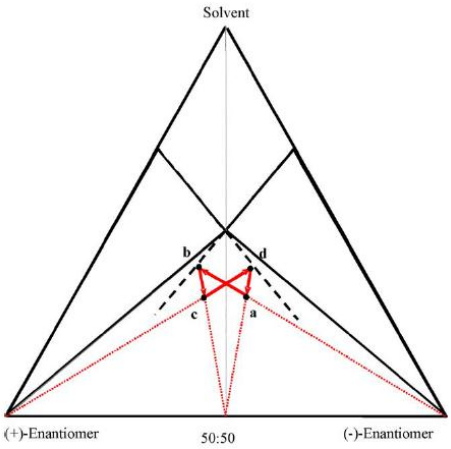

Figure 2.15 Trajectories for a sequential, cyclic preferential crystallisation process[79]

Figure 2.16 illustrates the experimental set-up used for the cyclic preferential crystallisation of threonine enantiomers in water by Elsner *et al*[80]. The aim of their investigation was to determine the feasibility of such a process and to identify the parameters influencing its operation. The system consists of two 1.2 litre vessels arranged in sequence with a 250 ml filtration unit between them to separate the solid product from the process solution. The optical rotation and density of the solution within the first vessel is measured externally by circulating a small amount the mother liquor. The temperature of the entire system, including the filtration unit, density metre, polarimeter, and all the lines between them, are thermostated and maintained at the process temperature to ensure no unwanted crystallisation occurs outside of each vessel.

During their experiments, a batch of each threonine enantiomer was crystallised from a solution with a concentration corresponding to saturation at 40˚C and an initial enantiomeric excess of 0% i.e. a racemic solution (i.e. two subsequent 'half-cycles' were employed for each enantiomer - *abcd* in Figure 2.15). Initially, the undersaturated racemic solution in vessel 1 was maintained at a temperature greater than its crystallisation temperature to ensure that any remaining particulate matter had been dissolved. After cooling 10 ˚C below the saturation temperature, 2.5 g of homochiral seed with a sieve fraction of 212-300 µm were added resulting in the desired enantiomer crystallising by growth or secondary nucleation mechanisms. The slurry produced was then passed through the filter unit to remove the crop of enantiopure crystals, after which a mass of racemate equivalent to the mass of crystals removed was added to the

solution. This was then passed to vessel 2 with the procedure described being repeated for the opposing enantiomer.

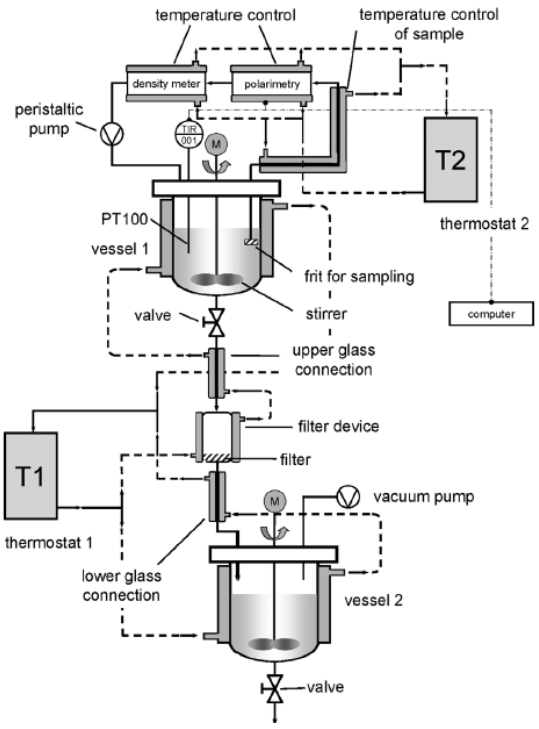

Figure 2.16 Experimental set-up for cyclic preferential crystallisation used by Elsner *et al*[80]

To avoid nucleation of the unwanted enantiomer in each vessel, the optical rotation of the solution was monitored with crystallisation being interrupted when the solution *ee* reached 2% for the counter-enantiomer which corresponds to an optical rotation of approximately $\pm 0.056^{\circ}$ (Figure 2.17 [79, 80]). This value was determined in similar preliminary experiments in which the counter enantiomer was instead allowed to crystallise whilst the solution *ee* was measured by polarimetry. The reversal of the optical rotation is indicative of the counter enantiomer nucleating therefore the process can be stopped at any value of optical rotation before the limit is achieved Obviously if crystallisation is interrupted closer this limit, the process will be more productive due to the greater crystallisation time for the desired enantiomer. However, it must be remembered that resolution will continue until the crystals are filtered from the mother liquor therefore an allowance must be made to compensate for the time taken for the slurry to be filtered - hence a lower *ee* that the actual limit is selected.

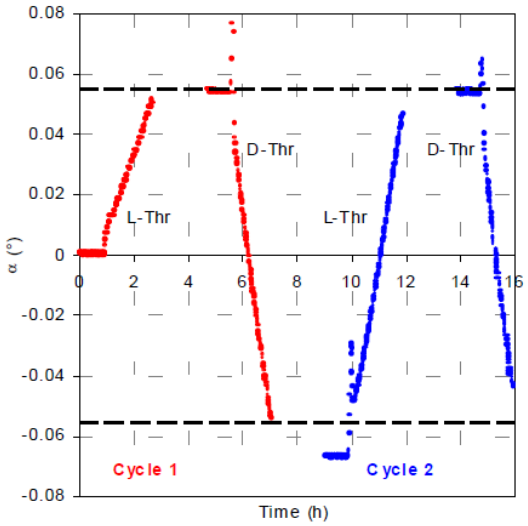

Figure 2.17 Optical rotation trajectories for two subsequent separation cycles crystallising L-Threonine and D-Threonine sequentially[79, 80]

Seeded Programmed Polythermic Preferential Crystallisation (S3PC) is a modification of SIPC whereby crystallisation occurs over a range of temperatures. Figure 2.18a shows the isopleth *R-Y-T* for such a process. when the solution becomes supersaturated at T_{homo}, seed crystals are introduced and controlled cooling is applied to favour crystal growth over secondary nucleation and the liquid phase composition follows the stable solubility curve *HL*[51] unit a racemic solution is achieved. Meanwhile the (*R)*-enantiomer leaves solution via secondary nucleation or crystal growth mechanisms as the system proceeds along L_F with the liquid phase composition now containing an excess of the (*S)*-enantiomer. Therefore in this method equilibrium is maintained between the temperatures T_A to T_L, whereas the (*S)*-enantiomer is non-equilibrated and the (*R*)-enantiomer in metastable equilibrium from T_L to T_F. The Pure crystals are filtered and an amount of racemate equal to the mass of that removed is added. The process is then repeated for the opposite enantiomer.

The SIPC and S3PC processes described are limited by the fact that they require seed crystals for each enantiomer (for cyclic operation) produced *ex situ*. An improvement of these processes involves the *in situ* partial crystallisation of the enantiomer in excess which is subsequently used as seed; Auto-Seeded Programmed Polythermic Preferential Crystallisation (AS3PC) (Figure 2.18b). Initially the composition is given by point E_B within the biphasic region of the phase diagram. At this temperature (T_B) a slurry exists consisting

of the pure (*R)*-enantiomer in thermodynamic equilibrium with its saturated solution. As with S3PC, an appropriate cooling profile from T_B to T_L, stirring mode and rate are selected so the system remains close to equilibrium favouring crystal growth rather than uncontrolled nucleation[81], and the liquid composition moves along the metastable solubility curve *BL*. This technique utilises the enantiopure crystals suspended in the slurry hence the title "Auto-Seeded". The Pure crystals are filtered and an amount of racemate equal to the mass of that removed is added. The system is then heated back to T_B resulting in selective dissolution of the (*R*)-enantiomer crystals as the composition enters the biphasic region comprised of (*S*)-enantiomer crystals in equilibrium with the saturated racemic solution. The rate of crystallisation i.e. the rate of secondary nucleation and growth is influenced not only by the degree of supersaturation but also on the quantity of seed present at the start of the process, with a greater amount favouring fast crystallisation[82] as a result of the increased surface area provided.

a) b)

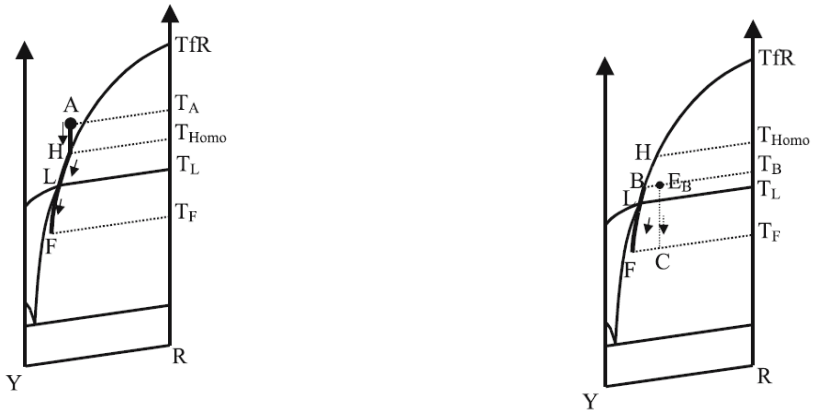

Figure 2.18 *R-Y-T* Isopleth from a ternary phase diagram showing the principle of a) Seeded Programmed Polythermic Preferential Crystallisation (S3PC) and b) Auto-Seeded Programmed Polythermic Preferential Crystallisation (AS3PC)[51]

3 Racemisation

3.1 Background

Racemisation involves the interconversion of enantiomers to irreversibly form a racemate from a pure enantiomer or an optically active mixture. Since the enthalpy change of the enantiomers undergoing racemisation, $\Delta H^{Rac} = 0$, the process is thermodynamically favourable only because of the increased entropy associated with the mixing of the enantiomers in the liquid phase, which is equal to RTln2 (Equation 2.46) [83].

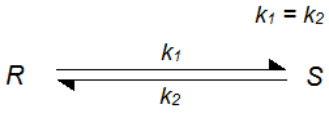

Equation 3.1

The rate of racemisation is proportional to the concentration of the excess enantiomer. Assuming $k_1 = k_2 = k$, the rate equation for a reversible first-order reaction for conversion of the pure enantiomer *R* to *S* is given as [84]:

$$\ln\left[\frac{1+S/R}{1-S/R}\right] = 2kt$$

Equation 3.2

where *S/R* is the stereoisomeric ratio which approaches unity as the excess *R*-enantiomer is racemised.

Alternatively, the racemisation kinetics can be described by the decay in enantiomeric excess from 100% to 50% i.e. the racemisation half-life, $t_{1/2}$:

$$t_{1/2} = \ln\frac{2}{2k}$$

Equation 3.3

Several racemisation methods exist which can be categorised as follows [85]:

- Thermal racemisation
- Base-catalysed racemisation
- Acid-catalysed racemisation
- Racemisation via Schiff bases
- Enzyme-catalysed racemisation
- Racemisation via redox and radical reactions

The application of these techniques remains limited due to the necessity of elevated temperatures, strongly acidic or basic environments, and their inherent specificity. A more effective approach is the use of "general purpose" organometallic racemisation catalysts which can be applied to chiral centres bearing the same functional groups in mild conditions.

3.2 Amine Organometallic Racemisation Catalysts

One of the first investigations into organometallic racemisation catalysts for chiral amines was performed by Murahashi *et al* [86]. (*S*)-(-)-*α*-phenylethylamine was quickly racemised using a palladium black catalyst under argon at 100 ˚C and 50˚C (Figure 3.1). However, only a 3% yield was possible as the reaction also produced a mixture of (*S*,*S*)-, (*S*,*R*)- and (*R*,*R*)- *α, α'*-dimethyldibenzylamine (77%, *ee* = 1.7%), and *N*-(methylbenzylidene)- *α*-methylbenzylamine *(*20%, *ee* = 6.6%*).*

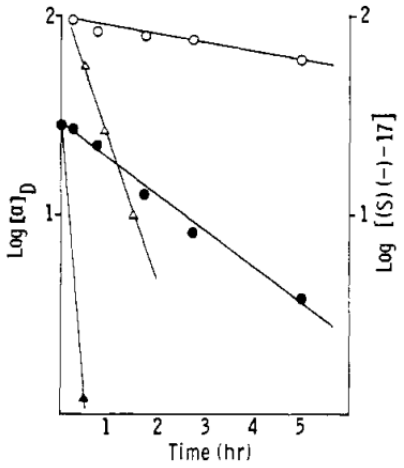

Figure 3.1 Optical rotation profiles for the palladium catalysed racemisation of *(S)*-(-)-*α*-phenylethylamine at 50˚C (●) and 100 ˚C (○) and the conversion at 50˚C (▲) and 100 ˚C (Δ) [86].

Palladium-based racemisation catalysts have since been used in the DKR of *α*-methylbenzylamine in toluene at 70˚C under hydrogen. Parvulescu *et al* [87] noticed that the amine could be better preserved during racemisation when an alkali earth metal support was used instead of charcoal. Using 5 wt% of $Pd/BaSO_4$, the selectivity was significantly improved up to 91% in 5 hours with the remainder being composed of ethylbenzene (ETB), however, the *ee* was 25%. 2% *ee* was achieved with a 56% conversion when the reaction was allowed to proceed for 24 hours although the selectivity was reduced to 81%.

The mechanism for the racemisation reaction involves dehydrogenating the amine to an imine with a subsequent hydrogenation to form the antipode (Scheme 3.1). When charcoal is used the imine is condensed with the amine to form a dimeric product with a high selectivity. However, it seems that the alkali earth metal supports act to minimise the formation of the condensation products.

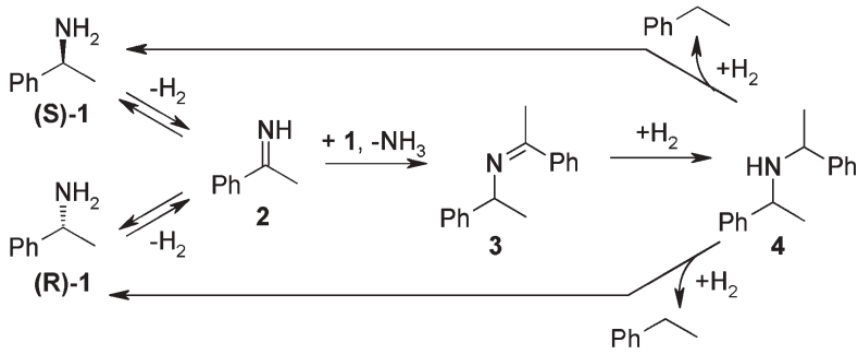

Scheme 3.1 Mechanism for the racemisation of 1-phenylethylamine showing the formation of the dimeric impurities [87]

Park *et al* [19] used a Pd-nanocatalyst entrapped in aluminium oxide (Pd/AlO(OH)) to effectively racemise chiral amines in a DKR process giving enantiomeric excesses and yields of up to 99%. (*S*)-1-phenylethylamine (*ee* > 99%) was racemised to 2% *ee* within 24 hours using 1 mol% of the Pd-nanocatalyst in toluene at 70˚C. However, 18% of the resultant reaction mixture consisted of impurities resulting from hydrolysis and condensation side reactions. Additionally, some amines required 12 mol % of catalyst for effective racemisation. The success of their DKR, with regards to yield and *ee,* was due to the rate of the enzymatic resolution being faster than that of racemisation thus the formation of the side products was minimised. Problems may therefore arise if this catalyst were to be used in a system whose resolution rate was slower than the racemisation rate.

Bäckvall *et al* [88] have developed an efficient ruthenium-based hydrogen-transfer catalyst for the racemisation of primary and secondary amines. This can be used in mild conditions and allows for high functional group tolerance, improving on the Pd catalysts performance. Previous studies by the group [15] have shown that low valent Ru-complexes are able to catalyse the transfer hydrogenation of amines to imines. (*S*)-1-phenylethlamine was racemised using 5 mo% of the Ru-complex **1** for 48 hours at 100˚C (Scheme 3.2). Complete racemisation was successful; however, a large proportion of the reaction mixture consisted of impurities **4a** and **5a**. To improve the process, several approaches were employed; dilution of the reaction mixture, addition of ammonia and addition of a hydrogen donor to increase the concentration of **1a**.

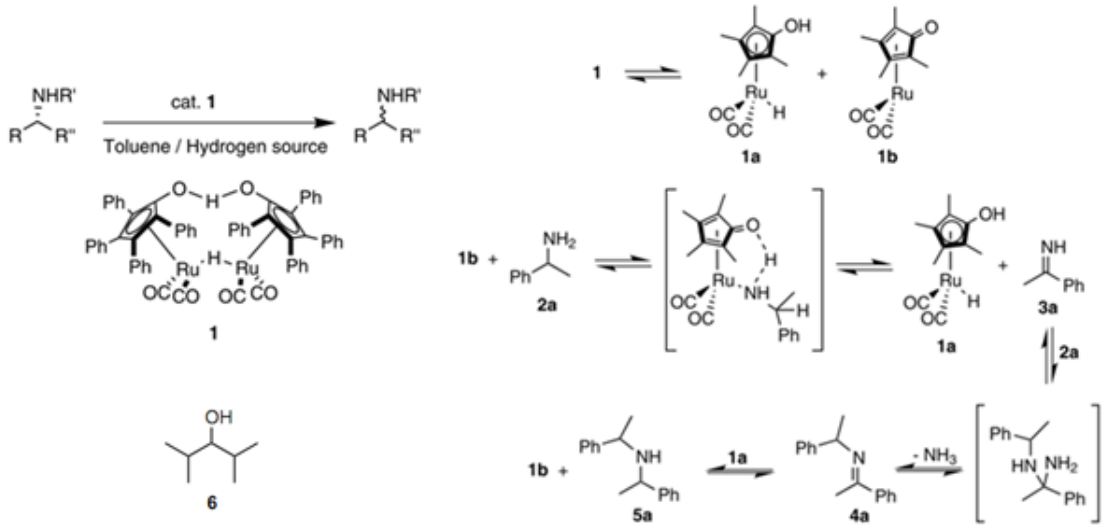

Scheme 3.2 Ru-catalyst (**1**), used by Backvall et al [88] in the racemisation of primary and secondary chiral amines. Right hand side - proposed mechanism for the the formation of the imine **4a** and amine **5a** impurities during racemisation. **6** – hydrogen donor 2,4-dimethyl-3-pentanol

A significant improvement was seen in the selectivity of the process from 5% to 91 % when the concentration was reduced; however, the *ee* increased from 0% to 6%. When ammonia was added to the system, the production of side products was effectively inhibited and an *ee* of 2% was obtained. Despite this, the use of ammonia resorts back to the harsh conditions seen with traditional base-catalysed racemisations, and as a consequence, the functional group tolerance of the Ru catalyst is reduced. To eliminate this problem 2,4-dimethyl-3-pentanol (**6**) was used as a hydrogen donor giving identical results; production of the impurities was inhibited with an ee of 2% being achieved .

Table 3.1 Racemization of (S)-1-phenylethylamine using an Ru-complex under a range of different conditions and with additives ammonia and 2,4-dimethyl-3-pentanol [88]

Entry	*t* (h)	Additive	Conc. **2a**[b]	% **2a**[c] (% ee[d])	% **4**[c]	% **5**[c]
1	48	–	1	5 (0)	12	29
2	48	–	0.5	21 (3)	8	15
3	48	–	0.25	84 (6)	5	11
4	48	–	0.125	91 (3)	3	6
5	48	1 equiv. NH_3	0.25	98 (2)	<1	<1
6	48	0.5 equiv. **6**	0.25	98 (2)	<1	<1
7	48	1 equiv. **6**	0.25	98 (2)	<1	<1

[a] Reaction conditions: (*S*)-**2a** (0.25 mmol), **1** (5 mol%) in toluene at 100°C.
[b] Concentration in M.
[c] Yield measured by GC on a CP-Chirasil-Dex CB column using pentadecane as internal standard based on the corresponding acetates after 24 h.
[d] Enantiomeric excess measured by GC on a CP-Chirasil-Dex CB column based on the corresponding acetates.

The catalyst was successful at racemising a number of different primary and secondary chiral amines. The later were found to racemise at a much faster rate requiring less than an hour to achieve 100% *ee*. The rate of racemisation was seen to be enhanced by the presence of electron-donating substituents with the opposite also being observed. Despite being shown to be effective at racemising a wide range of different chiral amines under mild conditions, use of the Ru-catalyst requires high loadings (5 %) and high temperatures (100˚C+) in order for racemisation to proceed at a sufficient rate.

The most robust racemisation catalyst to date has been developed by Blacker *et al* [17] which has been used in the DKR of chiral amines under mild conditions and with low catalyst loadings. Pentamethylcyclopentadienyl iridium(III) iodide dimer ($[Cp^*IrI_2]_2$) (Scheme 3.3a) acts as a pre-catalyst that reacts with primary, secondary or tertiary amines to form the SCRAM™ catalyst which is subsequently used for racemisation. Preliminary investigations showed that (*R*)- and (*S*)-6,7-dimethoxy-1-methyl-1,2,3,4-tetrahydroisoquinoline could be slowly racemised using a precursor to the CATHy catalysts pentamethylcyclopentadienyl-rhodium and iridium (III) chloride dimers ($[Cp^*IrCl_2]_2$) by forming an imine which can be reduced to either enantiomer. When $[Cp^*IrI_2]_2$ was used, the rate of racemisation was increased 120 fold as the effective charge on the metal was modified by the addition of a different halide ligand, which in turn acts to alter the activity of the catalyst.

The racemisation of a number of different primary, secondary and tertiary amines was performed using SCRAM^{TM} (catalyst loadings 0.1-1.0 mol%) in a range of solvents under mild conditions. Primary amines were shown to form large amounts of dimeric impurities (~70%) due to a combination of rapid dehydrogenation, and high reactivity of the resultant imine with the substrate. By contrast, secondary amines were shown to be efficient racemised within 22 min to 24 hrs, with a tertiary amine being racemised in less than 21 hrs.

The success of SCRAM^{TM} in racemising secondary amines led to it being used in the DKR of the API Sertraline [16]. Each chiral centre of the waste diastereomer was epimerised (conformational change of a single chiral centre) sequentially using SCRAM^{TM} for the amino-chiral centre and potassium *tert*-butoxide for the methine. SCRAM^{TM} showed high activity with low loadings (0.1 mol%) in a range of different solvents, although toluene was found to be the most effective. Scheme 3.3b illustrates the possible mechanism for sertraline epimerisation and imine formation using SCRAM^{TM}.

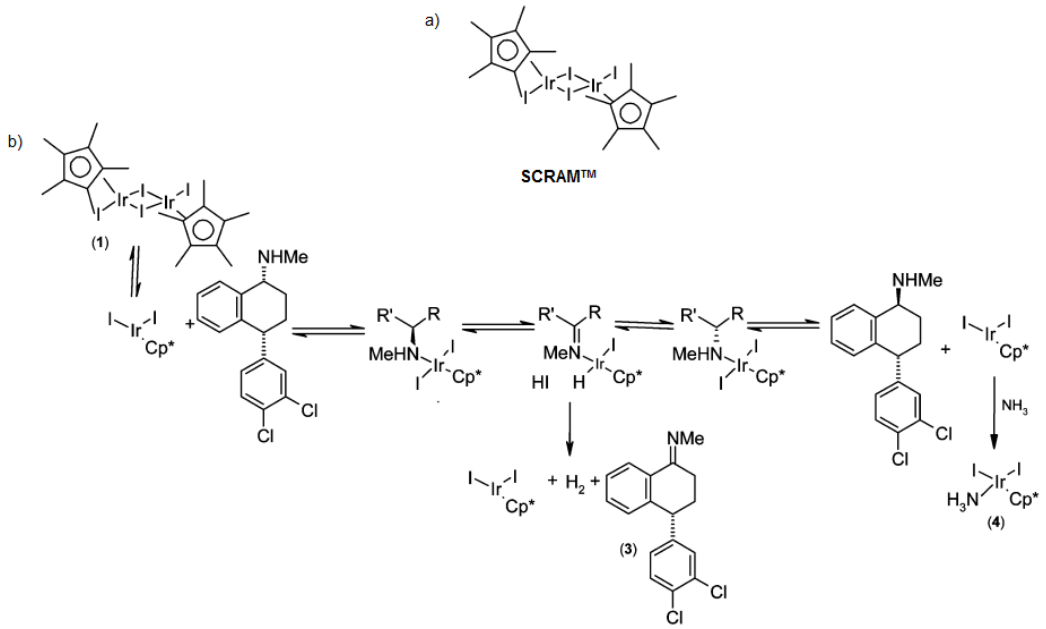

Scheme 3.3 a) SCRAM^{TM} racemisation catalyst (Pentamethylcyclopentadienyl iridium dichloride dimer or $[Cp^*IrCl_2]_2$), b) Possible mechanism for sertraline epimerisation and sertraline imine formation [16].

3.3 Alcohol Organometallic Racemisation Catalysts

Unlike amines, racemisation of chiral alcohols is comparatively well established with many examples of organometallic complexes being demonstrated as effective in DKR and asymmetric transfer hydrogenations. Ruthenium sports the greatest number of complex variations [19, 88-115] whilst palladium [14] , rhodium [116], and aluminium [117] based catalysts have also all been used successfully often being highly active and requiring relatively mild conditions.

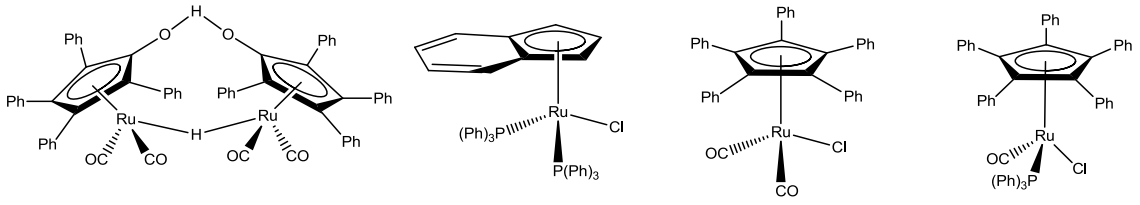

Figure 3.2 Examples of ruthenium-based organometallic complexes used for racemisation in DKR.

Perhaps the most well-known complex, Shvo's catalyst $[(\eta^4\text{-}Ph_4C_4CO)(CO)_2Ru]_2$ (**1**) [91] has been has been demonstrated to be a highly effective in hydrogen transfer reactions being capable of giving complete conversions of many different substrates within 10 min. Bäckvall *et al* [95] were the first to utilise Shvo's catalyst for racemisation in a DKR process for the resolution of a racemic alcohol (Figure 3.3). (*R*)-α-methylbenzyl alcohol was shown to be successfully racemised after 45 h using 2 mol% of complex (**1**) and 1 equivalent of acetophenone in *t*BuOH at 70°C. Combining in-situ solution phase racemisation using **1** with the transesterification enzyme *Candida antarctica* Lipase B, it was possible to selectively react the racemic mixture with a number of different acyl donors leading to the undesired enantiomer being converted in solution and > 99.5% *ee* being obtained. However, since the process required one equivalent of acetophenone, which remained present in the reaction mixture with most of the acyl donors trialled, relatively poor yields of the single enantiomer were obtained.

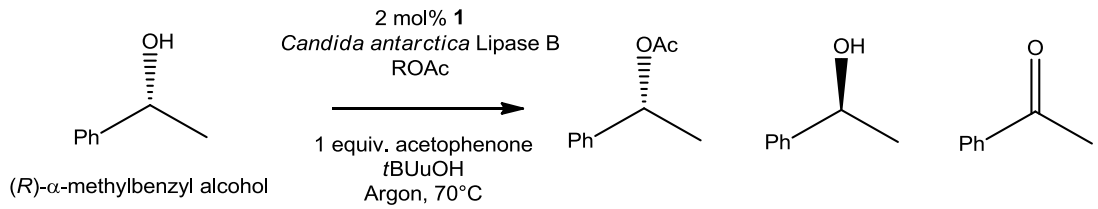

Figure 3.3 DKR of (R)-α-methylbenzyl alcohol using Shvo's catalyst (**1**), *Candida antarctica* Lipase B, an acyl donor, and 1 equivalent of acetophenone [95]

Following on from this, the same research group found that a specifically designed acyl donor, 4-chlorophenyl acetate, resulted in efficient DKR of a wide range of chiral alcohols using Shvo's catalyst (**1**), the enzyme *Candida antarctica* Lipase B for selective acylation, and 1 equivalent of benzophenone [118]. Using the racemate 1-phenylethanol, it was possible to obtain > 99% *ee* of the desired acylated enantiomer using 2 mol% 1 in a number of different solvents in as little as 20 h at 70°C. For the 13 chiral alcohols investigated, DKR in toluene resulted in consistently high enantiomeric purities (> 99% *ee* in the majority of cases) and considerable yields (up to 88%) demonstrating the effectiveness of catalyst **1** for in-*situ* solution phase racemisation. Furthermore, the DKR system developed by Bäckvall *et al* [95] was effectively applied [119] to the resolution of bifunctional alcohols such as hydroxyl acid esters [96, 120], diols, hydroxy aldehydes [120], β-halo alcohols [121], β-hydroxy nitriles [122], β-azido alcohols[123] and hydroxyalkanephosphonates [124].

Catalyst **2**, (η^5-indenyl)RuCl(PPh_3)$_2$, was shown to be highly active for the chiral alcohol racemisation [89]. Complete conversion (*S*)-1-phenylethanol to its corresponding racemate was achieved in < 20 at room temperature using 1 mol% **2** in dichloromethane (Figure 3.4). Unlike Shvo's complex, racemisation did not require 1 equivalent of ketone; however, the presence of KOH or *t*BuOK in solution was necessary for activation of the catalysts. In the same study, the versatility of catalyst **2** was further demonstrated where, under the reactions conditions, it was successfully applied in the racemisation of a number of different chiral alcohols with complete conversion always being observed.

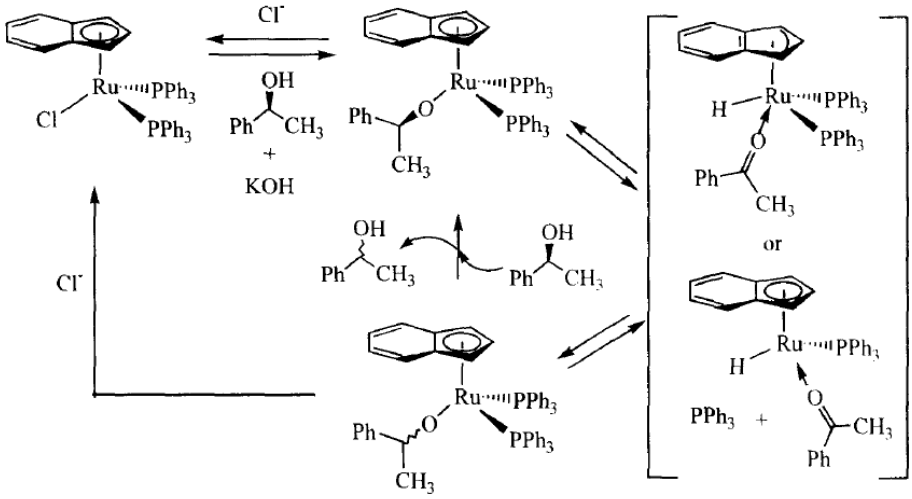

Figure 3.4 Proposed pathway for racemisation of (*S*)-1-phenylethan-1-ol with catalyst **2** [89].

In another study, Park et al [107] showed that catalyst **2** could be activated using a combination of molecular oxygen and triethylamine hence negating the requirement of low solubility KOH as shown in the previous study. Enzymatic resolution of 1-phenylenthanol was performed using *Pseudomonas cepacia* lipase to selectively acylate the desired enantiomer using **2** (2 mol%), oxygen (2 mol%), which was injected after degassing the system and refilling with argon, and 3 equivalents of triethylamine. The reactions were performed at temperatures =< 40°C for 5 h in a number of different solvents resulting in up to 99% ee of the desired acylated product being obtained. Furthermore, the process was also applied successfully to a number of different benzylic alcohols similarly giving enantiomeric purities of 99% with yields of up to 98%.

Complex **3** and an analogue were also demonstrated as being highly active alcohol racemisation catalysts [103]. Complete conversation of (*S*)-1-phenylethanol could be achieved within 10 min at room temperature using only 0.5 mol% 3 which was activated using *t*BuOK. In a subsequent study [125] DKR of a range of different chiral alcohols was successfully performed using catalyst **3** and isopropenyl acetate as an acyl donor (Figure 3.5) frequently giving > 99% *ee*, and when optimised within 3 h of reaction time. Additionally, unlike previous examples, DKR of **3** could also be applied to aliphatic alcohols broadening the application of these ruthenium-based complexes.

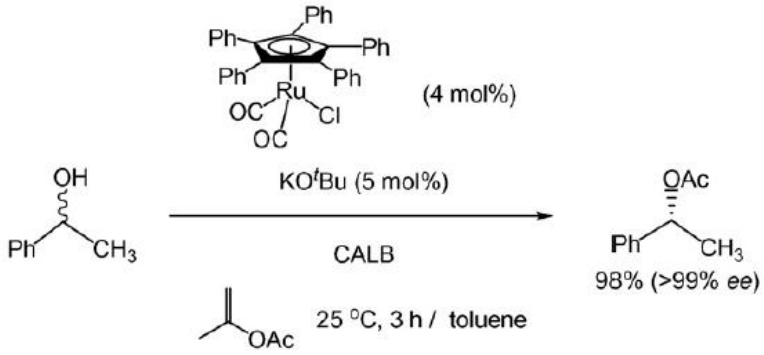

Figure 3.5 DKR of 1-pheylethanol in toluene using catalyst **3** and *Candida antarctica* Lipase B

Catalyst **4** is one of the few ruthenium based-complexes which remains active under aerobic conditions. Synthesising this complex by replacing a CO ligand in catalyst **3** with PPh_3, Park et al [126] were able to racemise many different benzylic alcohols and diols using 4 mol% **4** activated by Ag_2O at room temperature in toluene with reaction times ranging between 1 and 5 h for complete conversion to the racemate. Similar to previous investigations, **4** was paired with *Candida antarctica* Lipase B and the acyl donor isopropenyl acetate in a DKR process which was applied to a number of both benzylic and aliphatic chiral alcohols giving > 99% ee of the acylated single enantiomer in all cases in as little as 6 h operational time.

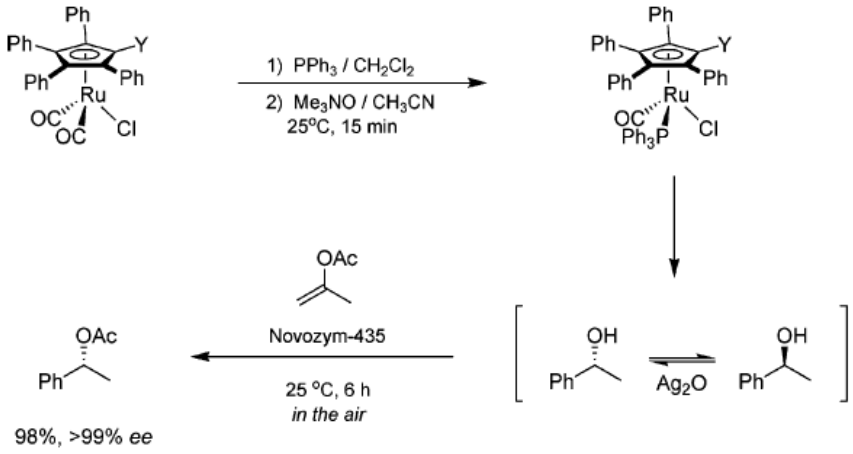

Figure 3.6 Synthesis of catalyst **4** from **3** and its use as an air stable racemisation catalyst in the DKR of 1-phenylethanol[126].

3.4 Crystallisation of Conglomerates with *In-situ* Racemisation

3.4.1 Crystallisation-Induced Asymmetric Transformation

Despite its attractiveness as a method of resolving racemates, preferential crystallisation of conglomerates is inherently limited to a maximum theoretical yield of 50% of the desired enantiomer. Coupling preferential crystallisation with in-situ solution phase racemisation in a crystallisation-induced asymmetric transformation (CIAT, also referred to as second order asymmetric transformation or SOAT) overcomes this issue increasing the potential maximum obtainable theoretical yield to 100%. Since addition of the catalyst to the solution results in the enantiomers existing in dynamic equilibrium, the ternary phase diagram for given racemate-solvent, used for development of a preferential crystallisation, is modified so that the areas within which the pure enantiomers exist are inaccessible. Figure 3.7 [82] illustrates the CIAT process in terms of the ternary phase equilibria for a racemate-solvent system. When a system of racemising enantiomers is seeded, solute is enantio-selectively removed from solution which (for fast racemisation) subsequently leads to conversion of the excess antipode to re-equilibrate the solution phase. Consequently, as the seed crystals grow, the total composition of the desired enantiomer in the system increases resulting in horizontal evolution of the synthetic mixture as depicted by the red arrow. Simultaneously, the solution phase composition follows a vertical trajectory (depicted by the blue arrow) since the dissolved racemate is maintained by the action of the catalyst. Figure 3.7d shows the progression of both the solution and solid phase compositions during polythermal CIAT. As the system is cooled to generate a crystallisation driving force, the system composition gradually moves towards enantiopure edge of the phase diagram whilst the solution continues towards the vertices being representative of the reduction in solute concentration as it is removed due to seeding.

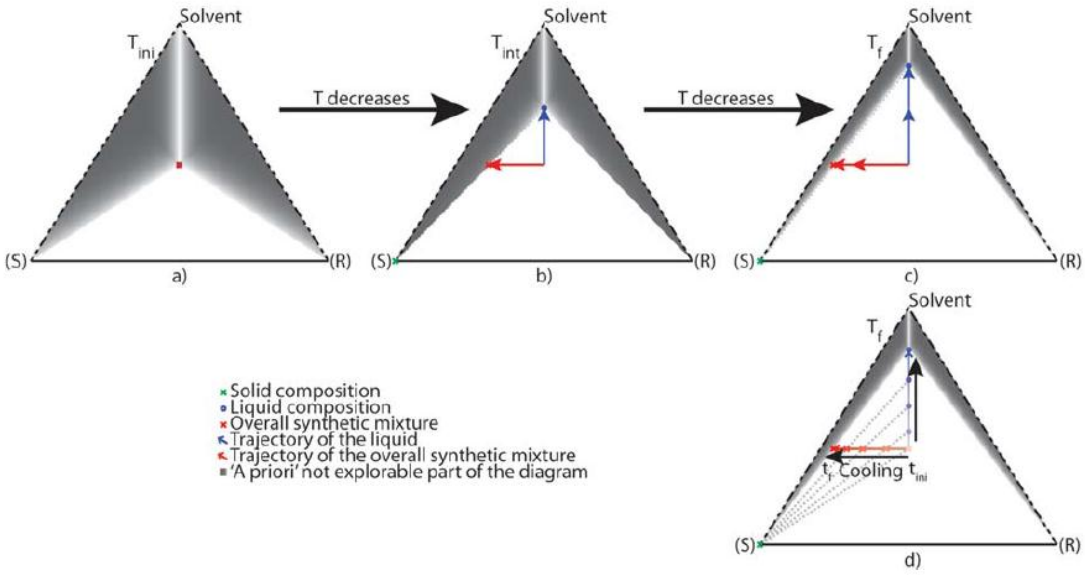

Figure 3.7 Description of crystallisation-induced asymmetric transformation in terms of the ternary phase equilibria for a racemate-solvent system [82].

Due to the strict requirements of the CIAT process, which necessitates a racemic conglomerate system that can undergo solution phase racemisation using a catalyst, the application of CIAT has been relatively limited [23, 29, 85, 127-131]. Chibata *et al* [127] successfully applied the CIAT process to the resolution and subsequent transformation of *N*-acetyl-leucine. A solution of the racemate in acetic acid was equilibrated using catalytic amounts of acetic anhydride and seeded with enantiopure crystals. Cooling at a controlled rate of 10°C h^{-1} from 100°C to 40°C to generate supersaturation led to an almost chirally pure product being obtained with a 140% yield being obtained of the desired enantiomer.

Carlson *et al* [29] isolated enantiopure crystals of the conglomerate narwedine from an initially racemic solution using CIAT. Racemic narwedine was dissolved in a binary solvent of 9:1 ethanol-triethylamine at 80°C in the presence of 1 mol% galanthamine which acted as the racemisation catalyst. This was then cooled to 40°C, resulting in precipitation, where it was held for 16 h. Unlike the previous example, no seed crystals were utilised during the process; however, analysis of the solid after filtration showed that it consisted entirely of a single enantiomer. This was postulated to be due to the mechanism of conversion using galanthamine which was thought to stereo-selectively interact with and

racemise one of the narwedine enantiomers in solution generating seed in-*situ* upon cooling. Subsequent growth of these crystals due to the solution being supersaturated further enhanced the catalytic process leading to ~150% yield of a single enantiomer in one operational stage. To highlight the efficiency of the process, 10 g of racemic starting material gave 9.02 g of enantiopure product in two crystallisation cycles.

CIAT was applied to the resolution and simultaneous antipode conversion of the cholecystokinin antagonist Asperlicin[132]. In preliminary experiments, separation of the racemate was achieved through crystallisation of its camphorsulphonic acid (CSA) salt from ethyl acetate leading to high yields and enantiomeric purities of the desired enantiomeric salt being obtained (80-84% yield and 99.5% *ee* respectively) albeit the counter enantiomer constituted as waste. During the investigation is was noticed that the undesired antipode could undergo thermal racemisation at 90°C in the presence of CSA, yet at this temperature crystallisation was not a suitable option. By increasing the acidity of the chiral proton through the addition of catalytic quantities of an aromatic aldehyde forming an intermediate imine, it was shown that the Asperlicin could be racemised at ambient temperatures opening up the possibility of using CIAT to recycle the waste enantiomer in-*situ.* Consequently, the optically pure enantiomer was obtained in as much as 91% yield, i.e. 182% considering the starting composition of the desired enantiomer.

The above brief review of several CIAT processes highlights its potential as a method of obtaining pure enantiomers from an initial racemate. However; in each of the cases discussed, and in those referenced, the common theme is that the applicability of each process has been limited to a single substrate since the mechanisms for racemisation are all system specific. Typically conversion of the undesired enantiomer occurs due to the presence of a low pKa chiral proton which can dissociate with relative ease allowing the chiral centre to be racemised by rehydrogenation of the resulting planar intermediate. Therefore the ability of a chosen species to undergo racemisation is determined by its functionality rather than the effectiveness of the selected catalytic method. In section 3.3 several organometallic complexes were discussed with each being capable of racemising a wide range of functionally related compounds in

DKR. If the capability of these catalysts could be utilised in preferential crystallisations, the applicability of CIAT could potentially be extended to a much broad range of racemates.

3.4.2 Viedma Ripening

Even when the conditions for resolution by crystallisation and racemisation coincide, CIAT is still limited due to the possibility of the counter enantiomer crystallising during the process. Viedma[31, 133, 134] has demonstrated an unusual method to lead to the emergence of single phase homochirality without counter enantiomer nucleation for inorganic chiral $NaClO_3$ crystals initially present as an equimolar mixture of two enantiomorphic crystalline phases in equilibrium with an achiral aqueous phase ($NaClO_3$ exists as achiral ions in solution which can crystallise as two enantiomeric crystals in the cubic chiral space group $P2_1/3$.

3 mm diameter glass balls were added to an initially, racemic (with regards to the solid phases), equilibrated slurry. Upon agitation, attrition between the balls resulted in the random emergence of only single crystalline enantiomeric phase. When the starting slurry had an initial crystalline enantiomeric excess of 5%, the crystals produced at the end of the process were always of a single chiral phase. Viedma was able to achieve compete homochirality within 10 hours with a symmetric starting composition, and 8 hours with an initial crystalline enantiomeric excess in a system that would otherwise maintain its starting composition indefinitely. It was also shown that an increase in the number of balls and stirring rate reduced the time taken to achieve a single chiral phase (Figure 3.8).

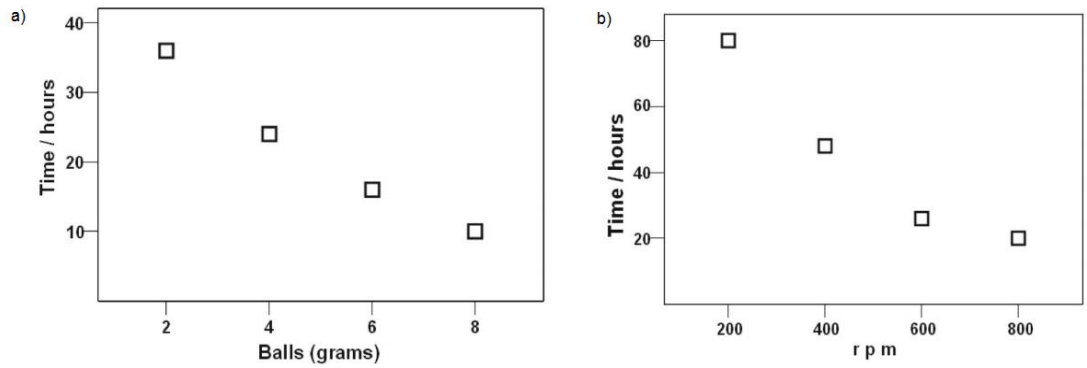

Figure 3.8 $NaClO_3$ achiral solutions with an initial equimolar mixture of enantiomeric crystals and glass balls showing a) the time taken to achieve complete symmetry breaking depedning on the number of balls (600 rpm) b) the time taken to achieve achieve complete symmetry breaking depedning on the stirring rate (4 g of balls)[31]

It is believed that abrasion and grinding provided by the glass balls results in the crystals breaking apart into smaller fragments including microcrystalline particles. As the solubility of the particles increases with a reduction in size (Gibbs-Thomson effect), these tend to dissolve back into solution subsequently "feeding" the larger crystals (Ostwald's ripening). Chirality is only a property of NaClO3 in the crystalline state as the unit cell is comprised of four molecules packing in a chiral space group. Molecular addition via mass transfer from the solution is therefore achiral so a dissolving particle can feed any crystal independent of its previous chirality. Growth of the larger crystal is favour by Ostwald's ripening so by chance, either chiral phase may result randomly due to the enhancement by attrition (when the slurry is initially racemic). For molecules that are chiral in both the liquid and solid phases, racemisation must be sufficiently fast to emulate this.

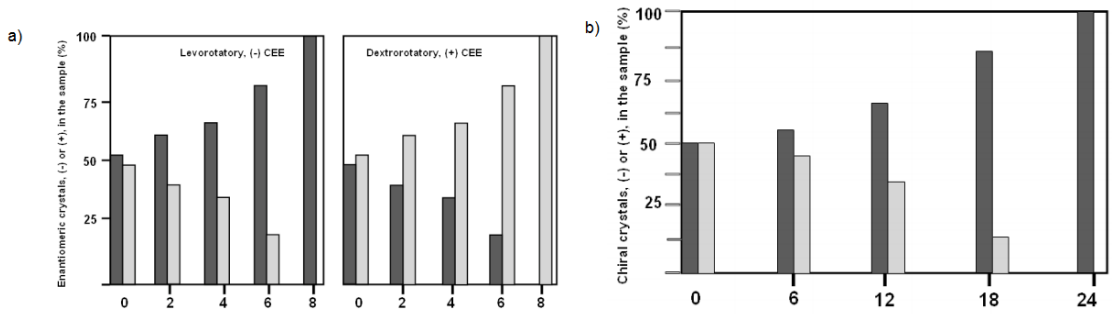

Figure 3.9 $NaClO_3$ achiral solutions with an initial 5% excess of enantiomeric crystals and glass balls showing the progression of symmetry breaking a) over 8 hours (8 g balls, 600 rpm) b) over 24 hours (4 g balls 600 rpm)[31]

Similar results were seen by Sainz-Diaz *et al*[28] using 1,1-binaphthyl enantiomers which spontaneously racemise in solution at room temperature over the course of several hours, or in the melt at 180˚C in a matter of seconds[135, 136]. A mixture of 1,1-binaphthyl was held at 180˚C to for 20 min to ensure complete racemisation. Crystallising from solution at 150˚C produces a racemic compound; however, crystallising at the same temperature whilst stirring eventually led to enhancement of chiral discrimination in the solid phase producing crystals with a large enantiomeric excess. Figure 3.10 shows the powder X-ray diffraction patterns for the two samples obtained with and without stirring, and for the enantiomeric and racemic forms of 1,1-binaphthyl. It is clear that stirring results in transformation from the racemic to enantiopure crystal forms. Analogous to grinding with balls, stirring induces the micro-fragmentation of crystals producing nuclei or clusters which dissolve due to their increased solubility feeding the growth of larger crystals.

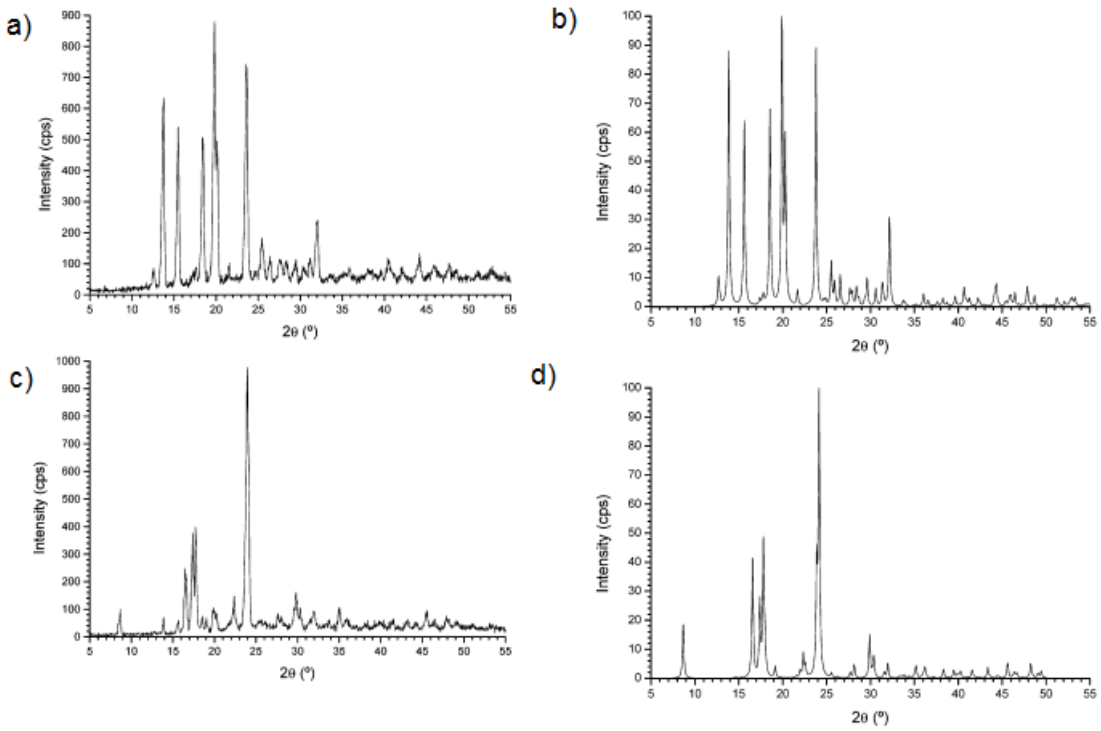

Figure 3.10 Powder X-ray diffraction patters of 1,1-binaphthyl a) crystallised from the melt whilst stirring b) crystallised from the melt without stirring c) pure enantiomer ($P4_12_12_1$) c) racemic compound ($C2/c$)[28].

Noorduin *et al*[24] were the first to apply Viedma's findings[31] to true molecular enantiomeric amino acid derivatives. The conglomerate forming imine of 2-methyl-benzaldehyde and phenylglycinamide underwent fast base-catalysed racemisation in methanol with the organic base 1,8-diazabucycloundec-7ene (DBU) . Equilibrated slurries, with an initial 2-10% solid phase enantiomeric excess of either crystalline enantiomer, were stirred at 1250 rpm under ambient condition with will 2.5 mm glass beads. Addition of DBU initiated racemisation (racemisation half-life = 2 min) leading to complete chiral discrimination (99.9% *ee*), at best, within approximately 6 days when the initial enantiomer excess was 10%. When glass beads were absent, the crystalline enantiomeric excess remained unchanged indefinitely. Perhaps even more interesting is that the handedness of the resulting crystalline phases from an initially racemic solution could be controlled by using a chiral additive to direct the evolution of a single solid phase. Using as little as 0.1 mol % of pure (*R*)-phenylglycine and (*S*)-phenylglycine resulted in the formation of only (*S*)-2-methyl-benzaldehyde and (*R*)-2-methyl-benzaldehyde respectively, with the time taken to achieve

complete chiral decimation being reduced with an increase in DBU concentration. This study proved that the concept of chiral “amnesia” observed in Viedma’s achiral $NaClO_3$ solutions applies to racemisable organic compounds that crystallise as conglomerates i.e. it is possible for a crystalline *S* enantiomer to dissolve (by attrition leading to increased surface area and hence solubility), racemise, and be deposited on the larger enantiopure *R* crystals.

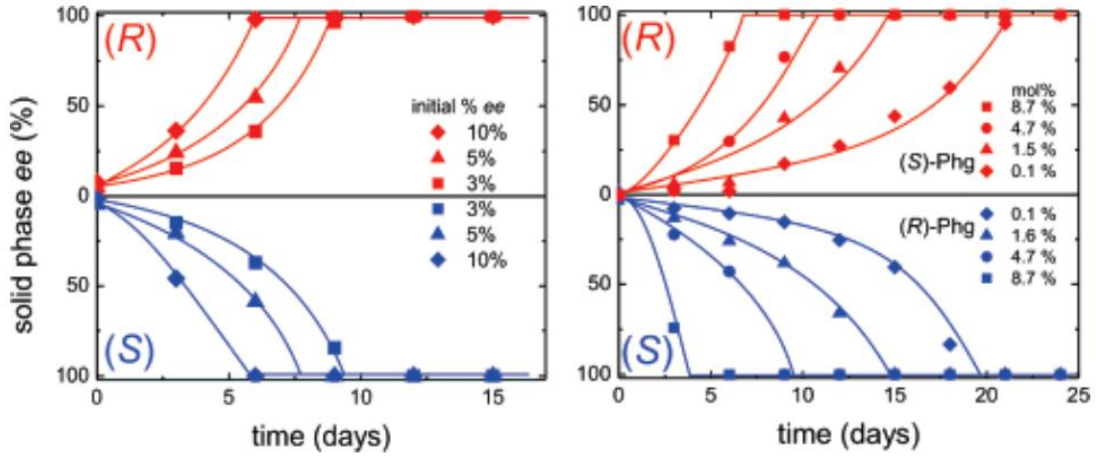

Figure 3.11 Attrition-enhanced evolution of solid-phase ee for 2-methyl-benzaldehyde-phenylglycinimine in MeCN a) starting with an initial crystalline enantiomeric excess as shown b) starting from a crystalline racemic mixture with chiral additive (*R*) and (*S*)-phenylglycine[24].

The method of Noorduin *et al* [24] was repeated by Viedma *et al* [134] using aspartic acid, one of only two amino acids that crystallise as a conglomerate under ambient conditions, in acetic acid with the catalyst racemisation salicylaldehyde. Near identical results were produced, with compete chiral discrimination of the solid phase occurring at 160˚C within 6 days with attrition enhancement and an initial enantiomeric excess (< 10%), and unlike Noorduin, this was also achieved without glass beads in around 8 days perhaps suggesting that agitation alone was sufficient to cause abrasion. Similarly Tsogoeve *et al*[30] confirmed that using glass balls was not necessary to induce chiral symmetry breaking in a reversible Mannich reaction; instead agitation is all that is required to produce secondary nuclei. Attrition enhanced deracemisation has since been applied to the production of enantiomeric compounds of industrial importance including the pharmaceuticals Naproxen[25] and Clopidogrel[137].

4 Conglomerate Selection

4.1 Introduction

The proposed CIAT process involves coupling preferential crystallisation with in-*situ* solution phase racemisation of the undesired counter enantiomer. A prerequisite of the former is that the chiral system exists as a stable conglomerate i.e. a mechanical mixture of discreet homochiral crystals, as opposed to a racemic compound whose racemic crystals contain a 1:1 mixture of both enantiomers within the unit cell, as conglomerates are able to be resolved by seeding since their enantiopure solid phases are more stable than the corresponding enantiomeric-co-crystals. Conversely, seeding a racemic solution of a racemic-compound-forming system with enantiopure crystals would lead to dissolution of the seeds as the eutectic point occurs at *ee*s ≠ 0%, hence solubility of the mixture increases with *ee* up to the eutectic. This leaves approximately 10% of chiral systems that may be suitable for CIAT; however, since the influences behind conglomerate formation are not fully understood, and the fact that the heterogeneous phase equilibria of chiral compounds are often overlooked, it is possible that in time this number will increase.

In addition to forming a conglomerate, it was also necessary that the selected chiral system was able to undergo efficient solution phase racemisation using available racemisation catalysts. Existing CIAT processes rely on chiral centres that can be easily racemised under the correct conditions, typically due to the presence of low pKa chiral protons, which limits its application. Using organometallic complexes, which have been successful racemisation catalysts in the DKR of chiral alcohols and amines, should overcome this problem potentially increasing the number of conglomerates that could be processed by CIAT.

4.2 Objectives

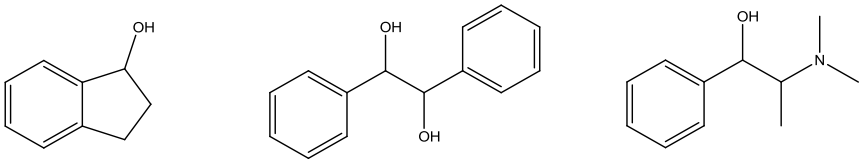

1 **2** **3**

Scheme 4.1 Conglomerate candidates investigated to identify model chiral systems for use in the CIAT process: 1-indanol (**1**), hydrobenzoin (**2**), *N*-methylephedrine (**3**).

In this chapter, three chiral systems were investigated for use as model CIAT compounds due to being reported as conglomerates in the literature and possessing chiral centres with the potential to undergo racemisation by organometallics; 1-indanol (**1**), hydrobenzoin (**2**) and *N*-methylephedrine (**3**) (Scheme 4.1). To explore their heterogeneous phase equilibria and confirm conglomerate formation from the solvents earmarked for CIAT (the choice of solvent being limited primarily by the catalysts – see section 4.3.1), binary phase diagrams were constructed for each of the potential candidates. The crystal structures of both their racemate and enantiopure forms were also investigated.

The melting point of the pure enantiomers and racemates, T_A^f and T_R^f respectively, were determined using DSC to give an indication of enantiomeric composition as melting a non-racemic mixture of enantiomers gives rise to two endotherms which correspond to the binary phase diagram solidus i.e. melting of the racemic portion of the mixture, and the liquidus, which results from melting the remaining pure enantiomer. Consequently, a truly racemic or an enantiopure sample should give rise to only a single endotherm over a narrow temperature range; however, it must be noted that, using DSC, for enantiomeric compositions close to 0% and 100% *ee* (100% *ee* and close to the eutectic composition for a racemic compounds), the endotherms of the solidus and liquidus tend to overlap as the temperature difference between them decreases, hence, this technique should be used in conjunction with more accurate methods, such as polarimetry or chiral HPLC.

In addition to giving an insight into enantiomeric composition, identifying T_R^f and T_A^f was used to give an indication of the type of crystalline racemate that is present. For chiral systems crystallising as a conglomerate, the difference between T_A^f and T_R^f is typically greater than 20°C, whereas the pure enantiomers of a corresponding racemic compound can melt at temperatures above, below or equal to that of T_R^f. This can be extended by considering the enthalpy of fusion of the pure enantiomer and the racemate, ΔH_A^f and ΔH_R^f respectively, since the difference between the two typically lies between 1.7 and 5.0 kJ mol^{-1} for a conglomerate [138] (section 2.6.2).

Binary phase diagrams were constructed by measuring the solidus and liquidus temperatures (melting points) of a range of mixtures of enantiomers prepared by solvent evaporation from toluene (see section 4.3.1 for a discussion on solvent selection). This allows for characterisation of the chiral solid phase equilibria since the eutectic point will always occur at 0% *ee* for conglomerates, whereas a racemic compound possess two eutectics at *ee*s ≠ 0%. Deviation from liquid phase ideality was qualitatively assessed by examining the coincidence of the measured liquidus temperatures with those predicted using the Schröder-Van Laar expression (Equation 2.43) and the measured T_A^f and ΔH_A^f values. This was extended by comparing the calculated entropy of mixing, ΔS_l^m, based on the measured calorimetric data (Equation 2.51) with that of in ideal conglomerate which can be shown to be equal to Rln2 or 5.77 J mol^{-1} K^{-1}.

Binary phase diagram construction may not always lead to a definitive conclusion on the chiral heterogeneous phase equilibria of a given system as the eutectic points of a racemic compound can occur at any non-racemic/enantiopure composition and in the case that this is close to racemic, it may appear that a conglomerate is present. To eliminate this problem, powder XRD and infra-red spectroscopy were used to identify the diffraction patterns of both the racemate and pure enantiomer. Since a conglomerate is a 1:1 mechanical mixture of the enantiopure phases, its racemic and enantiopure spectra should away be identical; however, racemic compounds are 1:1

mixtures of both enantiomers in the crystal lattice therefore their corresponding enantiopure spectra will differ from that of the racemate.

4.3 Conglomerate Selection

4.3.1 Selection Criteria

The choice of a suitable model chiral system for development of the CIAT process was dependent on satisfying a number of criteria:

- Stable conglomerate (~10% of all chiral systems) when crystallised under the prescribed operating conditions
- No possibility of solid solution or metastable racemic compound formation
- Crystalline at room temperature
- Ideally contain only a single stereogenic centre
- Able to undergo efficient racemisation using available organometallic complexes
- Exhibit a solubility in common solvents suitable for crystallisation and use with racemisation catalysts
- Available in both racemic and enantiopure forms
- Non-hygroscopic
- Chemically and thermally stable
- Available to purchase or synthesize at a relatively cheap price
- Safe to handle with the available personal protective equipment

Perhaps the most important prerequisite for development of the proposed process is that the chosen chiral system crystallises as a conglomerate with chiral discrimination in the solid phase allowing for resolution by seeding with the pure enantiomer. Since the CIAT process relies on seeding a racemising solution of enantiomers, it is essential the stability of homochiral crystals exceeds that of the corresponding racemic form (or solid solution) so that a single enantiomer can be selectively crystallised.

Examples of racemic compound resolution by entrainment have been demonstrated [139, 140], however, this process relies on seeding at eutectic compositions which, for this type of racemate, is at an *ee* ≠ 0. Consequently, coupling preferential crystallisation of racemic compounds with in-situ racemisation would not be possible since (in an ideal case) the solution phase *ee* would remain racemic throughout CIAT due to the action of the catalyst.

One-pot Crystallisation Induced Diastereomeric Transformations (CIDT) of racemic compounds are known [21, 22], however, these often rely on the presence of chiral centres than can be easily racemised. Additionally, the conditions used to form diastereomers, e.g. by reaction with a chiral acid, may not be suitable for the organometallic catalysts earmarked for use in the CIAT process. Performing diastereomeric crystallisation and racemisation in series a quasi-continuous process could eliminate these problems (this is currently under investigation within our research group), however, this project aims to perform crystallisation and racemisation simultaneously in a single-step batch process therefore the investigation was limited to conglomerate forming chiral systems.

In addition to being resolvable by entrainment, it was also essential that the chosen model compound could be efficiently racemised using available organometallic complexes. Typically these catalysts are capable of racemising chiral amines and alcohols by dehydration leading to the formation of intermediate imine/ketone species which are subsequently rehydrogenated to form the racemate. However, racemisation of primary amines and alcohols can lead to the irreversible formation of dimers, whereas few examples of tertiary structure racemisation exist in the literature. Hence, the search was limited to chiral secondary amines and alcohols which ideally had only a single stereogenic centre at the functional carbon. Racemisation of compounds with multiple centres leads to both antipode and diastereomer formation, and in the case that the latter exhibits a solubility lower than the corresponding enantiomers, their exclusive crystallisation may be inhibited since the diastereomer would be first to achieve saturation in solution. Additionally, the presence of the diastereomer in solution could influence the crystallisation characteristics of the enantiomers as it can be considered to be an impurity;

therefore, crystallisation kinetics or even formation of the conglomerate could be affected by its presence.

It is evident due to the criteria discussed so far that solvent selection is of paramount importance to the success of the CIAT process. The solvent must allow for crystallisation of the model system in conglomerate form, with the solute being readily soluble and easily deposited upon cooling. Additionally, racemisation in solution must also be possible whilst the solvent remains inert to the catalytic process. This requires that the catalyst is completely soluble under the conditions used to perform CIAT and remains undersaturated for the duration of the process. Generally, non-polar aprotic solvents are most suitable for use with organometallic racemisation catalysts as they appear to give the greatest racemisation cycle efficiencies. Toluene is the most widely used solvent due to its ability to dissolve many organic compounds, whilst also being suitable for use with racemisation catalysts. Hence, this was chosen to be the CIAT process solvent and is used throughout the subsequent chapters.

To perform CIAT it was necessary to obtain the chosen model system in both racemic and enantiopure forms for the solution being entrained and the seed crystals respectively, in addition to the preliminary analysis that was required. Since the racemate can be obtained by mixing equimolar quantities of each enantiomer, either the racemate and a single enantiomer, or both enantiopure forms were needed. Furthermore, the organometallic racemisation catalysts tend to require dry, oxygen free environments; therefore it was also necessary that the chosen chiral substrate was not hygroscopic in order to prevent inhibition of the catalysts activity during the process.

4.3.2 CIAT Candidates

Initial searches of the literature were focused on identifying a chiral amine that would be suitable for the CIAT process since these have been shown to be racemisable with iridium-based catalysts that are widely used within our research group [16, 17]. However, after a thorough review of the literature it was clear that there were few, if any, chiral amines that satisfied the criteria given in

section 4.3.1; primarily the requirement of conglomerate formation. The focus of the search for a model system was then turned to chiral secondary alcohols for which racemisation by organometallics is well established, despite the availability of conglomerates still being limited.

1-indanol (**1**, Scheme 4.1) was proposed as a possible candidate as it has been listed in the text by Jacques *et al* [9] as a conglomerate that can be resolved by preferential crystallisation. The molecule contains a single secondary alcohol stereogenic centre which can potentially be racemised by a number of different catalysts, particular ruthenium-based complexes [119], whilst its racemic and enantiopure forms can be readily synthesised or purchased from commercial sources.

Despite having two chiral centres, hydrobenzoin (**2**) was the second choice of model system. This has been shown to crystallise as a conglomerate allowing for its resolution by direct crystallisation [9, 141-143]. Similar to **1**, hydrobenzoin contains two secondary alcohol chiral centres which should undergo efficient racemisation with several available catalysts and is readily available in both racemic and enantiopure forms.

Although there was initial doubt about its ability to undergo racemisation due to its tertiary chiral amine, for which few racemisation examples exist in the literature, and its dual chiral functionality, having both a chiral amine and alcohol group, *N*-methylephedrine (**3**) was selected for investigation as it has been shown to form a stable conglomerate [138] and is readily available in both racemic and enantiopure forms.

4.4 Methodology and Analytical Techniques

4.4.1 Enantiomer Preparation

As a result of cost and commercial lead times, it was necessary to synthesise the pure enantiomers of **1** and **2** to confirm conglomerate formation and for subsequent use as model chiral systems for the CIAT process ((*R*,*S*)-**3** and (*S*,*R*)-**3** were obtained from Sigma Aldrich, purity taken as stated by the supplier, > 99%). Details of the synthetic literature procedures and materials

used can be found in the respective Enantiomer Synthesis sections for **1** and **2** (11.2.1 and 11.2.2 respectively). For each of the chiral systems investigated, the racemate was obtained by mixing equimolar quantities of the two enantiomers, heating them to form a racemic melt, and allowing this to recrystallise by natural cooing to room temperature. The resulting solid was ground to a fine powder using a pestle and mortar to ensure chiral homogeneity for subsequent analysis. Details of the analytical techniques used to characterise the materials, and for the analyses performed in the subsequent sections, can be found in 11.1.

4.4.2 Binary Phase Diagram

Binary phase diagrams for **1**, **2** and **3** were constructed by measuring the melting points of mixtures of antipodes with a range of enantiomeric excesses (0 – 100% *ee*) using the DSC instrument described in section 11.1.4. The samples were prepared by mixing known quantities of each enantiomer and dissolving them in toluene. The solvent was then left to evaporate yielding crystals of the racemate which were subsequently ground to a fine powder using a pestle and mortar to ensure chiral homogeneity. As discussed in section 4.3.1, toluene was earmarked as a possible process solvent as it has been used successfully with a number of different organometallic catalysts; hence it was used for preparation of the samples to identify if any changes crystal structure occurred as a result of its use. The enantiomeric mixtures were loaded into 40 µl aluminium pans and subjected to a heating programme which, for **1**, **2** and **3**, consisted of holding the pan temperature for 25 min at 25°C, 40°C and 80°C, and heating at a rate of 2°C min^{-1} to 90°C, 110°C and 170°C respectively. Using the resultant DSC curves, the solidus and liquidus melting temperatures were obtained and plotted against *ee* giving one half of the binary phase diagram which was sufficient for the analysis.

4.4.3 Crystal Structure

The powder X-ray diffraction pattern and infra-red spectra of the pure enantiomer and racemate was identified for **1**, **2** and **3** to determine if they

share the same crystal structure (and hence the same spectra) which would indicate conglomerate formation. For structures which could not be elucidated using the powder XRD and published databases of crystal structures, single crystal XRD was necessary. Details of the instruments used for both powder and single crystal X-ray diffraction can be found in section 11.1.6.

4.5 1-indanol Characterisation

4.5.1 Binary phase diagram

As a preliminary investigation into whether **1** belongs to the class of crystalline conglomerates, the melting points and enthalpies of fusion of (*R*)-/(*S*)-**1** and *rac*-**1** were determined using calorimetry. As previously discussed, a difference in racemate and pure enantiomer melting point ($\Delta T^f = \Delta T_A^f - \Delta T_R^f$) greater than 20°C is usually indicative of the presence of a conglomerate. Similarly, assuming ideal behaviour, a conglomerate will usually exhibit a difference in enthalpy of fusion between the pure enantiomer and racemate ($\Delta H^f = \Delta H_A^f - \Delta H_R^f$) in the range 1.7-5.0 kJ mol^{-1}. However, since racemic compound forming systems can also exhibit T_A^f>=20°C above that of the corresponding racemate, and varying differences in enthalpy of fusion, calorimetric assessment of the type of racemate present should only be used as *a* preliminary method of analysis.

Figure 4.1 shows the DSC thermogram for the synthesised material rac-**1**, (*R*)-**1** and (*S*)-**1** prepared from toluene. For each curve a single endotherm occurs with the peak corresponding to the melting temperature, whilst integration of the endotherms yields the enthalpies of fusion. These values for **1** are listed in Table 4.1. Considering the average melting point of the pure enantiomers (*R*)-**1** and (*S*)-**1**, 73.7°C, the difference in melting point, ΔT^f, between the average and *rac*-**1** is 18.8°C. Although close to the > 20°C difference typically observed between the pure enantiomers and the corresponding racemate for most conglomerate systems, this finding suggests, but is not conclusive, that **1** does not belong to the class of crystalline conglomerates. However, the difference between the average pure enantiomer and racemic enthalpies of fusion, ΔH_A^f-ΔH_R^f, of **1** is 1.8 kJ mol^{-1}, which is only just within the typical range normally

seen for conglomerates. These conflicting findings confirm that further analysis is required.

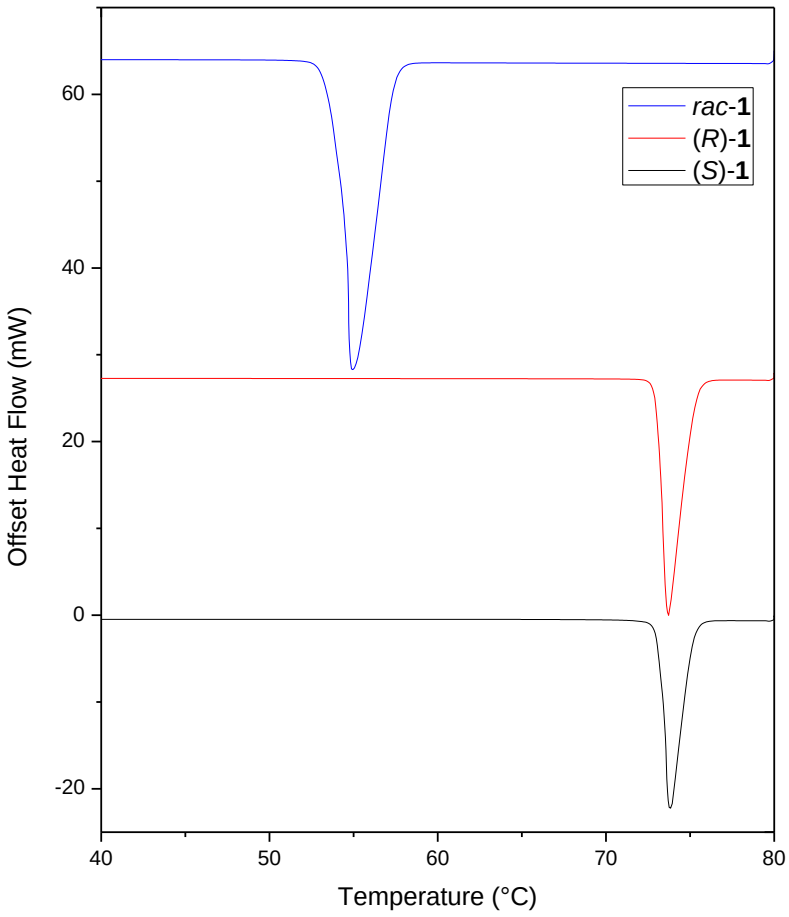

Figure 4.1 DSC thermogram of (*R*)- and (*S*)-**1** (synthesised according to the procedure by Li *et al* [144]), and racemic *rac*-**1** (obtained by melt-recrystallisation of an equimolar mixture of both enantiomers).

Table 4.1 Melting points, T^f, and fusion enthalpies, ΔH^f ,determined using DSC for (*R*)-, (*S*)- and racemic *rac*-**1**.

1-indanol (1)	**Melting point, T^f (°C)**		**Enthalpy of fusion, ΔH^f (kJ mol^{-1})**	
	T_R^f	T_A^f	ΔH_R^f	ΔH_A^f
(*R*)-	-	73.6	-	20.1
(*S*)-	-	73.7	-	18.7
***rac*-**	54.9	-	17.6	-

The use of calorimetry to investigate racemate behaviour can be extended by constructing the binary phase diagram for a given chiral system. Conglomerates can be identified by their single eutectic point which occurs at 0% *ee*, whilst racemic compounds exhibit two eutectics at compositions ≠ 0% *ee*.

Figure 4.2 shows the DSC thermogram for **1** with a range of enantiomeric excesses from 0-100% *ee*. It can be seen that for compositions other than 0 and 100% *ee*, two endotherms occur of varying sharpness with the peaks corresponding to the solids and liquidus temperatures; the areas of each being determined by the relative amounts of racemate and excess enantiomer present in the sample. At 0% *ee* a single endotherm occurs as the composition is racemic and each enantiomer melts simultaneously. As the *ee* is increased to 4%, a second smaller endotherm appears at a lower temperature, whilst the larger endotherm now occurs at a slightly lower temperature and has a smaller area than the 0% *ee* curve. This alone is a strong indicator of racemic compound formation since, as previously mentioned, the eutectic occurs at 0% *ee* for a conglomerate therefore for compositions greater than 0% *ee* the second endotherm should appear at a higher temperature (liquidus) whilst the racemic endotherm remains in the same position (solidus), albeit with a reduced area. Assuming at this stage that this does happen to be a racemic compound, the smaller endotherm occurs as a result of melting of the pure enantiomer in excess (4%) whereas melting of the 1:1 racemic solid gives rise to the larger endotherm, hence the relative areas.

As the composition is increased from 4 to 20% *ee,* the area of the endotherm at the lower temperature increases yet remains in the same position. However, the area of the racemic endotherm reduces in size whilst also occurring at progressively lower temperatures. Eventually the two peaks overlap becoming indistinguishable at 24 and 30% *ee* and only single endotherm is present which represents the liquidus point. As *ee* is increased beyond 30%, a second smaller endotherm reappears, this time at a higher temperature, with the area and peak position gradually increasing with *ee* until 100%, at which point the low temperature solidus endotherm disappears and only a single peak remains which corresponds to the pure enantiomer melting point. The behaviour

observed is highly characteristic of racemic compounds as the liquidus temperature initially decreases as the *ee* is increased beyond racemic until only a single endotherm occurs at 24 and 30% *ee*. This suggests that the eutectic point occurs between 24 and 30% *ee* which can never be the case for conglomerates (the exact *ee* could not be identified due to the overlapping of the endotherms).

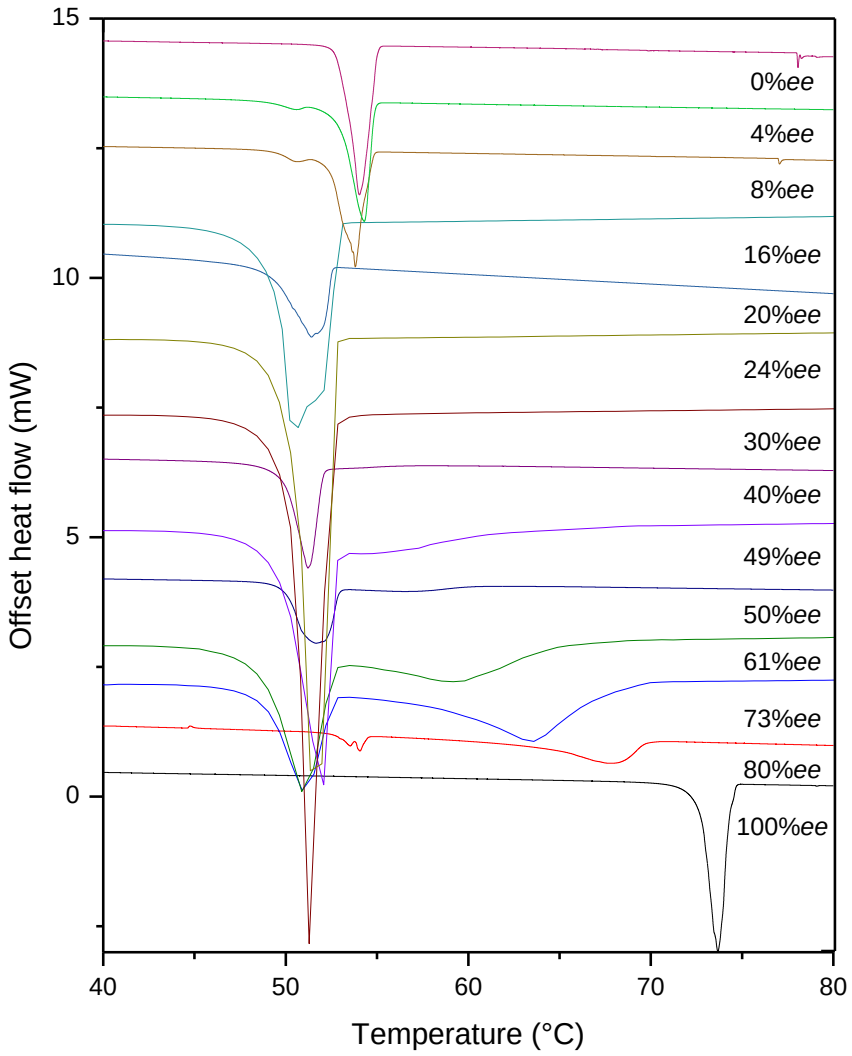

Figure 4.2 DSC curves for mixtures of **1** enantiomers showing the solidus and liquidus temperatures (note: heat flow DSC was used for some samples, e.g. 20% *ee*, whose thermograms were inverted for comparison hence the negative slopes).

Table 4.2 Melting points of mixtures of **1** enantiomers determined using DSC, and expected melting points calculated using the simplified Shröder van-Laar and Prigogine-Defay expressions (Equation 2.43 and Equation 2.44)

Enantiomeric Excess, *ee* (%) (*S*)-1	Measured melting point (°C)		Calculated liquidus (°C)		Expected solidus[a]
	Liquidus	Solidus	Schröder-Van Laar	Prigogine-Defay	
0	54.7	--		54.9	
4	54.3	50.6		54.8	
8	53.8	50.7		54.7	
16	52.1	50.4	--	54.2	
20	51.8	51.4		53.8	
24	51.7	--		53.3	
30	51.3	--		52.4	
40	54.3	51.2	55.4		52.2
49	55.7	51.6	58.4		
50	56.9	51.7	58.8		
61	59.8	50.9	62.2	--	
73	63.6	50.9	65.9		
80	66.1	51.5	68.1		
100	73.6	--	73.7		

[a]Based on observed intersection of the calculated liquidus curves

The peak temperatures for the endotherms of each curve in Figure 4.2 were identified and are listed in Table 4.2. Additionally, the corresponding racemic compound ideal liquidus temperatures are also given which were calculated for enantiomeric compositions between 0 and 30% *ee* using the Prigogine-Defay expression (Equation 2.44) and experimentally determined, ΔT_R^f and ΔH_R^f; and the Schröder-Van Laar expression (Equation 2.43) with ΔT_A^f and ΔH_A^f beyond the eutectic i.e 40 to 100% *ee*, as is the convention for racemic compound forming systems (note: only a liquidus temperature occurs at 0% *ee* as the enantiomers are present in equal quantities; for the samples with 24 and 30%

ee only a single endotherm could be identified as these correspond to the eutectic region therefore they were taken as liquidus temperatures). The last column in Table 4.2, the expected solidus, was determined by identifying the intersection between the two calculated liquidus curves.

Using the data presented in Table 4.2, half of the binary phase diagram for **1** was constructed using (*S*)-**1** as the excess enantiomer (Figure 4.3). With this graphical representation of the endotherm temperatures it is evident that **1** belongs to the racemic compound class of racemates as it possess the characteristic curved liquidus at compositions < 30%, and the lowest liquids temperature i.e. the eutectic occurs at an enantiomeric composition greater than 0% *ee*. Furthermore, the experimental and calculated data are in close agreement. Although the exact *ee* could not be elucidated due to overlapping endotherms, the eutectic occurs at an *ee* between 24 and 30% based on the experimental data, and approximately 31% *ee* based on the intersection of the two calculated liquidus curves.

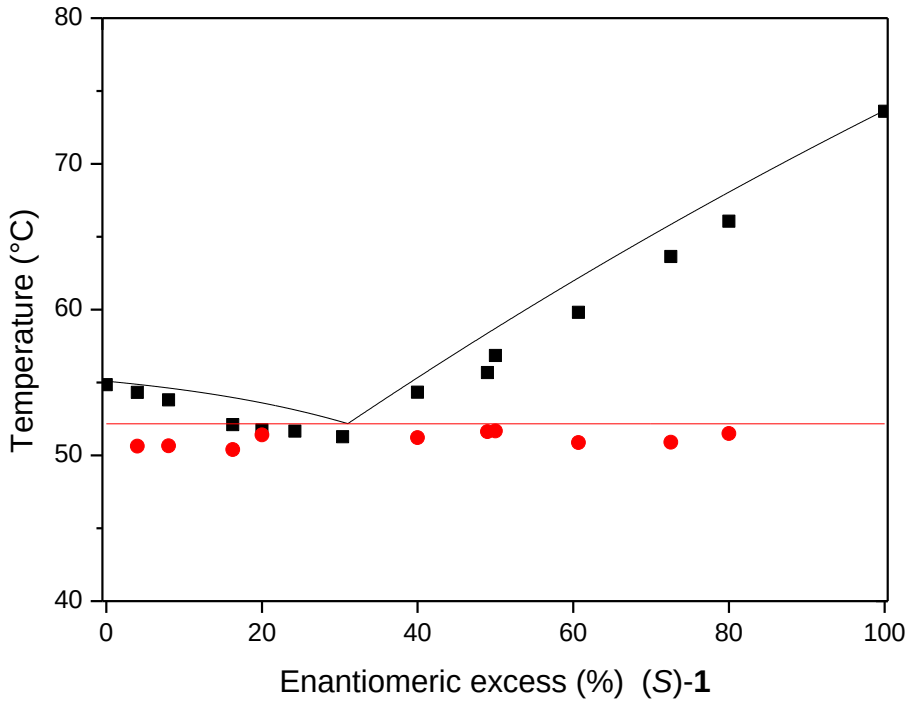

Figure 4.3 Half binary phase diagram for 1-indanol (**1**) with (*S*)-**1** in excess (■ measured liquids, ● measured solidus, ▬ calculated liquids, ▬ expected solidus).

4.5.2 Crystal Structure

Despite the data presented so far strongly suggesting that **1** forms a racemic compound, its racemate and enantiopure crystal structures were investigated. Figure 4.4 shows the powder XRD patterns for (*R*)-**1** and *rac*-**1**. As expected, examination of the peak positions shows that the two diffraction patterns are different which is true of racemic compounds as they are 1:1 crystals comprised of each enantiomer within the lattice and therefore have a different crystal structure than the corresponding pure enantiomer. Conversely, since a conglomerate is a mechanical mixture of discreet homochiral crystals, its racemate shares the same crystal structure as its pure enantiomer and therefore its diffraction patterns would be identical.

1 was further confirmed to exists as a racemic compound by identifying the infra-red spectra of (*R*)- and *rac*-**1**. As with powder XRD, the solid state structure influences the infra-red spectrum, however, this is due to the crystallographic positions of the characteristic absorption groups; hence the racemate of a racemic compound does not share the same spectrum as its pure enantiomer.

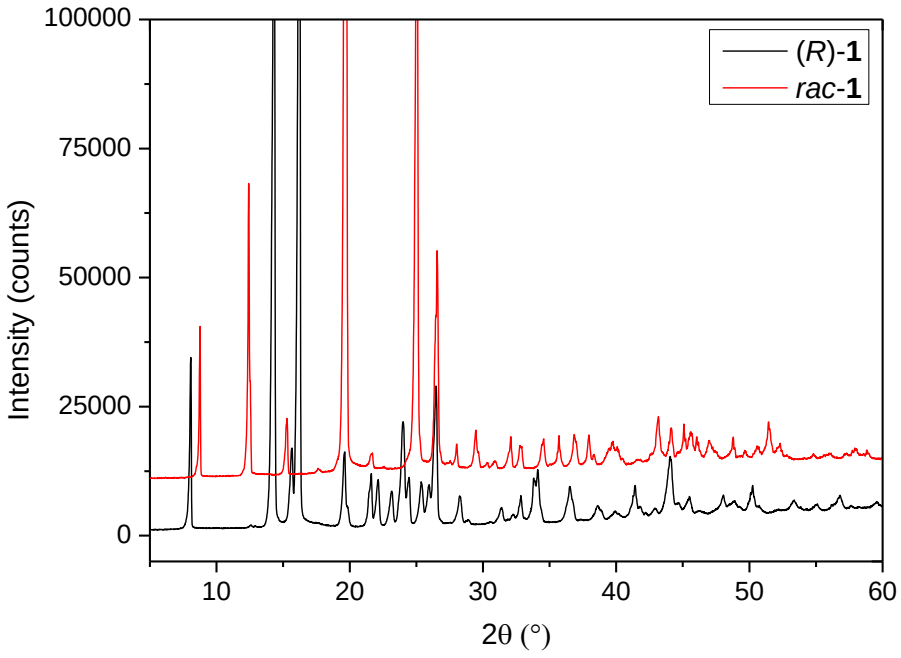

Figure 4.4 (*R*)- and *rac*-**1** powder X-ray diffraction spectra.

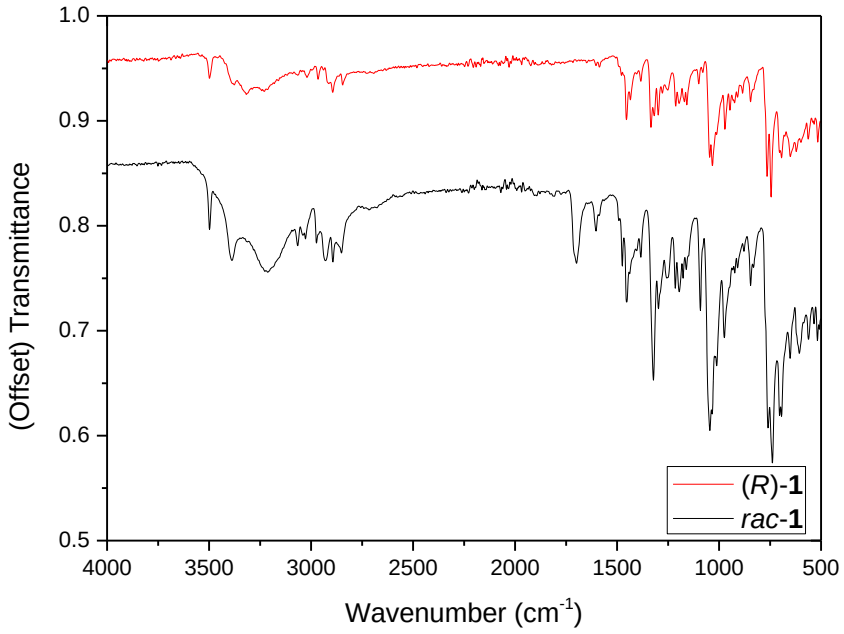

Figure 4.5 (*R*)- and *rac*-**1** FT-IR spectra.

Using the powder XRD data presented in Figure 4.4, attempts were made to deduce the crystal structure of the racemic compound *rac*-**1** by searching crystallographic databases with its diffraction pattern, yet no crystal structure was available for rac-1. This is typical for enantiomeric systems as chemists rarely investigate the type of racemate that a chiral system forms as two different synthetic routes are needed to produce enantiopure compounds and their racemic counterparts (where resolution is not used).

As a result of the lack of information available on the crystal structure of *rac*-**1**, single crystal XRD analysis was performed to elucidate is solid state arrangement. Figure 4.6 shows the crystal packing and unit cell structure for *rac*-**1**. The racemate crystallises in the body-centred tetragonal space group $I4_1/a$, indicating it has a 4-fold screw axis along the *a* direction, with 16 molecules of **1** in the unit cell (cell lengths $a = b \neq c$ where a = 20.19 Å, b = 20.19 Å, c = 7.60 Å, and cell angles $\alpha = \beta = \gamma = 90^{\circ}$). Since space group $I4_1/a$ is centrosymmetric both enantiomers are present in the crystal structure and it is therefore a racemic compound. Examination of the figure shows that there are two full and two half homochiral columns within the unit cell which possesses 16 molecules in total. The molecules are held together by two hydrogen bonds

between the hydroxyl hydrogen and corresponding oxygen on an identical molecule with van der Waals forces being responsible for the interactions between the homochiral columns.

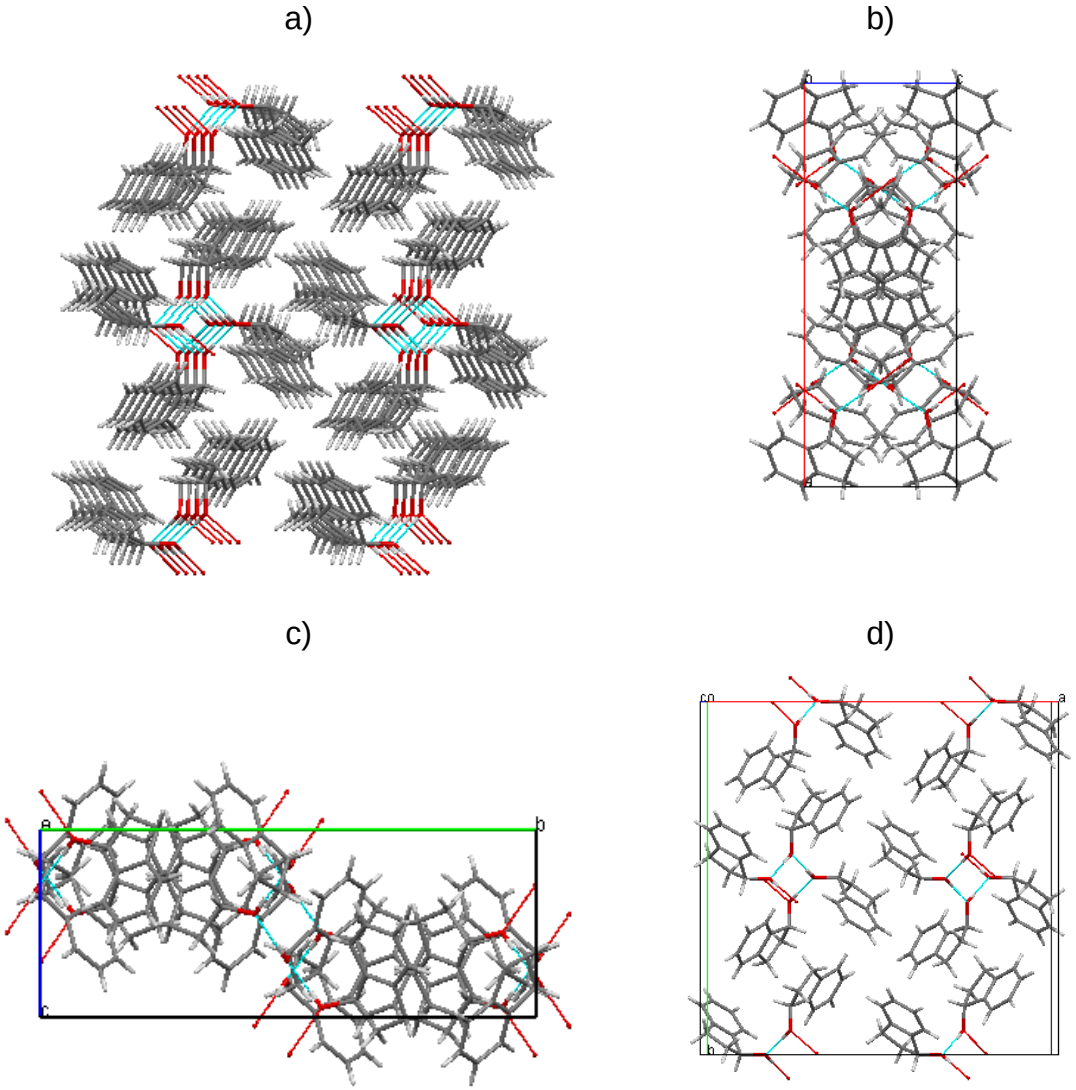

Figure 4.6 Crystal structure of *rac*-**1** showing a) molecular packing along the *c* axis and the contents of the unit cell along the b) *a* axis c) *b* axis and d) *c* axis. Blue and thin red lines indicate hydrogen bonging to other molecules and molecules not shown respectively. Hydrogen bonded distances and angles for O-H…O: O-H = 0.84 Å, H…O = 1.87 Å, O-…O = 2.71 Å, ∠OHO = 176.2°.

Figure 4.7 and Figure 4.8 show the crystal packing and unit cell structures for (*R*)- and (*S*)-**1**. The enantiomers crystallises in the chiral monoclinic space group $P2_1$ indicating a twofold screw axis with a half translation along the c axis, having two molecules in the unit cell (cell lengths $a \neq b \neq c$ where for (*R*)-**1**: a =

7.06 Å, *b* = 4.84 Å, *c* = 11.01 Å, and cell angles *α* = *γ*= 90˚, *β* = 95.75°, and (*S*)-**1**: *a* = 7.05 Å, *b* = 4.82 Å, *c* = 10.97 Å and *α* = *γ*= 90˚, *β* = 95.76°). Examination of the figures shows that the enantiomers exhibit the characteristic hydrogen bonding networks observed in the majority of chiral crystals. The crystal structure is comprised of homochiral 2_1 columns in which each molecule is held together by two hydrogen bonds between the hydroxyl hydrogen and corresponding oxygen on an identical molecule with van der Waals forces being responsible for the interactions between the homochiral columns.

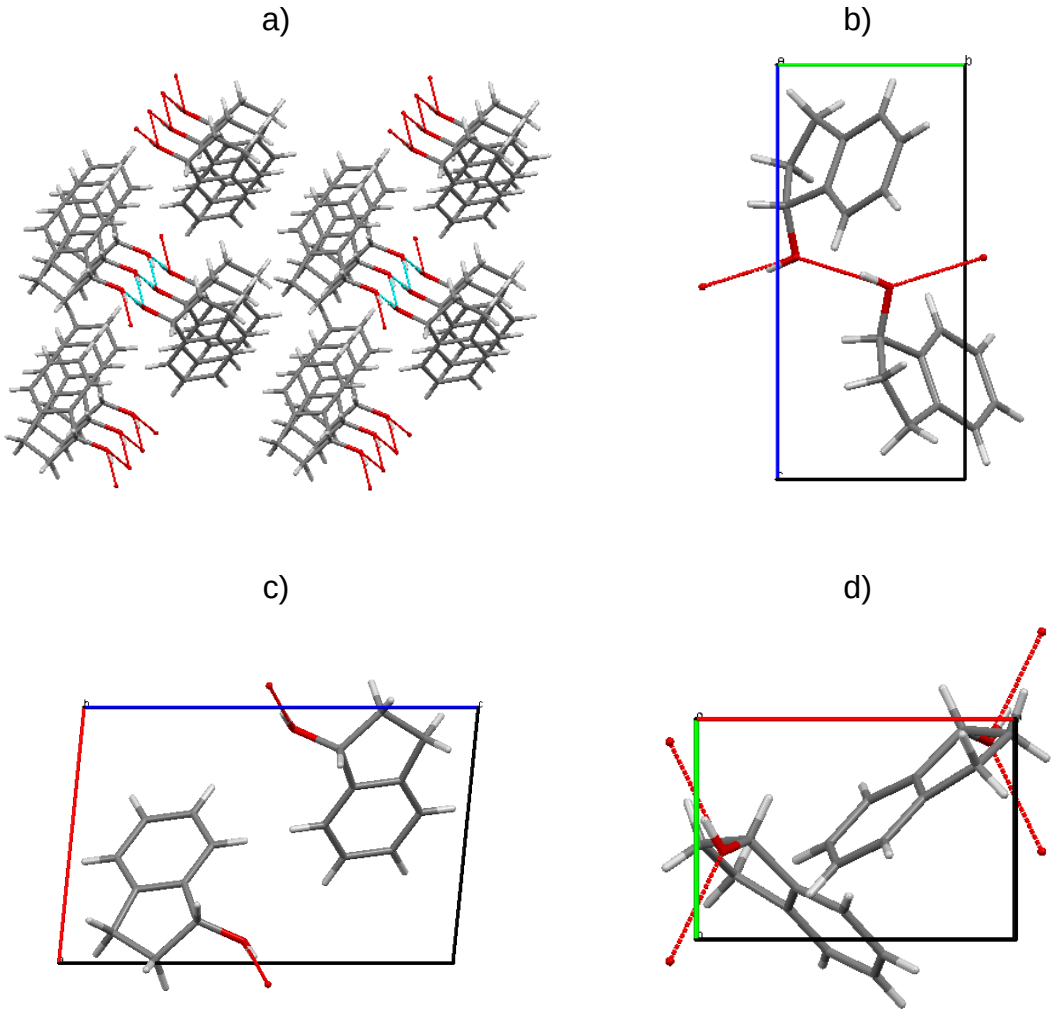

Figure 4.7 Crystal structure of (*R*)-**1** showing a) molecular packing along the *b* axis and the contents of the unit cell along the b) *a* axis c) *b* axis and d) *c* axis. Blue and thin red lines indicate hydrogen bonging to other molecules and molecules not shown respectively. Hydrogen bonded distances and angles for O-H…O: O-H = 0.84 Å, H…O = 1.94 Å, O-…O = 2.77 Å, ∠OHO = 170.4°.

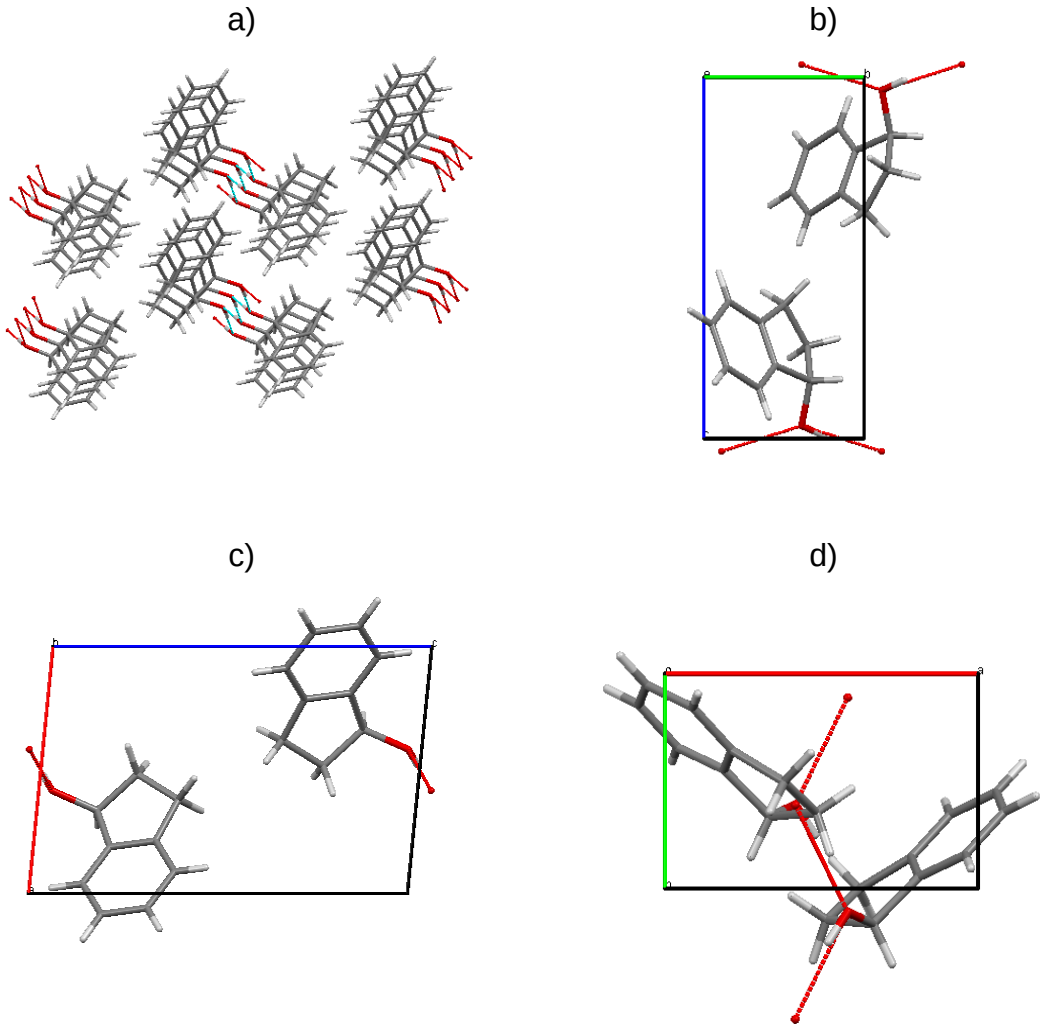

Figure 4.8 Crystal structure of (*S*)-**1** showing a) molecular packing along the *b* axis and the contents of the unit cell along the b) *a* axis c) *b* axis and d) *c* axis. Blue and thin red lines indicate hydrogen bonging to other molecules and molecules not shown respectively. Hydrogen bonded distances and angles for O-H…O: O-H = 0.84 Å, H…O = 1.93 Å, O-…O = 2.76 (9) Å, ∠OHO = 176.2°.

4.5.3 Metastable conglomerate formation

The findings from the powder and single crystal XRD analysis confirmed that **1** exists as a stable racemic compound crystallising in the centrosymmetric $I4_1/a$ space group. Further investigation revealed that **1** can also exist as a metastable conglomerate when crystallised under the correct conditions [52, 145].

Attempts were made to obtain **1** in its conglomerate form using a method from a 1960 study by Hückel *et al* [145]. 15 g of the racemic compound was melted and held at 120°C for 30 min in a round bottom flask. This was then cooled to 40°C using a water bath and combined with 180 ml of petroleum either 30-60°C to form a solution. After cooling to room temperature, the solution was seeded with a single crystal of (*R*)-**1** and refrigerated for several hours to induce crystallisation of the metastable conglomerate. The resulting solid was filtered, washed with cold solvent and dried under vacuum to give the product crystals.

Figure 4.9, the DSC curve for the product obtained using the methodology given above, shows that no transformation from racemic compound to conglomerate occurred as its melting point, T_R^f, has remained unchanged at 54.9°C, although some broadening of the peak has occurred for reasons which are unclear but could be linked to partial decomposition of the substrate at the high temperature isotherm. Using the Shröder van-Laar expression (Equation 2.43) and the experimentally determined values of T_A^f and ΔH_A^f (Table 4.1), the melting point of the conglomerate form of **1** was predicted to be 39.8°C which is in close agreement to the 37°C that has been reported but far below that of the sample analysed. The procedure was repeated several times holding the racemate for a longer duration in its molten state, and in refrigeration; however, each attempt at obtaining the conglomerate was unsuccessful.

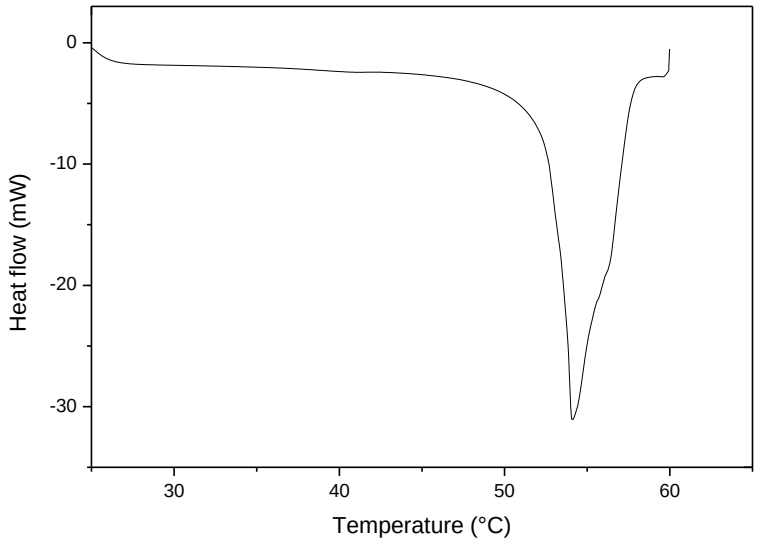

Figure 4.9 DSC spectra for *rac*-**1** after attempting to obtain the metastable conglomerate using the method by Hückel *et al* [145].

An alternative method [52] suggested simply holding the racemate in its molten state for several minutes at 80°C before cooling to room temperature, though this was performed by the authors at a ~ 5 mg scale using DSC. The method was attempted in a round bottom flask using 5 g of racemic material, holding it in the molten state for up to 1 h before cooling; yet, again the conglomerate could not be isolated. Observation of the round bottom flask at the end of the process revealed a web of thin fibrous crystals had occupied its entire volume suggesting that, upon melting the racemate, its vapours had condensed on the inner walls of the flask in racemic compound form and acted as sites for crystal growth thus preventing the formation of the less energetically favoured metastable conglomerate nuclei.

The procedure given above was repeated using DSC with a scaled down 8 mg sample. The racemate was held in its molten state for 30 min at 90°C before being cooled at a rate 1°C min^{-1} to 0°C. After maintaining this temperature for 2 hr, the sample was heated to 80°C at a rate of 2°C min^{-1}. Despite several attempts (including holding the sample at -5°C for up to 10 hr) the racemate remained in the molten state and would not crystallise therefore its melting point could not be obtained. However, when mixtures of **1** enantiomers with non-racemic compositions were analysed, crystallisation was observed after holding

the sample at the bottom temperature of the heating program, hence their melting points could be determined.

The DSC curves in Figure 4.10 show the melting points of a range of non-racemic enantiomeric compositions of **1** after being subjected to the heating programme described above. For each curve, two endotherms occur which correspond to the solidus melting temperature, which remains consistent for each composition, and the liquidus melting temperature, which can be seen to increase with enantiomeric excess; the areas of each peak being determined by the relative amounts of racemate and excess enantiomer present.

Comparison of the melting temperatures obtained from the DSC data (presented in Table 4.3) with those used to construct the racemic compound binary phase diagram of **1** (Table 4.2) shows that there has been a considerable reduction in solidus temperature from approximately 51°C to 37°C which happens to be in close agreement with the predicted conglomerate racemate melting point of 39.8°C. This trend is also seen in the liquidus temperatures of the 16 and 24% *ee* samples which are lower than those given in Table 4.2 with the same composition. The difference in melting points is indicative of a change in crystal structure as it implies that the magnitude of the intermolecular forces have been reduced due to molecular orientation changes within the crystal lattice.

In addition to the decrease seen in both solidus and liquid temperatures, the single endotherm for 24 and 30% *ee*, which corresponds to the eutectic region of the binary phase diagram for **1** (Figure 4.3), is no longer present in Figure 4.10; instead the difference between the solidus and liquidus temperatures increases with *ee,* thus the eutectic that existed at this composition is no longer present. These features of the calorimetry data presented are characteristic of conglomerate behaviour and show that the application of the above described DSC temperature programme has resulted in a crystal structure change from a 1:1 racemic compound to a mechanical conglomerate mixture, therefore **1** can be said to be stable and metastable with respect to the former and latter.

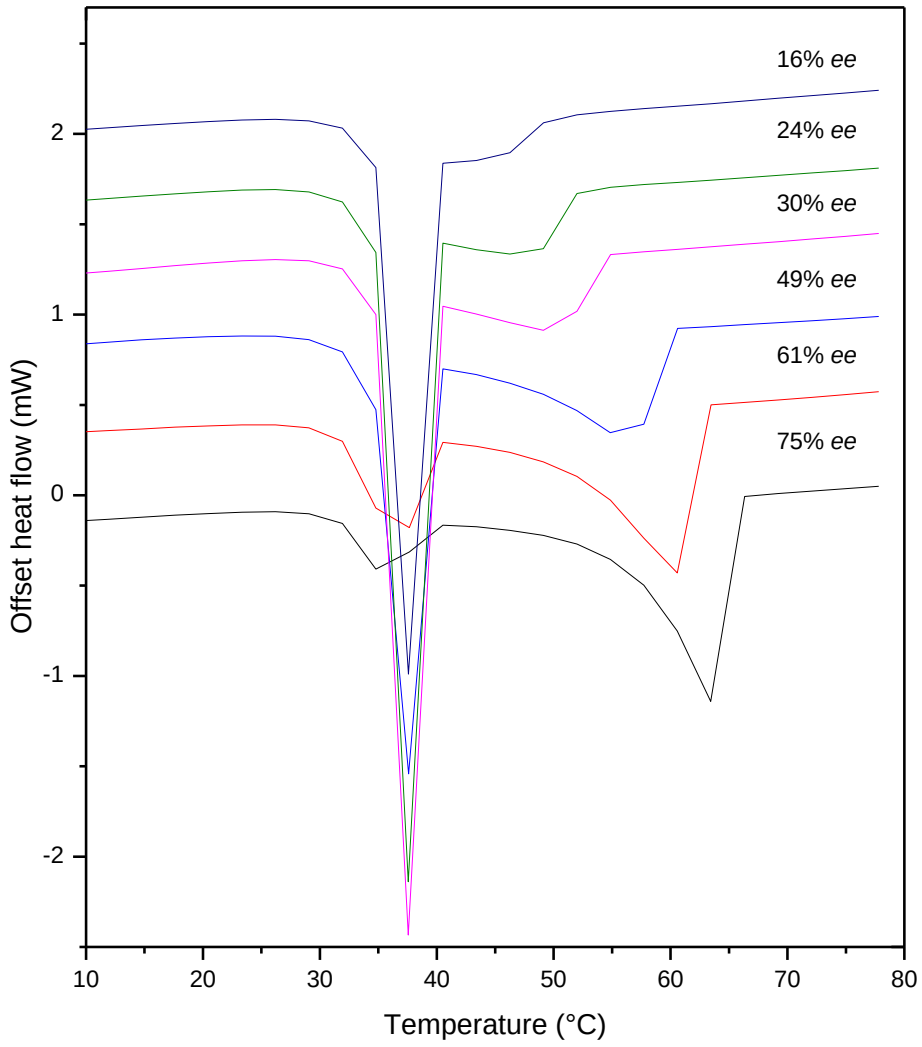

Figure 4.10 DSC curves showing the melting points of mixtures of **1** enantiomers after attempting to form its metastable conglomerate.

Table 4.3 Melting points of mixtures of **1** enantiomers for its metastable conglomerate determined using DSC, and expected melting points calculated using the simplified Shröder van-Laar expression (Equation 2.43) and the experimentally determined pure enantiomer melting point, T_A^f, and enthalpy of fusion, ΔH_A^f .

Enantiomeric Excess, *ee* (%) (S)-1	Measured melting point (°C)		Expected Solidus (°C)[a]	Calculated Liquidus (°C)
	Solidus	Liquidus		
0	--	--		39.8
16	37.6	43.4		46.6
24	37.6	47.7		49.7
30	37.6	49.1		51.9
49	37.6	55.0	39.8	58.8
61	37.7	60.6		62.2
75	35.8	63.4		66.5
100	--	--		73.6

[a]Based on the calculated liquidus curve

The metastable conglomerate solidus and liquidus temperatures obtained from the DSC data were combined with the racemic compound temperatures from section 4.4.2 and plotted to give half of the complete binary phase diagram for **1** with an excess of (*S*)-**1** (Figure 4.11). Furthermore, the corresponding ideal conglomerate liquids temperatures calculated using the Schröder-Van Laar expression (Equation 2.43) with the experimentally determined melting point and enthalpy of fusion of the pure enantiomer are also plotted.

Examination of the binary phase diagram shows that the DSC data from Table 4.3 is characteristic of a conglomerate as there is no evidence of a eutectic point at an *ee* > 0%, and the solidus temperatures are consistent whilst the liquidus temperatures increase with *ee*. For *ee*s greater than ~30% (the racemic compound eutectic) there is a close agreement between the liquidus temperatures of both the racemic compound and metastable conglomerate which is expected for systems for this type of system (stable racemic compound, metastable conglomerate) since there is of course no change in the

enthalpy of fusion of the pure enantiomer which is in excess. Below ~30% *ee* however, the metastable conglomerate liquid temperatures are always lower than the corresponding racemic compound samples with the same *ee* as the two types of racemic crystals have different structures, and hence different enthalpies of fusion.

As described in the methodology used to obtain the metastable conglomerate of **1**, the melting point of the racemate could not be obtained as it would not crystallise, even after prolonged cooling. Despite this, the data obtained for *ees* > 0% follow a clear trend which culminates close to the predicted racemate melting point of 39.8°C at 0% *ee* i.e. the eutectic occurs at this point hence it can be safely concluded that this is indeed the metastable conglomerate form of **1**. Ideally powder XRD would have been used to prove this, however, as mentioned previously, the metastable conglomerate of **1** could not be obtained on a scale larger that ~8 mg which is far below the sample requirements of the available powder XRD instrument. Despite this, the data presented can be taken as very strong evidence for **1** forming a metastable conglomerate.

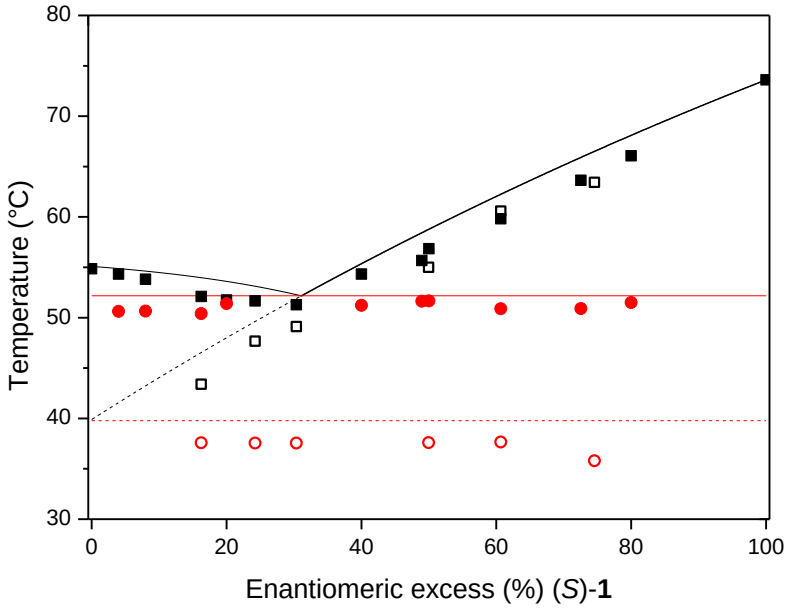

Figure 4.11 Binary phase diagram for 1-indanol (**1**) showing the solidus and liquidus temperatures for both its racemic compound, and metastable conglomerate forms (Racemic compound: ■ measured liquids, ● measured solidus, ▬ calculated liquids, ▬ expected solidus; metastable conglomerate: □ measured liquids, ○ measured solidus, --- calculated liquids, --- expected solidus).

4.5.4 Conclusion: 1-indanol (1) Characterisation

1-indanol (**1**) was investigated for use as a model chiral system for the CIAT process as it has been listed in the literature as a resolvable conglomerate [9] and has the potential to undergo racemisation at is 2° alcohol chiral centre using available organometallic complexes. The pure enantiomers were synthesised following the procedure given in section 11.2.1, and the racemate obtained by combining, and recrystallising equimolar quantities of the two pure stereoisomers. Calorimetry was then used to investigate the melting behaviour of the racemate and pure enantiomer, and to construct the binary phase diagram which gave a clear indication of racemic compound formation as the eutectic occurred at a non-racemic enantiomeric composition (~30% *ee*).

Differences in the powder XRD and infra-red spectra of the racemate and pure enantiomer confirmed the findings of the calorimetric data, indicating differences in crystal structures which would not occur for conglomerate forming systems as they are mechanical mixtures enantiopure crystals. Conversely, as racemic compounds are essentially 1:1 co-crystals of each enantiomer, their internal structure, and hence solid state spectra, will always differ from that of the pure enantiomer. Single crystal XRD showed that the racemate of **1** crystallises in the body-centred tetragonal space group $I4_1/a$ which is centrosymmetric and hence cannot consist of enantiopure crystals as their constituents are inherently asymmetric. The pure enantiomers on the other hand were shown to crystallise in the chiral monoclinic space group $P2_1$ which happens to be the most frequently occurring non-centrosymmetric space group.

Further investigation into the heterogeneous equilibria showed that a metastable conglomerate form of **1** could be obtained under the correct temperature program. Calorimetric analysis showed a significant reduction in solidus temperature from ~51°C to ~37°C with the latter being close to the conglomerate racemate melting temperature predicted using the Schröder van-Laar equation (39.8°C). Additionally, disappearance of the non-racemic eutectic was observed, with the liquidus temperature trend indicating the presence of a eutectic at 0% *ee*. The calorimetric data was combined with the racemic

compound binary phase diagram giving a complete description of the heterogeneous phase equilibria for **1** and showing that it exists as a stable racemic compound, and a metastable conglomerate.

Although examples of metastable conglomerate preferential crystallization have been demonstrated [139, 140], the data presented shows that **1** is an unsuitable candidate for use as a model CIAT system. In addition to being a stable racemic compound, which cannot be resolved by preferential crystallisation under normal circumstances, the conditions used to obtain the metastable conglomerate, consisting of heating well above the racemate melting point, and subsequent cooling and holding for a prolonged period at a low temperature far below the racemate melting point, are unsuitable for racemisation by organometallics. Not only would the racemisation rate be compromised at low temperatures, but it may be possible for the catalyst itself to become supersaturated and crystallise. Furthermore, the metastable conglomerate could only be obtained from the melt with all attempts of solution crystallisation being fruitless.

In conjunction with the ability of the racemate of **1** to form a conglomerate, it may be possible that the presence of the catalyst and enantiopure seed crystals could result in exclusive crystallisation of a single enantiomer due to lowering of the crystallisation energy barrier. This was to be investigated; however, **1** was shown to be extremely soluble in all organic solvents due to a combination of low molecular weight, potential for hydrogen bonding, and its aromaticity. Combinations of different solvents also proved to be inadequate for crystallisation, and when water was used in conjunction with organic solvents, oiling out of **1** was observed. Due to these factors, which would unnecessarily complicate the CIAT process, **1** was eliminated from the investigation and other chiral systems were considered.

4.6 Hydrobenzoin Characterisation

4.6.1 Binary Phase Diagram

Figure 4.12 shows the DSC thermogram for *rac*-***2***, (*R*,*R*)-**2** and (*S*,*S*)-**2**, with the corresponding melting points and enthalpies of fusion given in Table 4.4. Considering the average pure enantiomer melting point, 147.7°C, and that of the racemate, 120.7°C, the difference of 27.0°C between them is a strong indicator of conglomerate formation. Furthermore, the difference of 3.3 kJ mol^{-1} seen between the average pure enantiomer enthalpy of fusion, 32.3 kJ mol^{-1}, and that of the racemate, 29.0 kJ mol^{-1}, is typical of conglomerate forming systems which are usually in the range 1.7-5.0 kJ $mol^{-1.}$

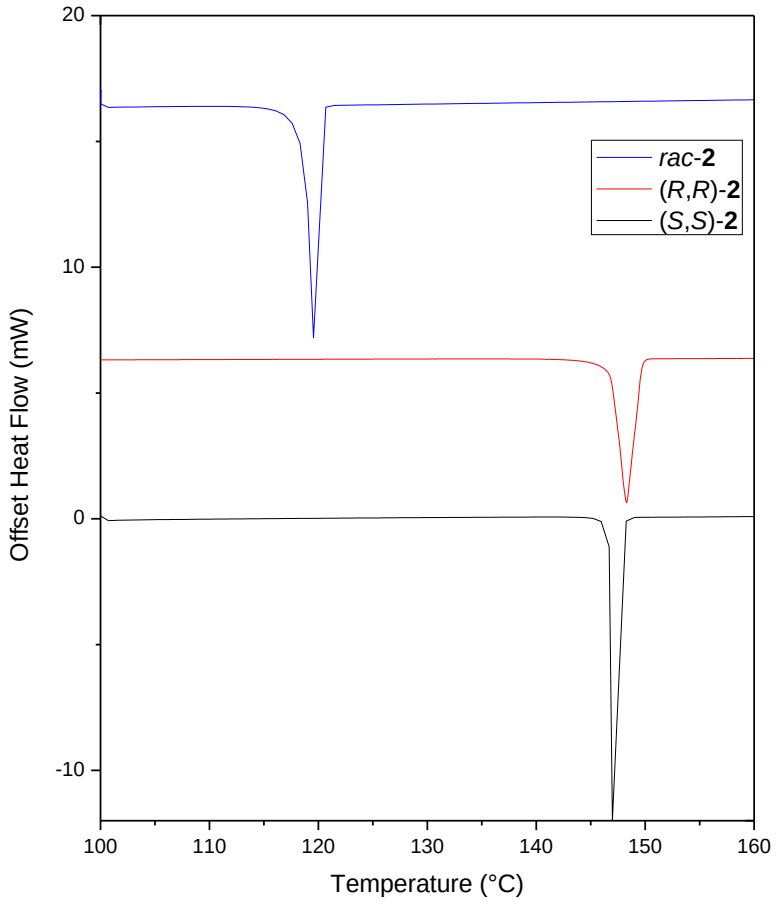

Figure 4.12 DSC thermograms of (*R*,*R*)- and (*S*,*S*)-**2** (synthesised according to the procedure by Ikariya *et al* [146]), and *rac*-**2** (obtained by melt-recrystallisation of an equimolar mixture of both enantiomers).

Table 4.4 Melting points, T^f, and fusion enthalpies, ΔH^f, determined using DSC for (*R*,*R*)-, (*S*,*S*)- and *rac*-**2**.

Hydrobenzoin (2)	Melting point, T^f (°C)		Enthalpy of fusion, ΔH^f (kJ mol^{-1})	
	T_R^f	T_A^f	ΔH_R^f	ΔH_A^f
(*R,R*)-	-	148.3	-	32.2
(*S,S*)-	-	147.0	-	32.3
***rac*-**	120.7	-	29.0	-

The DSC thermograms were obtained for a range of enantiomeric compositions of **2** prepared in toluene (Figure 4.13). It can be seen that for compositions other than 0 and 100% *ee*, two endotherms occur of varying sharpness with the peaks corresponding to the solidsus and liquidus temperatures; the areas of each being determined by the relative amounts of racemate and pure enantiomer present in the given sample. At 0% *ee* a single endotherm occurs since both enantiomers are present in equimolar quantities and melt simultaneously; only a single endotherm occurs at 100% *ee* as the sample is of course enantiopure.

As the *ee* is increased from 0 to 25% a second smaller and broader endotherm appears at a higher temperature (liquidus), whilst the racemic endotherm (solidus) remains at the same temperature despite now having a smaller area than the 0% *ee* peak (note: the solidus and liquidus peaks could not be discerned for *ee* < 25% due to endotherm overlapping). This behaviour alone is a strong indicator of conglomerate formation as its eutectic always occurs at 0% hence the liquidus for higher *ee*s will only be seen at higher temperatures, whereas racemic compounds will always show an initial reduction in liquidus temperature as the *ee* is increased beyond racemic. The appearance of the higher temperature endotherm is due to the presence of the excess enantiomer; as a result of the entropy of mixing associated with forming a binary liquid from a mechanical mixture of discreet homochiral solid phases (the liquid phase mixing lowering the overall free energy change of the melting process relative to that of an enantiopure solid melting to form an enantiopure liquid), the racemic portion of the sample will always be first to melt leaving the excess pure enantiomer which melts at a higher temperature.

As the *ee* is increased, the liquidus endotherm can be seen to become sharper, occurring at increasingly higher temperatures and with a greater area, whereas the solidus peak temperature remains consistent yet its area can be seen to reduce in size as its relative amount in the sample is decreased. Eventually, when the *ee* reaches 100%, the solidus endotherm disappears as there is no antipode present and hence the pure enantiomer that was originally in excess remains. As the liquidus temperature increases with *ee* to 100%, and is at its lowest when the *ee* = 0 %, the data in Figure 4.13 strongly indicates that **2** exists as a conglomerate.

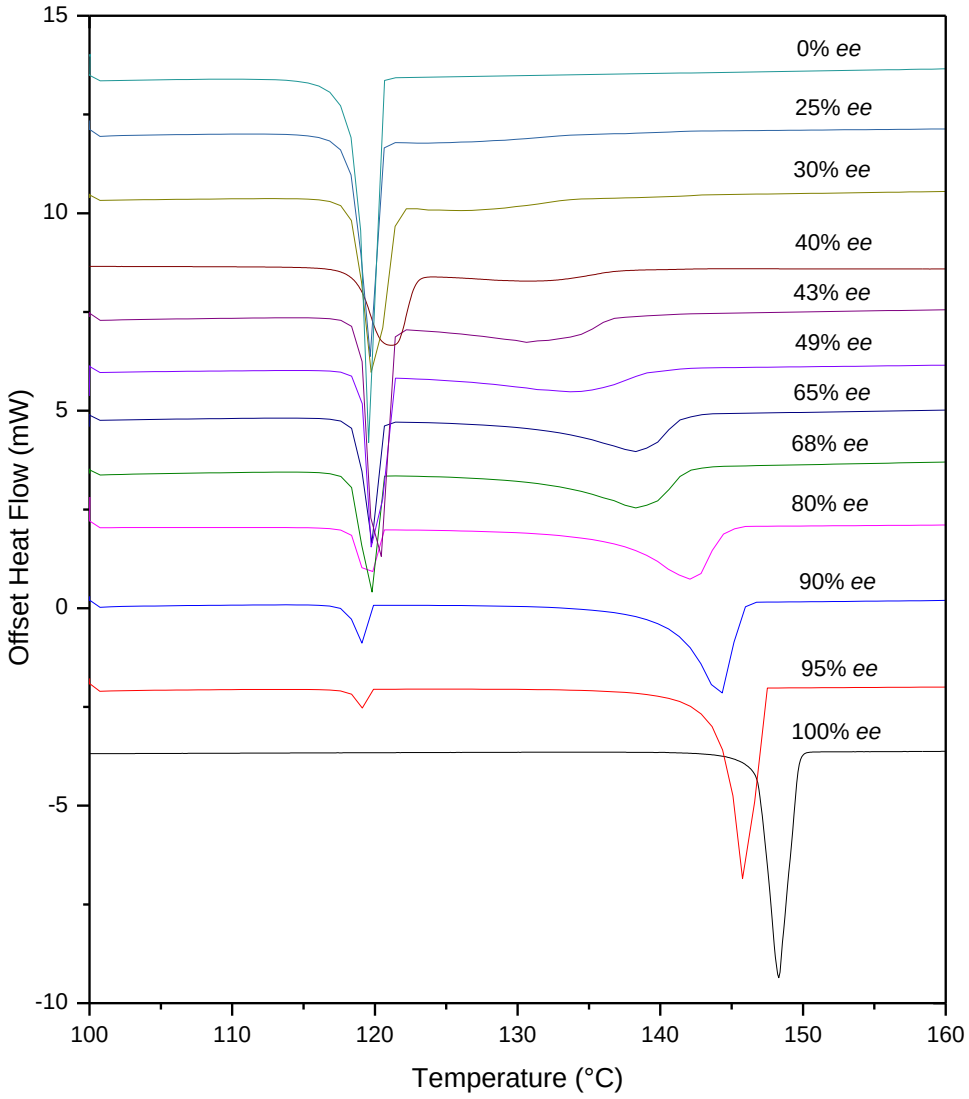

Figure 4.13 DSC curves for mixtures of **2** enantiomers showing the solidus and liquids temperatures.

Table 4.5 Melting points of mixtures of **2** enantiomers determined using DSC, and expected melting points calculated using the simplified Shröder van-Laar expression (Equation 2.43)

Enantiomeric Excess, *ee* (%) (*S*,*S*)-2	**Mole Fraction (*S*,*S*)-2**	**Measured Liquidus (°C)**	**Measured Solidus (°C)**	**Expected Solidus (°C)**	**Calculated Liquidus (°C)**
0	0.50	120.7	--	120.72	120.7
25	0.63	127.5	120.3		127.8
30	0.65	128.3	120.5		129.4
40	0.70	131.7	121.1		132.6
43	0.72	133.2	119.8		133.5
49	0.75	135.3	120.3		135.2
65	0.83	139.7	120.4		139.7
68	0.84	140.1	119.9		140.5
80	0.90	143.0	119.6		143.5
90	0.95	144.9	119.2		146.0
95	0.98	146.7	119.2		147.1
100	1.00	148.3	--		148.3

Table 4.5 lists the solidus and liquidus temperatures obtained from the calorimetry data presented in Figure 4.13. The corresponding ideal liquidus temperatures, determined using the Schröder van-Laar expression (Equation 2.43), are also given with the expected solidus temperature taken as the racemate melting point. Using this data half of the binary phase diagram was constructed for **2** with an excess of (*S*,*S*)-**2** (Figure 4.14). It is clear from examination of the phase diagram that **2** exists as conglomerate since the lowest liquidus temperature, i.e. the eutectic, occurs at 0% *ee* which is always the case for conglomerates.

Comparison of the experimentally determined liquidus and ideal liquidus temperatures shows that they are in very close agreement which implies that the enantiomers behave close to ideally in the liquid phase i.e. their enthalpy of mixing approaches zero. The entropy of mixing of the enantiomers in the liquid phase, calculated to be 5.2 J mol^{-1} K^{-1} (Equation 2.51), further suggests ideality as this is very close to the expected liquid phase entropy of mixing for ideal conglomerates, $R\ln 2$ = 5.8 J mol^{-1} K^{-1} (see section 2.6.2). The difference seen between the calculated and expected values occurs since, in practice, the magnitude of homochiral and heterochiral interactions in the liquid phase must

be different therefore an enthalpy change must accompany the mixing of antipodes. Despite this, several authors [147, 148] have shown that the scale of the heterochiral mixing enthalpy change represents approximately 1% of the enthalpy of fusion and can therefore be considered to be negligible; hence it is reasonable to assume that the enantiomers behave ideally in the liquid phase which is confirmed by the coincidence of the experimental and calculated liquidus temperatures in Figure 4.14.

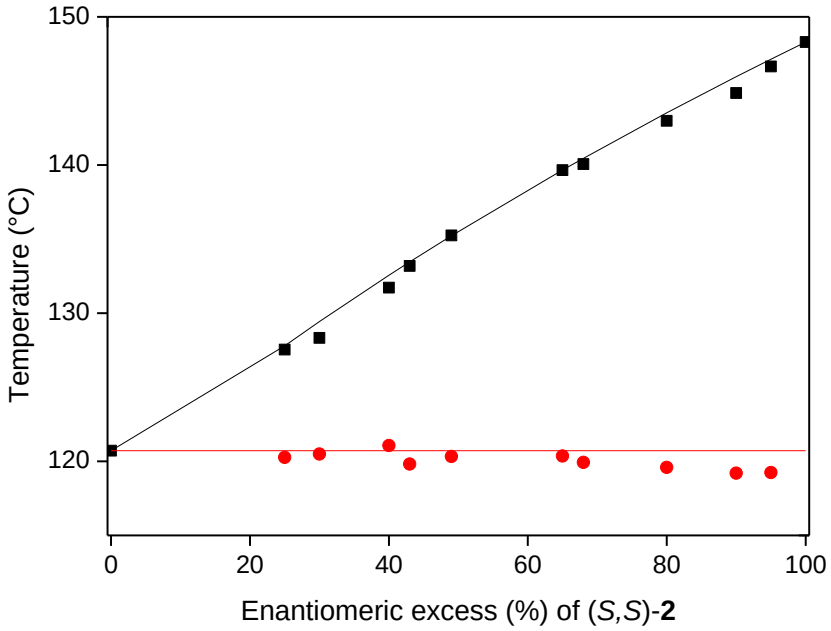

Figure 4.14 Half binary phase diagram for hydrobenzoin (**2**) with (*S*,*S*)-**2** in excess (■ measured liquids, ● measured solidus, ▬ calculated liquids, ▬ expected solidus)

4.6.2 Crystal Structure

The powder XRD pattern and infra-red spectra of *rac*-**2** and (*R*,*R*)-**2** prepared from toluene are presented in Figure 4.15 and Figure 4.16. The diffraction pattern for *meso*-**2**, the diastereomer with respect to (*R*,*R*)- and (*S*,*S*)-**2**, is also given for comparison. Considering *rac*-**2** and (*R*,*R*)-**2**, it can be seen that the number and positions of the peaks in each diffraction pattern are identical which is characteristic of a conglomerate since the racemate is a mechanical mixture of the two crystalline enantiomers. On the other hand, the diffraction

pattern for *meso*-**2** differs from that of the racemate and enantiomer since it has a different crystal structure.

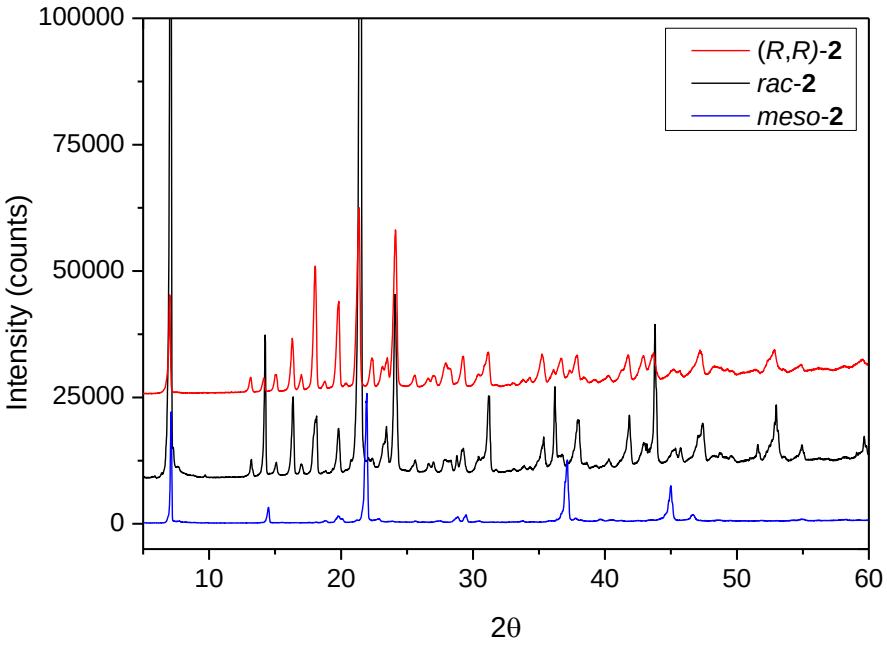

Figure 4.15 Powder X-ray diffraction patterns of the stereoisomers and racemate of **2**.

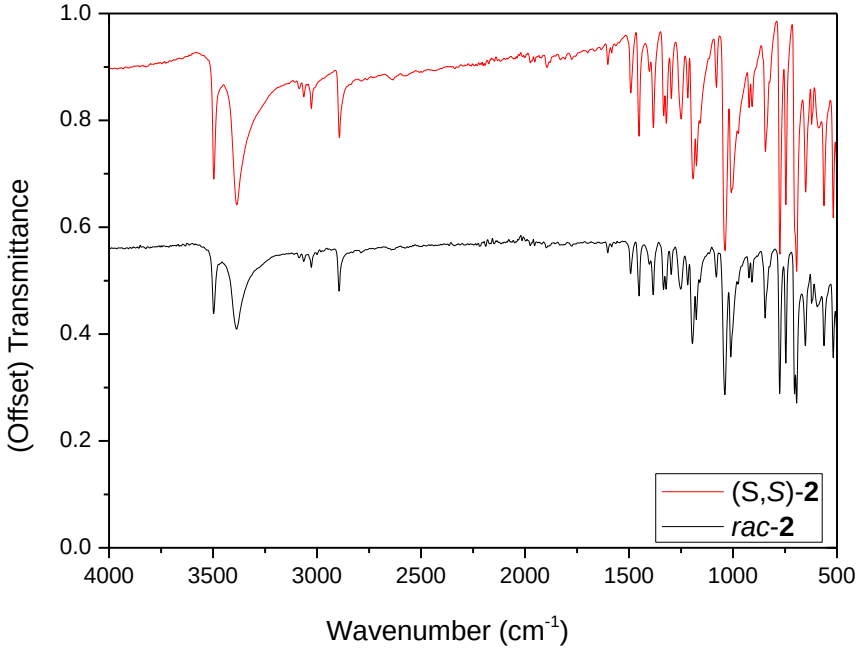

Figure 4.16 FT-IR spectra of (*R*,*R*)- and (*S*,*S*)-**2**.

Figure 4.17 shows the crystal packing and unit cell structures for (*R*,*R*)-**2** which were generated using crystallographic database data [149]. The enantiomer crystallises in the non-centrosymmetric chiral primitive monoclinic space group $P2_1$ indicating a twofold screw axis with a half translation along the *c* axis, having two molecules of (*R*,*R*)-**2** in the unit cell (cell lengths $a \neq b \neq c$ where *a* = 5.84 Å, *b* = 7.90 Å, *c* = 12.41 Å, and cell angles $\alpha = \gamma = 90^{\circ}$, $\beta = 93.04°$). The crystal structure is comprised of homochiral 2_1 columns in which each molecule is held together by two hydrogen bonds between the hydroxyl hydrogen and corresponding oxygen on an identical molecule with van der Waals forces being responsible for the interactions between the homochiral columns.

Considering the crystal structure of *meso*-**2** (Figure 4.18), the diastereomer crystallises in the centrosymmetric primitive monoclinic space group $P2_1/c$ indicating a two-fold screw axis perpendicular to a glide plane along the *c* axis, with four molecules in the unit cell (cell lengths $a \neq b \neq c$ where *a* = 12.54 Å, *b* = 5.08 Å, *c* = 9.31 Å, and cell angles $\alpha = \gamma = 90^{\circ}$, $\beta = 106.67°$) [149].

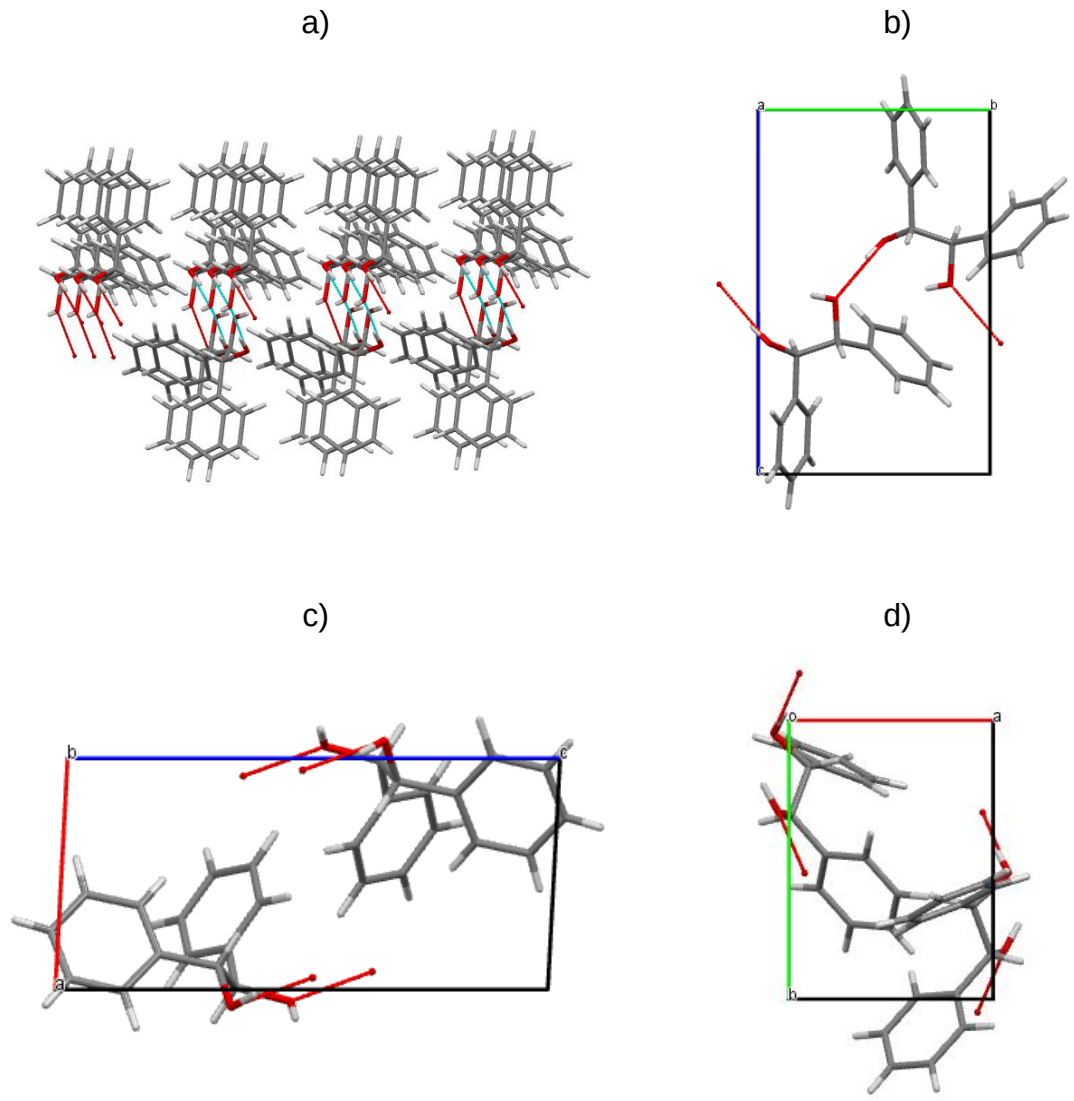

Figure 4.17 Crystal structure of (*R*,*R*)-**2** (space group $P2_1$) showing a) molecular packing along the *b* axis and the contents of the unit cell along the b) *a* axis c) *b* axis and d) *c* axis. Red lines indicate hydrogen bonds.

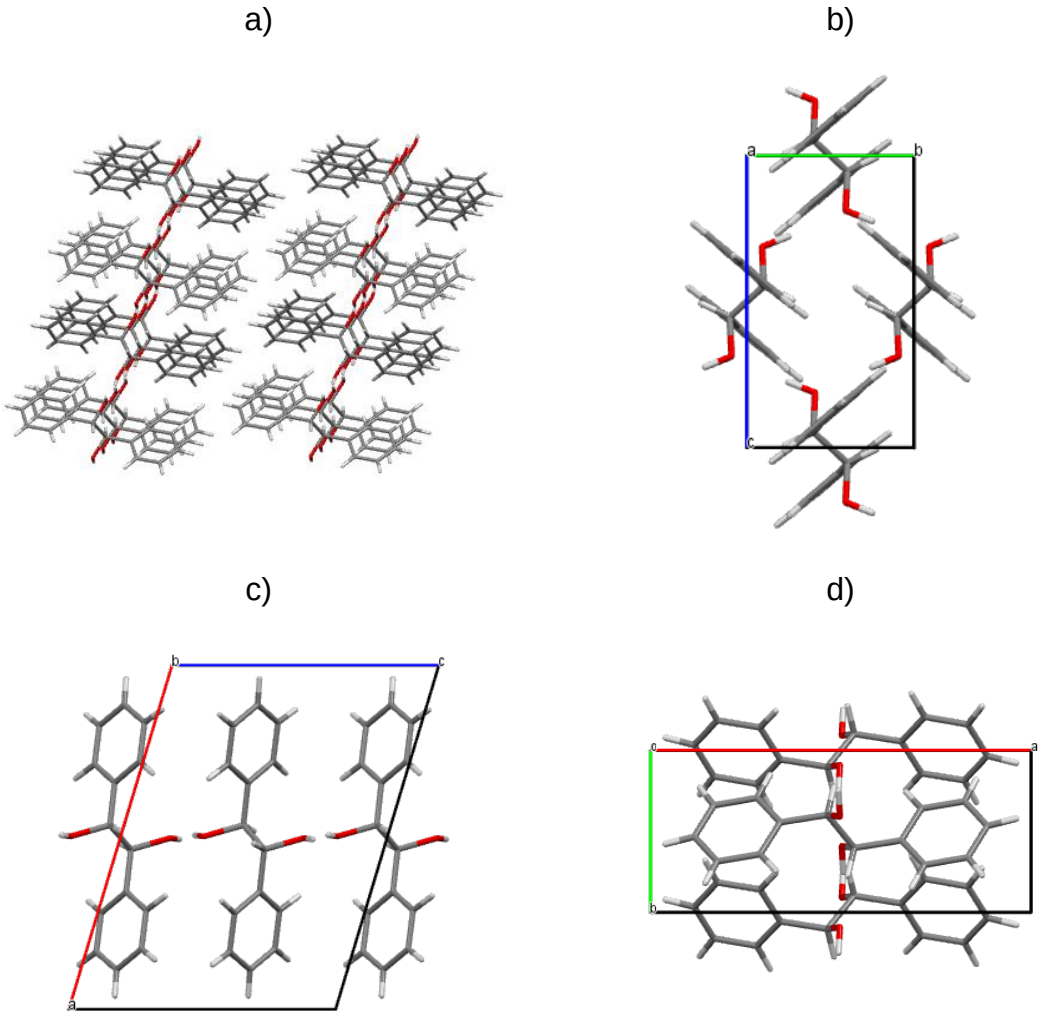

Figure 4.18 Crystal structure of *meso*-**2** (space group $P2_1/c$) showing a) molecular packing along the *b* axis and the contents of the unit cell along the b) *a* axis c) *b* axis and d) *c* axis. Red lines indicate hydrogen bonds.

4.6.3 Conclusion: Hydrobenzoin (2) Characterisation

Hydrobenzoin (**2**) was investigated for use as a model chiral system for the CIAT process as it has been listed in the literature as a conglomerate, is resolvable by preferential crystallisation, and has the potential to undergo racemisation at is two 2° alcohol chiral centres using available organometallic complexes. The pure enantiomers were synthesised following the procedure give in section 11.2.2, and the racemate was obtained by combining, and crystallising, equimolar quantities of the two enantiomers from the melt.

Calorimetry was used to investigate the melting behaviour of the racemate and pure enantiomers obtained by solvent evaporation from toluene, and to construct the binary phase diagram which gave a clear indication of conglomerate formation as the difference as the eutectic occurred at 0% *ee*, Coincidence of the experimental liquidus data with the predicted ideal liquidus, and the close agreement between the calculated entropy of mixing with that of an ideal system, suggested that the enantiomers behave close to ideally in the liquid phase which is generally observed for conglomerates.

The findings of the calorimetry data were confirmed by powder XRD and infra-red spectroscopy with the racemate and pure enantiomer having identical spectra since the former is a mechanical mixture of discreet enantiopure solid phases. The crystal structure of the pure enantiomer obtained from the literature [149], proved the existence of a conglomerate showing that (*R*,*R*)-**2**, and hence *rac*-**2**, crystallises in the non-centrosymmetric primitive monocline space group $P2_1$ which is the second most frequently observed chiral crystal structure for conglomerates accounting for approximately 30% [9].

Despite having two chiral centres, which upon racemisation would yield a diastereomeric *meso* form in addition to the two enantiomers, the characterisation results described above show that **2** could be a suitable candidate for use as a model chiral system in the CIAT process thus its use was further investigated in the subsequent chapters. To compensate for the formation of additional species, it was necessary to determine the solubility of the mixture that resulted upon racemisation, as opposed to the solubility of the racemate which would need to be identified for a system with a single chiral centre, as it is this that would need to be seeded with the pure enantiomer. Additionally, as the meso form was also present in the racemisation mixture, its solubility had to be identified and compared with that of the pure enantiomer to ensure that the later had the lower solubility and hence would be first to reach supersaturation.

4.7 *N*-Methylephedrine Characterisation

4.7.1 Binary Phase Diagram

Figure 4.19 shows the DSC spectra for *rac*-**3**, (*R*,*S*)-**3** and (*S*,*R*)-**3**, with the corresponding melting points and enthalpies of fusion given in Table 4.6.Considering the average pure enantiomer melting point, 87.7°C, and that of the racemate, 63.4°C, the difference of 24.3°C between them is a strong indicator of conglomerate formation. Furthermore, the difference of 3.4 kJ mol^{-1} between the average pure enantiomer enthalpy of fusion, 28.7 kJ mol^{-1}, and that of the racemate, 25.3 kJ mol^{-1}, is typical of conglomerate forming systems which are usually in the range 1.7-5.0 kJ $mol^{-1.}$

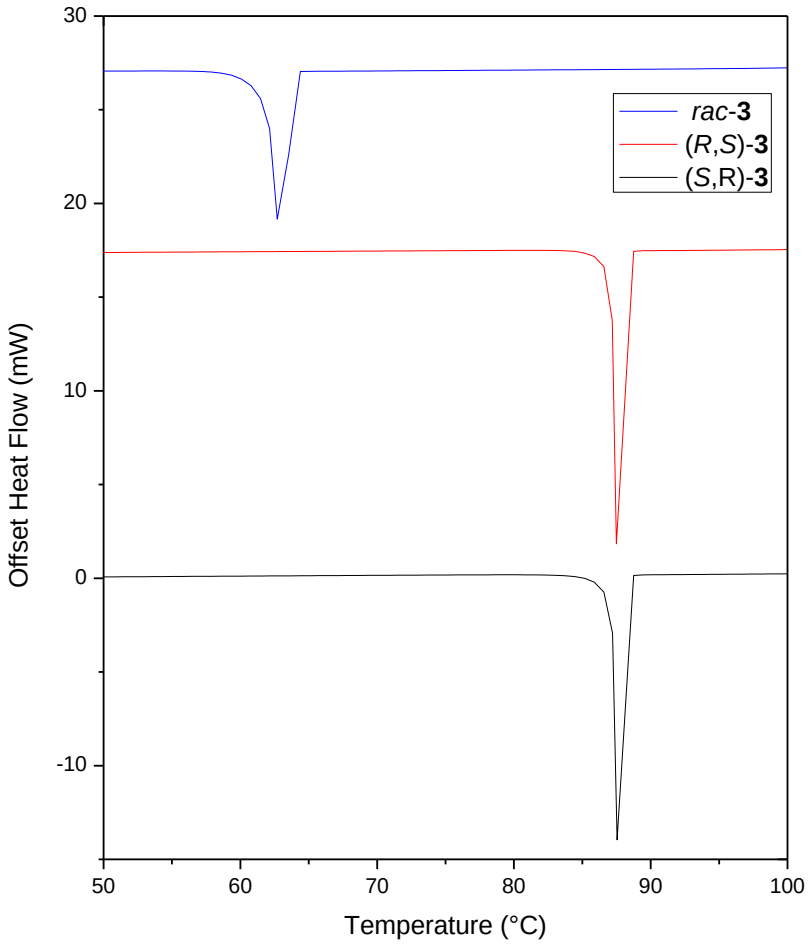

Figure 4.19 DSC thermogram of commercial (*R*,*S*)- and (*S*,*R*)-**3** (Sigma Aldrich), and *rac*-**3** (obtained by melt-recrystallisation of an equimolar mixture of both enantiomers).

Table 4.6 Melting points, T^f, and fusion enthalpies, ΔH^f, determined using DSC for (*R*,*S*)-, (*S*,*R*)- and *rac*-**3**.

***N*-methylephedrine (3)**	**Melting point, T^f (°C)**		**Enthalpy of fusion, ΔH^f (kJ mol^{-1})**	
	T_R^f	T_A^f	ΔH_R^f	ΔH_A^f
(*R*,*S*)-	-	87.9	-	28.9
(*S*,*R*)-	-	87.5	-	28.5
(±)-	63.4	-	25.3	-

The DSC spectra were obtained for a range of enantiomeric compositions of **3** prepared from toluene (Figure 4.20). The trends observed in the calorimetry data, which are characteristic of a conglomerate forming system since the lowest liquidus temperature i.e. the eutectic occurs at 0% *ee*, are identical to those described for **2** (see section 4.6.1 for discussion of calorimetric data trends for conglomerates).

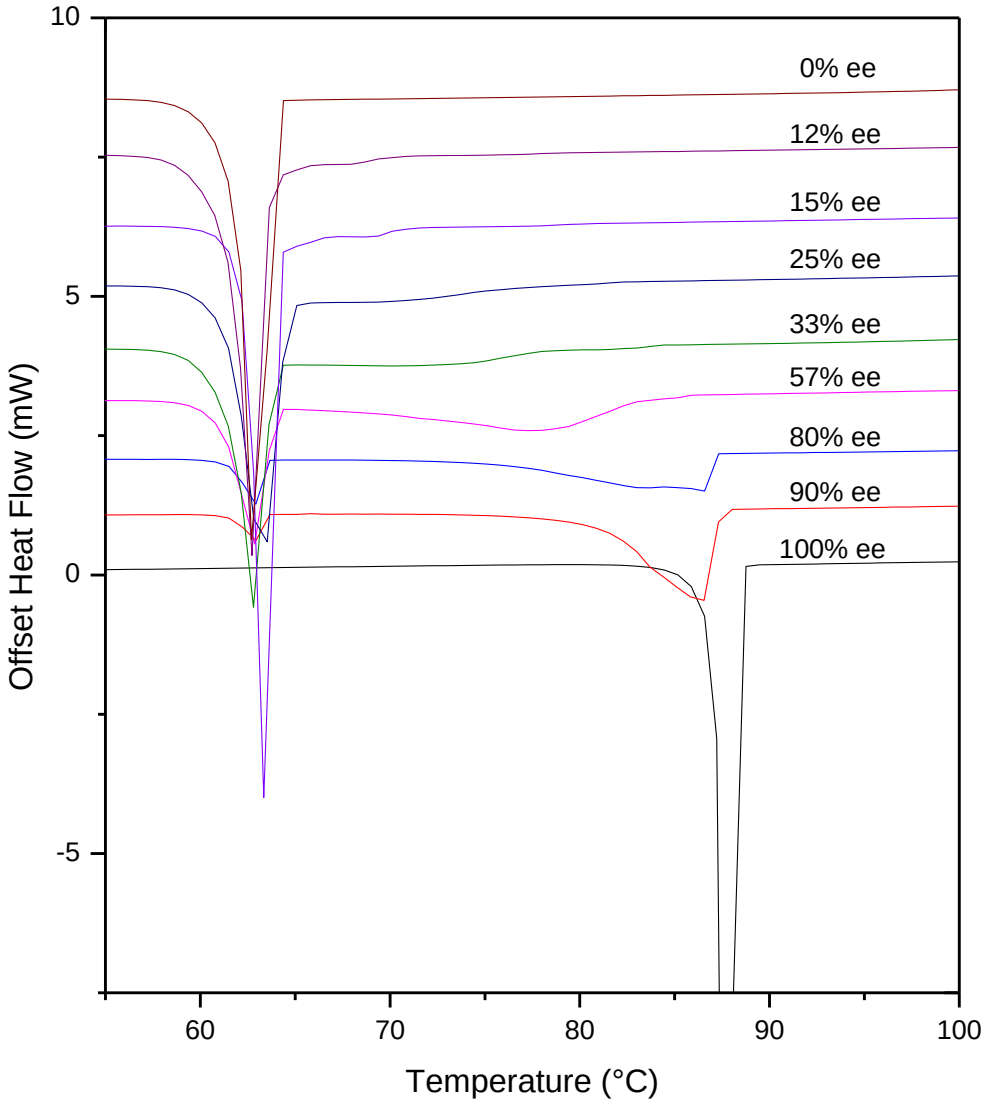

Figure 4.20 DSC curves for mixtures of **3** enantiomers showing solidus and liquidus temperatures.

Table 4.7 Melting points of mixtures of **3** enantiomers determined using DSC, and expected melting points calculated using the simplified Shröder van-Laar expression (Equation 2.43)

Enantiomeric Excess, *ee* (%) (*R*,*S*)-3	**Measured melting point (°C)**		**Expected Solidus (°C)**	**Calculated Liquidus (°C)**
	Solidus	**Liquidus**		
0	--	63.4		63.4
12	63.2	68.1		67.3
15	63.7	69.3		68.3
25	63.2	70.2		71.2
33	62.8	72.4	63.4	73.2
57	63.4	77.0		78.9
80	63.1	83.7		84.0
90	63.1	86.6		86.0
100	--	87.9		87.9

Table 4.7 lists the solidus and liquidus temperatures obtained from the calorimetry data presented in Figure 4.20. The corresponding ideal liquidus temperatures, determined using the Schröder van-Laar expression (Equation 2.43), are also given with the expected solidus temperature taken as the racemate melting point. Using this data half of the binary phase diagram was constructed for **3** with an excess of (*R*,*S*)-**3** (Figure 4.21). It is clear from examination of the phase diagram that **3** exists as conglomerate since the eutectic, occurs at 0% *ee* which is always the case for conglomerates.

Comparison of the experimentally determined liquidus and ideal liquidus temperatures shows that they are in very close agreement which implies that the enantiomers behave close to ideally in the liquid phase i.e. their enthalpy of mixing approaches zero. The entropy of mixing of the enantiomers in the liquid phase, calculated to be 5.44 J mol^{-1} K^{-1} (Equation 2.51), further suggests ideality as this is very close to the expected liquid phase entropy of mixing for ideal conglomerates, Rln2 = 5.78 J mol^{-1} K^{-1} (see section 2.6.2).

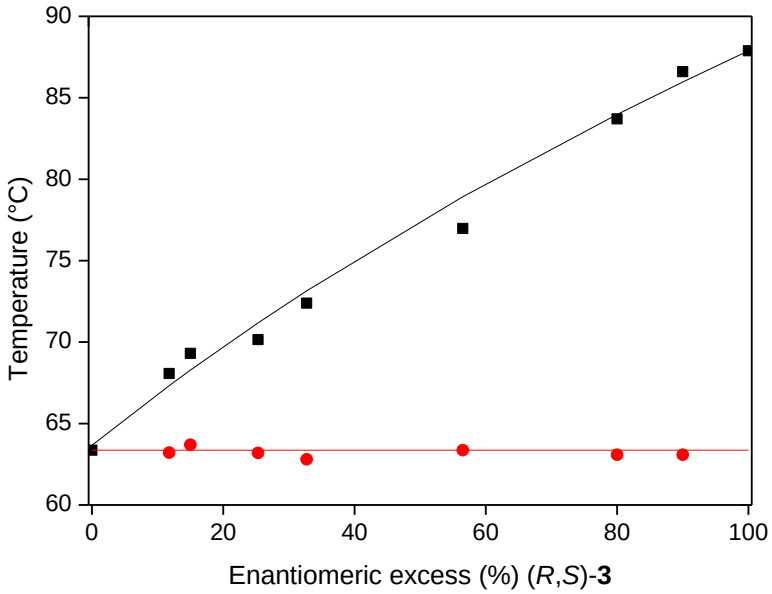

Figure 4.21 Half binary phase diagram for *N*-methylephedrine (**3)** with (*R*,*S*)-**3** in excess (■ measured liquids, ● measured solidus, ▬ calculated liquids, ▬ expected solidus).

4.7.2 Crystal Structure

The powder XRD pattern and infra-red spectra of *rac*-**3** and (*R*,*S*)-**3** prepared from toluene are presented in Figure 4.22 and Figure 4.23. Examination of the data shows that the number and positions of the peaks in each spectrum are identical which is characteristic of a conglomerate since the racemate is a mixture of the two discreet crystalline enantiomeric phases.

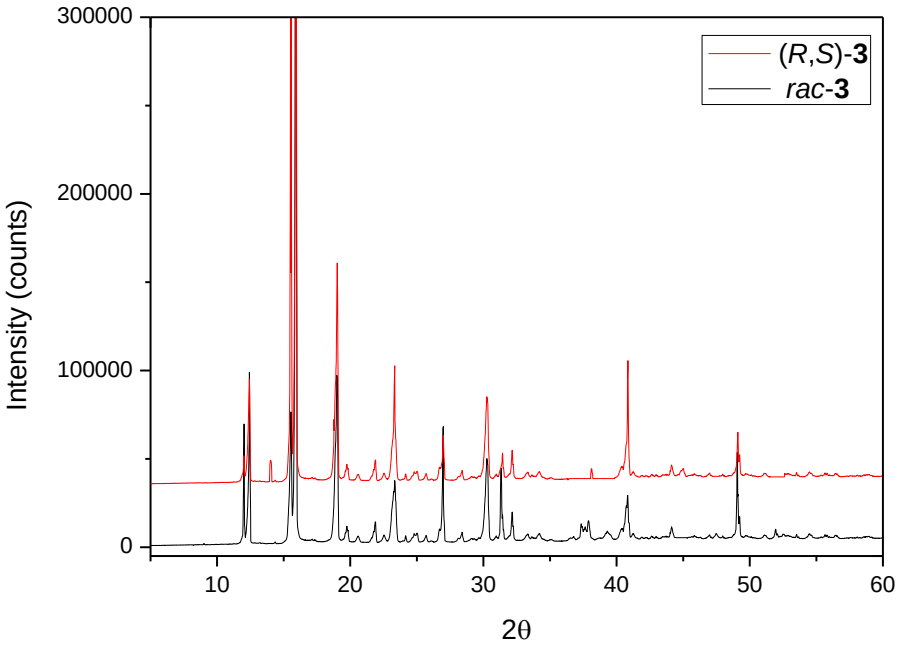

Figure 4.22 Powder X-ray diffraction spectra of (*R*,*S*)- and *rac*-**3**.

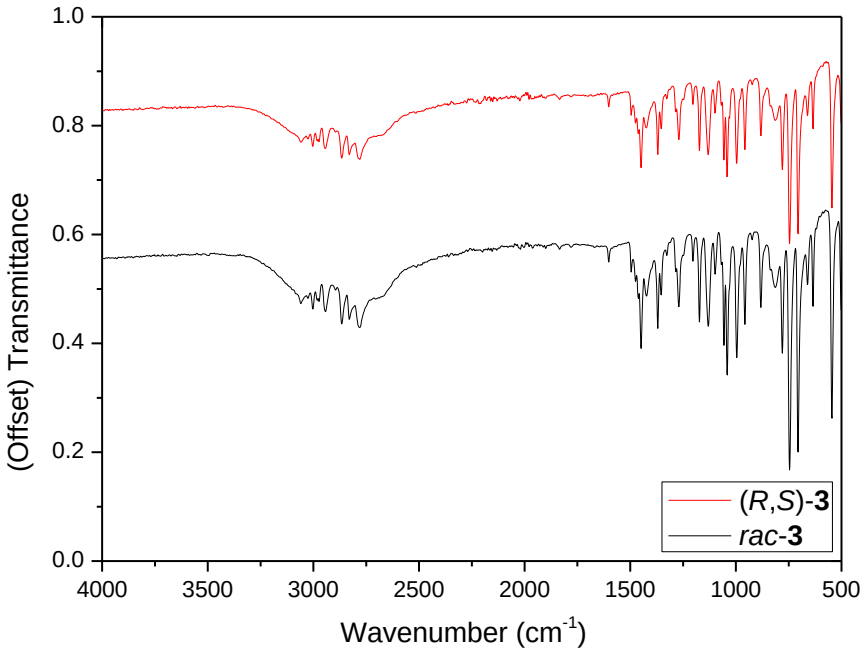

Figure 4.23 FT-IR spectra for (*R*,*S*)- and *rac*-**3**.

Figure 4.24 shows the crystal packing and unit cell structures for (*R*,*S*)-**3** which were generated using crystallographic database data [150]. The enantiomer crystallises in the non-centrosymmetric primitive orthorhombic space group $P2_12_12_1$ indicating a two-fold screw rotation axis with half a translation along the *a*, *b* and *c* unit cell axis, having four molecules of (*R*,*S*)-**3** in the unit cell (cell lengths $a \neq b \neq c$ where a = 8.08 Å, b = 8.90 Å, c = 14.57 Å, and cell angles $\alpha = \beta = \gamma = 90^{\circ}$). The crystal structure is comprised of homochiral 2_1 columns in which each molecule is held together by a hydrogen bond between the hydroxyl hydrogen and corresponding tertiary amine on an identical molecule with van der Waals forces being responsible for the interactions between the homochiral columns.

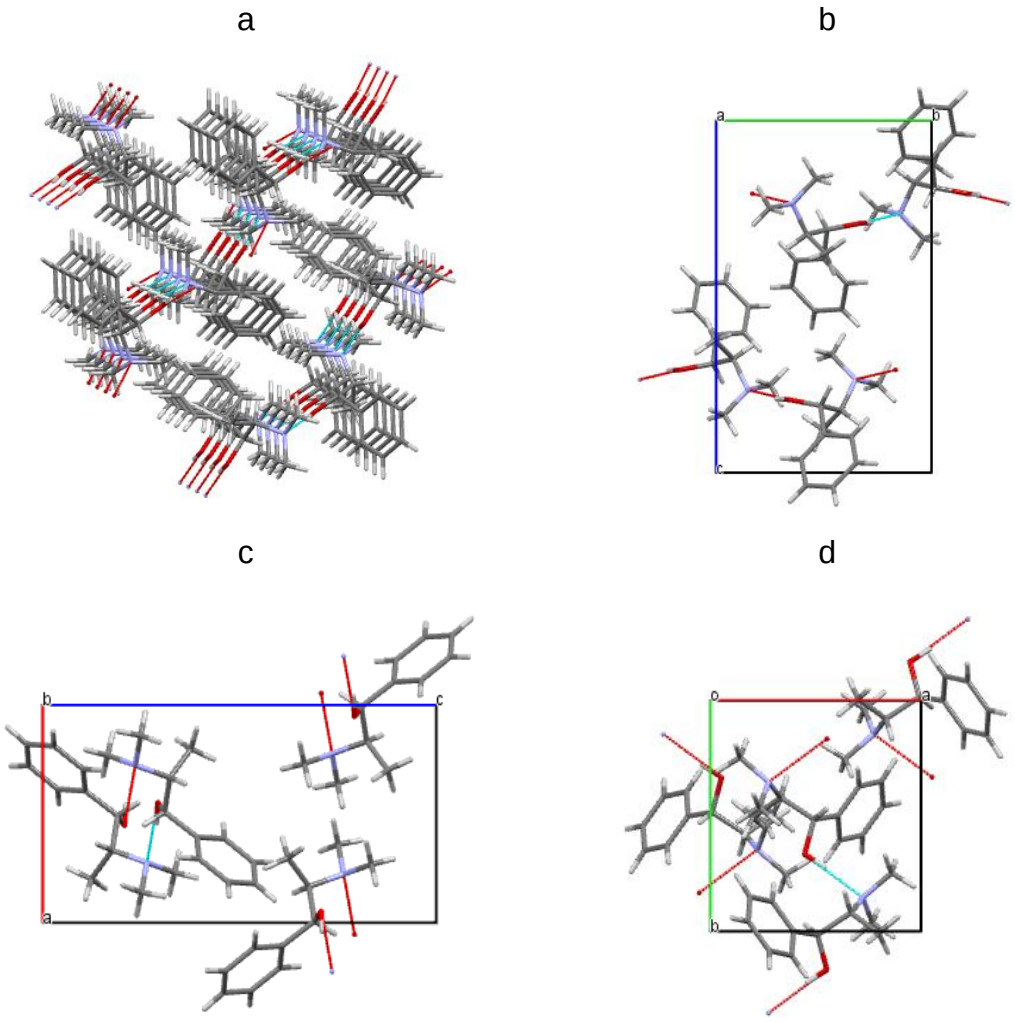

Figure 4.24 Crystal structure of (*R*,*S*)-**2** showing a) molecular packing along the *b* axis and the contents of the unit cell along the b) *a* axis c) *b* axis and d) *c* axis. Blue and thin red lines indicate hydrogen bonging to other molecules and molecules not shown respectively.

4.7.3 Conclusion: *N*-Methylephedrine (3) Characterisation

N-Methylephedrine (**3**) was investigated for use as a model chiral system for the CIAT process as it has been listed in the literature as a conglomerate and has the potential to undergo racemisation at its 2° alcohol and 3° amine chiral centres using available organometallic complexes. The pure enantiomers were obtained from commercial suppliers (Sigma Aldrich, > 99% *ee*) and the racemate prepared by mixing and recrystallising equimolar quantities of the two enantiomers from the melt. Calorimetry was used to investigate the melting behaviour of the racemate and the pure enantiomers obtained by solvent evaporation from toluene, and to construct the binary phase diagram which gave a clear indication the conglomerate formation as a single eutectic occurred at 0% *ee*. Coincidence of the experimental liquidus data with the predicted ideal liquidus, and the close agreement between the calculated entropy of mixing with that of an ideal system, suggested that the enantiomers behave close to ideally in the liquid phase which is generally observed for conglomerates.

The findings of the calorimetry data were confirmed by powder XRD and infra-red spectroscopy with the racemate and pure enantiomer having identical spectra since the former is a mechanical mixture of discreet enantiopure solid phases. The crystal structure of the pure enantiomer, obtained from the literature [150], proved the existence of a conglomerate showing that (*R*,*S*)-**3**, and hence *rac*-**3**, crystallises in the non-centrosymmetric primitive orthorhombic space group $P2_12_12_1$ which happens to be the most frequently observed chiral crystal structure for organic molecules.

Despite having two chiral centres with differing functionality, which upon racemisation would yield two diastereomeric forms of **3** in addition to the two enantiomers, the characterisation results described above suggested that **3** was a suitable candidate for use as a model chiral system in the CIAT process. However, subsequent investigations (results not presented) showed that the pure enantiomers of **3** could not be racemised by any of the organometallic catalysts tested. Several iridium and ruthenium-based catalysts were trialled under a range of different conditions however no appreciable drop in *ee* was observed even when the substrate was refluxed for long durations of time

suggesting that the quaternary iminium intermediate species necessary for racemisation could not be generated (the reactions were monitored by polarimetry). Although it was hoped that this would not be the case, the behaviour observed was anticipated since there are few examples of tertiary amine racemisation, and as a result of these findings **3** was not investigated any further.

4.8 Chapter Summary

The investigation into coupling preferential crystallisation with in-situ solution phase racemisation required a model chiral system that crystallises as a conglomerate and has the potential to undergo racemisation in solution with available organometallic complexes. A thorough search of the literature revealed only three suitable candidates that satisfied the selection criteria outlined in the chapter. 1-indanol (**1**), hydrobenzoin (**2**) and *N*-methylephedrine (**3**) were investigated for use as model chiral systems for development of the CIAT process as they have all been reported to exist as conglomerates in the literature.

Calorimetric data were obtained for each of the systems investigated allowing for comparison of their racemate and pure enantiomer temperatures and fusion ($\Delta T_R^f / T_A^f$ and $\Delta H_R^f / \Delta H_A^f$ respectively) and identification of the eutectic *ee* by binary phase diagram construction, and calculation of the liquid phase entropy of mixing, ΔS_l^m, as these can be used as characterisation techniques for chiral heterogeneous equilibria. The ideal liquid curves and liquid phase entropy of mixing were also identified using the calorimetric data to examine the proximity of chiral system to ideality. In addition to melting behaviour, the solid state structure of both the racemate and pure enantiomer were investigated by comparing their powder XRD and FT-IR spectra and identifying their crystal structures.

1 was found to be and unstable model system as it was shown to crystallise as a stable racemic compound despite being listed as a resolvable conglomerate [9]. A difference of 18.8°C and 1.8 kJ mol^{-1} between the pure enantiomer and racemate melting points implied the presence of a racemic compound which was confirmed by binary phase diagram construction, the eutectic occurring at ~30% *ee*, and PXRD and FT-IR, the racemate and pure enantiomer having different spectra. Single crystal XRD analysis showed that the racemate of **1** crystallises in the centrosymmetric body centred tetragonal space group *I*41/a, whilst its enantiomers crystallise in the centrosymmetric monoclinic space group $P2_1$.

Further investigation revealed that **1** is in fact able to form a metastable conglomerate under the correct conditions. DSC was used to obtain this by using a prescribed programme in which the mixtures of enantiomers were held in their molten state well in excess of the melting point of the pure enantiomer (90°C) before being cooled to 0°C under a controlled cooling rate. The conglomerate was obtained for non-racemic mixtures of **1** enantiomers (the conglomerate for 0% *ee* could not be obtained as it remained molten) with a reduction in solidus temperature (and liquidus temperatures at *ee*s below the racemic compound eutectic) from ~51 to ~37°C, and construction of the complete binary phase diagram yielding a single eutectic at 0% *ee*, confirming the ability of **1** to form a metastable conglomerate.

Although chiral discrimination in the solid phase of **1** was shown to be possible, the condition required to obtain the conglomerate i.e. the prolonged period of low temperature cooling, conflicted with the condition requirements of the racemisation catalysts. Furthermore, the conglomerate could only be obtained in the melt, and 1 was shown to be extremely solubility in all of the organic solvents tested therefore it was not taken forward in the CIAT investigation.

Despite having two chiral centres, **2**, was proposed as a possible candidate as it has been shown to crystallise as a conglomerate and has been resolved by preferential crystallisation [9], and has the potential to undergo racemisation. **2** crystallised from toluene was confirmed to be a conglomerate as the difference between its racemate and enantiomer melting point was greater than 20°C (26.9°C), the binary phase diagram contained only a single eutectic at 0% *ee*, and the PXRD and FT-IR spectra for the racemate and enantiomers were identical. The presence of two chiral centres complicates is use as a model CIAT system as a *meso* form of **2** one results upon racemisation therefore this must be considered by identify its solubility relative to the enantiomers to ensure that the latter is the most stable and hence will be the first to achieve supersaturation. Furthermore, since CIAT involves seeding a racemising i.e. equilibrated solution of enantiomers, the solubility of the racemisation mixture of **2** must be determined (as oppose to that of the racemate which would be required if the model system had a single chiral centre) to identify suitable

conditions for CIAT. In spite of these potential complications, **2** was selected as model system for investigation.

Also having two chiral centres, albeit with different functionality, **3** was considered as it has been shown to crystallise as a conglomerate , despite initial reservations about the ability of the tertiary chiral amine stereogenic centres potential to undergo racemisations. **3** crystallised from toluene was confirmed to be a conglomerate as the difference between its racemate and enantiomer melting point was greater than 20°C (23.4°C), the binary phase diagram contained only a single eutectic at 0% *ee*, and the PXRD and FT-IR spectra for the racemate and enantiomers were identical. Even with the ability of the enantiomer of **3** to be resolved by seeding, further investigation (results not included) showed that it was unable to undergo racemisation. Several different iridium and ruthenium-based racemisation catalysts (see section 5.3.2) were trialled under a range of different conditions; however, even under reflux for prolonged reaction times, racemisation of 3 was not observed. It was therefore unable to be used as a model CIAT system and is not discussed any further.

5 Racemisation Catalyst Selection

5.1 Introduction

To recycle the waste enantiomer in-*situ* during the CIAT process, a suitable racemisation catalyst was required that can efficiently convert the optically active solution that results after enantio-selective crystallisation, back to one that is racemic. Organometallic complexes based on transition metals such as ruthenium, rhodium and iridium, have shown great promise as racemisation catalysts in the DKR of chiral alcohols and amines, in many cases giving quantitative yields of a single enantiomer from an initially racemic solution. Their ability to racemise a wide range of functionally related compounds with low catalysts loadings (~1-5 mol%), high functional group tolerance, requirement of mild conditions, and high solubility in organic solvents, make them a suitable candidate for CIAT. Other racemisation techniques, such as acid/base or heat catalysed racemisations, tend to be specific to each system requiring chiral centres that can be easily racemised e.g. due to the presence of low pKa chiral protons, and are thus limited in their application.

Racemisation of optically active alcohols and amines by organometallics proceeds by dehydrogenation at the chiral centre to produce the corresponding ketone/imine followed by rehydrogenation either side of the planar intermediate. Typically, racemisation with these complexes occurs via inner-sphere electron transfer in which the active catalytic species is first generated by the addition of base (or thermal dissociation in the case of dimeric organometallics) which leads to ligand exchange with the optically active substrate, followed by hydride elimination and subsequent addition at the stereogenic carbon. Ruthenium-based complexes are the most widely used for alcohol racemisation particularly in DKRs where a number of different catalysts have been used successfully [89, 90, 98, 99, 101, 102, 104, 106, 109, 110, 115, 151]. Rhodium [116], palladium [14, 113], aluminium [117] and vanadium-based [111] complexes have also been shown to racemise chiral alcohols and have been utilised in DKRs; however, their use has been limited compared with those based on ruthenium.

5.2 Objectives

Organometallic complexes were screened to identify a suitable catalyst for the racemisation of the chiral diol, **2**, the model system identified in chapter 4, to be used in the CIAT process. Due to their success in DKRs and hydrogen transfer reactions, three potential candidates were investigated: chloro(indenyl)-bis-(triphenylphosphine)-ruthenium(II) (**4**); chlorodicarbonyl-(1,2,3,4,5-pentaphenyl-cyclopentadienyl)-ruthenium(II) (**5**); and chlorocarbonyl-triphenylphosphene-(1,2,3,4,5-pentaphenylcyclopentadienyl)-ruthenium(II) (**6**).

Racemisation of **2** was attempted with each catalyst under a range of conditions, primarily varying the temperature and catalysts load to identify a complex that was capable of giving sufficient rates of conversion of the pure enantiomer, (*S*,*S*)-**2**, to the racemate, *rac*-**2**. For catalysts that were shown to successfully racemise **2**, observed kinetics for the overall reaction were identified, the effect of temperature and catalysts load on the reaction rate considered, and a possible catalytic cycle proposed. Since, as previously discussed, racemisation of **2** leads to the formation of *meso*-2 (in addition to the antipode) and other reaction intermediates, the relative composition of the resulting mixture was also determined to allow for characterisation of its solubility in the subsequent chapter which was necessary to identify conditions for CIAT.

Racemisation of **3**, which was shown to crystallise as a conglomerate from toluene, was also attempted using the complexes listed above under a range of different conditions (results not given). However; in each case no racemisation was observed, even when refluxed for long durations of time, which was most likely a due to the resistance of its tertiary chiral amine for which few examples of racemisation by organometallics exists.

5.3 Racemisation Catalyst Selection

5.3.1 Selection Criteria

Selection of a suitable organometallic complex for racemisation of **2** was dependent on satisfying a number of criteria:

- Able to efficiently racemise the selected model system
- Racemisation rate equal to or in excess of crystallisation rate
- Remains undersaturated in solution for the duration of the CIAT process
- Does not inhibit chiral discrimination in the solid phase
- Minimal influence on crystallisation characteristics
- Cheap to obtain or synthesise

As CIAT consists of coupling preferential crystallisation with in-*situ* solution phase racemisation, the relative rates of the two processes had to be considered. For the process to be successful the rate of racemisation had to exceed that of crystallisation, i.e. the rate at which solute is deposited from solution. In an ideal case the rate of racemisation would be fast enough to maintain a racemic or near racemic solution phase *ee*, which would allow the process to operate close to equilibrium between the solid and solution phases potentially leading to quantitative yields of the seeded enantiomer.

If the racemisation rate were not to exceed that of crystallisation, eventually growth of the seed crystals and secondary nuclei formation of the desired enantiomer would lead to an rise in the *ee* of its antipode in solution which, in turn, would increase its chance of spontaneous crystallisation as its degree of supersaturation would be greater than that of the desired enantiomer. To compensate for the latter case occurring, the crystallisation conditions could of course be tuned (to a certain degree) so that the relative rates of the two processes are as required; however, catalysts found to give slow rates of racemisation e.g. in the order of days, would be unsuitable for CIAT as even with modified crystallisation conditions, it is likely that this would result in sufficient time for the nucleation induction period to elapse.

Considering the preferential crystallisation of **2** from ethanol reported in the literature [143], a crystal yield of approximately 8% of the desired enantiomer was recovered after allowing the process to run for 20 min, which corresponds to a 4% increase in the solution phase *ee* of the undesired enantiomer in this time period. Therefore, in theory, for a crystal yield of 100% of the desired enantiomer 250 min would be required based on the observed rate of crystallisation (assuming size independent growth). For CIAT to be successful the selected catalyst would thus need to be able to completely racemise the pure enantiomer within this time period, ideally with a racemisation time considerably less than this for the reasons described above.

In addition to achieving fast rates of racemisation, the selected catalysts also had to exhibit sufficient solubility in the process solvent. Since the driving force for crystallisation during CIAT is generated by cooling, it was essential that the catalyst remained dissolved for the duration of the process and did not itself become supersaturated and precipitate from solution. On the other hand, the presence of the catalyst in solution had to have minimal influence of the crystallisation characteristics of both the desired and undesired enantiomer, particularly, the ability of the racemate to form a conglomerate or the seed crystals to grow, or the potential for the catalyst to act as centres for nucleation.

Finally, by their very nature, being comprised of precious metals, the organometallic complexes earmarked for use as CIAT catalysts are often expensive to purchase or synthesise. Therefore the ideal candidate had to be available for the investigation in sufficient quantities (tens of grams) at a reasonable cost.

5.3.2 CIAT Candidates

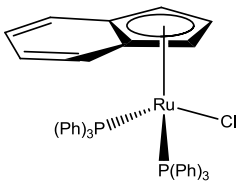

4

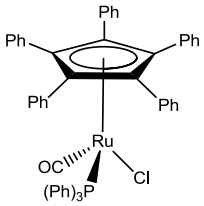

5

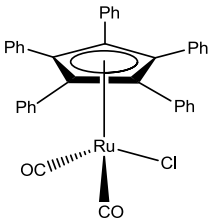

6

Figure 5.1 Organometallic complexes investigated for use as a racemisation catalyst in the CIAT process: Chloro(indenyl)-bis-(triphenylphosphine)-ruthenium(II) (**4**); chlorocarbonyl-triphenylphosphene(1,2,3,4,5-pentaphenylcyclopentadienyl)-ruthenium(II) (**5**); chlorodicarbonyl-(1,2,3,4,5-pentaphenylcyclopentadienyl)-ruthenium(II) (**6**);

The ruthenium-based complexes **4**-**6** were investigated for use in the CIAT process as they have all been shown to be capable of racemising a wide range of chiral alcohols and have been successfully used in DKRs ([107, 126, 152]). Each of the complexes are active in toluene, which as a result has been earmarked for use as the CIAT process solvent (see section 5.3.3 for discussion), being capable of efficient racemisation at room temperature, in some cases within 30 min with low catalyst loads of 0.5 mol%.

Generation of the active catalytic species of **4**-**6** takes place by the addition of base, typically *t*-BuOK or KOH, which results in ligand loss, and hence the formation of a reactive 16 electron ($16e^-$) complex, leaving it susceptible to subsequent ligand re-addition which leads to racemisation of the substrate. Despite the high activities seen, one drawback associated with the use of ruthenium-based catalysts (**4** and **6**) is that they require dry anaerobic conditions. **5** on the other hand, is the only air stable catalyst that has been reported in the literature [126]. Due to the similarities seen in the CIAT obtained for catalysts **4** and **6**, and since a great deal of work was done using **4**, the results for catalyst **6** are not presented in the subsequent chapters.

The iridium-based complexes pentamethylcyclopentadienyl iridium(II) dichloride dimer ($[Cp^*IrCl_2]_2$) and pentamethylcyclopentadienyl iridium(II) diiodide dimer ($[Cp^*IrI_2]_2$) were investigated due to their success in hydrogen transfer reactions

and DKRs ([16, 17, 144, 152-154]); however all attempts at racemising **2** were unsuccessful even when the reaction mixture was refluxed for 24 h under relatively high catalyst loads (0.117 mol l^{-1}, 3 mol%). Shvo's catalyst (1-Hydroxy-tetraphenyl-cyclopentadienyl-(tetraphenyl-2,4-cyclopentadien-1-one)-μ-hydro-tetracarbonyl-diruthenium(II)) was also considered due to its use in hydrogen transfer and DKR [61, 91-94, 118], and proved successful at racemising **2** within 1 h (0.117 mol l^{-1}, 80°C, 2 mol%). However the high cost of the catalyst, coupled with the fact that it is structurally analogous to **5** (Shvo's catalyst essentially being a dimer of **5**) meant that was not used for CIAT (results for Ir-based and Shvo's catalyst not given).

5.3.3 Solvent Selection

As previously discussed (see section 4.3.1) toluene was chosen to be the CIAT process solvent as it has been successfully used for racemisation using a wide range of catalysts including **4**-**6**. It has been shown to have the ability to dissolve a wide range of organometallics, whilst also remaining inert to the catalytic cycle. As will be seen in chapter 6, it is also suitable for the crystallisation of **2** as a conglomerate, allowing for its complete dissolution upon heating, and deposition of a sufficient quantity of material upon cooling.

5.4 Methodology and Analytical Techniques

5.4.1 Catalyst Preparation

4 and **5** were synthesised using the literature procedures given by Oro *et al* [155] and Ko *et al* [126] respectively. See section 11.2 for a description of the synthetic routes used.

5.4.2 Racemisation

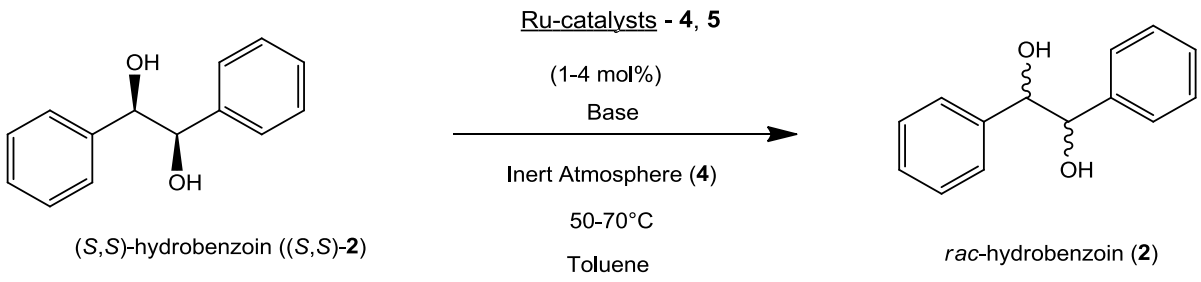

Scheme 5.1 Conditions for (*S*,*S*)-**2** racemisation using Ru-based complexes **4** and **5**.

Procedure for racemisation of (S,S)-hydrobenzoin ((*S*,*S*)-***2***) *with ruthenium-based catalysts **4-5** (0.93 mmol scale):* To a 25 ml Schlenk flask equipped with a reflux condenser, thermometer and inert gas supply (catalysts **4** and **5**, N_2 or Ar) was dissolved 0.93 mmol of (*S*,*S*)-***2***) (0.2 g) and 10 mol% base (*t*-BuOK or KOH) in 8 ml of dry toluene at 50-80°C. 0.5-4 mol% of **4** or **5** was then added and the reaction left to proceed for 1 h.

Sampling procedure for (S,S)-hydrobenzoin ((*S*,*S*)-***2***)*:* 0.5 ml samples of the reaction mixture, obtained using a glass syringe through an air tight septum, were quenched with 1 M HCl and topped up with diethyl ether to ensure compete dissolution of the substrate (due to a low solubility in toluene at room temperature). The organic top layer was separated, evaporated, and subsequently dried under vacuum. The samples were then dissolved in propan-2-ol and analysed by chiral HPLC (see section 11.1.5 for HPLC method details)**.**

5.5 Racemisation of (*S*,*S*)-Hydrobenzoin ((*S*,*S*)-2)

5.5.1 Chloro(indenyl)-bis-(triphenylphosphine)-ruthenium(II) (4)

5.5.1.1 Reaction Rate

Figure 5.2 shows the progress of the racemisation of (*S*,*S*)-**2** by complex **4** (0.117 mol l^{-1}, 2 mol% **4**, 60°C). It is evident that **4** is highly active under the conditions used as complete racemisation of the substrate has occurred after 5 min. As expected, in addition to forming its antipode, the reaction of (*S*,*S*)-**2** with **4** also leads to the formation of near equal amounts *meso*-**2** and the di-ketone intermediate benzil (1,2-diphenylethane-dione). Interestingly, benzaldehyde was also seen to be formed which indicates that the alkane C-C bond has undergone cleavage due to the action of the catalyst which could have been a result of (*S*,*S*)-**2** acting as a bidentate ligand due to it possessing two chiral centres.

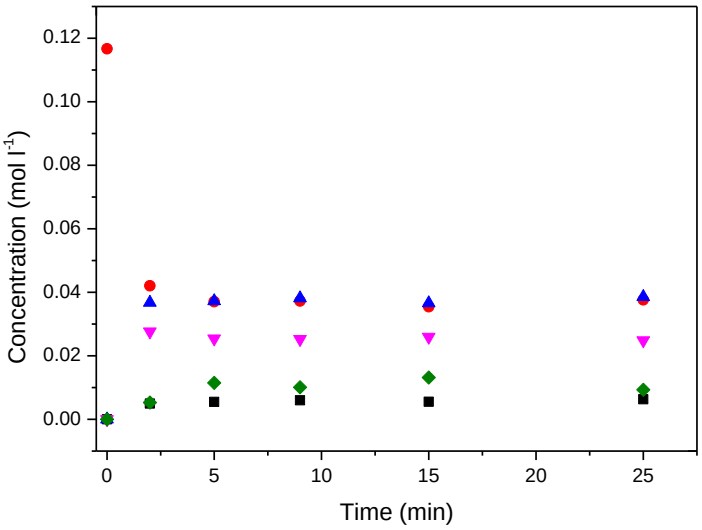

Figure 5.2 Racemisation of (*S*,*S*)-**2** with **4** (0.117 mol l^{-1}, 2 mol% **4**, 60°C) (● (*S*,*S*)-**2**, ▲ (*R*,*R*)-**2**, ▼ *meso*-**2,** ■ benzil, ◆ benzaldehyde).

Using differential analysis [156] the observed kinetics for the racemisation of (*S*,*S*)-**2** by **4** were estimated. As the reaction proceeded at such a fast rate it was difficult to obtain data points before equilibrium was achieved. Consequently, the values used for estimation of the racemisation rate were taken from the curve that was fitted to the experimental data. It is possible that

that racemisation rate could have been reduced by lowering the temperature or catalysts load; however, with regards to the former, the low solubility of the pure enantiomer (*S*,*S*)-**2** did not permit dissolution bellow ~50°C, whereas reduction of the catalyst load to 0.5 mol% did not result in complete racemisation.

Using the OriginPro software package, the data from Figure 5.2 was fitted with an exponential decay function whose derivatives at selected points were subsequently calculated to obtain the rate of change of (*S*,*S*)-**2** concentration with respect to time (Table 5.1). Logarithms of the derivatives and the corresponding concentrations were then taken and plotted to give Figure 5.3. Using this the order, *n*, and observed rate constant, k_{obs}, of the racemisation reaction were obtained from the *y*-intercept and slope of the fitted line and estimated to be 2.183 and 12.877 $l^{1.183}$ $mol^{-1.183}$ s^{-1} respectively giving the racemisation rate function for (*S*,*S*)-**2** by **4** (Equation 5.1).

Table 5.1 Differential analysis of (*S*,*S*)-**2** racemisation with **4** (0.117 mol l-1, 2 mol% **4**, 60°C).

Time (min)	**Concentration (*S*,*S*)-hydrobenzoin ($C_{(S,S)-2}$) (mol l^{-1})**	**$\log_{10}(C_{(S,S)-2})$**	**$dC_{(S,S)-2}/dt$**	**$\log_{10}(-dC_{(S,S)-2}/dt)$**
0.0	0.117	-0.933	-0.107	-0.970
0.5	0.077	-1.112	-0.055	-1.259
1.0	0.057	-1.242	-0.028	-1.556
1.5	0.047	-1.327	-0.014	-1.852

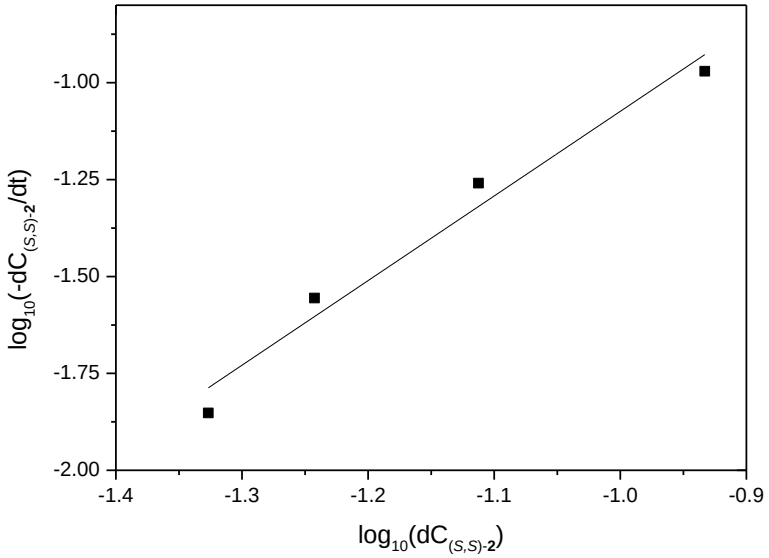

Figure 5.3 $\log_{10}(-dC_{(S,S)\text{-}\mathbf{2}}/dt)$ vs. $\log_{10}dC_{(S,S)\text{-}\mathbf{2}}$ for the racemisation of (*S*,*S*)-**2** by **4**.

Estimated rate function for the racemisation of (*S*,*S*)-**2** by **4**:

$$-r_{(S,S)-\mathbf{2}} = k_{obs}C^{n}_{(S,S)-\mathbf{2}} = \left(12.877\frac{l^{1.183}}{mol^{1.183}\,s}\right)C^{2.183}_{(S,S)-\mathbf{2}}\ mol\ l^{-1}s^{-1} \qquad \text{Equation 5.1}$$

5.5.1.2 Temperature Dependence

As the proposed CIAT process relies on cooling to induce supersaturation of the desired enantiomer, the temperature dependence of the racemisation rate was investigated to ensure it remains sufficiently fast to maintain a racemic or near racemic solution composition during CIAT as the temperature is reduced. Figure 5.4 shows the progress of the racemisation of (*S*,*S*)-**2** by **4** at 50°C, 60°C and 70°C (0.117 mol l^{-1}, 2 mol% **4**). As expected, the time take for complete racemisation reduces with an increase in temperature occurring within 10 min, 5 min, and 2 min, at reaction temperatures of 50°C, 60°C and 70°C respectively highlighting the suitability of 4 for use in the proposed CIAT process. Ideally the reaction rate would have been investigated over a wider range of temperatures; however as is implied from examination of Figure 5.4, the racemisation rate becomes immeasurably fast at beyond 70°C therefore it would not be possible to accurately deduce any kinetic information using data obtained under this condition. On the other hand, as mentioned previously, at temperatures less

than 50°C, (*S*,*S*)-**2** becomes insoluble in toluene therefore this could not be performed. A temperature difference of 5°C between each successive measurement was attempted; however, it was difficult to resolve any differences between the data generated therefore 10°C intervals had to be selected.

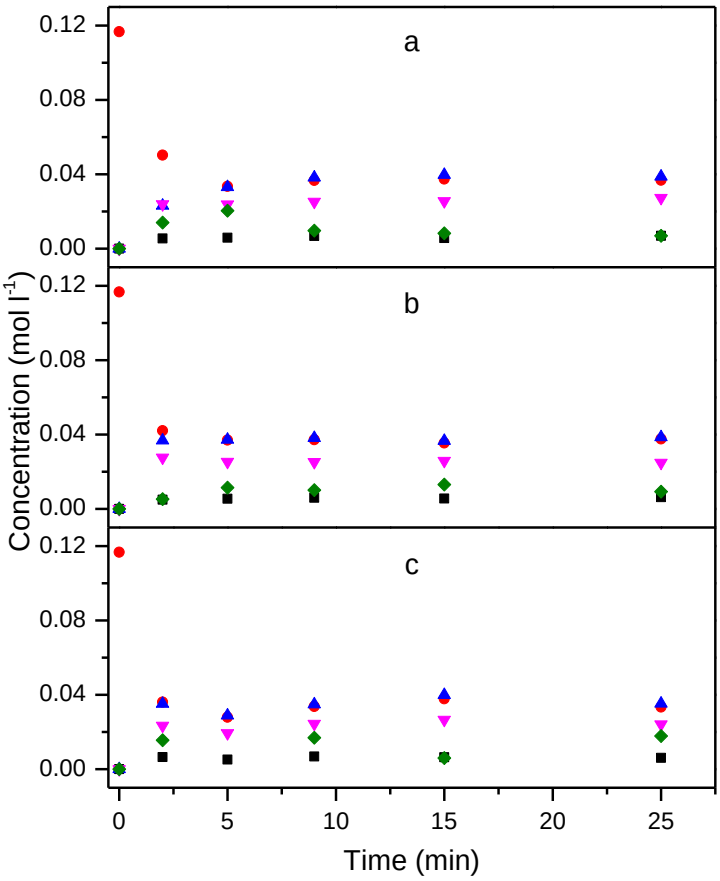

Figure 5.4 Racemisation of (*S*,*S*)-**2** by **4** at a) 50°C, b) 60°C and c) 70°C (0.117 mol l^{-1}, 2 mol% **4** (● (*S*,*S*)-**2**, ▲ (*R*,*R*)-**2**, ▼ *meso*-**2,** ■ benzil, ◆ benzaldehyde).

Using the same method described in the previous section, the observed kinetics for the racemisation were estimated at the three temperatures examined (Figure 5.5). The observed rate constants for each temperature (Table 5.2 Graphically determined observed rate constants for the racemisation of (*S*,*S*)-2 with catalysts **4** for a range of temperatures (0.1167 mol l-1, 2 mol%)) show that the rate of racemisation is approximately doubled for an increase 10°C; however, the observed rate constant for 70°C is less than expected, considering those obtained at the lower temperatures, which is likely due to the rate of concentration change of (*S*,*S*)-**2** being faster than that which was observed

between the concentration at t = 0, and the first sample that was taken. Using the data in Table 5.2, the activation energy, E_A, and pre-exponential factor, A, were estimated as being 56.8 kJ mol^{-1} and $9.5x10^9$ $l^{1.183}$ $mol^{-1.183}$ s^{-1} respectively from the slope and y-intercept of an Arrhenius plot (Figure 5.6) leading to an expression for the temperature dependency of the observed racemisation rate constant (Equation 5.2).

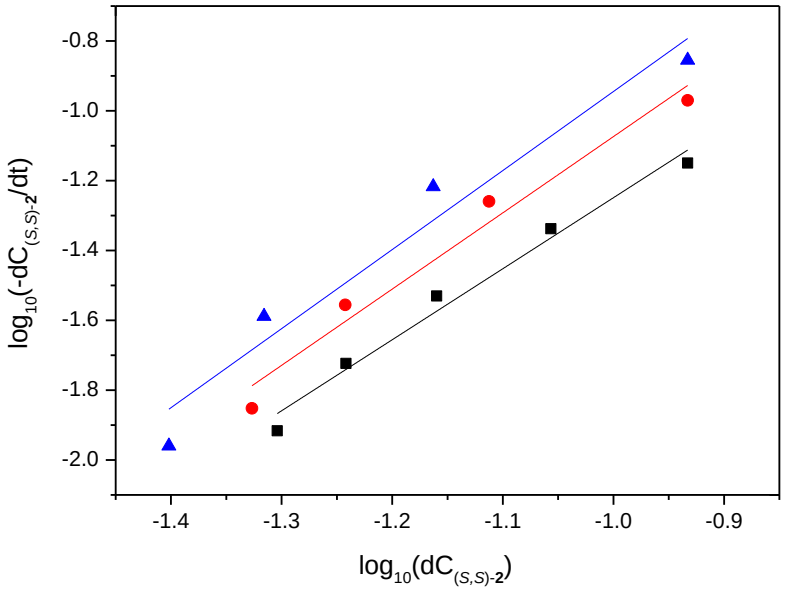

Figure 5.5 $\log_{10}(-dC_{(S,S)\text{-}2}/dt)$ vs. $\log_{10}dC_{(S,S)\text{-}2}$ for the racemisation of (*S*,*S*)-**2** by **4** at ▲ 50°C, ● 60°C and ■ 70°C

Table 5.2 Graphically determined observed rate constants for the racemisation of (*S*,*S*)-**2** with catalysts **4** for a range of temperatures (0.1167 mol l-1, 2 mol%)

	Temperature (°C)		
	50	**60**	**70**
Rate constant, k_{obs} ($l^{1.183}$ $mol^{-1.183}$ s^{-1})	6.097	12.877	20.845

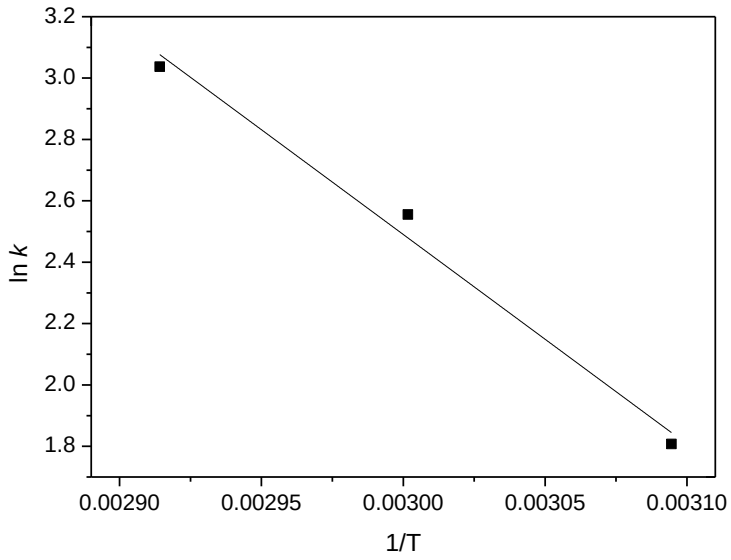

Figure 5.6 Natural log of the observed racemisation rate constant, k_{obs}, vs. 1/T, for the racemisation of (*S*,*S*)-**2** with **4.**

Estimated temperature dependency of the observed rate constant for the racemisation of (*S*,*S*)-**2** by **4**:

$$k_{obs}(T) = A\, e^{\frac{-E_A}{RT}} = 9.523 \times 10^9\, e^{\left(\frac{-56.768}{RT}\right)} \qquad \text{Equation 5.2}$$

5.5.1.3 Catalysts Load

To investigate the dependency on the racemisation rate on the catalyst loading used, racemisation of (*S*,*S*)-**2** was performed with 1, 2 and 4 mol% of **4** (0.117 mol l^{-1}, 60°C) (Figure 5.7). As expected, the time taken for complete racemisation is reduced from 10 to 2 min with catalyst quantity. Examination of the observed rate constants, k_{obs} (Table 5.3), determined using the graphical technique applied previously, shows that the rate is approximately three times as fast when the concentration of the catalyst is doubled. Interestingly, when the racemisation was performed using 4 mol% of **4**, a higher level of benzaldehyde was observed than when lower quantities of **4** were used. Initially it was postulated this could be due to competition between racemisation of (*S*,*S*)-**2** to (*R*,*R*)-**2** / *meso*-**2**, with the C-C cleavage reaction required to form benzaldehyde which may have been promoted by higher catalyst loadings.

However, repeats of these runs did not support this as no trends could be observed between benzaldehyde formation and catalyst load. In fact, the high levels of benzaldehyde seen occurred randomly from sample to sample, with discontinuities observed within the same run (as can be seen in from 5 to 9 min in Figure 5.7). It is therefore likely that, due to the strong chromophore exhibited by benzaldehyde that this was due to analytical deviations whereby small differences in the quantity of benzaldehyde present in each sample gave rise to large difference in the resulting HPLC spectra. Compositional analysis at different wavelengths was attempted yet this was not successful at resolving different components of the racemisation.

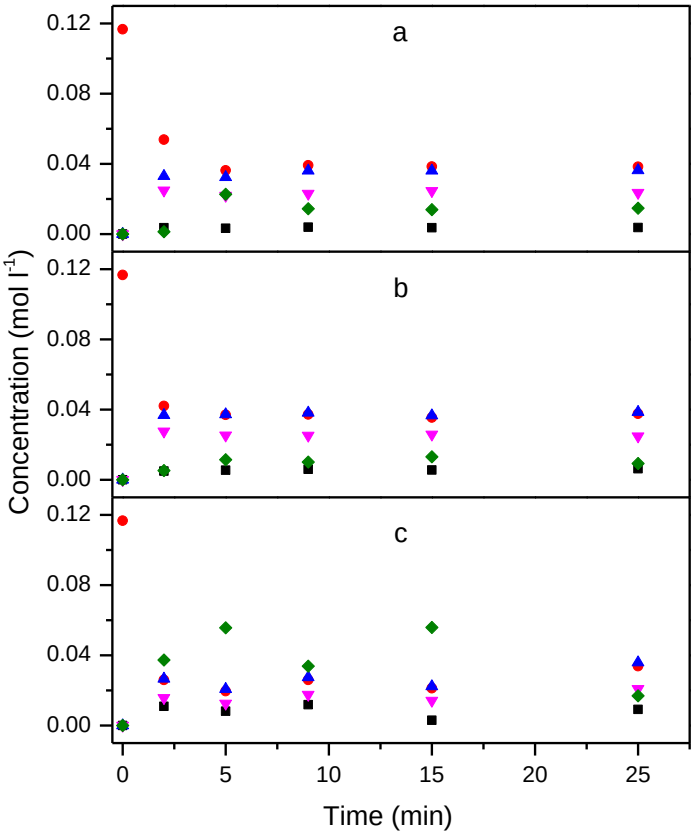

Figure 5.7 Racemisation of (*S*,*S*)-**2** by **4** a) 1 mol% , b) 2 mol% and c) 4 mol% **4** (0.117 mol l^{-1}, 60°C) (■ benzil, ● (*S*,*S*)-**2**, ▲ (*R*,*R*)-**2**, ◆ benzaldehyde, ▼ *meso*-**2**).

Table 5.3 Graphically determined rate constants for the racemisation of (*S*,*S*)-**2** with catalysts **4** for a range catalyst loadings (0.1167 mol l^{-1}, 60°C)

	Catalyst mol%		
	1	**2**	**4**
Rate constant, *k* ($l^{1.183}$ $mol^{-1.183}$ s^{-1})	3.614	12.877	35.156

5.5.2 Chlorocarbonyl-triphenylphosphene(1,2,3,4,5-pentaphenylcyclopentadienyl)-ruthenium(II) (5)

5.5.2.1 Reaction Rate

Figure 5.8 shows the progress of (*S*,*S*)-**2** racemisation by complex **5** (0.117 mol l^{-1}, 2 mol% **5**, 60°C). As with the complex investigated in the previous section, efficient racemisation takes place resulting in the enantiomers of **2** becoming equimolar after ~25 min has elapsed. In addition (*R*,*R*)-**2** and *meso*-**2**, significant quantities of benzil, stilbene and benzaldehyde were also formed. Using the data presented in Figure 5.8, the observed kinetics for the racemisation of (*S*,*S*)-**2** by **5** were estimated using the methodology described in section 5.5.1.1 with the resulting values given in Table 5.4 and plotted in Figure 5.9. The reaction order, *n*, and observed rate constant, k_{obs}, were obtained from the *y*-intercept and slope of the fitted line and estimated to be 0.984 and 1.266 $l^{0.984}$ $mol^{-0.984}$ s^{-1} respectively giving the racemisation rate function for (*S*,*S*)-**2** by **5** (Equation 5.3).

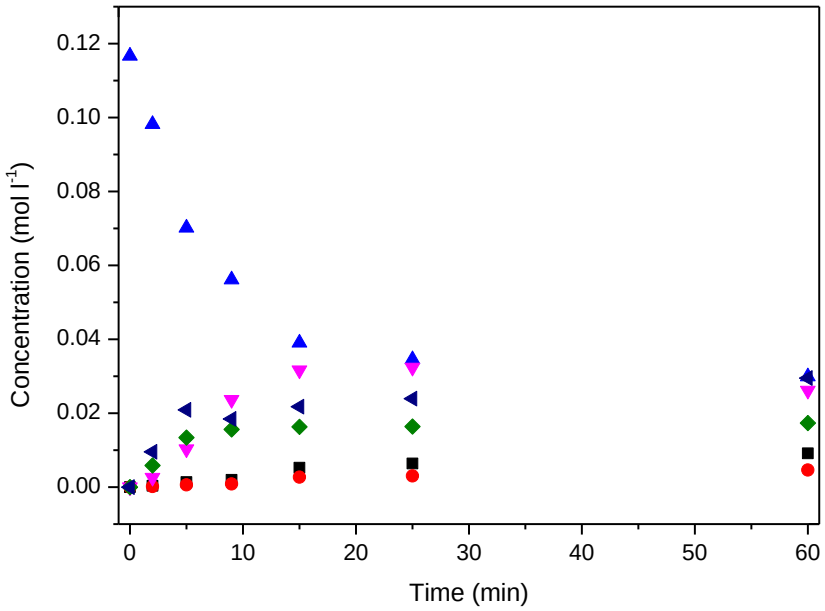

Figure 5.8 Racemisation of (*S*,*S*)-**2** with **5** (0.117 mol l^{-1}, 2 mol% **5**, 60°C) (■ benzil, ● stilbene, ▲ (*S*,*S*)-hydrobenzoin, ▼ (*R*,*R*)-hydrobenzoin, ◀ benzaldehyde, ◆ *meso*-hydrobenzoin)

Table 5.4 Differential analysis of (*S*,*S*)-**2** racemisation with **5** (0.117 mol l-1, 2 mol% **5**, 60°C).

Time (min)	**Concentration (*S*,*S*)-hydrobenzoin ($C_{(S,S\text{-HB})}$) (mol l^{-1})**	**$\log_{10}(C_{(S,S\text{-HB})})$**	**$dC_{(S,S\text{-HB})}/dt$**	**$\log_{10}(-dC_{(S,S\text{-HB})}/dt)$**
0	0.117	-0.933	-0.0164	-1.786
2	0.098	-1.008	-0.0122	-1.914
5	0.070	-1.154	-0.0078	-2.106
9	0.056	-1.251	-0.0044	-2.359
15	0.039	-1.408	-0.0018	-2.742

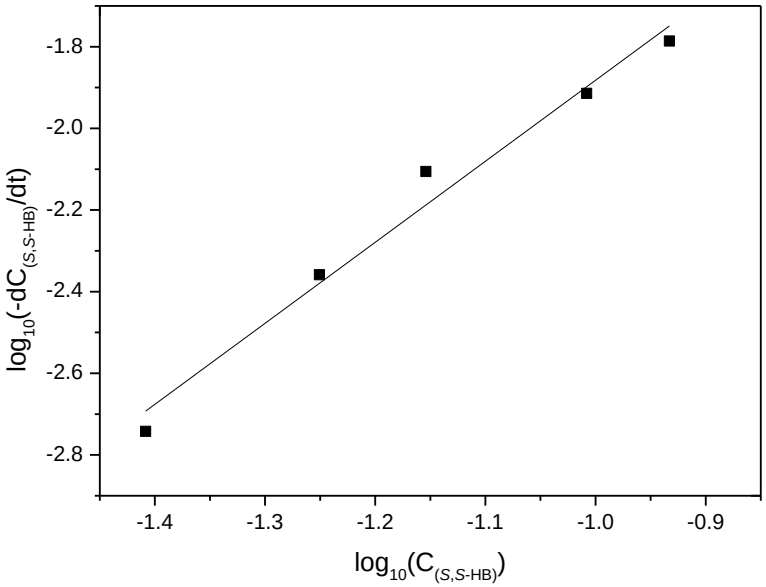

Figure 5.9 $\log_{10}(-dC_{(S,S)\text{-}\mathbf{2}}/dt)$ vs. $\log_{10}dC_{(S,S)\text{-}\mathbf{2}}$ for the racemisation of (*S*,*S*)-**2** by **5.**

Estimated rate function for the racemisation of (*S*,*S*)-**2** by **5**:

$$-r_{(S,S)-\mathbf{2}} = k_{obs}C^{n}_{(S,S)-\mathbf{2}} = \left(1.266\frac{l^{0.984}}{mol^{0.984}\,s}\right)C^{1.984}_{(S,S)-\mathbf{2}}\ mol\ l^{-1}s^{-1} \qquad \text{Equation 5.3}$$

5.5.2.2 Temperature Dependence

Figure 5.10 shows the progress of (*S*,*S*)-**2** racemisation by **5** at 50°C, 60°C and 70°C (0.117 mol l^{-1}, 2 mol% **5**). As expected, the time taken for complete racemisation reduces with an increase in temperature occurring within < 60 min, ~25 min, and ~9 min, at reaction temperatures of 50°C, 60°C and 70°C respectively. The observed kinetics were estimated at the three temperatures examined (Figure 5.11) leading to the rate constants presented in Table 5.5. As the temperature is increased to 60°C and 70°C, the estimated rate is seen to increase by a factor of ~4 and ~6 respectively. Unlike complex **4**, the relative levels of benzaldehyde remain consistently low and do not appear to be influenced by a change in the process temperature. Using the data in Table 5.5

the activation energy, E_A, and pre-exponential factor, A, were estimated as being 146.0 kJ mol^{-1} and $1.2x10^{23}$ $l^{0.984}$ $mol^{-0.984}$ s^{-1} respectively from the slope and *y*-intercept of an Arrhenius plot (Figure 5.12) leading to an expression for the temperature dependency of the observed racemisation rate constant (Equation 5.4).

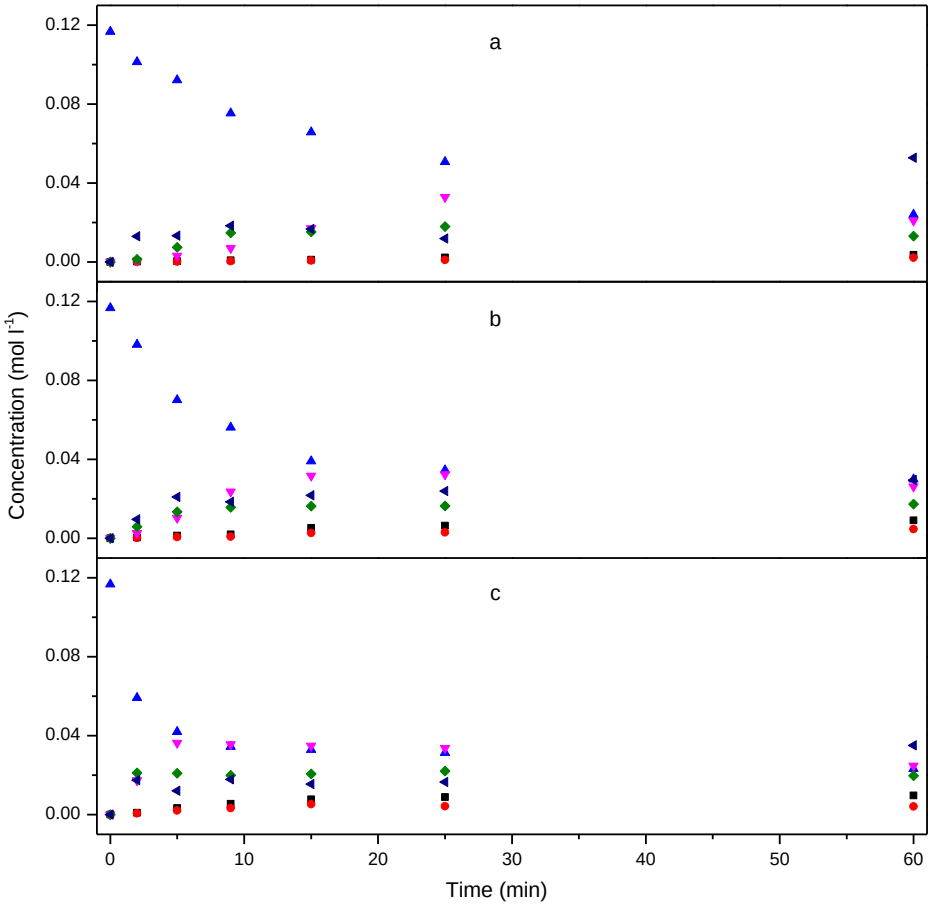

Figure 5.10 Racemisation of (*S*,*S*)-**2** by **5** at a) 50°C, b) 60°C and c) 70°C (0.117 mol l^{-1}, 2 mol% **5**) (■ benzil, ● stilbene, ▲ (*S*,*S*)-hydrobenzoin, ▼(*R*,*R*)-hydrobenzoin, ◀ benzaldehyde, ◆ *meso*-hydrobenzoin).

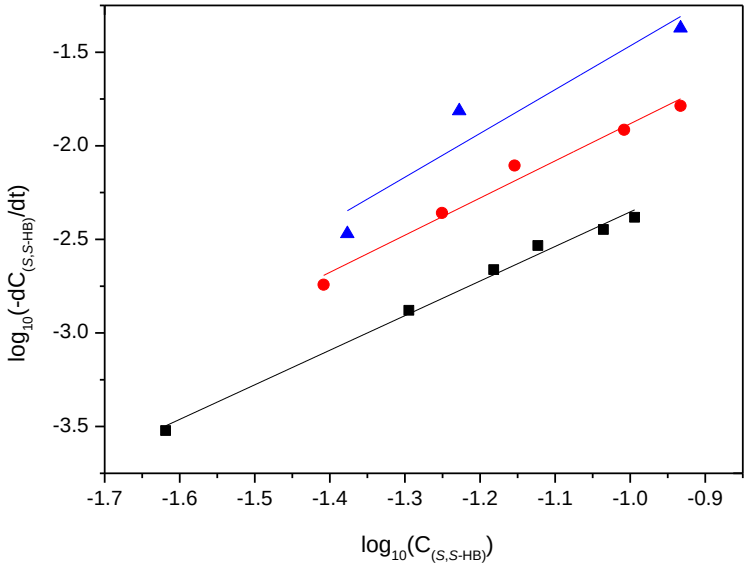

Figure 5.11 $\log_{10}(-dC_{(S,S)\text{-}\mathbf{2}}/dt)$ vs. $\log_{10}dC_{(S,S)\text{-}\mathbf{2}}$ for the racemisation of (*S*,*S*)-**2** by **5**at ▲ 50°C, ● 60°C and ■ 70°C.

Table 5.5 Graphically determined observed rate constants for the racemisation of (*S*,*S*)-**2** with catalysts **5** for a range of temperatures (0.1167 mol l-1, 4 mol% **5**)

	Temperature (°C)		
	50	**60**	**70**
Rate constant, *k* ($l^{0.984}$ $mol^{-0.984}$ s^{-1})	0.312	1.266	7.454

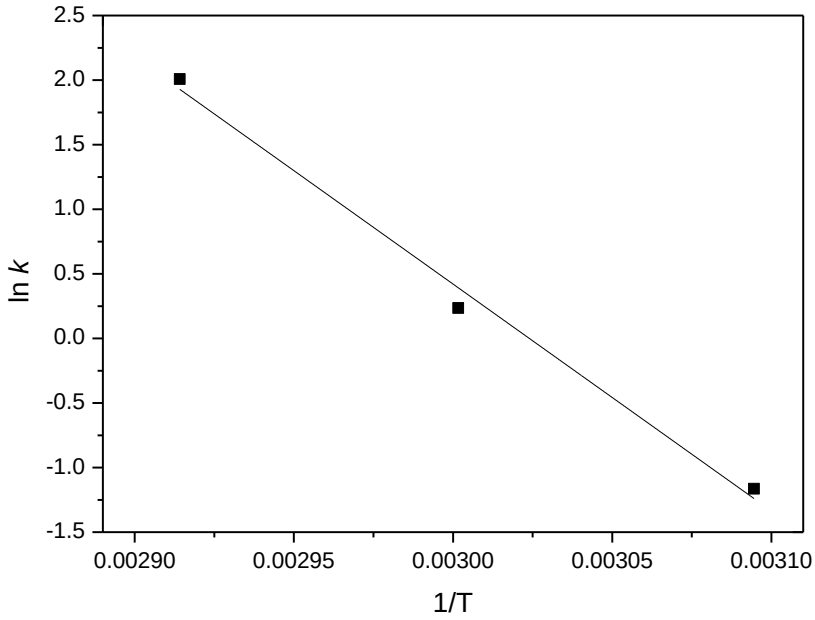

Figure 5.12 Natural log of the observed racemisation rate constant, *k*, vs. 1/T, for the racemisation of (*S*,*S*)-**2** with **5.**

Estimated temperature dependency of the observed rate constant for the racemisation of (*S*,*S*)-**2** by **5**:

$$k_{obs}(T) = A\, e^{\frac{-E_A}{RT}} = 1.170 \times 10^{23}\, e^{\left(\frac{-146036}{RT}\right)} \qquad \text{Equation 5.4}$$

5.5.2.3 Catalyst Load

Racemisation of (*S*,*S*)-**2** was performed with 1, 2 and 4 mol% of **5** (0.117 mol l^{-1}, 60°C) (Figure 5.13). Increasing the catalyst loading resulted in only a slight reduction in the time required for the enantiomers of **2** to become equimolar when 2 and 4 mol% **5** was used. However; unlike complexes **4**, complete racemisation of (*S*,*S*)-**2** was not achieved over the duration of time in which the reaction was monitored when 1 mol% of **5** was used indicating its lower relative activity. The rate constants determined at each catalyst loading (Table 5.6) indicate that the reaction rate is approximately 100% and 25% greater when the quantity of **5** is successively doubled from 1 to 4 mol%. Despite this, efficient

racemisation could still be achieved at => 2 mol% **5** making it a suitable candidate for CIAT.

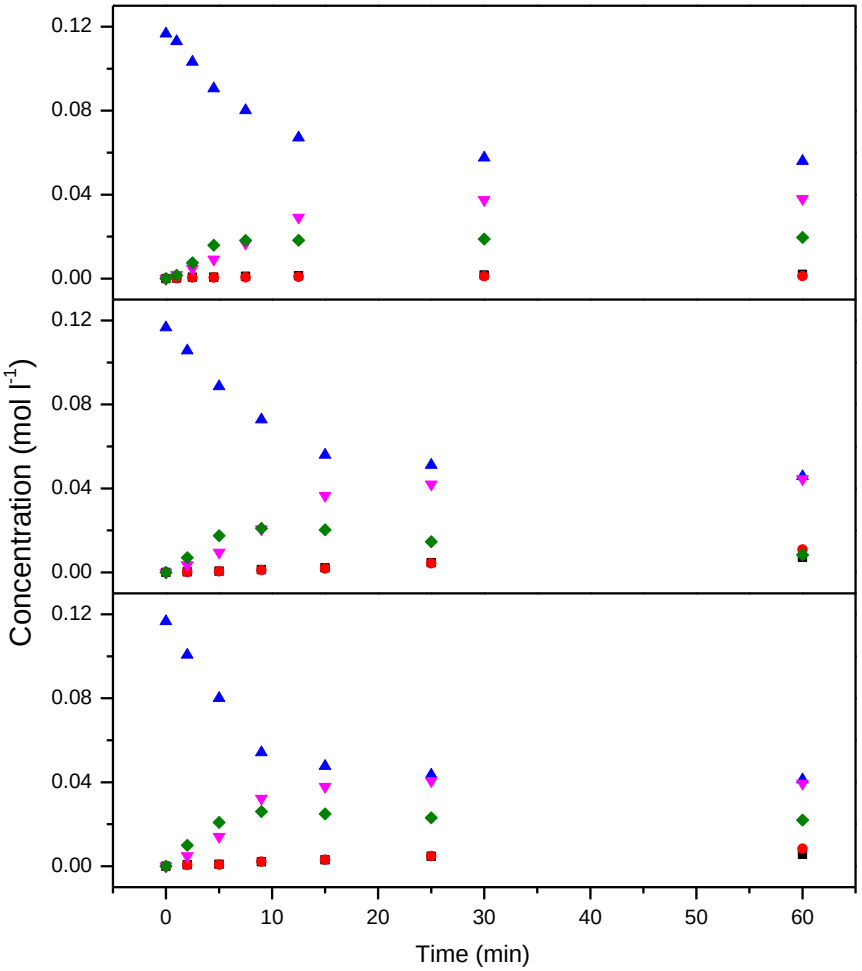

Figure 5.13 Racemisation of (*S*,*S*)-**2** by **5** a) 1 mol% , b) 2 mol% and c) 4 mol% **5** (0.117 mol l^{-1}, 60°C) (■ benzil, ● stilbene, ▲ (*S*,*S*)-hydrobenzoin, ▼(*R*,*R*)-hydrobenzoin, ◀ benzaldehyde, ◆ *meso*-hydrobenzoin).

Table 5.6 Graphically determined rate constants for the racemisation of (*S*.*S*)-**2** with catalysts **5** for a range catalyst loadings (0.1167 mol l-1, 60°C)

	Catalyst mol%		
	1	**2**	**4**
Rate constant, *k* ($l^{0.984}$ $mol^{-0.984}$ s^{-1})	0.494	1.028	1.266

5.5.3 Catalytic Cycle

Due to the structural resemblances of complexes **4** and **5**, and with each requiring base activation, it is likely that racemisation proceeds via similar mechanisms. As an example, the proposed mechanism for the racemisation of (*S*,*S*)-**2** by catalyst **4** is given in Scheme 5.2 to describe the catalytic cycle of the Ru-based complexes investigated.

Activation of the precatalyst **4** occurs via the addition of *t*-BuOK, resulting in loss of the Cl ligand to produce KCl, which in turn leads to the formation of the ruthenium *tert*-butoxide complex **4a**. The *tert*-butoxide group is then exchanged for the chiral diol (*S*,*S*)-**2** forming the *sec*-alkoxide species **4b**. For the next stage of the cycle, moving from **4b** to **4c** or **4d**, two mechanisms have been suggested [157, 158]. **4b** is an $18e^-$ species i.e. it is coordinatively saturated, therefore formation of the η^2-π-coordinated ketone complex via β-hydride elimination is likely to be due to either η^5 to η^3 ring slippage [100, 114], or by loss of a ligand (PPh_3 in this example). Considering complex **4**, the indenyl ligand is known to undergo η^5 to η^3 ring slippage [159] which results from the stabilisation of the benzene ring due to the attainment of full aromaticity; therefore it is possible that **4c** occurs as an intermediate. Ring slippage is less likely for **5**, which instead exhibit a pentaphenylcyclopentadienyl ligand, with recent studies suggesting that β-hydride elimination does in fact occur by ligand loss forming a $16e^-$ species which leaves a vacant coordination site for the hydride [160, 161]. From **4c**/**4d** to **4e**, hydride re-addition from Ru to either side of the planar ketone results in racemisation of the stereogenic centre and formation of the η^1-coordinated ketone complex. This is then exchanged with a molecule of (*S*,*S*)-**2** and the catalytic cycle is repeated.

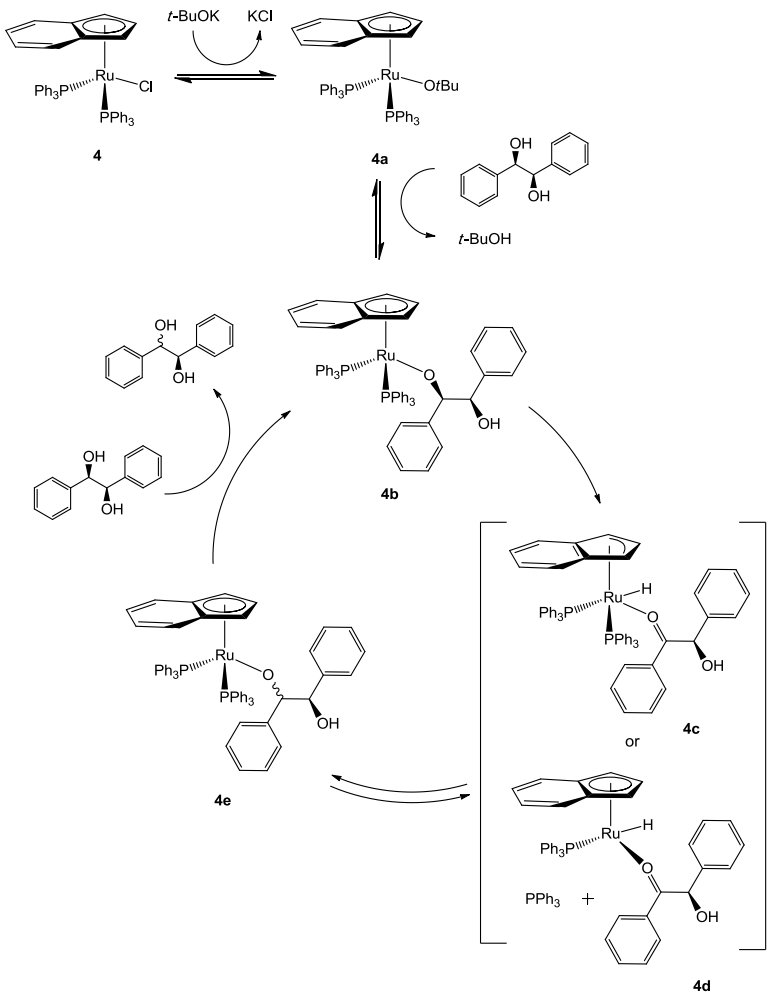

Scheme 5.2 Suggested catalytic cycle for the racemisation of (*S*,*S*)-**2** using complex **4** as an example.

5.6 Chapter Summary

Three ruthenium-based organometallic complexes, chloro(indenyl)-bis-(triphenylphosphine)-ruthenium(II) (**4**), chlorodicarbonyl-(1,2,3,4,5-pentaphenylcyclopentadienyl)-ruthenium(II) (**5**) and chlorocarbonyl-triphenylphosphene(1,2,3,4,5-pentaphenylcyclopentadienyl)-ruthenium(II) (**6**) (results not presented) were investigated for use as racemisation catalysts in the proposed CIAT process with the model enantiomeric compound, hydrobenzoin (**2**), identified in the previous chapter. Racemisation of (*S*,*S*)-**2** was performed using each of the complexes in toluene under a range of different conditions to quantify their rates of reaction and to determine the dependency of these rates on temperature and catalyst loading. Temperature was varied as the proposed CIAT process involves controlled cooling to generate supersaturation of the desired enantiomer therefore it was necessary to identify whether each of the complexes remained active as the temperature is reduced. It was also necessary to investigate the effect of catalyst loading to identify the levels of catalyst that would be required to perform CIAT.

Each of the complexes investigated were shown to efficiently racemise (*S*,*S*)-**2**. **4** was the most active catalyst with complete racemisation occurring within 2 min at temperatures and catalysts loads greater than 60°C and 2 mol% respectively. At the lowest temperature and catalyst loading examined (50°C and 1 mol%) the complex remained highly active allowing for complete racemisation within 5 min highlighting its suitability as a racemisation catalyst for the CIAT process.

5, the only air stable complex investigated, was shown to be the least active of each of the catalysts investigated. At the highest temperature and catalyst loading examined (70°C and 4 mol%) racemisation could be achieved within 9 and 25 min respectively. However, at 50°C (2 mol%) and 1 mol% (60°C) complete racemisation was not observed within the duration of each experimental run (60 min). Despite this, the proportion of by-products formed was relatively low and therefore, if sufficient quantities were used, and the process conditions were tailored to be in favour of racemisation (i.e. slow cooling ramp to allow adequate time for racemisation), being the most robust

catalyst due to its inherent stability, **5** was shown to be a suitable candidate for used as a catalysts in the proposed CIAT process.

6 Hydrobenzoin Crystallisation for CIAT

6.1 Introduction

In developing a preferential crystallisation process for two enantiomers, it is necessary to identify the phase equilibria for the three component system, i.e. both enantiomers and the solute, by constructing the ternary phase diagram which is then used to identify the conditions for the process. For a racemising system however, the ternary phase diagram is modified so that the regions in which the pure solid phase components exists cannot be accessed; hence, for CIAT an alternative approach must be taken.

CIAT involves introducing optically pure seed crystals into a supersaturated solution of racemising enantiomers. Therefore it is essential to identify the solid-solution phase equilibria of the racemate, i.e. the equilibrium and metastable solubility temperatures of the two enantiomers for a range of concentrations allowing for construction of the racemic solubility curve. Using this information, conditions can be selected so that enantiopure crystals will be added to the system whilst it is in the metastable zone. Within this region a thermodynamic driving force for crystallisation exists but, for a homogenous solution free of any foreign matter, spontaneous nucleation will not be observed until a characteristic induction time period has elapsed. However, introducing seeds to the system will lead to selective deposition of solute through seed growth and secondary nuclei formation, since the energy barrier for two-dimensional crystal formation is lower than that which needs to be overcome to form three-dimensional nuclei.

In the previous chapter it was shown that, as a result of possessing two stereogenic centres, racemisation of the selected model conglomerate hydrobenzoin (**2**) with either catalyst **4** or **5** results in the formation of its antipode but also near equivalent quantities of the corresponding meso stereoisomer (small amounts of other reaction intermediates were also observed). Consequently, to determine suitable conditions for CIAT, identifying the equilibrium solubility curve for the racemate of **2** would not have provided

the required information. Instead, it was necessary to determine that of the equilibrated mixture that resulted upon complete catalytic transformation of **2** using catalyst **4** or **5**, **4**-*rac*$_{mix}$-**2** and **5**-*rac*$_{mix}$-**2** respectively.

6.2 Objectives

Conditions for were identified for CIAT of **2** by catalyst **4** and **5** by identifying the crystallisation and dissolution temperatures for the mixtures that resulted upon catalytic conversion in toluene, **4**-*rac*$_{mix}$-**2** and **5**-*rac*$_{mix}$-**2**, as shown in the previous chapter. Doing this for a range of concentrations led to construction of the solubility diagram for each system and hence determination of their MSZW allowing for CIAT conditions to be selected whereby the seed could be entrained in a supersaturated solution of the reaction mixture without spontaneous crystallisation of the undesired species.

In addition to identifying the solid-solution phase equilibria of **4**-*rac*$_{mix}$-**2** and **5**-*rac*$_{mix}$-**2**, enantiopure (*S*,*S*)-**2** and (*R*,*R*)-**2** seed crystals for use in the CIAT process were prepared and characterised.

6.3 Methodology and Equipment

6.3.1 HEL Automate Parallel Vessels

The solubility of **4**-*rac*$_{mix}$-**2** was identified using the HEL Automate reactor system (Figure 6.1) consisting of four 30 ml parallel jacketed glass vessels. Each reactor was equipped with a variable speed agitator, a PT100 thermocouple, a turbidity probe and inlet ports, with the system being fully automated and controlled via HEL WinIso software located on an external PC. Heating and cooling was provided by a Julabo HD oil bath which circulates the heat transfer fluid sequentially through each reactor. Additional heating was supplied by way of an internal hot plate to account for heat loss from the fluid as it is circulated.

The turbidity probes were used to identify the crystallisation and dissolution temperatures. An LED emits a beam of red light through a length of quartz fibre housed within the probe shaft. A mirror at the base of the probe, submerged in the

process solution, reflects the light beam back to a signal converter logging the data. As crystals appear in the solution, the transmission of the light beam is hindered reducing the intensity of the signal. The probe was calibrated by recording the signal produced when submerged in a clear solution and a slurry, allowing this to be used to determine the dissolution and crystallisation temperatures respectively of the system under a prescribed temperature programme.

Figure 6.1 HEL Automate parallel overhead-stirred jacketed reactor system (30 ml scale) used to conduct determine the solubility curve of **4**-*rac*$_{mix}$-**2**.

6.3.2 Crysta16

The solubility of **5**-*rac*$_{mix}$-**2** was identified using the Crystal16 system (due to technical problems that occurred with the turbidity probes on the HEL Automate rig). This consists of 16 parallel 1.3 ml vessels with magnetic stirring, on-line turbidity measurement, and heating provided by way of four independently controlled aluminium blocks

6.3.3 Racemisation Mixture Preparation

The equipment used to determine the solubility of **4**-*rac*$_{mix}$-**2** and **5**-*rac*$_{mix}$-**2** described in the previous sections rely on using optical turbidity analysis to identify the crystallisation and dissolution temperatures. Consequently, to determine these points it is essential that the system being examined permits transmission of the light source when the solution is free of solid. However, when catalyst **4** or **5** was added to **2**, a dark opaque solution resulted through which the incident light was unable to travel (see Figure 7.1 in chapter 7 for an image of the CIAT process solution containing **4**-*rac*$_{mix}$-**2** and **4**). Consequently

it was not possible to determine the solubility of the mixtures with the catalysts present in solution therefore **4** and **5** had to be removed without altering the equilibrated composition.

To prepare material for the solubility measurements, a known quantity of (*S*,*S*)-**2** was first racemised by catalysts **4** and **5** for 1 h in toluene (60°C, 4 mol% catalyst, argon atmosphere for **4**) to yield the equilibrated reaction mixtures **4**-*rac*$_{mix}$-**2** and **5**-*rac*$_{mix}$-**2**. This was then immediately crash cooled to -40°C whilst stirring using a bath of dry ice in isopropanol leading to crystallisation of the mixture. The solids were filtered under vacuum, and washed twice with toluene that had also been cooled to -40°C, which separated the catalyst rich liquor leaving white crystals. After drying for 24 hr, the product was weighed and compared with that of (*S*,*S*)-**2** used at the beginning of the process to determine whether any mass had been lost by remaining dissolved in solution. Due to the low temperatures used to deposit the crystals from solution, in conjunction with the relatively large scales used (~100 g of starting material), negligible losses were observed indicating that there was an insignificant change in the composition of **4**-*rac*$_{mix}$-**2** and **5**-*rac*$_{mix}$-**2**. Furthermore, due to the high solubility of the catalyst in toluene, it was efficiently separated allowing the solubility of the mixture to be determined since it yielded a clear solution upon dissolution.

Figure 6.2 and Figure 6.3 show the chiral HPLC chromatograms for **4**-*rac*$_{mix}$-**2** and **5**-*rac*$_{mix}$-**2** respectively after preparation using the method described. Analysis of the chromatograms shows that for **4**-*rac*$_{mix}$-**2** and **5**-*rac*$_{mix}$-**2** approximately 35% and 33% were comprised of the enantiomers (*S*,*S*)-/(*R*,*R*)-**2** respectively, whilst the remainder consisted of *meso*-**2** with very small amounts of benzaldehyde and some unknown present. Comparison of this data with that presented in chapter 5 shows that there was in fact a slight change in the composition, with the small quantities of benzil and stilbene not being seen. However, since they were present in very low amounts, their effect on the equilibrium solubility temperature of the significantly more dominant enantiomers and meso form would be minimal (although this many have had a minor effect on the crystallisation kinetics). However; this was satisfactory for the investigation leading to it being used for the solubility analysis, and also as a starting material for the subsequent CIAT experiments.

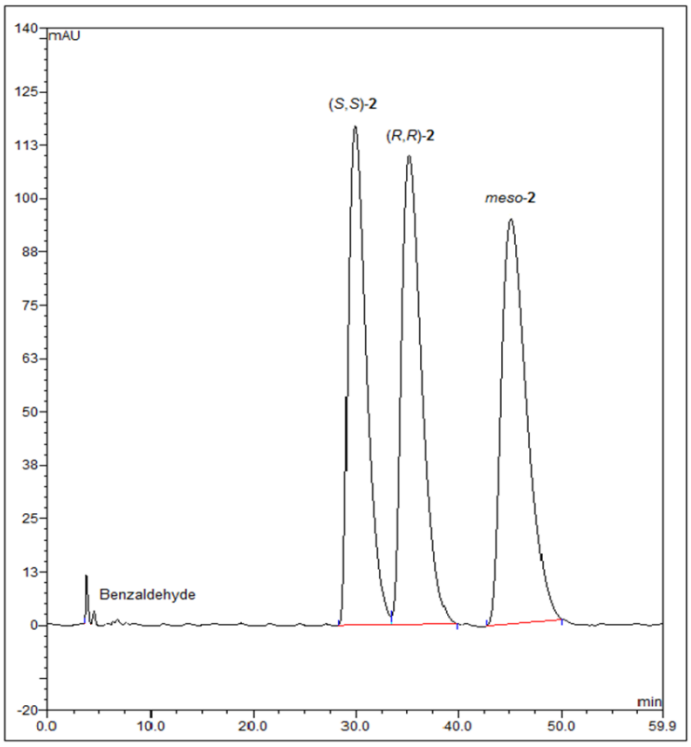

Figure 6.2 Catalyst **4** hydrobenzoin racemisation mixture (**5**-*rac*$_{mix}$-**2)**.with a composition of approximately 35% (*R*,*R*)-/(*S*,*S*)-**2**, 28.5% *meso*-2, 0.5% benzaldehyde and 1% unknown.

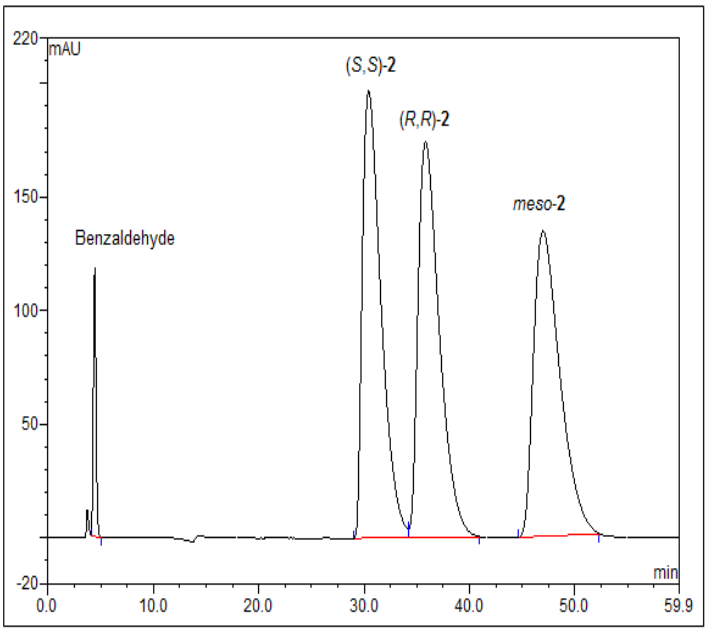

Figure 6.3 Catalyst **5** hydrobenzoin racemisation mixture (**5**-*rac*$_{mix}$-**2**).with a composition of approximately 33% (*R*,*R*)-/(*S*,*S*)-**2**, 31.5% *meso*-**2**, 2% benzaldehyde, 0.5% unknown.

6.3.4 Solubility Measurements

The methodology used for determining the solubility of **4**-*rac*$_{mix}$-**2** and **5**-*rac*$_{mix}$-**2** using both the HEL Automate and Crystal 16 system was identical; however this was performed at differing scales of 30 ml and 1.3 ml respectively. Known quantities of the equilibrated mixtures and toluene were added to the respective vessels and sealed to give a range of concentrations to be examined. A temperature programme was applied which consisted of initially holding the system at least 15°C above the equilibrium saturation temperature (an estimate of which was determined during preliminary runs) for at least 1 h to ensure that no solution phase molecular order remained which would act to influence the crystallisation kinetics by reducing the MSZW. The solution was then cooled at a controlled rate of -0.25°C min^{-1}, -0.5°C min^{-1}, -0.75°C min^{-1} and -1°C min^{-1}, to at least 10°C below the temperature at which crystallisation was observed by the on-line turbidity analysis, where it was held isothermally for a further 1 h to ensure crystallisation was complete so that the solid and solution phases were in equilibrium. Using rates of heating opposite but equal in magnitude to those applied when cooling, the solution temperature was increased to the initial starting temperature and the dissolution point recorded.

The cycle of controlled cooling and heating was repeated a number of times to obtain average values for the crystallisation and dissolution temperatures as a function of cooling rate. This data was then plotted, linearly fitted, and extrapolated to a theoretical cooling rate of 0°C min^{-1}, i.e. an infinitely slow rate thus eliminating the influence of the rate of temperature change on the crystallisation and dissolution temperatures, yielding the true equilibrium and metastable solubility temperatures for a given concentration which allowed the solubility diagram to be constructed (section 6.4).

6.3.5 Seed Preparation

To prepare the seed crystals used in the CIAT experiments, (*S*,*S*)-**2** was dissolved in toluene and held isothermally for 1 h to ensure that no solution phase order remained. This was then left to cool to room temperature resulting in deposition of the solute which was subsequently filtered, washed twice with

toluene, and dried. To minimise the possibility of impurities being present in the solid, the recrystallisation procedure described was repeated 5 times and the resulting liquor discarded. On the final run, after holding the solution isothermally it was crash cooled to -40°C whilst stirring using a bath of dry ice in isopropanol yielding very fine crystals which were filtered and washed twice with room temperature toluene. By cooling to this temperature at such a fast rate, the aim was to produce small crystals with an even CSD and hence a large surface area as it was postulated that this would lead to higher rates of selective solute removal during CIAT which, in turn, would result in the undesired species being transformed by the action of the catalyst at a quicker rate therefore lowering their concentrations in solution which would reduce the likelihood of them reaching their metastable limits and crystallising. By washing the filtered crystals with room temperature toluene, the aim was to give a smooth surface on the seed crystals so that any high energy sites were reduced, and also to dissolve any micro-nuclei since the presence of either could have potentially acted as nucleation sites for the undesired species during CIAT. The seed crystals obtained were analysed using chiral HPLC and DSC to ensure enantio-purity, the results being presented in section 6.5.

6.3.6 Solvent Selection

As mentioned in chapter 5, toluene was earmarked to be the process solvent for the CIAT investigation as it was known to be inert to the catalytic process for a number of different organometallic complexes. In preliminary runs, it was also shown to be suitable for crystallisation of **2** and its enantiomers allowing a sufficient quantity to be dissolved upon heating which was readily deposited when cooled.

6.4 Hydrobenzoin Solubility in Toluene

6.4.1 Chloro(indenyl)-bis-(triphenylphosphine)-ruthenium(II) (4) Racemisation Mixture (4-*rac*$_{mix}$-2) in Toluene

Table 6.1 gives the average observed crystallisation and dissolution temperatures, T_{Cryst} and T_{Diss} respectively, as a function of cooling rate for a range of **4**-*rac*$_{mix}$-**2** concentrations in toluene which were determined by turbidimetric measurements using the HEL Automate parallel reactor system (see section 11.5 for raw data). Using this information, for each concentration T_{Cryst} and T_{Diss} were plotted against cooling rate and fitted with a linear trend line which was extrapolated to a cooling rate of 0°C min^{-1} to give the equilibrium and metastable solubility temperatures allowing the MSZW for a given concentration to be identified (Figure 6.4).

As discussed in the methodology section, the rate of cooling affects the observed temperatures T_{Cryst} and T_{Diss} as a result of the kinetics of each process. For T_{cryst}, examination of the values presented in Table 6.1 and their corresponding plots in Figure 6.4, show that for a given concentration the observed crystallisation temperature is inversely proportional to the cooling rate.

To deposit crystals from a solution, it is first necessary to create a thermodynamic driving force, either by cooling or through evaporation of solvent, which leads to the solution becoming supersaturated i.e. the system exists away from equilibrium between the solid and solution phases since there is more solute dissolved than the solution can accommodate. However, instantaneous crystallisation is not observed as soon as supersaturation is achieved since nuclei of a critical radius, r_c, must first be formed which consist of three-dimensional clusters of molecules for whom the rates of molecular addition and molecular dissolution are equivalent. In order for the clusters to grow, the critical free energy barrier ΔG_{crit}, must be overcome which subsequently leads to a reduction the total free energy of the system and hence the formation of thermodynamically stable macroscopic crystals (see section 2.3 for a more detailed discussion). Therefore in short, crystallisation is governed by the kinetics of critical nuclei formation, and the necessity for these nuclei to reach a size at which they become stable (which in turn are influenced by the characteristics of the system).

When supersaturation is generated by continuously cooling a solution (or by solvent removal), the degree of sub-cooling reduces the critical nuclei radius lowering the crystallisation energy barrier, whilst the rate at which this occurs determines the crystallisation temperature (assuming the solution is truly homogeneous) since sufficient time is required for the formation of critical nuclei through solute-solute addition. Therefore, as the rate of cooling is increased, crystallisation is observed at lower temperatures with the relationship between the two being linear as can be seen in Figure 6.4. Conversely, reducing the rate of cooling results in an increase in the crystallisation temperature to a point where the rate cannot be lowered any further, i.e. infinitely slow cooling, which corresponds to the true thermodynamic crystallisation temperature or, more precisely, the metastable solubility temperature.

Figure 6.4 shows that for each concentration examined, the dissolution temperature was seen to increase linearly with cooling rate. For dissolution to occur, the solvent surrounding each crystal must be undersaturated so that mass can be transferred from the solid surface into the solution phase, which is dependent on the magnitude of interaction between the solute and solvent, i.e. the enthalpy of mixing that results, the entropy change associated with the phase change, the surface energy of a given crystal face, and the system temperature. Since no thermodynamic barrier exists, dissolution would be expected as soon as the solution becomes undersaturated; however, in practice this is also seen to have a dependency on the rate of heating which the system experiences and is also affected by to crystal size.

As crystal size is reduced, the ratio of molecules in contact with the solution relative to those in the bulk is increased hence the observed rate of mass transfer is also increased i.e. for two populations of crystals with the same total mass but different sizes, those that are smaller will dissolve first since there is less mass per crystal despite the kinetics of molecular mass transfer for the two populations being identical. Below a certain size threshold, the comparatively high surface to volume ratio results in high surface energies leading to a solvent being able to dissolve more solute than is observed at the macroscopic scale hence the observed equilibrium solubility is increased. For macroscopic crystals of the same size, as the cooling rate is increased, dissolution is seen to occur at

higher temperatures as shown in Figure 6.4 since there is insufficient time for the entire crystal mass to be transferred into the solution phase; however, due to the lack of thermodynamic energy barrier, less of a temperature rate change dependency is seen for dissolution temperatures compared with those for crystallisation.

For similar reasons, less variability is seen for the observed dissolution temperatures as is shown by the size of the standard error displayed in Figure 6.4. Despite being thermodynamically favourable, the formation of critical nuclei is governed by the likelihood of a group of molecules in solution colliding and ordering together in a cluster. This results in a probability distribution with time for a given set of conditions which therefore leads to a certain degree of variation in crystallisation temperature. On the other hand, since the observed rate is simply a result of crystal size, with no barrier hindering the process, little variation is seen in the temperature at which dissolution occurs.

Using the data presented in Figure 6.4, the equilibrium and metastable solubility temperatures, and hence the MZSW, were obtained at a zero cooling rate (see Table 6.2 for values). As would be expected, the temperature at which these occur increases with solution concentration since the amount of solute a solvent can accommodate is determined by the system temperature as described by the free energy change for the solubility process. It is also evident that the MSZW, i.e. the difference between the equilibrium and metastable solubility temperature within which the system is supersaturated but instantaneous homogeneous crystallisation does not take place, becomes narrower as concentration is increased. From a molecular perspective, at a higher solution concentration there is a greater likely hood of successful clustering due to the increased collision frequency. Furthermore, the critical nuclei size is reduced with temperature so the critical free energy barrier to crystallisation is lower. Therefore, for a higher concentration and hence higher temperature, upon generation of supersaturation, crystallisation is observed to occur sooner which leads to the MSZW being reduced.

Figure 6.5 shows the solubility curve for **4**-*rac*$_{mix}$-**2** which was constructed by plotting the equilibrium and metastable solubility temperatures (obtained from Figure 6.4) against their corresponding solution concentrations which gives light

to the trends described above. As predicted by the van't Hof expression, these show a clear exponential relationship illustrating that the magnitude of dissolution becomes more sensitive as the temperature increases, whilst the MSZW becomes increasingly narrower. Figure 6.5 was used as a basis to select the seeding conditions during the CIAT experiments for **2** by catalyst **4** presented in chapter 7. In order to grow the seed, temperatures had to be selected for a given concentration which resulted in the system being within the MSZW so that a driving force for crystallisation existed. As will be seen in chapter 7, in some of the isothermal CIAT runs, sub-cooling beyond the metastable limit was possible so long as the rate of cooling was sufficient to widen the MSZW. For the polythermal temperature programmes utilised during CIAT, due to the longer run times potentially leading to the nucleation induction time being achieved, attempts were made to allow the system to stay as close to the equilibrium solubility curve as possible to minimise the chance of spontaneous nucleation occurring.

Through close examination of Figure 6.5, it is evident that upon extrapolation to higher concentrations, the solubility and metastability curves would be expected to intersect at which point the MSZW = 0°C and hence $T_{Cryst} = T_{Diss}$, whilst continuing beyond this point T_{Cryst} would be seen to be greater than T_{Diss} which is clearly impossible since no crystallisation driving force would exist above the equilibrium solubility temperature. Although a reduction in MSZW would be anticipated as temperature is increased, due to the reduction in the nuclei critical radius, this observation is likely due to experimental issues which occurred whilst the data was being obtained. For the higher concentration data, examination of the interior of the vessel at the end of the runs revealed that when the temperature was reduced beyond the metastable limit, unavoidable crystallisation occurred on the agitator above the solution level. Consequently, since some of the solute was no longer in contact with the solution, the temperature at which dissolution was seen to occur was reduced as there was less solute to dissolve. Therefore at higher concentrations (> 0.4 mol l^{-1}) it is likely that the equilibrium solubility temperature has been underestimated. However, despite this all CIAT runs were performed well below this concentration and, furthermore, the CIAT experiments were not preceded by crystallisation which would have resulted in solute depositing on the agitator.

Table 6.1 Average crystallisation (cloud point), T_{Cryst}, and dissolution (clear point), T_{Diss}, temperatures for the hydrobenzoin racemisation mixture, obtained using catalyst **4** (**4**-*rac*$_{mix}$-**2**), in toluene (see section 11.5 for raw data).

Cooling rate (°C min^{-1})	**Concentration (mol l^{-1})**					
	0.0467		**0.117**		**0.233**	
	T_{Cryst}	T_{Diss}	T_{Cryst}	T_{Diss}	T_{Cryst}	T_{Diss}
0.25	7.8	24.2	22.4	36.1	36.2	44.5
0.5	5.4	24.6	21.3	38.0	32.5	49.4
0.75	3.8	25.1	20.6	40.9	30.7	50.1
1	2.4	25.4	16.9	41.0	27.2	51.3

Cooling rate (°C min^{-1})	**Concentration (mol l^{-1})**			
	0.350		**0.467**	
	T_{Cryst}	T_{Diss}	T_{Cryst}	T_{Diss}
0.25	45.1	52.5	49.7	55.9
0.5	38.5	54.9	47.2	58.4
0.75	36.1	54.8	43.1	57.9
1	34.4	58.2	40.8	62.2

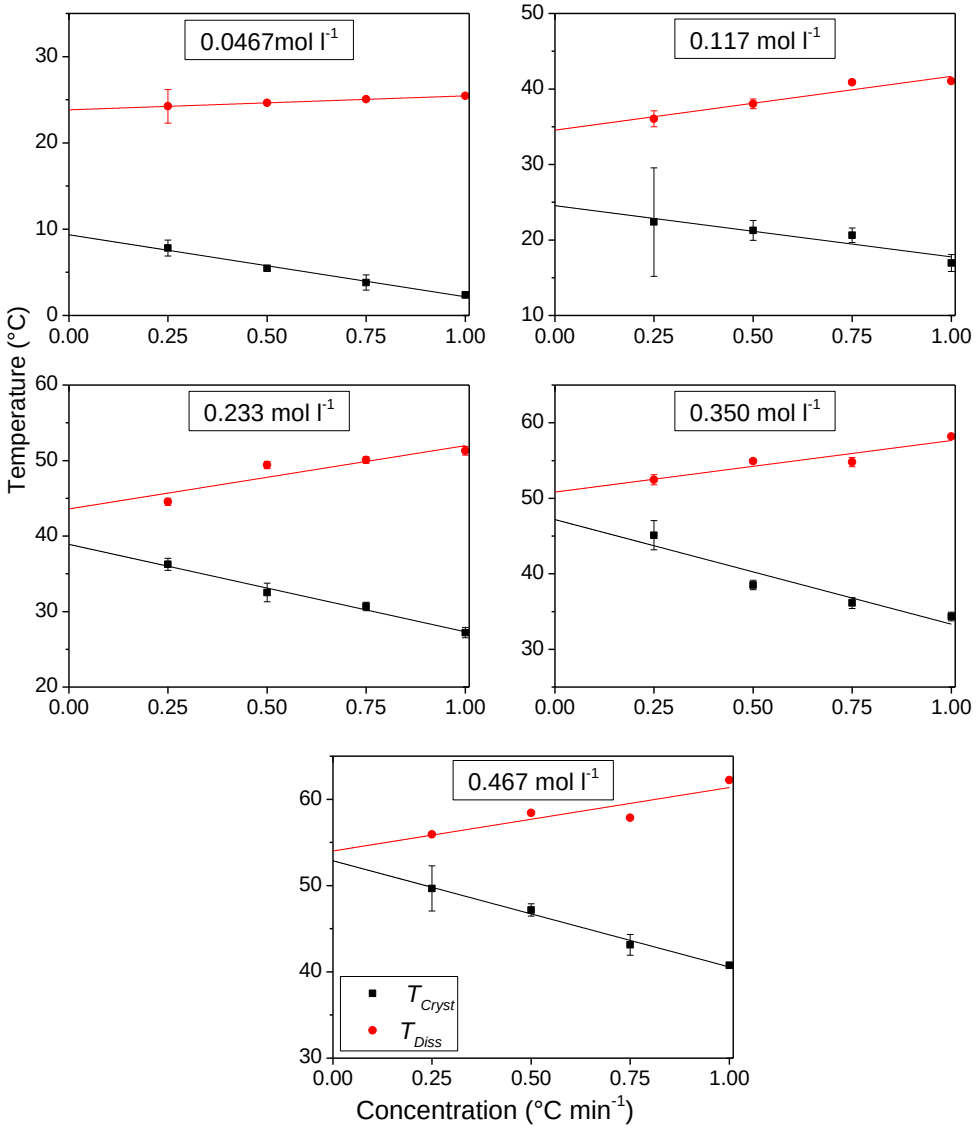

Figure 6.4 Average crystallisation, T_{cryst}, and dissolution, T_{Diss}, temperatures vs. cooling rate for five concentrations of **4**-*rac*$_{mix}$-**2** in toluene.

Table 6.2 Equilibrium and metastable solubility temperatures for **4**-*rac*$_{mix}$-**2** in toluene obtained from the data given in Figure 6.4

Concentration (mol l^{-1})	**Equilibrium Solubility Temperature (°C)**	**Metastable Solubility Temperature (°C)**	**Metastable Zone Width (°C)**
0.0467	23.8	9.4	14.5
0.117	34.5	24.5	10.0
0.233	43.6	38.9	4.7
0.350	50.8	47.2	3.6
0.467	54.0	52.9	1.1

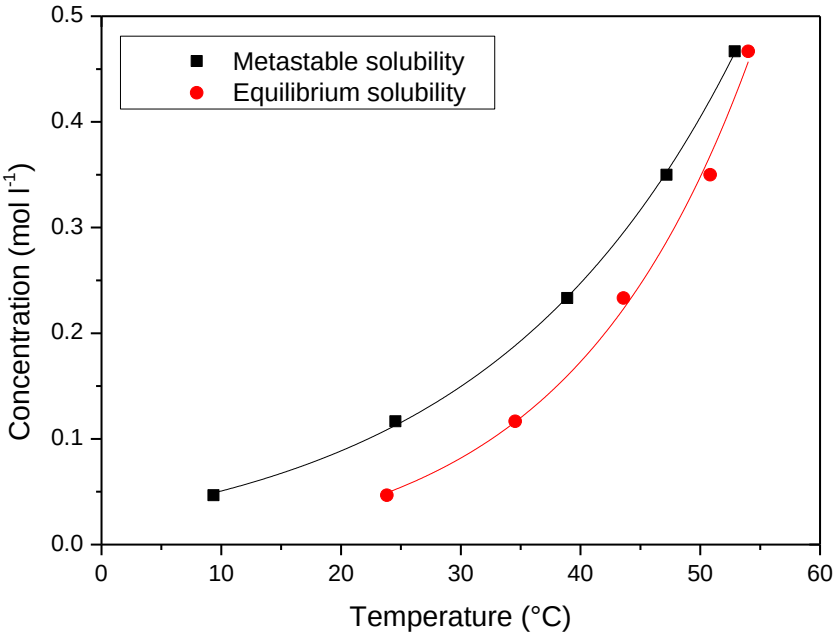

Figure 6.5 Solubility diagram for **4**-*rac*$_{mix}$-**2** in toluene.

6.4.2 Chlorocarbonyl-triphenylphosphene(1,2,3,4,5-pentaphenylcyclopentadienyl)-ruthenium(II) (5) racemisation mixture (5-*rac*$_{mix}$-2) in toluene

Table 6.3 gives the average observed crystallisation and dissolution temperatures, T_{Cryst} and T_{Diss} respectively, as a function of cooling rate for a range of **5**-*rac*$_{mix}$-**2** concentrations in toluene which were determined by turbidimetric measurements using the Crystal16 parallel reactor system (see section 11.7.1 for raw data). Using this information, for each concentration T_{Cryst} and T_{Diss} were plotted against cooling rate and fitted with a linear trend line which was extrapolated to a cooling rate of 0°C min^{-1} to give the equilibrium and metastable solubility temperatures allowing the MSZW for a given concentration to be identified (Figure 6.4).

Through comparison of the solubility data presented for **5**-*rac*$_{mix}$-**2** with that of **4**-*rac*$_{mix}$-**2**, it is evident that the same characteristic solution crystallisation relationships exists which were discussed in the previous section. However; it is apparent that there is a greater variability in the **5**-*rac*$_{mix}$-**2** data as is shown by

the size of the standard error bars in Figure 6.4, the magnitude of which being larger at lower concentrations.

This can attributed to the scale at which the solubility measurements were determined. **5**-*rac*$_{mix}$-**2** solubility was determined using a 1.3 ml scale solution with the Crystal16 system, whereas **4**-*rac*$_{mix}$-**2** was at 30 ml using the HEL Automate. As previously discussed, in a supersaturated solution a probability distribution exists for nuclei formation with time. Essentially, the 30 ml scale experiments for **4**-*rac*$_{mix}$-**2** can be approximated as being 23 1.3 ml volumes; therefore, there are 23 volumes within which nucleation will result in the entire solution crystallising. Hence, for the 30 ml scale the probability distribution for nucleation occurring within any of the volume elements becomes cumulative so that the variability is reduced with scale [162]. It can be seen in Figure 6.4 that the variability also appears to be more significant at lower concentrations. As mentioned previously, to form critical nuclei it is necessary for an ordered cluster to form through successful bi-molecular collisions. At low concentrations, the frequency of these collisions is reduced therefore more variation would be expected in the crystallisation temperatures.

Figure 6.7 shows the solubility curve for **5**-*rac*$_{mix}$-**2** which was constructed by plotting the equilibrium and metastable solubility temperatures (obtained from Figure 6.5) against their corresponding solution concentrations. As with **5**-*rac*$_{mix}$-**2**, the solubility curve was used to identify the conditions for CIAT of **2** using catalyst **5** presented in chapter 7. However; the greater variability seen in the crystallisation temperatures, and hence the larger MSZW, had to be considered when selecting seeding temperatures.

Table 6.3 Average crystallisation (cloud point), T_{Cryst}, and dissolution (clear point), T_{Diss}, temperatures for the hydrobenzoin racemisation mixture, obtained using catalyst **5** (**5**-*rac*$_{mix}$-**2**), in toluene.

Cooling rate (°C min^{-1})	Concentration (mol l^{-1})			
	0.078		0.155	
	T_{Cryst}	T_{Diss}	T_{Cryst}	T_{Diss}
0.25	11.2	32.3	24.0	43.7
0.5	12.9	32.3	20.9	43.9
0.75	6.9	32.8	18.3	44.4
1	4.8	33.1	16.1	44.9

Cooling rate (°C min^{-1})	Concentration (mol l^{-1})			
	0.233		0.311	
	T_{Cryst}	T_{Diss}	T_{Cryst}	T_{Diss}
0.25	29.3	47.0	34.5	50.8
0.5	27.3	48.1	30.4	50.9
0.75	23.5	48.5	24.4	51.2
1	20.8	48.9	23.1	51.7

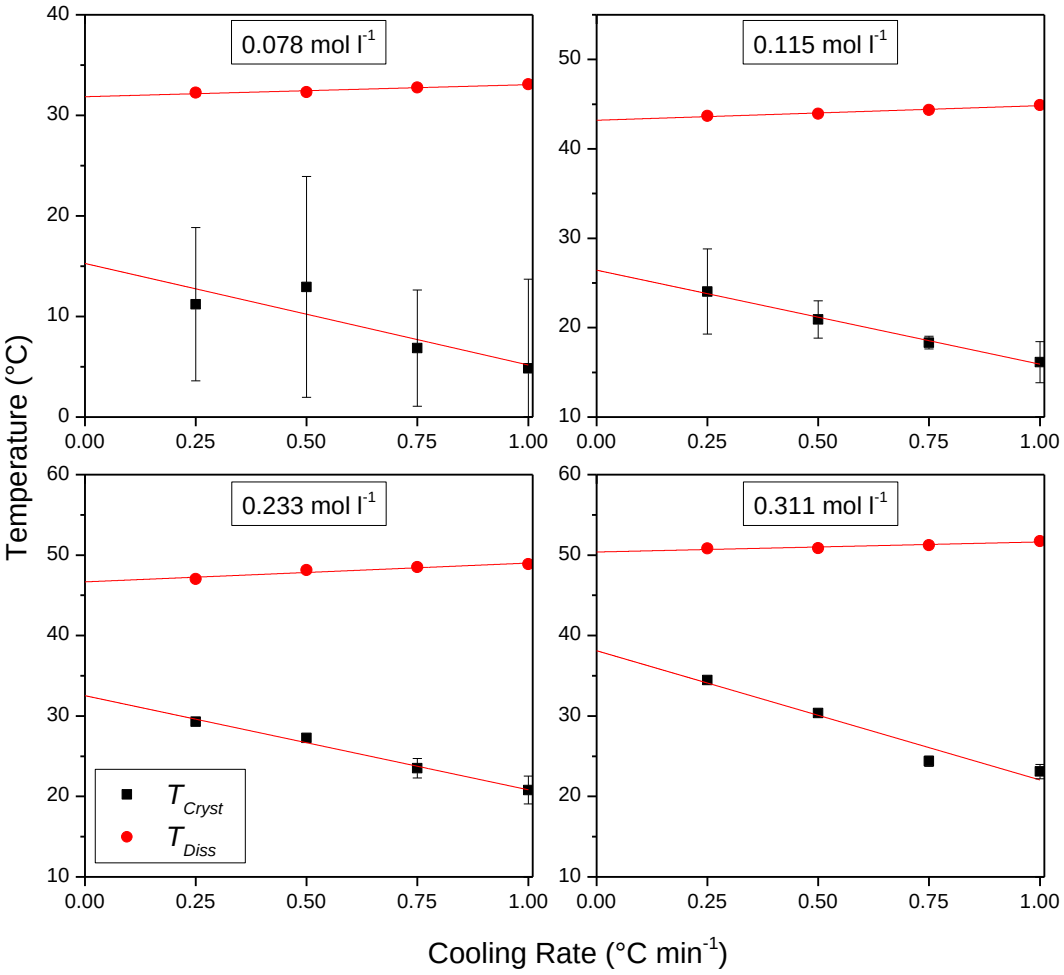

Figure 6.6 Crystallisation, T_{cryst}, and dissolution, T_{Diss}, temperatures vs. cooling rate for four concentrations of **5**-*rac*$_{mix}$-**2** in toluene

Table 6.4 Equilibrium and metastable solubility temperatures for **5**-*rac*$_{mix}$-**2** in toluene obtained from the data given in

Concentration (mol l^{-1})	Equilibrium Solubility Temperature (°C)	Metastable Solubility Temperature (°C)	Metastable Zone Width (°C)
0.078	31.9	15.3	16.6
0.155	43.2	26.4	16.8
0.233	46.7	32.5	14.1
0.311	50.4	38.1	12.3

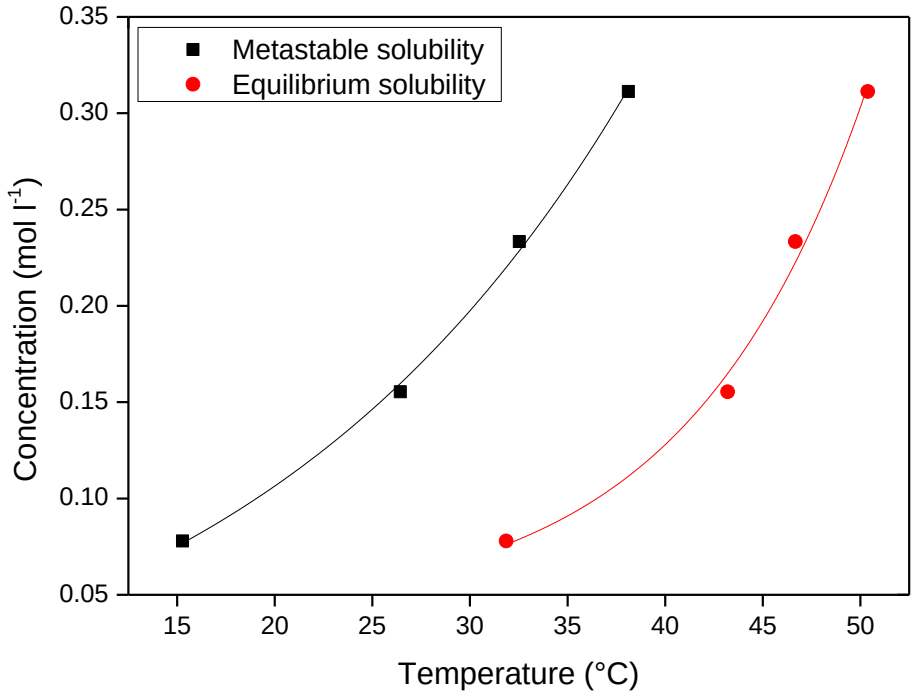

Figure 6.7 Solubility diagram for **5**-*rac*$_{mix}$-**2** in toluene

6.5 Seed Characterisation

Seed crystals for CIAT were prepared using the methodology outlined in section 6.3.5. As a result of their equivalent solubilities, it was essential to show that the counter enantiomer and meso forms of **2** were absent from the seed crystals since their presence during CIAT would increase the likelihood of them

crystallising since the energy barrier is lower for two-dimensional crystallisation compared with that of three-dimensional nuclei formation.

Figure 6.8 shows the chiral HPLC chromatogram for the (SS)-2 seed crystals prepared for CIAT. It is evident that, using the prescribed methodology, a high enantiomeric purity was obtained. Based on peak area the seed crystals were shown to be composed of > 99% (*S*,*S*)-**2** with the remainder being attributed to benzaldehyde and an unknown species which could not be identified. Despite many recrystallisations, it was not possible to completely eliminate these impurities; however, as shown by the chiral HPLC chromatograms for **4**-*rac*$_{mix}$-**2** and **4**-*rac*$_{mix}$-**2**, the mixtures are predominantly composed of the two enantiomers and meso form of with low levels of other reaction by-products (Figure 6.2 and Figure 6.3). Since the latter were present in low quantities, it was anticipated that their concentrations would not permit them to reach supersaturation under the conditions used to perform CIAT. Furthermore, since the seed crystals did not contain any (*R*,*R*)-**2**, which being the antipode exhibits the same solubility and hence would be supersaturated during CIAT, it was concluded that a composition > 99% (*S*,*S*)-**2** was sufficient for the CIAT experiments.

To complement the chiral HPLC analysis, the DSC and ^{1}H-NMR spectra for the (*S*,*S*)-**2** seed crystals were also identified (see section 11.2.2 for ^{1}H-NMR). Analysis of the DSC curve in Figure 6.9 shows that a peak occurs at 148.47°C which corresponds to the pure enantiomer melting point. Furthermore, its sharp nature combined with a lack of any other peaks at lower temperature backs the findings of the HPLC analysis. Similar conclusion can be drawn from the ^{1}H-NMR spectra; however, due to the higher sensitive of the technique, some peaks with negligible intensities relative to that generated by (*S*,*S*)-**2** can be observed which can be attributed to the < 1% impurities identified by chiral HPLC. Figure 6.10 shows a microscope image of the (*S*,*S*)-**2** seed crystals illustrating their elongated plate-like like habit which is often a characteristic feature of non-centrosymmetric chiral crystals. Particle size analysis was also performed using an imaging technique however the results of which are not presented.

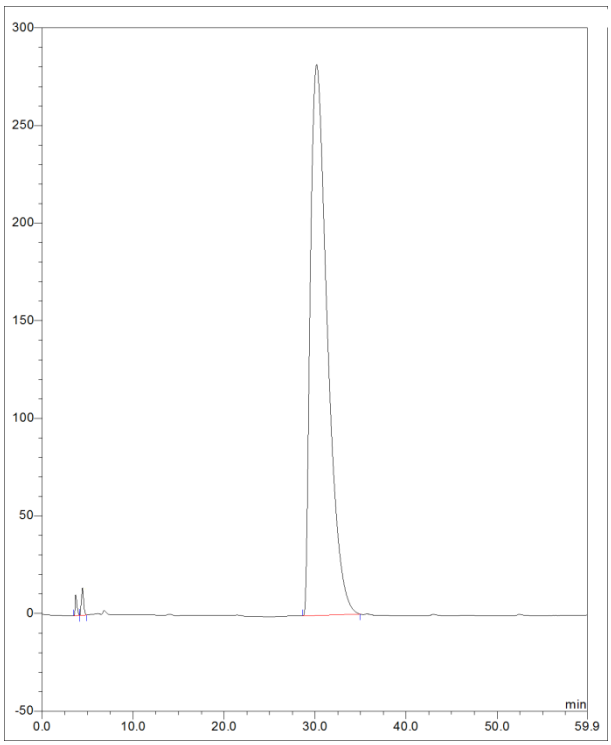

Figure 6.8 Chiral HPLC chromatogram for (*S*,*S*)-**2** seed crystals.

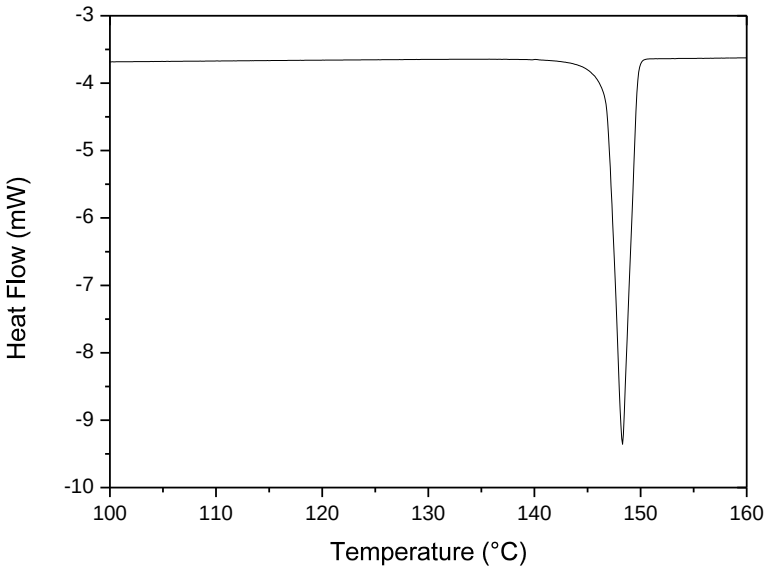

Figure 6.9 DSC spectra for the (*S*,*S*)-**2** seed crystals.

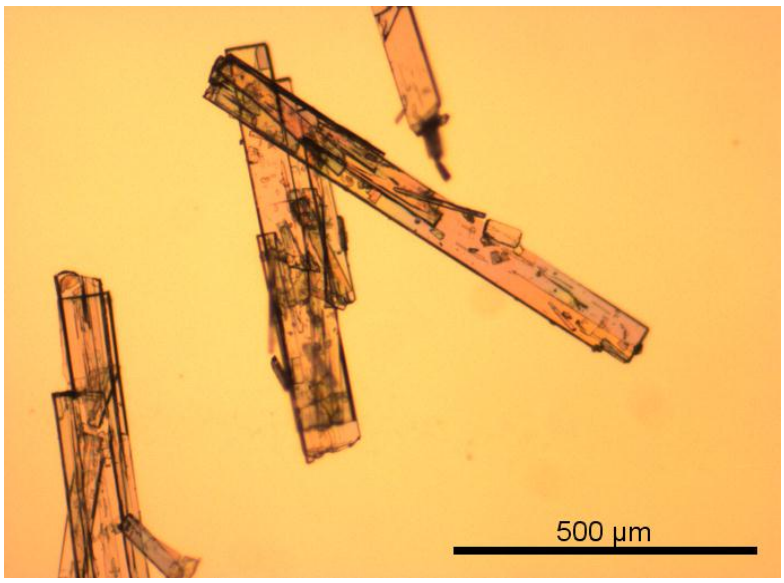

Figure 6.10 (*S*,*S*)-**2** seed crystals.

6.6 Chapter Summary

As the proposed CIAT process involves seeding an supersaturated solution of equilibrated **2** stereoisomers, for which the presence of two chiral centres yields both the enantiomers (*S*,*S*)-**2** / (*R*,*R*)-**2** and the corresponding diastereomer *meso*-**2**, it was necessary to determine the solubility and MSZW of the mixtures that resulted upon catalytic transformation of **2** by catalysts **4** and **5** in the selected process solvent toluene, **4**-*rac*$_{mix}$-**2** and **5**-*rac*$_{mix}$-**2**, to identify the conditions under which CIAT would be performed.

For a range of concentrations of **4**-*rac*$_{mix}$-**2** and **5**-*rac*$_{mix}$-**2** in toluene, the crystallisation and dissolution temperatures were identified by turbidimetric analysis under varying cooling rates. Using this information, the equilibrium and metastable solubility temperatures were obtained from the data extrapolated to a zero cooling rate allowing the MSZW to be determined. This yielded the solubility curves for both **4**-*rac*$_{mix}$-**2** and **5**-*rac*$_{mix}$-**2** which were used as a basis to select the seeding conditions used during the CIAT experiments. Due to differences in the scales of the equipment used to identify the solubility of each mixture, with **4**-*rac*$_{mix}$-**2** being determined using a 30 ml solution volume and **5**-*rac*$_{mix}$-**2** using 1.3 ml of solution, significantly more variation was seen in the crystallisation temperatures of the latter despite the collection of a greater number of data points, which had to be considered when designing the experiments for CIAT of **2** using catalyst **5**.

In addition to solubility measurements, the methodology used to prepare the seed crystals used in the CIAT investigation was also presented and justified. Characterisation data for the (*S*,*S*)-**2** seed showed that it exhibited > 99% purity with no (*R*,*R*)-**2** or *meso*-**2** present; however, < 1% benzaldehyde and an unknown species were shown to be present which could not be eliminated despite many attempts.

7 Crystallisation-Induced Asymmetric Transformation (CIAT) using Racemisation Catalysts

7.1 Introduction

Crystallisation-Induced Asymmetric Transformation (CIAT) is a method of obtaining a single enantiomer from an initially racemic mixture of a conglomerate forming chiral system. Establishing a dynamic equilibrium between two stereoisomers in a supersaturated solution, and subsequently seeding with pure crystals of the desired enantiomer, leads to enatioselective growth whilst the undesired antipode remains dissolved in solution. Removal of the seeded enantiomer from solution through growth and secondary nucleation results in the composition becoming non-racemic which, in turn, causes the excess enantiomer to racemise thus re-forming an equimolar mixture and re-establishing solution phase equilibrium. If the rate of racemisation is sufficiently fast and exceeds that of crystallisation the ternary phase equilibria is modified so that the regions of the phase diagram where a given enantiomer is in excess cannot be accessed. Therefore, the solution phase remains observably racemic whilst the desired enantiomer is crystallised with the antipode remaining dissolved and being readily converted; hence, a quantitative yield of a single enantiomer can theoretically be achieved if the process is operated to completion.

Previous examples of CIAT demonstrated in the literature (see section 3.4.1) have all utilised asymmetric molecules whose chiral centres are easily racemised typically due to the presence of low pKa chiral protons which are liable to be removed by the addition of base to the process solution. Once dehydrogenated, a planar intermediate results (ketones and imines for alcohols and amines respectively) which is subsequently non-selectively rehydrogenated reducing optical activity and eventually leading to the formation of a racemate. Due to racemisation by this method being system specific, in addition to the prerequisite of conglomerate formation (~10% of chiral compounds), the application of CIAT has remained underutilised for the industrial scale production of single enantiomers from synthesised racemates.

7.2 Objectives

Using the information presented in the previous chapters, it was possible to move forward and perform the primary investigation into the possibility of coupling solution phase organometallic catalysed racemisation with preferential crystallisation in a CIAT process. CIAT was attempted using the model chiral system **2**, and the three ruthenium-based complexes **4**, **5** and **6** (results for **6** not presented), under a range of different process conditions, based on the racemisation mixture–toluene phase equilibria, to initially attempt to identify the key parameters that result in only a single enantiomer being produced, and to ultimately try to identify the optimum operating conditions under which the maximum quantity of the desired enantiomer could be obtained. The parameters varied during the investigation were selected due to their fundamental influence on the success of preferential crystallisations, whilst also considering the combined effect of in-*situ* solution phase racemisation with variable rates. In the following sub-sections, the general procedure used for each CIAT experiment is outlined and the parameters varied discussed.

7.2.1 General Methodology

CIAT Equipment: The CIAT experiments were performed using the HEL Automate reactor system described in section 6.3.1. CIAT runs for catalysts **4** were performed under an inert atmosphere using argon supplied by an external gas cylinder.

*Procedure for CIAT of **2** using racemisation catalysts **4***: A prescribed quantity of the racemisation mixture (see section 6.3.3 for preparation details and section 7.2.2.2 for quantities of each mixture used) and base (*t*BuOK or KOH for activation of the catalyst) was added to the glass automate vessel. The reactor head was lowered and sealed after which the vessel was purged with argon through an airtight port for 1 h followed by the addition of 30 ml of dry toluene by syringe to form the initial process slurry. The prescribed temperature programme was then applied (see section 7.2.2.1 for details) which for all runs began by heating the reactor contents to the maximum temperature, T_{max}, whilst

stirring for 1 h to ensure complete dissolution of the racemisation mixture and base. At the end of the isothermal stage, catalyst **4** was added to the vessel and the contents cooled after which seed crystals of (*S*,*S*)- or (*R*,*R*)-**2** were added at the seed temperature, T_{seed}, which was selected to be in proximity to the saturation temperature of the racemisation mixture, T_{sat}. In some of the runs performed the racemisation catalyst was introduced after the addition of seed crystals at T_{seed} which allowed for a prescribed initial excess of the desired enantiomer to be added to the reactor at the beginning of the process (since any excess enantiomer would be racemised in the unsaturated solution where the catalyst was added prior to seed at temperatures above T_{sat}). With the seed crystals and catalyst present in the vessel, the temperature programme was applied, either consisted of maintaining a constant temperature for a period of time, cooling, or cycling the temperature of the reactor to induced growth of the seed crystals. Once complete, the vessel contents was immediately filtered at the final temperature, T_{filt}, yielding a solid which was washed twice with chilled toluene and dried under vacuum to give crystals of the final product.

*Procedure for CIAT of **2** using racemisation catalyst **5***: The same procedure described for catalyst **4** was used; however, since **5** is known to be air stable it was not necessary to perform the experiments under inert conditions.

Process Analysis: The dried samples obtained at the end of CIAT runs were weighed and analysed using chiral HPLC to determine the stereoisomeric composition. In some instances PXRD was used to determine the diffraction pattern of the samples which was compared with that of the enantiopure seed material. Due to the dark colour that resulted upon addition of the catalyst to the solution (Figure 7.1), it was not possible to monitor the progress of the experimental runs using online-analytical techniques such as FBRM, turbidity or polarimetry.

Figure 7.1 HEL Automate reactor vessel illustrating the dark colour solution that resulted upon addition of catalysts **4** and **5** to substrate **2** which prevented the use of on-line analytical techniques

7.2.2 Significant Process Parameters

Using the methodology given above, several experimental conditions were varied or were of significance to the investigation and had to be considered:

- Cooling programme
- Seed conditions
- Catalyst load
- Solution concentration
- Stirring rate

These are discussed at greater depth in the following sub-sections. Precise details of the conditions used for each run are presented with the corresponding results in tables from section 7.3 onwards.

7.2.2.1 Cooling Programme and Seeding Conditions

As a result of the competition between the enantio-selective crystallisation rate, i.e. the rate removal of the desired enantiomer from solution, and the racemisation rate, i.e. the rate at which it is replaced, investigation of the optimum cooling programme and seeding conditions was perhaps the most

important attribute of the CIAT process which needed to be investigated. Ideally, the racemisation rate would be sufficiently fast to allow the solution phase stereoisomers to remain equilibrated whilst the desired enantiomer is crystallised from solution. In doing so, equimolar quantities of each enantiomer would be maintained in solution which would minimise the chance of the undesired enantiomer spontaneously nucleating as long as the system remained far from the metastable solubility limit. As the racemisation rate becomes slower relative to that of crystallisation, there is the possibility that the antipode's concentration relative to the seeded enantiomer would increase in solution until eventually it would reach its metastable limit, with the rate at which this occurs increasing with the difference between the observed kinetics of racemisation and crystallisation.

As shown in chapter 5, the racemisation rate using each of the catalysts investigated is favoured by a high temperature. Conversely, in chapter 6, as expected the likelihood of spontaneous nucleation was shown to increase with higher temperatures as the MSZW becomes smaller. Therefore, considering temperature alone, the most favourable conditions would be a compromise whereby the temperature invokes a sufficient rate of racemisation whilst allowing the solution to remain metastable, ideally close to equilibrium between the solid and liquid phases so that the driving force for crystallisation is low but maintained. It is also necessary that the increase in racemisation time that results upon cooling of the solution is also accounted for when the temperature profile is applied.

In conjunction with CIAT process temperature, the seeding regime i.e. the position within the temperature programme at which the enantiopure seed crystals are introduced to the system, is also of key importance to the success of the proposed process. Seeding an enantiomeric system has the benefit that the enantiopure crystals are half as soluble as the racemate therefore a certain quantity can be introduced above the racemic saturation temperature, T_{sat}, with the degree of dissolution occurring being determined by the ternary phase equilibria. For CIAT however, the racemisation catalyst is present therefore addition and subsequent partial dissolution of enantiopure seed above T_{sat} would result in the solution deviating from a racemic composition which, in turn,

would lead to racemisation of the excess enantiomer and dissolution of double the amount seed compare with preferential crystallisation. On the other hand, if the seed crystals were introduced below T_{sat}, i.e. whilst the solution is metastable, the chance of spontaneous nucleation is increased due to the presence of the seed lowering the energy barrier to crystal formation. Consequently, theory would suggest that seeding temperatures should be selected to be close to but below T_{sat}.

In practice, for polythermal CIAT cooling programmes, the seed could be introduced above T_{sat} as long as a sufficient quantity was used to offset the effects of the ternary phase equilibria so that some enantiopure solid would remain after racemisation of the excess in solution occurred. However; the doubling of solubility that would occur upon racemisation would have to be considered when prescribing the seed quantity and temperature. Despite this, the loss in solid would of course be compensated for by the selective crystallisation that would result upon cooling and reestablishment of a driving force. For isothermal cooling programmes however, whereby the system temperature remains constant after addition of seed, the quantity of desired solute that could be recovered and hence the success of CIAT (for a single stage process), is determined by how far below T_{sat} the system can be seeded without inducing crystallisation of the antipode.

Several different temperature programmes and seeding regimes were trialled during the CIAT study, due to the anticipated effects described above and as a result of experiences during the investigation, aiming to provide conditions that favoured growth of the seeded enantiomer and racemisation kinetics whilst also minimising the possibility of spontaneous crystallisation of the antipode. Figure 7.2 shows a qualitative representation of the different temperature programmes used consisting of isothermal (**a**) and polythermal (**b**, **c** and **d**) temperature profiles.

Considering Figure 7.2**a**, initially the pre-prepared racemisation mixture and base required for catalyst activation were dissolved in toluene and held at T_{max} for a minimum of 1 h to ensure complete dissolution. T_{max} was selected to be at least 15°C above the saturation temperature of the racemisation mixture to ensure that upon dissolution no liquid phase order remained which could have

resulted in the crystallisation kinetics being affected due to the MSZW potentially being reduced. At the end of T_{max}, the racemisation catalyst was added to the system and the solution cooled to T_{seed}, where the enantiopure seed crystals were introduced into the system, either under a prescribed cooling rate or by crash cooling. The latter condition was chosen as it was postulated that the likelihood of spontaneous crystallisation of the antipode is partly a function of the time that the system is metastable. Hence, it may be favourable to achieve the desired level of supersaturation, i.e. T_{seed}, at the fastest rate possible in order to maximise the period of time that the seed crystal spend suspended in solution. After allowing crystallisation of the seed to proceed for a period of time by both growth and secondary nucleation, the solution was filtered at T_{filt} (where for the isothermal program $T_{cryst} = T_{filt}$) to yield the product crystals which were washed and dried using the procedure described in section 7.2.1.

The polythermal temperature programme depicted in Figure 7.2**b** is an extension of **a** where instead of filtering the crystals at the end of the isothermal section of the profile, the solution temperature is reduced under a controlled cooling rate. Assuming the rate of racemisation is sufficiently fast, enough time has elapsed, and the antipode has not reached its metastable limit and crystallised, at the end of the isotherm the system should consist of a racemic solution in equilibrium with enantiopure solid. By subsequently cooling the resulting slurry, a driving force for crystallisation will be induced therefore a greater quantity of solute can theoretically be obtained as the solubility is reduced as the temperature is lowered. To allow for the solution phase to remain as close to racemic as possible during the process, a slow cooling rate would be most favourable as the rate at which solute is removed would be minimised. Temperature programme **b** was applied using a range of different cooling rates and different seed temperatures, T_{seed}, with the slurry being filtered as soon as T_{filt} was achieved.

For the scenario where the rate of racemisation was thought to become too slow to maintain an observably racemic solution during cooling, the temperature program illustrated in Figure 7.2**c** was utilised. Instead of continuously reducing the temperature to T_{filt}, the programme consisted of alternating between cooling

and constant temperature stages. After addition of the seed crystals, the system temperature was reduced by a small amount and subsequently held constant for a period of time. The hypothesis was that lowering the temperature would generate supersaturation inducing crystallisation of the desired form; however, not to the degree that the antipode would reach its metastable limit as a result of the difference in relative concentrations of the two enantiomers in solution becoming significant. Subsequently maintaining the temperature would inhibit the system becoming increasingly supersaturated, allowing time for crystallisation to reach equilibrium and for racemisation to proceed to re-establish a racemic composition in solution.

The final cooling programme investigated, shown in Figure 7.2**d**, was proposed for the event where the relative rates of racemisation and seeded crystallisation were unfavourable and resulted in spontaneous crystallisation of the undesired enantiomer. This consisted of crash cooling the seeded system followed by a period of heating to just below T_{sat}, at which point a constant temperature was maintained. The cycle of crash cooling, heating and constant temperature was then repeated with the minimum and maximum temperatures in each cycle being gradually reduced until T_{filt} was achieved which corresponded to the end of the maximum constant temperature stage of the last cycle. Considering the first cycle, initially a driving force is created when the system is crash cooled resulting in crystallisation of the seeded enantiomer; however, as a result of the slow relative racemisation rate, crystallisation of the antipode is also eventually observed. By increasing the temperature as soon as the minimum is achieved, the magnitude of supersaturation is reduced and hence the rate of crystallisation of the undesired enantiomer (and that of the desired) decreases. The system is heated to and held at a point in close proximity but below T_{sat} resulting dissolution of the predominately racemic portion leaving only the pure enantiomer as the solid phase, and racemisation of any excess, with the quantity of desired solute yielded from solution corresponding to the difference between T_{sat} and the constant temperature stage of the current cycle. Thus, in theory repeating this cycle until T_{filt}, should yield enantiopure crystals where the racemisation rate is too slow to allow utilisation of a constant cooling rate.

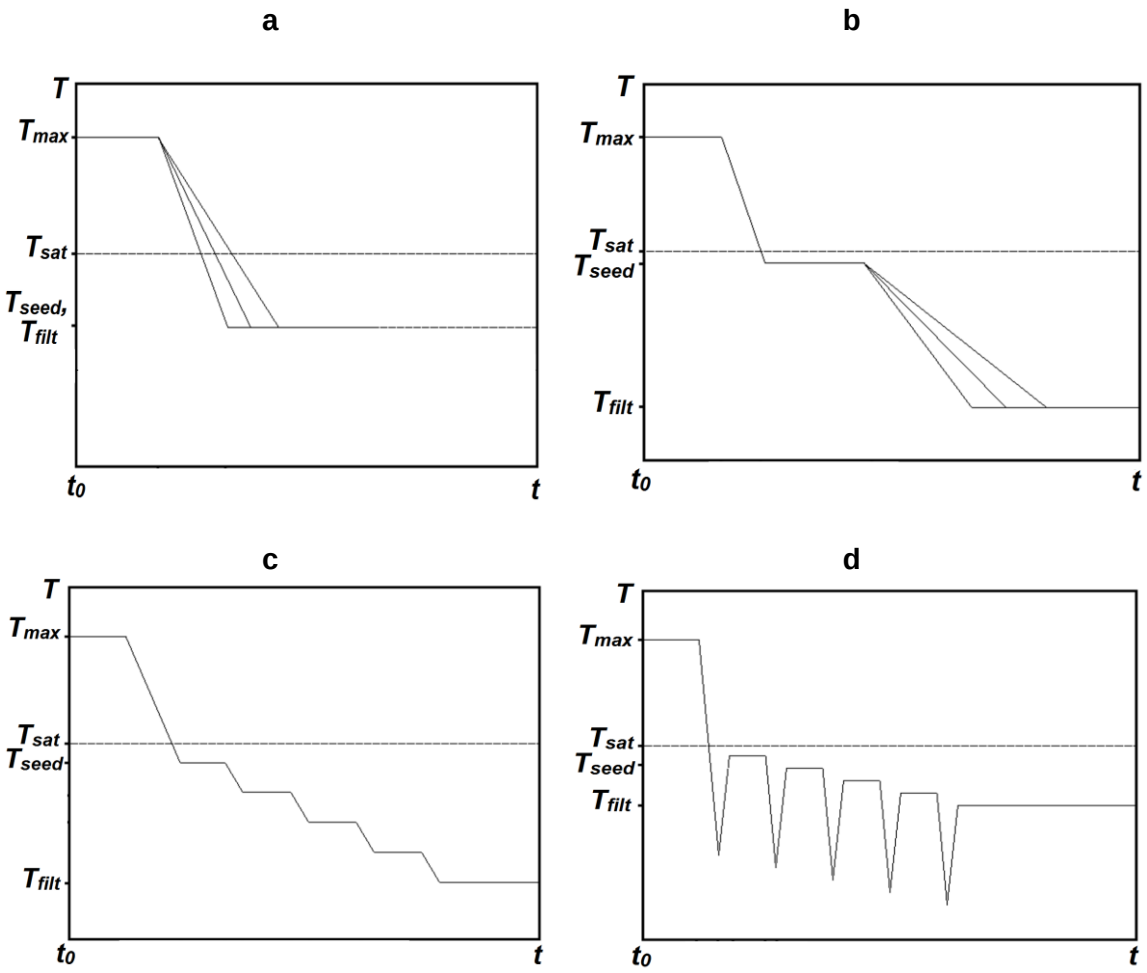

Figure 7.2 Graphical representation of the cooling profiles used for the CIAT experiments.

7.2.2.2 Solution Concentration

Since the MSZW is reduced with an increase in temperature, the concentration of the racemisation mixture used will influence the period of time the solution can remain metastable during enantio-selective crystallisation. Ideally a relatively low concentration would be used as this would result in a large MSZW; however, this would compromise the rate of racemisation increasing the likelihood of the antipode spontaneously crystallising due to a build-up of its concentration, and hence its supersaturation, relative to the desired enantiomer. Conversely, a high concentration would enhance the probability of spontaneous nucleation occurring, despite the faster racemisation kinetics, as the frequency of the molecular collisions required for crystal formation would increase. Therefore the choice of racemisation mixture concentration used is a compromise between these conflicting conditions and, consequently, the results

for runs using two different concentrations are presented to investigate these effects.

7.2.2.3 Seed Mass

As with the seeding regime, the quantity of seed used during the proposed CIAT process could have a significant influence over its success. It is postulated that the quantity of seed required is primarily influenced by a combination of the racemisation kinetics and the temperature programme used. For a seeded crystallisation, remaining within the MSZW will always result in spontaneous crystallisation after the induction time period has elapsed. Therefore for CIAT, to prevent antipode crystallisation in the case of a slow racemisation rate, it is favourable that the process is operated in the shortest time possible or as close to solid-liquid equilibrium as allowable whilst still maintaining a crystallisation driving force and maximising product yield.

In this scenario, use of a small quantity of seed would supply a comparatively small area for enantio-selective crystallisation hence reducing the rate at which solute is removed from solution; therefore the system would remain close to equilibrium and the relative difference in concentration between the enantiomers in solution as the process progresses would be low and effectively compensated for by the action of the racemisation catalyst. It is thus also necessary in this case to use a temperature profile which keeps the system close to equilibrium and prevent excessive build-up of supersaturation. If large volumes of seed were to be used, solute would be removed at a much faster rate due to the larger surface area provided, and as the racemisation rate would not be sufficient to minimise the excessive build-up of the antipodes relative concentration, it would reach its metastable limit much sooner.

For the case of relatively fast racemisation kinetics, it is possible to remove the desired enantiomer from solution at a much faster rate since it is efficiently replaced by the catalyst; therefore much larger volumes of seed could be used. This could be particularly useful when applying an isothermal temperature programme since, under these conditions, for the same T_{sat} the rate of crystallisation would be dictated by the surface area provided hence larger

quantities of seed should result in shorter process runs for a given solid yield which in turn would reduce the chance of the antipodes induction time being achieved. As a result of the different conditions investigated, several different quantities of seed crystals were used during the study.

7.2.2.4 Catalyst Load

The rate of racemisation is perhaps the most significant parameter influencing the success of the proposed CIAT process since it has a direct impact on each of the process parameters described. For the reasons already discussed, it is essential that that the racemisation kinetics are sufficiently fast to allow for efficient in-*situ* conversion of the waste enantiomer whilst the antipode remains dissolved. Not considering the effect of temperature on racemisation kinetics (which was previously discussed), it would therefore seem logical to use large quantities of catalyst to maximise the rate; however, there are several issues concerning this approach.

It is vital that the catalyst remains dissolved for the duration of the process since, if it were to crystallise, it could potentially act as a crystallisation centre for the enantiomers as a result of the presence of a solid surface lowering the nucleation energy barrier. In preliminary investigations however, it was shown that each of the catalysts used were sufficiently soluble in the earmarked process solvent toluene with approximately 0.2 g being dissolved in 1 ml of solvent at room temperature. Despite this, each of the catalysts required activation by excess base in the form of KOH which is considerably less soluble (< 1 mg ml^{-1}) which was thus a limiting factor in the quantity of catalysts that could be employed to prevent any solid being present during the process (several alternative bases were investigated for use with the catalysts, for which the results are not presented; however, complete racemisation was only possibly with KOH and tBuOK, with essentially all of the bases showing no activity).

Addition of any foreign body to a crystallising solution will affect the kinetics of the process typically reducing the MSZW promoting spontaneous nucleation or alternatively acting as a nucleation inhibitor. Foreign bodies can also affect

crystal growth kinetics by becoming incorporated within the crystal lattice which can also lead to the formation of different crystal habits. The effect of the catalyst being present in solution during CIAT on the crystallisation behaviour was hence investigated (seed section 7.3.4)

For the CIAT experiments presented, 4 mol% of catalyst was selected as the quantity used with the exception of several runs where 8 mol% was utilised. This choice ensured that both the catalyst and base remained dissolved for the duration of the process under the varying temperatures experienced. It was also sufficient to allow for efficient racemisation of the undesired enantiomer as was shown in chapter 5, whilst also remaining economically viable considering the high value of the complexes used and the number of runs performed.

7.2.2.5 Stirring Rate

Stirring rate has been shown to have a considerable influence in preferential crystallisations being a factor that determines the resolution time i.e. the duration under which the seed crystals can remain entrained in solution before filtration [9]. At low stirring rates crystal growth is limited by the diffusion rate of solute from the bulk solution to the crystal surface. Increasing the stirring rate is therefore beneficial in this respect. However, the diffusional resistance becomes less of an influence as stirring speed is increased until a plateau occurs and it has no further effect. For preferential crystallisation and CIAT, since the antipode is metastable throughout the process, high stirring rates are detrimental as the mechanical system-shock can reduce the nucleation induction time therefore the possible entrainment time will be reduced. Furthermore, high stirring rates could increase the likelihood of crystal breakage which can lead to exposure of high energy surface sites which may promote nucleation of the antipode. Consequently, an optimum exists whereby sufficient mass transfer is achieved whilst minimising the mechanical influence that the system experiences. Furthermore, considering the experimental rig used for the CIAT runs, the level of stirring had to allow for efficient heat transfer to eliminate any temperature gradients between the vessel wall and the bulk of the process slurry. A stirring rate of approximately 100 rpm was used for the majority of the CIAT runs performed and for all of the data presented as this was sufficient to

allow the solids to remain suspended and visibly well mixed, and was also shown in preliminary investigations to give an even distribution of temperature within the process solvent.

7.2.3 Presentation of Experimental Conditions and Results

Due to the number of experimental conditions investigated, and to maintain clarity, the precise conditions varied in each CIAT run are presented with the corresponding results in the following sections for a selection of experimental runs of interest. For each catalyst the data is grouped according to the temperature programme used for comparison and presented in four-part tables being divided into:

- Part 1: CIAT process conditions
- Part 2: Theoretical and obtained crystal yields
- Part 3: Product composition
- Part 4: System composition

Part 1 list the conditions used for each CIAT run consisting of the seed temperature, T_{seed}, temperature programme, which is referenced to the graphical representations shown in Figure 7.2, filtration temperature, T_{filt}, quantity of seed used (wt% of **4** or **5**-*rac*$_{mix}$-**2**), and total quantity of the desired enantiomer ((*S*,*S*)-**2** for the results presented with one exception where (*R*,*R*)-**2** is used) initially present in the system (%) which incorporates the contribution from both the racemisation mixture in solution, **4** or **5**-*rac*$_{mix}$-**2**, and the enantiopure seed crystals.

Part 2 gives the theoretical product mass (g), which is deduced from the solubility curves for the racemisation mixtures determined in section 6.4, the prescribed temperature programme i.e. the difference between T_{sat} and T_{filt}, and the seed/initial excess contributions. The theoretical mass of (*S*,*S*)-**2** in the product (g) is given which incorporates both the recovered solid mass and seed/initial excess used, and assumes no racemisation i.e. the theoretical quantity of (*S*,*S*)-**2** that would be received upon seeding it into a solution of **4** or **5**-*rac*$_{mix}$-**2** with no catalyst present and allowing the solid and liquid phases to reach equilibrium. The product mass (g) for each run is presented both with and

without seed/initial excess. Finally the crystal yield (%) is given which does not include seed/initial excess.

Part 3 gives the product composition which was determined by HPLC using the method described in section 11.1.5.

Part 4 presents the mass of (*S*,*S*)-**2** (g) that is present in the product (using the HPLC analysis from Part 3), the quantity of (*S*,*S*)-**2** remaining in the equilibrated solution and the total quantity of (*S*,*S*)-**2** present in the system in both the solid and solution phases (g, %). This is used to determine the change in total (*S*,*S*)-**2** composition in the system based on the initial composition (solid and solution), and is used as a measure to determine whether the action of the catalyst has increased the fraction of (*S*,*S*)-**2** present through CIAT i.e. through conversion of the antipode in the solution phase by seeding the solution with enantiopure crystals. Changes > 0 % indicate that (*S*,*S*)-**2** has been generated from it stereoisomers, (*R*,*R*)- and *meso*-**2**, by the CIAT process.

7.3 CIAT of Hydrobenzoin (2) using Chloro(indenyl)-bis-(triphenylphosphine)-ruthenium(II) (4)

7.3.1 Isothermal and Cyclic Polythermal Temperature Programmes

Table 7.1a lists the conditions used for a selection of CIAT runs using **2** and catalyst **4** under the temperature programmes that correspond to **a** and **d** in Figure 7.2, with the total quantity of (*S*,*S*)-**2** initially present in the system as solid and solution also given.

Considering entry **1**, the solution was crash cooled from 75°C to 49°C upon which 1 wt% of pure (*S*,*S*)-**2** seed was added to the solution. This was then held at 49°C for 60 min after which the solution was immediately filtered. Despite the operating temperature being considerably lower than the metastable equilibrium temperature, T_{cryst}, for **4**-*rac*$_{mix}$-**2** (section 6), preliminary experiments showed that the solution could remain metastable well below T_{cryst} for a period of time when crash cooled without spontaneous nucleation. This is due to the rate of supersaturation generation not allowing sufficient time for the molecular addition process that is required to form a 3-D crystal which can be observed by the

increasing and decreasing gradients of the dissolution and crystallisation temperatures respectively verses the rate of cooling (see section 5).

Based on the solubility curve for **4**-*rac*$_{mix}$-**2** and the quantity of seed used, theoretically 0.94 g of product could be obtained if the solid and liquid phases were in equilibrium at the end of the process (0.91 g from solution, 0.03 g from seed), and of this 0.35 g would consist of (*S*,*S*)-**2** if no racemisation had occurred (35% of 0.91 g from **4**-*rac*$_{mix}$-**2** solution**,** 0.03 g of seed) (Table 7.1b). At the end of the experimental run, 0.23 g of solid was obtained for entry **1,** with the quantity of solute being removed from solution being 0.2 g if the seed used is not considered, leading to a crystal yield of 21.94% (see Figure 7.4a for a microscope image of product crystals).

Table 7.1c shows the composition of the crystalline product determined by chiral HPLC. For entry **1**, 99.59% of the solid obtained was comprised of (*S*,*S*)-**2** with the remainder consisting of small quantities of benzaldehyde, whilst no (*R*,*R*)- or *meso*-**2** were found to be present. Figure 7.3, the chiral HPLC chromatograms for the product and solution phases at the end the process for entry **1**, show that the product is comprised almost solely of (*S*,*S*)-**2** whereas the solution phase exhibits the catalytically equilibrated composition of **4**-*rac*$_{mix}$-**2**. Using this data and a simple mass balance, the solution phase composition of (*S*,*S*)-**2** was calculated as 0.98 g, whilst the total quantity within the system equated to 1.21 g or 39.90%. Comparing the initial and final state of the system, the total composition of (*S*,*S*)-**2** present, both in solution and as solid, increased by 11.95% over the duration of the CIAT run. This finding confirms that through the action of seeding enantiopure crystals into a supersaturated solution of stereoisomers equilibrated by way of an organometallic racemisation catalyst, it is possible to transform the antipode in-*situ* in solution (and in this particular case the corresponding *meso*-**2** stereoisomer) into the desired crystalline form and obtain a pure chiral product.

Similar results were seen for entry **2** which was performed under identical conditions to entry **1**. Based on the chiral HPLC analysis, in the solid product recovered at the end of the process, 99.71% consisted of (*S*,*S*)-**2** with the remainder being composed of benzaldehyde, giving a higher purity product than that obtained in entry **1**. However, a lower crystal yield resulted with 0.15 g of

solute being removed from solution through crystallisation (16.46% crystal yield) which translates to 1.18 g or 38.84% of the system being composed of (*S*,*S*)-**2** considering both solid and solution phase. Comparing this with the initial state of the system, a 8.98% change in the total composition of (*S*,*S*)-**2** was observed at the end of the process also confirming that the undesired stereoisomers were converted in solution through the action of seeding and subsequent catalytic equilibration.

Despite the successes seen in entries **1** and **2**, a relatively low crystal yield was obtained in both cases indicating that at the end of the process the solid and solution phases were far from achieving equilibrium. In entry **3**, an attempt was made to improve on this by performing a CIAT run under the same conditions but instead holding the system at the operating temperature for a longer duration of time (90 min).

As anticipated, a greater mass of product was obtained as a result with 0.31 g being recovered (34.01% crystal yield); however, considering the chiral HPLC analysis, at the end of the process the crystalline product had a lower enantiomeric purity with 78.16% being comprised of (*S*,*S*)-**2** whilst the undesired antipode (*R*,*R*)-**2** and small quantities of *meso*-**2** were seen to be present (21.49% and 0.35% respectively). Based on this 0.27 g of (*S*,*S*)-**2** was present in the product obtained whereas 0.89 g remained in solution which translates to 1.21 g or 39.90% of the system being comprised of (*S*,*S*)-**2**. Comparing this with the initial state of the system, a total increase of 11.78% of (*S*,*S*)-**2** present in both the solid and solution phases was observed. In spite of the latter finding and the greater yield obtained, the presence of the antipode and *meso*- form in the resulting product indicates that both species reached their metastable limits over the duration of the CIAT run as their induction times had been achieved. Therefore, under the conditions used, increasing the run is not sufficient to increase the productivity of the process due to the limitation of the crystallisation kinetics.

Continuing the quest to obtain a high purity product and increased crystal yield, an alternative approach was attempted whereby the system was cooled to a lower temperature to establish a greater magnitude of supersaturation. However, based on the previous findings and the understanding of

crystallisation behaviour, it was anticipated that the induction would be reduced as a result of the lower operating temperature hence the run time was shortened to 30 min. Furthermore, to attempt to maximise the crystal yield, enantiopure (*S*,*S*)-**2** was added to the system as its equilibrium saturation temperature was achieved to initiate crystallisation as soon as the system became supersaturated. Lastly, a greater quantity of seed crystals was introduced into the system with the aim of providing a larger surface area for crystallisation which in turn was anticipated to increase the quantity of solute that was recovered.

Entries **4**-**6** give the data for the runs where the conditions described above were utilised. In each run 10 wt% (*S*,*S*)-**2** seed was added to the system at the approximate saturation temperature (54°C – 53.5°C) whilst crash cooling to 40°C, 35°C and 25°C for entries **4**, **5** and **6** respectively, at which point the system was held for 30 min before filtration. In entry **4** 0.32 g of solute was recovered from solution giving a high purity product with 99.21% (*S*,*S*)-**2** being present; however (*R*,*R*)-**2** was also seen to crystallise (0.56%) with a small quantity of benzaldehyde being present (0.24%). Moreover, a crystal yield of 16.95% was achieved which is comparable with those seen in the previous entries; therefore, despite obtaining a greater overall mass of crystalline product, the crystal yield was not improved, and in spite of the high purity, crystallisation of the antipode through it achieving its metastable limit occurred which was not seen when the process was operated at a higher temperature.

In entries **5** and **6**, as a result of the increasingly lower operating temperatures, a greater proportion of the resulting product consisted of the antipode with *meso*-**2** also being present due to the higher levels of supersaturation. In entry **5**, 76.03%, 23.13% and 0.3% of the resulting solid were comprised of (*S*,*S*)-**2**, (*R*,*R*)-**2** and *meso*-**2** respectively. The higher levels of (*R*,*R*)-**2** in addition to the presence of *meso*-**2**, indicates that the system was well beyond the metastable limit of the undesired species. This is also evident in the yield of product obtained where 0.97 g of solute was recovered from solution which equates to a crystal yield of 43.54%. As (*R*,*R*)-**2** and *meso*-**2** crystallised, additional solute was transferred from solution to the crystalline phase thus increasing the mass of the solid and the resulting yield. Since the magnitude of supersaturation was

greater than in previous entries, at the end of the process the system was closer to equilibrium and hence a greater quantity of (*S*,*S*)-**2** was also deposited from solution resulting in an increase in its total final composition since the solution phase remained catalytically equilibrated which translates to a 24.16% enhancement compared with the initial state of the system.

Entry **6** shows the same trend but to a greater extent due to the lower operating temperature used. A greater proportion of the product consisted of (*R*,*R*)-**2** and *meso*-**2** with 18.17% of the latter being present in the sold phase and, as a result, the crystal yield increased to 66.01%. However, due to the higher rates of (*R*,*R*)-**2** and *meso*-**2** crystallisation, there was insufficient time for the catalyst to convert their excesses in solution that occurred as a result of (*S*,*S*)-**2** being deposited; hence, the change in total (*S*,*S*)-**2** composition considering the initial and final state of the system reduced to 8.15%.

Due to the limitations seen using the conditions applied in the entries discussed, where a low magnitude of supersaturation gave a high purity product but low crystal yields, whist on the other hand increasing the level of supersaturation enhance yields but at the expense of product purity, an alternative temperature programme was used to attempt to incorporate the benefits of both methodologies. In entries **7**-**9**, the system was crash cooled to 25°C whilst seeding at the approximate equilibrium saturation temperature (54°C/53°C). As soon as 25°C was achieved the slurry temperature was increased to 51°C i.e. just below the saturation temperature, and held for 30 min. In entries **8** and **9**, the crash cool–heating cycle was repeated whilst gradually lowering the isothermal temperature. It was postulate that crash cooling to a low temperature would generate a high magnitude of supersaturation which in turn would result in relatively high quantities of the desired enantiomer being deposited from solution. Similarly, eventual crystallisation of the undesired species after some time had elapsed was also anticipated; however, by heating the solution and maintaining at a temperature below that of the equilibrium solubility, dissolution of the unwanted stereoisomers was expected yielding a slurry consisting of pure (*S*,*S*)-**2** in the solid phase and an equilibrated solution. Hence, repeating the cycle whilst gradually lowing the isothermal temperature with each stage would

result in an increase in the quantity of (*S*,*S*)-**2** crystals present corresponding to the **4**-*rac*$_{mix}$-**2** phase equilibria.

Entry **7** shows that for a single cooling-heating cycle the approach described above successfully gave high purity crystals at the end of the CIAT run consisting of 98.54% (*S*,*S*)-**2** with benzaldehyde constituting the remainder. However, since the temperature of the isothermal stage was only slightly below the saturation temperature, only a small enhancement in the total quantity of (*S*,*S*)-**2** present in the system was observed (3.44%). For entry **8**, the cycle was repeated to the final temperature of 48°C, yet, unlike entry **7**, a significant amount of (*R*,*R*)-**2** (22.31%) was found to present in the resulting product indicating that it had achieved its induction time, which explains the increased crystal yield of 39.99% (see Figure 7.4b for a microscope image of product crystals). Repeating the cycle for a third time (entry **9**) acted only to enhance the levels of undesired stereoisomers seen (36.26% (*R*,*R*)-**2**, 0.81% *meso*-**2**) whilst, due to the greater time of exposure to the solution that the solid experienced, a higher change in total (*S*,*S*)-**2** composition occurred (20.17%).

Table 7.1a Conditions used and results for CIAT experiments using catalyst **4** (4 mol%) and seeding **4**-*rac*$_{mix}$-**2** with (*S*,*S*)-**2**, 0.467 mol l^{-1}, 30 ml scale, temperature programmes a and d (Figure 7.2)[a].

Part 1: **CIAT process conditions**

Entry	T_{Seed} (°C)	Temperature Programme[a]	T_{filt} (°C)	Seed quantity (wt%)	(*S*,*S*)-2 in system (%)[b]
1	49	[a] Crash cool to 49°C,maintain 49°C for 60 min.	49	1	**35.64**
2	49		49	1	**35.64**
3	49	[a] As above, maintain 49°C for 90 min.	49	1	**35.64**
4	54	[a] Crash cool to 40°C, maintain for 30 min.	40	10	**40.91**
5	53.5	[a] Crash cool to 35°C, maintain for 30 min.	35	10	**40.91**
6	54	[a] Crash cool to 25°C, maintain for 30 min.	25	10	**40.91**
7	54	[d] Crash cool to 25°C, maintain for 30 min, increase to 51°C, maintain for 30 min.	51	10	**40.91**
8	53	[d] As entry 7, crash cool to 25°C, increase to 48°C, maintain for 30 min.	48	10	**40.91**
9	54	[d] As entry 8, crash cool to 25°C, increase to 44°C, maintain for 30 min, crash cool to 25°C, increase to 40°C, maintain for 30 min.	40	10	**40.91**

[a]See Figure 7.2 for a graphical presentation of the temperature programmes used corresponding to the value in square brackets. [b]Initial (*S*,*S*)-**2** in system (%) based on **4**-*rac*$_{mix}$-**2** composition in solution (35% (*S*,*S*)-**2**) and seed fraction.

Table 7.1b Conditions used and results for CIAT experiments using catalyst **4** (4 mol%) and seeding **4**-*rac*$_{mix}$-**2** with (*S*,*S*)-**2**, 0.467 mol l^{-1}, 30 ml scale, temperature programmes a and d.

Part 2: Theoretical and obtained crystal yields

Entry	Theoretical yields		Product Yields		
	Product mass including seed (g)[c]	Mass of (*S*,*S*)-2 in product (g)[d]	Product mass including seed (g)	Product Mass (g)[e]	Crystal Yield (%)[e]
1	0.94	0.35	0.23	0.2	21.94
2	0.94	0.35	0.18	0.15	16.46
3	0.94	0.35	0.34	0.31	34.01
4	2.19	0.96	0.62	0.32	16.95
5	2.53	1.08	1.27	0.97	43.54
6	2.95	1.23	2.05	1.75	66.01
7	0.91	0.51	0.38	0.08	13.22
8	1.35	0.67	0.72	0.42	39.99
9	2.19	0.96	1.7	1.4	74.16

[c]Theoretical mass from **4**-*rac*$_{mix}$-**2** solubility curve (Figure 6.5). [d]Theoretical mass of (*S*,*S*)-**2** in product with no racemisation, based on **4**-*rac*$_{mix}$-**2** composition (35% (*S*,*S*)-**2**) and seed fraction. [e]Not including seed.

Table 7.1c Conditions used and results for CIAT experiments using catalyst **4** (4 mol%) and seeding **4**-*rac*$_{mix}$-**2** with (*S*,*S*)-**2**, 0.467 mol l^{-1}, 30 ml scale, temperature programmes a and d.

Part 3: Product Composition (%)[f]

Entry	(*S*,*S*)-2	(*R*,*R*)-2	*meso*-2	Benzil	Stilbene	Benz-aldehyde
1	99.59	0.00	0.00	0.00	0.00	0.41
2	99.71	0.00	0.00	0.00	0.00	0.29
3	78.16	21.49	0.35	0.00	0.00	0.00
4	99.21	0.56	0.00	0.00	0.00	0.24
5	76.03	23.13	0.30	0.00	0.00	0.54
6	49.88	30.27	18.17	0.00	0.00	1.68
7	98.54	0.00	0.00	0.00	0.00	1.46
8	77.30	22.31	0.00	0.00	0.00	0.39
9	62.49	36.29	0.81	0.00	0.00	0.40

[f]Determined by chiral HPLC (see section 11.1.5 for method details).

Table 7.1d Conditions used and results for CIAT experiments using catalyst **4** (4 mol%) and seeding **4**-*rac*$_{mix}$-**2** with (*S*,*S*)-**2**, 0.467 mol l^{-1}, 30 ml scale, temperature programmes a and d.

Part 4: System Composition

Entry	Mass of (*S*,*S*)-2 in product (g)[g]	Remaining (*S*,*S*)-2 in solution (g)[h]	(*S*,*S*)-2 in system[i]		Change in total (*S*,*S*)-2 composition (%)[j]
			(g)	(%)	
1	0.23	0.98	1.21	39.90	**11.95**
2	0.18	1.00	1.18	38.84	**8.98**
3	0.27	0.94	1.21	39.84	**11.78**
4	0.62	0.94	1.55	47.06	**15.04**
5	0.97	0.71	1.68	50.79	**24.16**
6	1.02	0.44	1.46	44.24	**8.15**
7	0.37	1.02	1.40	42.32	**3.44**
8	0.56	0.90	1.46	44.23	**8.11**
9	1.06	0.56	1.62	49.16	**20.17**

[g]From chiral HPLC data and product mass. [h](*S*,*S*)-**2** in solution based on solubility curve, product mass and **4**-*rac*$_{mix}$-**2** composition (35% (*S*,*S*)-**2**). [i]Both solid and solution phase contributions. [j]Percent change in (*S*,*S*)-**2** composition considering initial and final solid and solution phases.

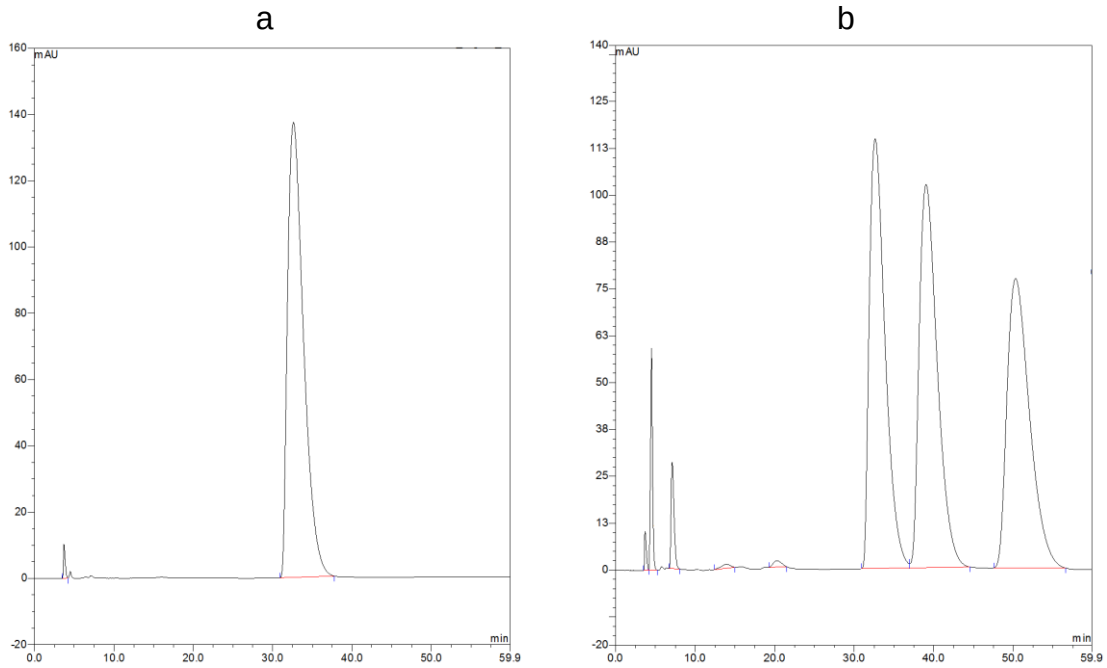

Figure 7.3 Entry **1** chiral HPLC chromatograms for a) the product obtained and b) the solution phase at the end of the run. (approximate component positions: 3 min benzaldehyde; 13 min stilbene; 21 min benzil; 33 min (*S*,*S*)-**2**; 40 min (*S*,*S*)-**2**; 51 min *meso*-**2**)

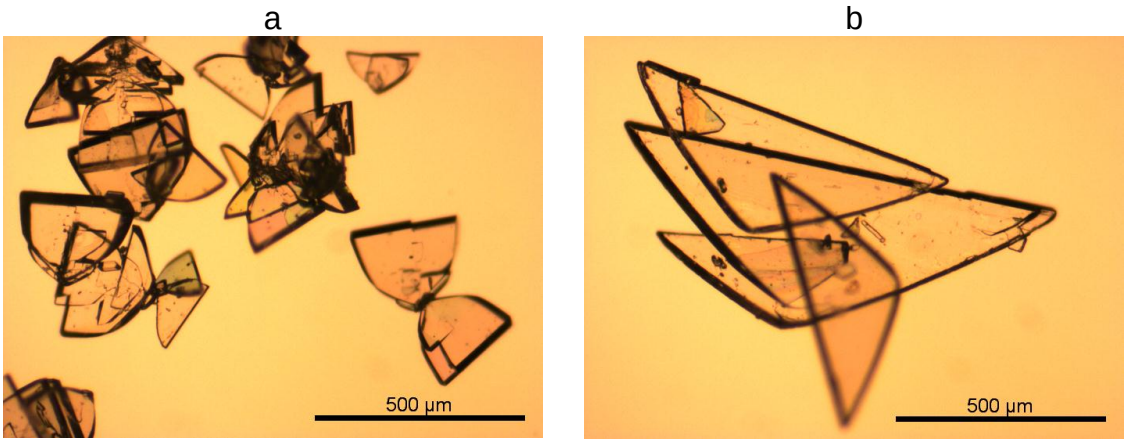

Figure 7.4 CIAT product crystal from Table 7.1 entries a) **1** and b) **8**.

7.3.2 Polythermal Temperature Programmes

Table 7.2 lists the conditions used for a selection of CIAT runs using **2** and catalyst **4** under the temperature programmes that correspond to **b** and **c** in Figure 7.2, with the total quantity of (*S*,*S*)-**2** initially present in the system as solid and solution also given.

The polythermal temperature programmes used are an extension of findings presented as entries **1**, **2** and **3** in the previous section (Table 7.1). Enantiopure crystals were obtained, and the total quantity of (*S*,*S*)-**2** present in the system increased, when pure (*S*,*S*)-**2** seed was introduced to the equilibrated solutions and held isothermally below the saturation temperature (49°C/40°C). However, as a result of maintaining the latter condition (with further reductions in temperature resulting in crystallisation of the undesired stereoisomers), low yields were obtained as the thermodynamic driving force was insufficient to maximise solute recovery and hence the productivity of the CIAT process. In the results presented in Table 7.2, the temperature programme began by replicating the entries that resulted in high chiral purity products, yet, to maintain supersaturation and hence increase the quantity of solute recovered, controlled cooling was subsequently applied to the system.

In entries **1** and **2** in (Table 7.2), the solution was seeded at 54°C which was maintained for a further 30 min. Unlike the lower temperature conditions used in the entries in the previous section discussed above, the seed temperature was selected to be approximately the saturation temperature to minimise the possibility of antipode and *meso*- form crystallisation due to them being close to their metastable limits. The solution was then cooled at a controlled rate of -0.1°C min^{-1} to 42°C at which point the solution was immediately filtered.

Considering entry **1** (Table 7.2), the solution was seeded with 5 wt% (*S*,*S*)-**2** which after cooling resulted in 1.24 g of solid being obtained. This equates to 1.09 g of solute being deposited from solution giving a crystal yield of 63.47%. Of this, chiral HPLC showed that 64.07% consisted of (*S*,*S*)-**2** with the remainder being comprised predominantly of (*R*,*R*)-**2** (35.25%) leading to a 21.91% change in total (*S*,*S*)-**2** present in the system. Similar results were seen when the quantity of seed was increased to 10 wt% (entry **2**); however, as a result of the greater crystallisation surface area provided, the crystal yield was

improved (68.13%) since, for a given time and set of process conditions, a larger quantity of solute would be expected to be deposited. Despite this, the presence of more surface area was observed to have a detrimental effect on the fraction of (*S*,*S*)-**2** in the product crystal obtained, with a considerable amount of *meso*-**2** also being present. Crystallisation of the antipode and *meso*-form indicates that either its nucleation induction time was achieved, the enantiopure crystals added to the system were acting as non-selective nucleation centres, or that the controlled cooling programme applied was not sufficiently slow enough to allow the system to remain close to equilibrium between the solid and liquid phases leading to the undesired stereoisomers reaching their metastable limits through a progressive increase in supersaturation.

In entries **3**-**6** the process cooling rate was reduced to -0.23°C min^{-1} in an attempt to allow the system to remain closer to the equilibrium solubility curve under cooling without excessive build-up of supersaturation. Furthermore, the time spent at the initial isothermal stage was increased to 60 min in order to provide more time for the system to approach equilibrium between the solid and solution phases. With the exception of entry **5,** as anticipated the crystal yield was seen to increase as a result of the reduced cooling rate allowing greater time for crystallisation. Despite this, little change was seen in the composition of (*S*,*S*)-**2** in the product obtained; however, unlike entries **1** and **2**, a greater proportion benzaldehyde was present in the crystal phase at the end of the run (with entries **3** and **5** containing 9.02% and 8.99% respectively compared with 0.38% and 0.84% for entries **1** and **2**). Interestingly, entry **4**, where 10 wt% seed was introduced in to the system, yielded the greatest quantity of (*S*,*S*)-**2** from solution with no benzaldehyde being observed in the final product.

These findings suggest that for a slow cooling rate, which results in the crystals being suspended in solution for a longer period of time, and a low crystallisation surface area provided by the seed, which reduces the rate of (*S*,*S*)-**2** deposition and hence minimises the quantity of material being converted by way of the catalyst since the solution phase is closer to catalytic equilibrium, sufficient time is given for benzaldehyde to become increasingly more supersaturated eventually leading to its spontaneous nucleation. However, it is known that

benzaldehyde is far more soluble in toluene than **2**, and coupled with the low levels seen in the racemisation mixture, it is unlikely that it would independently reach its metastable limit and nucleate. A more plausible explanation for its presence in the product crystals is that, due to similarities in their molecular structures, the (*S*,*S*)-**2** seed acts as a crystallisation centre for benzaldehyde thus lowering the energy barrier for crystal formation resulting in it being deposited from solution.

Based on this assumption, it is reasonable to expect the quantity of benzaldehyde present in the product to increase with the amount of seed introduced to the system due to the larger surface area yet the results presented in Table 7.2 (and the vast majority of the results presented in the report) suggest the opposite is true i.e. generally for the same given process conditions, and if sufficient time is available, an increase in the quantity of seed results in less benzaldehyde being deposited. For a conventional seeded crystallisation this would appear to be counterintuitive; however, it is likely that this is a result of the catalyst being present in solution. When large quantities of seed are introduced into the system, comparatively higher rates of (*S*,*S*)-**2** removal are observed as a result of the greater surface area. Consequently, the other catalytically equilibrated species in solution are transformed a faster rate which lowers their concentration and therefore reduces their tendency to crystallise, even in the presence of a crystal surface. On the other hand, if small volumes of seed are used, the rate of solute removal, and hence the rate of undesired species transformation by the catalyst is comparatively slower, therefore their concentrations remain higher and they are more likely to crystallise given the opportunity either through achievement of the metastable solubility limit or by non-selective molecular addition onto the seed crystal surface. Examination of the data presented for CIAT of **2** using catalyst **4** shows that this trend occurs in the majority of cases but is not always observed which is most likely due to the statistical dependency of this phenomena occurring

Considering entries **5** and **6**, for which the difference in process conditions was the seed temperature, T_{seed} (53.5°C and 52°C respectively), a similar effect is observed to that described previously for differing seed quantities. When the seed is introduced at a lower temperature, a greater quantity of solute is

deposited due to the greater magnitude of supersaturation. Consequently, a greater crystal yield is obtained, and the levels of benzaldehyde seen are significantly lower since the faster rate of solute removal gives correspondingly faster catalytic transformation hence its concentration is comparatively lower and its less likely to crystallise. Conversely, despite the superior yield, the fraction of (*S*,*S*)-**2** present in the product is lower for entry **6** since the relative difference in the concentration of its antipode, which unlike benzaldehyde is supersaturated, is higher therefore it is more likely to reach its metastable limit.

In entries **7**-**11** a similar temperature programme was applied whereby the system was held isothermally for 60 min at T_{seed} and subsequently cooled at a rate of 0.025°C min^{-1}; however, unlike the previous entries this was continued to the lower temperature of 25°C.

Considering entry **7**, relatively high crystal yield of 81.85% was obtained which is a result of the crystals remaining in solution for a longer duration of time allowing for equilibrium between the solid and solution phases to be approached. Despite this, a low chiral purity product was obtained as similarly the antipode was also given a longer process time for it to both achieve its nucleation induction time and for it to be subsequently deposited through growth and secondary nuclei formation. Comparing entry **7** with **8**, in which the amount of seed introduced was increased from 1 to 10 wt%, similar results were obtained, yet, for the reasons described previously, benzaldehyde was only found to be present when 1 wt% of seed was used and was absent for the 10 wt% case.

Entries **9** and **10** were performed using the same controlled cooling rate; however, in **9** the seed was introduced at the lower temperature of 49°C. Despite being introduced at a greater magnitude of supersaturation, and with entry **9** having a shorter process time, little difference was seen between the results of the two runs. However, in each case a significant change in the total (*S*,*S*)-**2** composition present in the system in both the solid and solution phase was observed being 42.19% and 37.79% respectively for the two entries **9** and **10**. Similar results were seen in entry **11**, which was simply a repeat of entry **10** for comparison. Interestingly, identical yields of crystalline product were received in both cases (83.74%), yet, the resulting compositions did differ. The

difficulty in reproducing data for identical conditions was a common theme throughout the investigation which was of course a result of the many different process and experimental parameters that influenced the CIAT process.

For entries **12**-**14** the cooling rate was further reduced to 7 x 10^{-4}°C min^{-1} with each entry being performed under the same process conditions. However, in entry **12** enantiopure (*R*,*R*)-**2** seed was used instead of (*S*,*S*)-**2** whereas entry **14** used 8 mol% of catalyst **4** (with (*S*,*S*)-**2** seed). Comparing entries **12** and **13**, as expected very similar results are obtained when either (*R*,*R*)-**2** or (*S*,*S*)-**2** seeds are used since there should be no difference in phase equilibria between the two. A slightly higher yield was observed when (*S*,*S*)-**2** was used however which is likely due to unavoidable experimental variations between the two runs. Despite this, as a result of the higher purity product obtained when (*R*,*R*)-**2** was used, near identical changes in the total composition of the desired enantiopure present in the system as solid and solution were seen (15.54% and 16.19% respectively when (*R*,*R*)-**2** and (*S*,*S*)-**2** seed was used).

Comparing entries **13** and **14**, it can be seen that a higher catalyst loading resulted in similar performance albeit giving a slightly lower yield and a lower change in total (*S*,*S*)-**2** system composition at the end of the run (which could be due to unavoidable experimental variations between the two runs). It would be expected that by increasing the solution phase transformation rate, a higher quantity of catalyst would improve the productivity of the process since the stereoisomers will be closer to equilibrium in solutions whilst the desired enantiomer is being deposited on the enantiopure seeds. However, as mentioned previously, presence of foreign species can have a considerable influence on crystallisation kinetics by reducing the MSZW, altering crystal growth, or by supressing nucleation. In the data presented, it appears that increasing the catalyst load does not have a considerable effect on the outcome of the process warranting the acceptable use of lower quantities.

Entries15 and 16 give the data for the CIAT runs that were performed under the temperature programme that corresponds to **c** in Figure 7.2. For each of the entries, the solution was seeded at T_{seed} and held isothermally for 16 min, after which a controlled cooling rate of -0.25°C min^{-1} was applied for a 1°C temperature change i.e. 4 min of cooling. The solution was again held

isothermally for an addition 16 min with cooling/isothermal temperature programme being repeated unit T_{filt} was achieved, at which point the slurry was immediately filtered. By inducing a low magnitude of supersaturation with a small temperature change, then allowing the system to sit isothermally, it was postulated that the latter condition would allow the system to approach equilibrium between the solid and solution phases. Generation of a small driving force would minimise the chance of the undesired species crystallising since their concentrations would be reduced by the catalyst during the isothermally stages. Through repetition of the cycle, the system would therefore remain close to the equilibrium solubility.

Considering entry **15**, the solution was seeded at 52°C with the temperature programme described above being repeated to 42°C. By attempting to stay close to the equilibrium solubility, a considerable crystal yield of (*S*,*S*)-**2** was achieved (71.04%). Furthermore, a relatively high enantiomeric purity was obtained with 78.72% of the product being comprised of (*S*,*S*)-**2** which lead to its total composition in the system as both solid and solution being increased by 43.40%. As anticipated, by staying close to equilibrium, the relative supersaturation of the undesired species was reduced which was further enhanced due to conversion by the catalyst.

Entry **16** was performed under the same conditions; however, the quantity of seed crystals used was twice that of entry **15** (8 wt%). As a result of the larger crystallisation area, leading to a greater quantity of solute being deposited, a slight increase in the crystal yield was observed. However, the composition of (*S*,*S*)-**2** in the final product was approximate 7% lower than what was seen in entry **15**. With a larger quantity of seed resulting in correspondingly faster rates of crystal growth and secondary nucleation, and with the rate of catalytic transformation being unchanged, it is likely that the concentrations of the antipode and *meso*- form was not reduced at a sufficient rate by the catalyst to compensate for the increased rate of removal by the seed hence they experienced a greater magnitude of supersaturation leading to larger quantities of them being deposited.

Table 7.2a Conditions used and results for CIAT experiments using catalyst **4** (4 mol%) and seeding **4**-*rac*$_{mix}$-**2** with (*S*,*S*)-**2**, 0.467 mol l^{-1}, 30 ml scales temperature programmes **b** ad **c**[a].

Part 1: CIAT process conditions

Entry[b]	T_{Seed} (°C)	Temperature Programme	T_{filt} (°C)	Seed quantity (wt%)	(*S*,*S*)-2 in system (%)[c]
1	54	[b] Isothermal at T_{Seed} for 30 min, -0.1°C min^{-1}	42	5	**38.10**
2	54		42	10	**40.91**
3	53.5	[b] Isothermal at T_{Seed} for 60 min -0.023°C min^{-1}	43.5	5	**41.44**
4	53.5		43.5	10	**43.97**
5	53.5		43.5	2	**39.81**
6	52		43.5	2	**39.81**
7	53.5	[b] Isothermal at T_{Seed} for 60 min -0.025°C min^{-1}	25	1	**39.25**
8	53.5		25	10	**43.97**
9	49		25	1	**39.25**
10	53		25	1	**39.25**
11	53		25	1	**39.25**
12[d]	54	[b] Isothermal at T_{Seed} for 30 min, -7x10^{-4}°C min^{-1}	40	10	**40.91**
13	54		40	10	**40.91**
14[e]	54		40	10	**40.91**
15	52	[c] Isothermal at T_{Seed} for 16 min, -0.25°C min^{-1} for 1°C, isothermal for 16 min, repeat to T_{Filt}	42	4	**36.5**
16	52		42	8	**38.9**

[a]See Figure 7.2 for a graphical presentation of the temperature programmes used corresponding to the value in square brackets. [b]6% initial excess of (*S*,*S*)-**2**. [c]Initial (*S*,*S*)-**2** in system (%) based on **4**-*rac*$_{mix}$-**2** composition in solution (35% (*S*,*S*)-**2**) and seed fraction. [d]Seeding with (*R*,*R*)-**2**. [e]8 mol% **4**.

Table 7.2b Conditions used and results for CIAT experiments using catalyst **4** (4 mol%) and seeding **4**-*rac*$_{mix}$-**2** with (*S*,*S*)-**2**, 0.467 mol l^{-1}, 30 ml scale temperature programme b.

Part 2: Theoretical and obtained crystal yields

Entry	Theoretical yields		Product Yields		
	Product mass including seed/initial excess (g)[f]	Mass of (*S*,*S*)-2 in product (g)[g]	Product mass including seed/initial excess (g)	Product Mass (g)[h]	Crystal Yield (%)
1	1.87	0.75	1.24	1.09	63.47
2	2.02	0.90	1.47	1.17	68.13
3	1.90	0.88	1.50	1.17	74.32
4	2.05	1.03	1.63	1.15	73.05
5	1.81	0.79	1.11	0.87	55.27
6	1.81	0.79	1.32	1.08	68.61
7	2.86	1.14	2.38	2.17	81.85
8	3.13	1.41	2.51	2.03	76.57
9	2.86	1.14	2.38	2.17	81.85
10	2.86	1.14	2.43	2.22	83.74
11	2.86	1.14	2.43	2.22	83.74
12[c]	2.19	0.96	0.88	0.58	30.70
13	2.19	0.96	1.10	0.80	42.38
14[d]	2.19	0.96	0.96	0.66	34.96
15	1.84	0.72	1.34	1.22	71.04
16	1.96	0.84	1.51	1.27	73.95

[f]Theoretical mass from **4**-*rac*$_{mix}$-**2** solubility curve (Figure 6.5). [g]Theoretical mass of (*S*,*S*)-**2** in product with no racemisation, based on **4**-*rac*$_{mix}$-**2** composition (35% (*S*,*S*)-**2**) and seed fraction. [h]Not including seed/initial excess.

Table 7.2c Conditions used and results for CIAT experiments using catalyst **4** (4 mol%) and seeding **4**-*rac*$_{mix}$-**2** with (*S*,*S*)-**2**, 0.467 mol l^{-1}, 30 ml scale temperature programme b.

Part 3: Product Composition (%)[i]

Entry	(*S*,*S*)-2	(*R*,*R*)-2	*meso*-2	Benzil	Stilbene	Benz-aldehyde
1	64.07	35.25	0.30	0.00	0.00	0.38
2	61.73	31.97	5.46	0.00	0.00	0.84
3	62.47	28.23	0.29	0.00	0.00	9.02
4	71.60	28.10	0.30	0.00	0.00	0.00
5	65.16	25.57	0.28	0.00	0.00	8.99
6	54.12	44.47	0.78	0.00	0.00	0.63
7	54.83	39.83	0.46	0.00	0.00	4.88
8	57.02	42.72	0.25	0.00	0.00	0.00
9	63.07	34.67	1.35	0.00	0.00	0.90
10	60.21	34.00	3.94	0.00	0.00	1.84
11	53.86	41.24	3.17	0.00	0.00	1.73
12[c]	8.72	80.93	0.74	0.00	0.00	9.61
13	72.59	24.91	0.31	0.18	0.06	1.94
14[d]	68.16	31.32	0.00	0.00	0.00	0.52
15	78.72	19.79	0.34	0.00	0.00	1.15
16	71.69	26.10	0.16	0.00	0.00	2.05

[i]Determined by chiral HPLC (see section 11.1.5 for method details).

Table 7.2d Conditions used and results for CIAT experiments using catalyst **4** (4 mol%) and seeding **4**-*rac*$_{mix}$-**2** with (*S*,*S*)-**2**, 0.467 mol l^{-1}, 30 ml scale temperature programme b.

Part 4: System Composition

Entry	Mass of (*S*,*S*)-2 in product (g)[j]	Remaining (*S*,*S*)-2 in solution (g)[k]	(*S*,*S*)-2 in system[l]		Change in total (*S*,*S*)-2 composition (%)[m]
			(g)	(%)	
1	0.79	0.67	1.46	46.44	**21.91**
2	0.91	0.64	1.55	46.91	**14.66**
3	0.94	0.64	1.58	47.37	**14.31**
4	1.17	0.65	1.81	52.14	**18.60**
5	0.72	0.75	1.47	45.33	**13.86**
6	0.71	0.67	1.39	42.79	**7.47**
7	1.30	0.29	1.60	49.70	**26.63**
8	1.43	0.34	1.77	50.89	**15.74**
9	1.50	0.29	1.79	55.81	**42.19**
10	1.46	0.27	1.74	54.09	**37.79**
11	1.31	0.27	1.58	49.27	**25.53**
12[c]	0.71	0.85	1.56	47.25	**15.49**
13	0.80	0.77	1.57	47.53	**16.19**
14[d]	0.65	0.82	1.47	44.65	**9.14**
15	1.05	0.62	1.68	53.78	**43.40**
16	1.08	0.61	1.69	52.10	**30.85**

[j]From chiral HPLC data and product mass. [k](*S*,*S*)-**2** in solution based on solubility curve, product mass and **4**-*rac*$_{mix}$-**2** composition (35% (*S*,*S*)-**2**). [l]Both solid and solution phase contributions. [m]Percent change in (*S*,*S*)-**2** composition considering initial and final solid and solution phases.

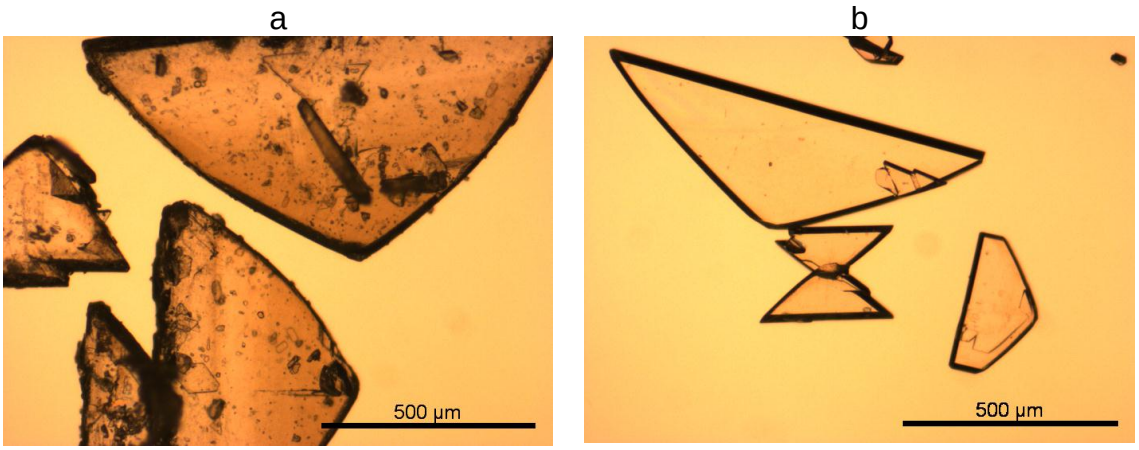

Figure 7.5 CIAT product crystals from Table 7.2 entries a) **7** and b) **12**

7.3.3 Reduced Concentration

Table 7.3 lists the conditions used for a selection of CIAT runs using **2** and catalyst **4** under the temperature programme that corresponds to **b** in Figure

7.2, with the total quantity of (*S*,*S*)-**2** initially present in the system as solid and solution also given. In all of the entries presented, a reduced **4**-*rac*$_{mix}$-**2** concentration of 0.233 mol l^{-1} was used (compared with the data presented previously). Since the MSZW for a solid-solution system generally increases with decreasing temperature, CIAT was performed at a lower concentration to investigated whether the productivity of the process could be improved as a result of potentially more time being available for the seed crystals to be entrained, and hence the reduced possibility of undesired species reaching there metastable solubility limit. In all of the entries presented, the solution was seeded at 43.5°C, held isothermally for 75 min, and cooled under a controlled rate to 20°C at which point the solution was immediately filtered.

Entries **1** and **2** were performed under identical conditions; however, in the former 8 mol% of catalyst **4** was used since, at these comparatively lower process temperatures, the racemisation rate is reduced therefore is was essential to know whether the productivity of the process could be enhanced by using larger catalyst loadings. Considering the resulting data, little difference was seen between the crystal yields of entries **1** and **2**; however, for the case where the lower 4 mol% of catalyst was used, a higher chiral purity product was obtained and significantly less benzaldehyde was present in the resulting crystalline product. This may have been due to the presence of additional foreign material in solution (entry **1**) influencing the crystallisation kinetics of benzaldehyde by acting as centres for nucleation as discussed previously. In both cases however, considerably more benzaldehyde was observed in the final product compared with the subsequent entries (**3**-**5**) which were performed under the same conditions but with slower cooling rates. This suggest that benzaldehyde may have approached or exceeded its metastable limit under the comparatively faster cooling rate which, in conjunction with the reduced rate of its catalytic conversion upon removal of the seeded enantiomer (*S*,*S*)-**2** (due to the low relative operating temperatures), may have resulted in its concentration being higher than what it would be if a slower cooling rate was used and hence more time provided for the solution to catalytically equilibrate.

Examination of entries **3**-**5**, for which the cooling rates were reduced to 0.01°C min^{-1}, 0.0075°C min^{-1} and 0.001°C min^{-1} respectively, provides further evidence

for this hypothesis; low levels of benzaldehyde were found to be present in the product crystals in each case. Crystal yields were comparable to entries 1 and 2; however, the chiral purity of the product obtained was considerably higher. Furthermore the change in the quantity of (*S*,*S*)-**2** present in the system at the end of the process in both the solid and solution phases was significantly improved with entry **5** giving a 61.57% increase. Of the three entries, 5 used the median cooling rate of 0.0075°C min^{-1} which implies that an optimum exists. For faster rates of cooling, it is more likely that the undesired species will reach their metastable solubility limits since the rate of catalytic conversion is not sufficient to minimise their concentrations in solution. On the other hand, for very slow cooling rates, and hence longer process times, it is possible that crystallisation of the undesirables may occur through them achieving their induction times.

Comparing the entries in Table 7.3 with those given in the previous sections using a higher **4**-rac_{mix}-**2** concentration, it is evident that there has been an improvement in the change in total quantity of (*S*,*S*)-**2** present in the system i.e. more of the undesired species were converted compared with the previous high relative-concentration runs. Similarly, increased chiral-purity products were also obtained under these conditions. As anticipated, the improvement in CIAT productivity seen when lower concentrations were used is likely due to the wider MSZW allowing the process to operate further from the metastable solubility points for each of the system components hence allowing more time for seeded enantiomer to crystallise. However, despite this slight improvement, it must be noted that in all of the polythermic CIAT experiments conducted it was not possible to recover an enantiopure product.

Table 7.3a Conditions used and results for CIAT experiments using catalyst **4** (4 mol%) and seeding **4**-*rac*$_{mix}$-**2** with (*S*,*S*)-**2**, 0.233 mol l^{-1}, 30 ml scale, temperature programme b[a].

Part 1: CIAT process conditions

Entry	T_{Seed} (°C)	Temperature Programme	T_{Filt} (°C)	Seed quantity (wt%)	(*S*,*S*)-2 in system (%)[b]
1[c]	43.5	[b] Isothermal at T_{Seed} for 75 min, -0.05°C min^{-1}	20	10	**1.28**
2	43.5		20	10	**1.28**
3	43.5	[b] As above -0.01°C min^{-1}	20	10	**1.28**
4	43.5	[b] As above -0.0075°C min^{-1}	20	10	**1.28**
5	43.5	[b] As above -0.001°C min^{-1}	20	10	**1.28**

[a]See Figure 7.2 for a graphical presentation of the temperature programmes used corresponding to the value in square brackets. [b]Initial (*S*,*S*)-**2** in system (%) based on **4**-*rac*$_{mix}$-**2** composition in solution (35% (*S*,*S*)-**2**) and seed fraction. [c]8 mol% **4**

Table 7.3b Conditions used and results for CIAT experiments using catalyst **4** (4 mol%) and seeding **4**-*rac*$_{mix}$-**2** with (*S*,*S*)-**2**, 0.467 mol l^{-1}, 30 ml scale, temperature programme b.

Part 2: Theoretical and obtained crystal yields

Entry	Theoretical yields		Product Yields		
	Product mass including seed (g)[d]	Mass of (*S*,*S*)-2 in product (g)[e]	Product mass including seed (g)	Crystal Yield (g)[f]	Crystal Yield (%)
1[c]	1.43	0.60	1.17	1.02	79.74
2	1.43	0.60	1.26	1.11	86.78
3	1.43	0.60	1.03	0.88	68.80
4	1.43	0.60	1.19	1.04	81.31
5	1.43	0.60	1.03	0.88	68.80

[d]Theoretical mass from **4**-*rac*$_{mix}$-**2** solubility curve (Figure 6.5). [e]Theoretical mass of (*S*,*S*)-**2** in product with no racemisation, based on **4**-*rac*$_{mix}$-**2** composition (35% (*S*,*S*)-**2**) and seed fraction. [f]Not including seed.

Table 7.3c Conditions used and results for CIAT experiments using catalyst **4** (4 mol%) and seeding **4**-*rac*$_{mix}$-**2** with (*S*,*S*)-**2**, 0.467 mol l^{-1}, 30 ml scale, temperature programme b.

Part 3: Product Composition (%)[g]

Entry	(*S*,*S*)-2	(*R*,*R*)-2	*meso*-2	Benzil	Stilbene	Benz-aldehyde
1[c]	46.07	6.73	2.55	0.00	0.00	44.65
2	55.11	31.12	0.27	0.93	0.00	12.57
3	63.47	35.24	0.16	0.00	0.00	1.12
4	78.12	21.31	0.34	0.00	0.00	0.23
5	69.20	28.68	0.86	0.00	0.00	1.26

[g]Determined by chiral HPLC (see section 11.1.5 for method details).

Table 7.3d Conditions used and results for CIAT experiments using catalyst **4** (4 mol%) and seeding **4**-*rac*$_{mix}$-**2** with (*S*,*S*)-**2**, 0.467 mol l^{-1}, 30 ml scale, temperature programme b.

Part 4: System Composition

Entry	Mass of (*S*,*S*)-2 in product (g)[h]	Remaining (*S*,*S*)-2 in solution (g)[i]	(*S*,*S*)-2 in system[j]		Change in (*S*,*S*)-2 composition (%)[k]
			(g)	(%)	
1	0.54	0.17	0.71	42.85	**4.75**
3	0.69	0.14	0.83	50.36	**23.10**
4	0.65	0.22	0.87	52.77	**29.00**
5	0.93	0.16	1.09	66.10	**61.57**
6	0.71	0.22	0.93	56.35	**37.74**

[h]From chiral HPLC data and product mass. [i](*S*,*S*)-**2** in solution based on solubility curve, product mass and **4**-*rac*$_{mix}$-**2** composition (35% (*S*,*S*)-**2**). [j]Both solid and solution phase contributions. [k]Percent change in (*S*,*S*)-**2** composition considering initial and final solid and solution phases.

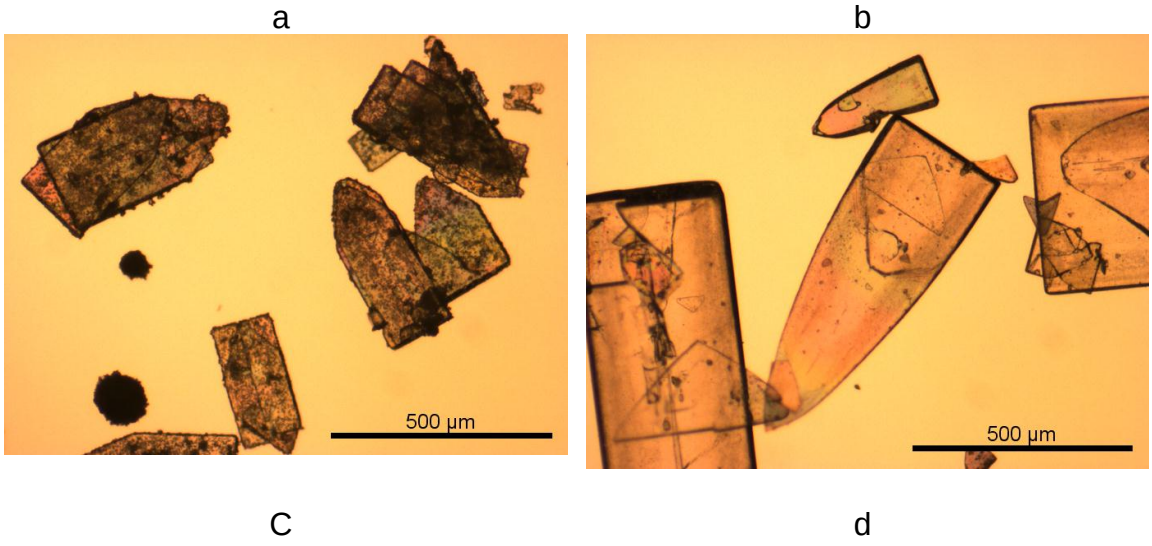

Figure 7.6 Product crystals from Table 7.3 Entries a) **1** and b) **4**.

7.3.4 Effect of Catalyst 4 on Crystallisation

As a result of the mixed success seen in the CIAT experiments using catalyst **4** presented in the previous sections, in which it was possible to obtain enantiopure product under an isothermal temperature programme but with low yields, whereas under a polythermal temperature program a comparatively

higher yield could be obtained but crystallisation of the antipode and the other species present in racemisation mixture could not be avoided, the effect on crystallisation due to the catalyst being in solution was investigated. PXRD was used to identify whether the catalyst was being incorporated to the crystalline product by comparing the diffraction patterns of the enantiopure (*S*,*S*)-**2** seed crystals with that of the enantiopure product obtained using the isothermal temperature programme. Although single crystal XRD would have allowed for a more thorough examination, it was not possible to obtain crystals large enough from the CIAT experiment.

Figure 7.7 shows the XRD diffraction patterns for the (*S*,*S*)-**2**seed used throughout the investigation and the enantiopure product crystals from entry **1** in Table 7.1. It is evident from close examination of the figure that the two diffraction patterns are a very close match despite the relative peak intensities differing for the two sets of data as a result of the differing crystal morphologies seen between the crystal samples due to them being obtained under different conditions. Each of the characteristic peaks occur at the same location with no additional peaks being present the pattern for entry **1** which would indicate a change in crystal structure or the presence of another species. This strongly indicates that it is not being incorporated into the crystal lattice although it is very likely that the catalyst has an effect on the crystallisation kinetics of **2** which is suggested by the strong exhibition of vicinal faces in the CIAT product crystals (Figure 7.4-7.6). Ideally single crystal XRD analysis would have been used to provide conclusive evidence for the lack of catalyst incorporation into the crystal lattice; however, under the conditions of CIAT it was not possible to grow a single crystal off sufficient size.

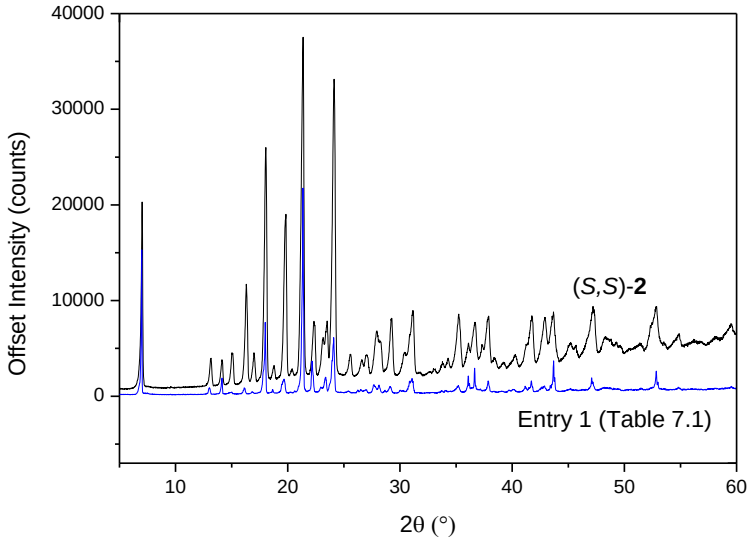

Figure 7.7 X-ray powder diffraction spectra for (*S*,*S*)-**2** and entry **1** from Table 7.1.

7.3.5 Catalyst 4 Activity

For the reasons mentioned in the previous section, the activity of catalyst **4** was investigated to identify whether it was the cause for the mixed success seen in the CIAT runs in which it was used. The length of time that **4** remained active in solution was determined by performing a simple experiment (results not presented) in which a fixed quantity of stock solution consisting of catalytically equilibrated **2** was added to solutions of enantiopure (*S*,*S*)-**2** in toluene at different time intervals, giving a catalyst load of 4 mol%, and left for a period of time to observe if any change in composition occurred due to the activity of the catalyst. Since the time that the stock solution spent racemising was known, it was possible to identify how long it took for catalyst **4** to become inactive since addition of the stock solution to the enantiopure solution at a given time would not result in the latter being equilibrated (the composition being determined by chiral HPLC).

Despite the findings in chapter 5, where the rate of racemisation was shown to be exceptionally fast, the experiment showed that catalyst **4** became deactivated after approximately 1 to 2 hours of operation, since the resulting composition after combing to two solutions exhibited an excess in (*S*,*S*)-**2** corresponding to what was present in the enantiopure solution.

This was investigated further by monitoring the catalytic transformation of (*S*,*S*)-**2** by catalyst **4** using online temperature controlled ^{31}P NMR analysis. Known quantities of (*S*,*S*)-**2**, **4** and KOH were added to an air tight NMR tube, evacuated and purged with argon, after which dry toluene was added using a syringe to give a prescribed concentration and a catalyst load of 4 mol%. The sample was immediately submitted for analysis where it was heated to 50°C with a spectra being recorded every 10 min for a period of 3 hours.

Figure 7.8 shows a selection of the resulting ^{31}P NMR spectra for the racemisation of (*S*,*S*)-**2** by **4** over time. Catalyst **4** gives rise to the peak positioned at δ = 47.6 whilst those occurring at δ = 64.9-63.8 and δ = 57.8 are attributed to the catalyst-substrate complexes that are formed during the catalytic transformation (note: at *t* = 0 there was approximately a 1-2 min delay between initiation of the reaction and recording the first spectra due to the time taken for the instrument to load the sample, hence the *t* = 0 spectra represents a racemising composition, not catalyst **4** alone). At δ = 28.9 triphenylphosphine oxide (PPh_3=O) can be seen to be formed in increasing quantities over the duration of the reaction. Conversely, the peak corresponding to catalyst **4** is gradually reduced, becoming absent from the spectra after around 80 to 90 min of reaction time has elapsed, with those representing the catalyst-substrate intermediates also becoming comparatively less intense. This shows that over the course of the reaction, and hence also during the CIAT runs, catalyst **4** was gradually converted predominantly to PPh_3=O, either through reaction with the oxygen in **2** or with that present in the air in the case that it was not sufficiently removed from the system (although the mechanism is not known). This occurred until **4** was completely void from solution at approximately 80 to 90 min at which point catalytic conversion ceased.

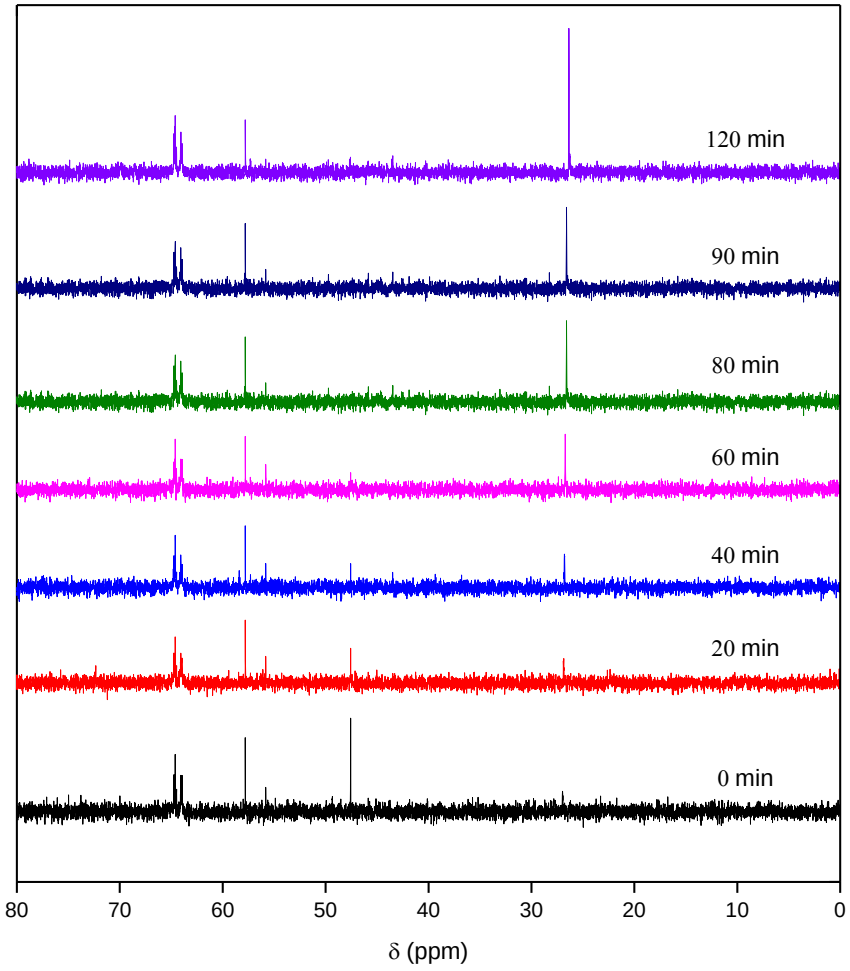

Figure 7.8 ^{31}P NMR (500 MHz, toluene) racemisation of (*S*,*S*)-**2** with catalyst **4** at 50°C: δ = 64.9-63.8 / δ = 57.8 unknown catalyst-substrate intermediates; δ = 47.6 catalyst **4** (s, 2P, PPh_3), δ = 28.9 triphenylphosphine oxide (PPh_3=O) (s, 1P, PPh_3).

The findings from the ^{31}P NMR experiment discussed above can be used to explain the mixed success seen in the data presented in the previous sections for CIAT of **2** with catalyst **4**. For the shorter isothermal runs, for which the process operation time did not exceed 90 min, high enantiomeric purities and in some cases enantiopure product was obtained. However, for those runs operated for greater that 90 min, the antipode was always seen to be present in the resulting crystalline product, with *meso*-**2** and other reaction intermediates also being frequently deposited. The fact that catalytic transformation was shown to cease after 80 to 90 min can be used to interpret the findings of the CIAT experiments.

Upon seeding the catalytically equilibrated solution with enantiopure (*S*,*S*)-**2** at the beginning of the process run, the desired enantiomer was deposited

exclusively without crystallisation of the undesired species since their concentrations were subsequently reduced by the action of the catalyst as soon as the solution phase composition deviated from that observed at equilibrium as a result of growth and secondary nucleation of (*S*,*S*)-**2**. For runs that exceeded 90 min, transformation of the undesired species to (*S*,*S*)-**2** had ceased due to catalyst **4** being absent from solution since it had been converted to PPh_3=O. Consequently, despite the magnitude of supersaturation experienced by the undesired components in solution remaining constant for the isothermal runs, the increased process times lead to their nucleation induction time periods being achieved hence they were deposited from the solution. For the polythermal runs, their magnitude of supersaturation increased with the reduction in temperature since they were not being converted leading to them reaching the metastable solubility limits and crystallising from solution. Thus, for runs in excess of approximately 90 min of operation, the solution phase components were no longer in dynamic catalytic equilibrium and, due to the solid phase equilibria, crystallisation of the undesired species was always observed.

7.4 CIAT of Hydrobenzoin (2) using Chloromonocarbonyltriphenylphosphine-(1,2,3,4,5-pentaphenylcyclopentadienyl)-ruthenium(II) (5)

Complex **5** was investigated for use as a CIAT catalyst due to the findings shown in the previous sections where CIAT of (*S*,*S*)-**2** was attempted using catalyst **4**. During these runs catalytic transformation of the undesired species in solution ceased after approximately 90 min due to the catalyst being converted to PPh_3=O leading to low chiral purity products being obtained since crystallisation of the other system components could not be avoided. Using the same methodology described in the opening paragraph of section 7.3.5, where a fixed quantity of a racemising stock solution was added to enantiopure solutions at prescribed time intervals, catalyst **5** was shown to remain active for up to 5 days of operation. Furthermore, it was shown in section 5.5.2 that **5** is air stable, and can in fact be operated under a pure O_2 atmosphere according to

a literature investigation [126], therefore it was anticipated that the issue seen with **4** disappearing from the reaction mixture due to being converted to PPh_3=O would not occur for **5**.

7.4.1 Isothermal and Cyclic Polythermal Temperature Programmes

Table 7.4 lists the conditions used for a selection of the CIAT runs using **2** and catalyst **5** under the temperature programmes that correspond to **b** and **d** in Figure 7.2, with the total quantity of (*S*,*S*)-**2** initially present in the system as solid and solution also given. The conditions selected were based on the findings of the CIAT experiment using catalyst **4**. A relatively low process temperature was used as this was shown to be favourable since it resulted in the MSZW being wider therefore the seed crystals could remain entrained in the solution for a longer duration of time leading to greater crystal yields. Furthermore, for the majority of the entries present in Table 7.4, comparatively large quantities of seed were used since it was observed that the undesired species in solution were less likely to crystallise during the process since fast removal of solute from solution by seeding resulted in their concentrations being subsequently reduced due to the action of the catalyst.

In entry **1**, the solution was seeded with 10 wt% of (*S*,*S*)-**2** at 38°C at which it was held for 1 h before being immediately filtered. A crystal yield of 13.79% was achieved of which 44.54% and 44.28% were shown by chiral HPLC to be composed of (*S*,*S*)-**2** and (*R*,*R*)-**2** respectively. Considering the initial and final state of the system, this gave a negative change of -5.18% for the total quantity of (*S*,*S*)-**2** present in the system at the end of the process. Initially it was thought that this may have been due to an experimental or measurement error; however, a similar result was seen when repeated, and in entries **2**-**4,** where the largest reduction in the quantity of (*S*,*S*)-**2** present was -9.24%.

This finding suggests that the solution was undersaturated in **5**-rac_{mix}-**2** when the enantiopure crystals were added to the system which would have resulted in (*S*,*S*)-**2** being partially dissolved upon introduction, the extent of which being determined by how far the solution was above the saturation temperature. This would have led to the solution becoming non-equimolar which, in turn, would

have initiated catalytic conversion of the excess enantiomer to re-establish equilibrium. However, from the solubility curve for **5**-*rac*$_{mix}$-**2** (identified in section 6), it is known that the equilibrium solubility temperature at this concentration is 43.2°C; therefore, the system was well within the MSZW which happens to be relatively large at 16.6°C. Furthermore, if the sequence of events described above were to have occurred, it would be expected that only (*S*,*S*)-**2** would be left in the solid phase (assuming it hadn't completely dissolve) since once equilibrated in solution, there would be no driving force for crystallisation. Analysis of the data given for entries **1**-**4** shows that this is not the case, and in fact, for each entry the quantities of (*S*,*S*)-**2** and (*R*,*R*)-**2** present in the product crystals were almost identical, with considerable amounts of *meso*-**2** also being present.

Perhaps even more unexpected were the findings presented in entries **5**-**7**. For each run, the solution was held isothermally for 2 h at 38°C with between 10-50 wt% of seed present. A temperature programme was applied which consisted of initially heating the system by 2°C to 40°C for 30 min, followed by crash cooling by 4°C to 36°C, at which point the system was held for 2 h. This cycle of heating by 2°C and crash cooling by 4°C was repeated to 26°C upon which the solution was immediately filtered. It was though that by initially heating the system above the seed temperature whilst remaining within the MSZW, any undesired species that may have been deposited would be re-dissolved. Subsequent crash cooling would increase the thermodynamic driving force thus resulting in crystallisation of the desired enantiomer onto the seed and inducing catalytic transformation in solution. Repeating the heating stage of the temperature programme would again result in any unwanted solid phase components of the system that may have formed being dissolved; therefore, the process would potentially operate close to equilibrium between the solid and solution phases leading to enantiopure product.

Examination of the data given for entries **5**-**7** shows that, even when 50 wt% of seed crystals were introduced into the system, and in spite of the reduction in process temperature to 26°C, no solids were received at the end of each run i.e. complete dissolution of the seed crystals occurred. Comparing this with entries **1**-**4**, it would be expected that sufficiently more product would be obtained due

to the reduction in temperature changing the position of equilibrium. Furthermore, considering the possibility that the initial heating stage of the temperature programme resulted in the solution becoming unsaturated, with the solubility of the pure enantiomer being double that of its racemate, and again with the comparatively low final process temperature, it would be impossible that the seed would have completed dissolved particularly when 50 wt% was used. Therefore the only conclusion that can be drawn from the findings in entries **1**-**7** is that the phase equilibria is being altered as a result of the catalyst being present in solution.

Table 7.4a Conditions used and results for CIAT experiments using catalyst **5** (4 mol%) and seeding **5**-*rac*$_{mix}$-**2** with (*S*,*S*)-**2**, 0.156 mol l^{-1}, 30 ml scale, temperature programmes a and d (Figure 7.2)[a].

Part 1: **CIAT process conditions**

Entry	T_{Seed} (°C)	Temperature Programme	T_{filt} (°C)	Seed quantity (wt%)	(*S*,*S*)-2 in system (%)[b]
1	38	[a] Isothermal for 1 h	38	10	**38.18**
2	38	[a] Isothermal for 2 h	38	10	**38.18**
3	35.5	[a] Isothermal for 1 h	35.5	10	**38.18**
4	35.5		35.5	20	**38.18**
5	38	[d] Isothermal for 2 h, 40°C for 30 min,	26	10	**38.18**
6	38	crash cool to 36°C, isothermal for 2 h,	26	20	**38.18**
7	38	38°C for 30 min, crash cool to 36°C, isothermal for 2 h, repeat to T_{filt}	26	50	**38.18**

[a]See Figure 7.2 for a graphical presentation of the temperature programmes used corresponding to the value in square brackets. [b]Initial (*S*,*S*)-**2** in system (%) based on **5**-*rac*$_{mix}$-**2** composition in solution (33% (*S*,*S*)-**2**) and seed fraction.

Table 7.4b Conditions used and results for CIAT experiments using catalyst **5** (4 mol%) and seeding **5**-*rac*$_{mix}$-**2** with (*S*,*S*)-**2**, 0.156 mol l^{-1}, 30 ml scale, temperature programmes a and d (Figure 7.2)[a].

Part 2: Theoretical and obtained crystal yields

Entry	Theoretical yields		Product Yields		
	Product mass including seed (g)[c]	Mass of (*S*,*S*)-2 in product (g)[d]	Product mass including seed (g)	Product Mass (g)[e]	Crystal Yield (%)[e]
1	0.39	0.19	0.14	0.04	13.79
2	0.39	0.19	0.18	0.08	27.57
3	0.50	0.23	0.21	0.11	27.61
4	0.60	0.33	0.47	0.27	67.02
5	0.72	0.30			
6	0.82	0.40	Seed dissolved		
7	1.12	0.70			

[c]Theoretical mass from **5**-*rac*$_{mix}$-**2** solubility curve (Figure 6.5). [d]Theoretical mass of (*S*,*S*)-**2** in product with no racemisation, based on **5**-*rac*$_{mix}$-**2** composition (33% (*S*,*S*)-**2**) and seed fraction. [e]Not including seed.

Table 7.4c Conditions used and results for CIAT experiments using catalyst **5** (4 mol%) and seeding **5**-*rac*$_{mix}$-**2** with (*S*,*S*)-**2**, 0.156 mol l^{-1}, 30 ml scale, temperature programmes a and d (Figure 7.2)[a].

Part 3: Product Composition (%)[f]

Entry	(*S*,*S*)-2	(*R*,*R*)-2	*meso*-2	Benzil	Stilbene	Benz-aldehyde
1	44.45	44.28	10.57	0.00	0.00	0.70
2	44.22	43.99	11.04	0.00	0.00	0.75
3	43.06	37.97	18.97	0.00	0.00	0.00
4	46.12	40.38	13.18	0.00	0.00	0.32
5						
6			Seed dissolved			
7						

[f]Determined by chiral HPLC (see section 11.1.5 for method details).

Table 7.4d Conditions used and results for CIAT experiments using catalyst **5** (4 mol%) and seeding **5**-*rac*$_{mix}$-**2** with (*S*,*S*)-**2**, 0.156 mol l^{-1}, 30 ml scale, temperature programmes a and d (Figure 7.2)[a].

Part 4: System Composition

Entry	Mass of (*S*,*S*)-2 in product (g)[g]	Remaining (*S*,*S*)-2 in solution (g)[h]	(*S*,*S*)-2 in system[i]		Change in total (*S*,*S*)-2 composition (%)[j]
			(g)	(%)	
1	0.06	0.34	0.40	36.20	-5.18
2	0.08	0.32	0.40	36.51	-4.38
3	0.09	0.31	0.40	36.54	-4.30
4	0.22	0.26	0.47	39.33	-9.24
5					
6			Seed dissolved		
7					

[g]From chiral HPLC data and product mass. [h](*S*,*S*)-**2** in solution based on solubility curve, product mass and **5**-*rac*$_{mix}$-**2** composition (33% (*S*,*S*)-**2**). [i]Both solid and solution phase contributions. [j]Percent change in (*S*,*S*)-**2** composition considering initial and final solid and solution phases.

7.4.2 Catalyst 5 Activity

The activity of the complex **5** during catalytic transformation of **2** was investigated as a result of the unexpected events described in the previous section whereby attempts of **2** CIAT using catalyst **5** led to either a reduction in the total quantity of (*S*,*S*)-**2** present in the system for short relative process times, or complete dissolution of the seed when longer times were utilised despite large quantities of seed being introduced into the system. To determine what was occurring in solution, a mixture of **5**-*rac*$_{mix}$-**2** and KOH was dissolved in toluene-d8 at 50°C. 4 mol% of catalyst **4** was then added and known solution volumes samples at regular intervals to be analysed by chiral HPLC.

Figure 7.9 shows the chiral HPLC data for the solution phase over time. Unexpectedly, it evident that there is a significant change in composition over time with (*S*,*S*)-**2**, (*R*,*R*)-**2** and *meso*-**2** eventually disappearing from solution. At 15 h the solution was free of the enantiomers and the meso form being composed predominantly of benzaldehyde, with some stilbene and benzil present in small quantities, indicating that C-C bond cleavage had occurred. This finding can be used to give a possible explanation for the observations seen when CIAT of **2** was attempted with **5**.

For short process times of 1 to 2 h where crystals were recovered with roughly equimolar quantities of each enantiomer (entries **1**-**4** in Table 7.4), addition of the seed to the supersaturated solution would have resulted in (*S*,*S*)-**2** initially being deposited from solution followed by catalytic transformation of the other species. Simultaneously, (*S*,*S*)-**2** and (*R*,*R*)-**2** were being converted to the considerably more soluble benzaldehyde in solution reducing their concentrations which, in turn, would have led to a portion of the (*S*,*S*)-**2** seeds dissolving to compensate, whilst it is likely that, despite the drop in concentration, (*R*,*R*)-**2** eventually crystallised since it was still supersaturated with its loss being compensated for through catalytic conversion of (*S*,*S*)-**2**. Hence, at the end of the process, when the mass balance was calculated, the total composition of (*S*,*S*)-**2** was shown to reduce since it was converted to benzaldehyde, and was likely also transformed to (*R*,*R*)-**2**. For the runs in

excess of 2 h (entries **5**-**7** in Table 7.4), as they were gradually transformed to benzaldehyde, the concentration of the enantiomers and meso form in solution would have subsequently reduced leading to dissolution of the seeds and any additional solids that may have formed due to crystallisation of the undesired species. Therefore, despite the high activity of the catalyst, the tendency of **5** to convert the desired enantiomer and its stereoisomers into by-products over time rendered it unsuitable for CIAT thus the experimental runs in which it was used were unsuccessful.

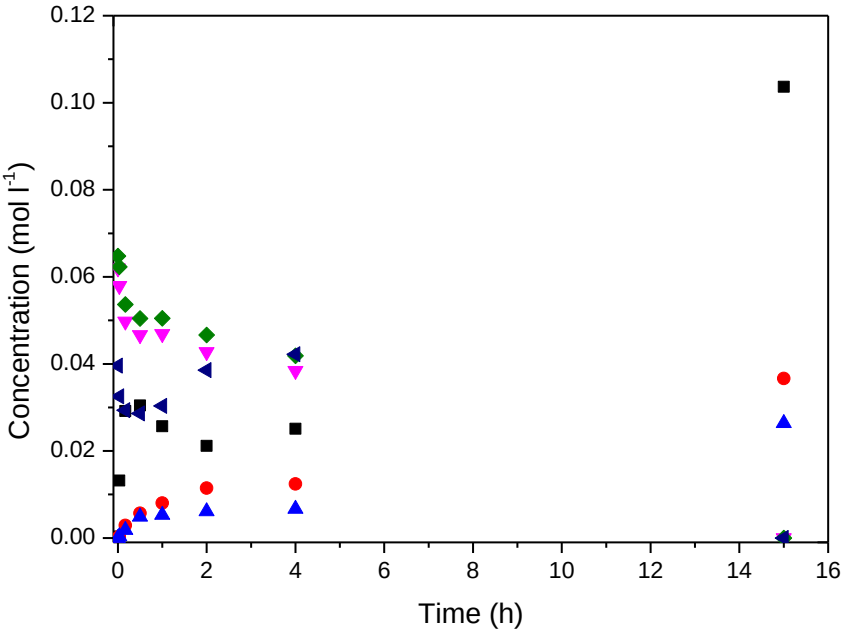

Figure 7.9 Drop in **5**-*rac*$_{mix}$-**2** concentration with time under catalytic conditions using complex **5** (*S*,*S*)-**2**, (*R*,*R*)-**2**, *meso*-**2**, benzaldehyde, benzil, stilbene. (◆ (*S*,*S*)-**2**, ▼ (*R*,*R*)-**2**, ◀ *meso*-**2,** ● benzil, ■ benzaldehyde, ▲ stilbene).

7.5 CIAT Using Other Catalysts Investigated

CIAT of **2** was also attempted using chlorodicarbonyl-(1,2,3,4,5-pentaphenylcyclopentadienyl)-ruthenium(II) as a racemisation catalyst (results not presented). Comparable results to **4** were seen using this catalyst which is likely due to their structural similarities, differing only by a single ligand. This complex was also observed to become inactive after period of time and was also significantly more expensive therefore its use through the CIAT investigation was limited relative to catalyst **4**.

7.6 Attrition-Enhance De-racemisation (Viedma Ripening)

In addition to the CIAT process, the attrition-enhanced de-racemisation system was also investigated using **2** as a substrate and catalysts **4** and **5** (results not presented). In a round bottom flask, **4**- or **5**-*rac*$_{mix}$-**2** were added with a known excess of (*S*,*S*)-**2** (10-50%) followed by **4** or **5** and KOH. 3 mm glass beads were then introduced to the vessel which was subsequently sealed. A known quantity of toluene was then syringed into the system giving a slurry which had a fixed excess of the desired enantiomer (note: for runs using **4**, the system was purged with argon, with degassed dry toluene being used as the process solvent). The slurry was heated to the desired temperature and stirred vigorously for time periods of several days to weeks, at which point the reactor contents were filtered, washed with cold toluene, and the product analysed by chiral HPLC.

Due to the problems seen with catalysts **4** and **5** when used in CIAT, none of the Viedma ripening runs resulted in successful de-racemisation of the system. The product obtained using **4** exhibited a composition corresponding to that at the start of the process which would be expected knowing that the complex becomes in active after approximately 90 min, whilst the experimental runs lasted up to several weeks. When **5** was used as the catalyst, no solids were obtained at the end of the process due to conversion of the enantiomers and meso form to benzaldehyde as discussed in the previous sections.

7.7 CIAT Modelling

In addition to the experimental work performed during the investigation, a model for the CIAT system was proposed to simulate the process of selective crystal growth by preferential crystallisation of a single enantiomer from solution using a population balance model, with simultaneous replacement of the crystallised solute through the racemisation reaction. However, due to the mixed successes seen during the experimental investigations, particularly the difficulty in obtaining enantiopure crystal using CIAT, implementation of the model was not

taken forward. The discussion below gives a general outline of the proposed model and the associated assumptions.

For a batch crystallisation, assuming perfect mixing and no particle breakage or agglomeration, the crystal number density distribution, $n(t,L)$ (# crystals m^{-3}), as a function of time, t (s), and of a one-dimensional characteristic length, L (m), can be obtained using the population balance equation which can be written as[163]:

$$\frac{\partial n(t,L)}{\partial t} + \frac{\partial [n(t,L)G(t)]}{\partial L} = 0 \qquad \text{Equation 7.1}$$

where $G(t)$ is the crystal linear growth rate (m s^{-1}) in the direction of the characteristic length, L, i.e.

$$G = \frac{dL}{dt} \qquad \text{Equation 7.2}$$

Equation 7.1 can be solved in discretised form to yield $n(t,L)$ by applying a backward finite difference approximation with a time step Δt and characteristic length step ΔL. For CIAT, under ideal conditions, crystallisation of the desired enantiomer occurs solely through growth on the crystal seeds whilst the undesired enantiomer remains dissolved in solution therefore it can be assumed that no nucleation occurs during the process or:

$$B = \frac{dN}{dt} = 0 \qquad \text{Equation 7.3}$$

where B is the nucleation rate (# crystals m^{-3} s^{-1}) and N is the number of crystals. Since CIAT involves introducing seed crystals to the solution, at the beginning of the process

$$n(0,L) > 0 \qquad \text{Equation 7.4}$$

i.e. the number of crystals initially present is determined by the quantity and characteristic length, L, of the seeds. Using the population balance equation,

the rate of mass deposition of the desired enantiomer (e.g. the (*S*)-enantiomer) from solution, $J_{S\text{-}crys}$ (kg m^{-3} s^{-1}) can be determined by numerically solving the expression:

$$J_{S-crys} = \frac{dM_{S-crys}}{dt} = 3k_v\rho_{crys}G(t)\int_{Lmin}^{L_{max}} n(t,L)\,L^2 dL \qquad \text{Equation 7.5}$$

where $M_{S\text{-}crys}$ is the mass of desired solute (in this case the (*S*)-enantiomer) crystallised (kg), k_v is the geometric shape factor (k_v = 1 for a cubic particle) and ρ_{crys} is the crystal density (kg m^{-3}).

During the CIAT process, as the desired enantiomer is deposited onto the seed crystals, it is simultaneously replaced in solution due to the action of the catalysts by converting the excess antipode thus re-establishing an equimolar enantiomeric composition. In Chapter 5 it was shown that the rate of racemisation can be fitted to the form

$$J_{R\to S} = \frac{dM_{R\to S}}{dt} = M_w k C_R^n \qquad \text{Equation 7.6}$$

where $J_{R\to S}$ is the rate of mass conversion of the undesired enantiomer (in this case (*R*)-) to the desired (*S*)-enantiomer (kg m^{-3} s^{-1}), M_w is the molecular weight (kg $kmol^{-1}$), C_R is the concentration of (*R*)-enantiomer which is in excess as a result of crystallisation of (*S*)- (kmol m^{-3}), *n* is the reaction order, and *k* is the reaction rate constant ($m^{(n-1)}$ $mol^{-(n-1)}$ s^{-1}). Hence combining the expressions for crystallisation given above with the kinetic equation for the racemisation reaction leads to a description for the rate of solution (and solid) phase change in mass of the desired (*S*)-enantiomer, $dM_{S\text{-}sol}/dt$ (kg m^{-3} s^{-1}), which assumes that crystallisation proceeds via crystal growth only and that crystallisation of the undesired enantiomer does not occur:

$$\frac{dM_{S-sol}}{dt} = -J_{S-crys} + J_{R\to S} \qquad \text{Equation 7.7}$$

7.8 Chapter Summary

Crystallisation-induced asymmetric transformation (CIAT) of the conglomerate alcohol hydrobenzoin (**2**) was attempted using the organometallic catalysts chloro(indenyl)-bis-(triphenylphosphine)-ruthenium(II) (**4**) and chloromonocarbonyltriphenylphosphine-(1,2,3,4,5-pentaphenylcyclopentadienyl)-ruthenium(II) (**5**) for solution phase racemisation.

Based on the racemisation kinetics (chapter 5) and the solubility of the stereoisomeric mixtures that resulted upon catalytic transformation of **2** with **4** and **5**, **4**-*rac*$_{mix}$-**2** and **5**-*rac*$_{mix}$-**2** respectively (chapter 6), conditions were selected for CIAT to allow the enantiopure crystals (prepared using methodology outlined in chapter 6) to be introduced into the system whilst the solution was within the metastable zone so that a sufficient driving force for crystallisation existed. Taking the rates of racemisation and crystallisation into consideration, the parameters suspected to be influential to the success of the process were highlighted to attempt to identify a suitable methodology for operation of the CIAT system which were the cooling programme, seeding temperature i.e. degree of supersaturation, seed quantity, solution concentration and catalyst load, which were all varied to attempt to identify conditions that would yield optically pure product.

Using catalyst **4**, it was possible to obtain enantiopure (99.71% chemical purity) product crystals of the desired enantiomer (*S*,*S*)-**2**, albeit with a relatively low crystal yield (16.46%), using an isothermal temperature programme which consisted of crash cooling a slurry of the seed to well below the saturation temperature of **4**-*rac*$_{mix}$-**2** and holding for a period of up to 90 min. This translated into an increase of 8.98% in the total quantity of (*S*,*S*)-**2** present in the system in both the solid and solution phases, indicating that, through the action of seeding the equilibrated solution, the undesired stereoisomers had been converted to (*S*,*S*)-**2.** For a slight reduction in purity (99.59%), the maximum crystal yield obtained for the runs in which enantiopure products were recovered was 21.94% which consequently gave the largest change in the quantity of (*S*,*S*)-**2** present in the system (11.95%). Despite the operating temperature being considerably lower than the metastable equilibrium temperature, T_{cryst}, for **4**-*rac*$_{mix}$-**2,** the solution was seen to remain metastable

well beyond the metastable solubility due to the rate of supersaturation generation not allowing sufficient time for the molecular addition process that is required to form a 3-D crystal.

For CIAT runs using **4** in excess of 90 min, for both isothermal and polythermal temperature programmes, enantiopure crystals were never obtained. Investigation into the activity of the catalyst showed that, in addition to converting the undesired species, **4** itself was gradually converted to triphenylphosphine oxide in solution leading to racemisation ceasing. As a result, the antipode and *meso* form were found to be present in the product crystals obtained at the end of the process due to them reaching their metastable limits and crystallising. Despite this, changes in total (*S*,*S*)-**2** system compositions of up to 61.57% (81.31% crystal yield) were seen when the polythermal temperature program was applied indicating that a substantial quantity of the undesired species had be transformed into (*S*,*S*)-**2**.

Issues related to the catalyst during CIAT were also observed for complex **5**. In contrast to **4**, **5** remained active for the duration of the process; however, instead of maintaining an equilibrated solution, the stereoisomers (*S*,*S*)-**2,** (*R*,*R*)-**2** and *meso*-**2** were all consumed being converted almost entirely to benzaldehyde. Consequently, despite large quantities of seed being introduced well below the saturation temperature of **5**-rac_{mix}-**2**, complete dissolution of the solid was observed in all of the runs that exceeded 2 h. Furthermore, for the shorter runs in which product was recovered, as a result of the solution concentration being reduced to the by-product formation, negative changes in the (*S*,*S*)-**2** total system composition were observed which was due to the seed crystals partially dissolving

In addition to CIAT, the attrition-enhanced de-racemisation process (Viedma Ripening) was also attempted using the conglomerate **2** and the racemisation catalysts **4** and **5**. Due to the issues with the catalysts described above, de-racemisation was not observed in any of the runs attempted. For **4**, the resulting composition was equivalent to that at the start of the process since it was consumed after a short period of time hence no solution phase transformation was occurring. On the other hand, use of **5** led to complete dissolution of the slurry since the stereoisomers in solution were converted to benzaldehyde

which as a result reduced their concentration in solution leading to it become undersaturated in solute.

Finally, a model for CIAT was proposed based on combining a population balance model for batch cooling crystallisation with the kinetics for in-*situ* solution phase racemisation of the excess undesired enantiomer.

8 Conclusions

A novel approach to the CIAT process was investigated by using organometallic catalysts **4** and **5** for solution phase racemisation to obtain a single enantiomer of **2** from an initially racemic mixture of a conglomerate forming system. Use of these complexes to establish dynamic equilibrium between solution phase enantiomers does not necessitate the presence of low pKa chiral protons, which has been the prerequisite for previously demonstrated CIAT examples limiting its use as an industrial scale method of producing pure enantiomers. Therefore the application of organometallics as racemisation catalysts in CIAT could potentially increase the number of conglomerates that can be resolved by this process.

To attempt CIAT with racemisation catalysts it was first necessary to identify a suitable model chiral compound which meets the requirements of the process, the most essential of which being that it crystallises as a stable racemic conglomerate (see chapter 4.3 for a discussion of the model chiral system selection criteria). It was also necessary that the chosen compound had the potential to undergo racemisation using available organometallic complexes which resulted in chiral alcohols and amines being earmarked for selection as extensive examples of their racemisation have been demonstrated. In chapter 4 several compounds listed as conglomerates in the literature were screened to identify a model system for use in the CIAT process. Of these hydrobenzoin (1,2-diphenylethane-1,2-diol), **2**, a chiral system containing two identical 2° alcohol stereogenic centres, was selected to be taken forward in the study as it was shown to form a stable conglomerate when crystallised.

In chapter 5, racemisation of (*S*,*S*)-**2** was attempted using a number of known iridium and ruthenium-based racemisation catalysts. The iridium-based complexes were found to be unsuccessful at racemising the chiral alcohol; however, as anticipated due to their success in DKR, those based on ruthenium were shown to be highly active with complete racemisation being possible within ~2 min under some of the conditions investigated. Three organometallic

complexes were selected for use as CIAT racemisation catalysts; Chloro(indenyl)-bis-(triphenylphosphine)-ruthenium(II) (**4**), chlorodicarbonyl-(1,2,3,4,5-pentaphenylcyclopentadienyl)-ruthenium(II) (**5**) and chlorocarbonyl-triphenylphosphene(1,2,3,4,5-pentaphenylcyclopentadienyl)-ruthenium(II) (**6**).

With the model chiral system and potential racemisation catalysts selected, the conditions required for CIAT were identified in chapter 6. Racemisation of (*S*,*S*)-**2** resulted in the formation of its antipode but also led to equivalent amounts of *meso*-**2** being formed in addition to small quantities of other related by-products including benzaldehyde. As a consequence, it was necessary to identify the equilibrium and metastable solubilities of the mixtures that resulted upon racemisation (*S*,*S*)-**2** with catalysts **4** and **5** (**4**-*rac*$_{mix}$-**2** and **5**-*rac*$_{mix}$-**2**) using each of the chosen complexes (as opposed to that of the true racemate which would be required for non-catalytic preferential crystallisation) since addition of the catalyst to any mixture of **2** stereoisomers would eventually lead to the corresponding equilibrated composition. The metastable zone width was determined for each of the racemisation mixtures **4**-*rac*$_{mix}$-**2** and **5**-*rac*$_{mix}$-**2** to be used as a basis to select conditions for CIAT. Finally enantiopure crystals of **2** enantiomers were prepared to be used for seeding.

The results of the CIAT experiments performed using the model conglomerate **2** and the racemisation catalysts **3** and **4** were presented in chapter **7**. Enantiopure product crystals with up to 99.71% purity were obtained with catalysts **4** using an isothermal temperature programme in which the undersaturated solution was crash cooled to well below the saturation temperature of **4**-*rac*$_{mix}$-**2** where it was held for periods of up to 90 min. However; for each of the optically active products recovered at the end of the CIAT process, low crystals yields were observed with the maximum being 21.94% which consequently gave the largest change in the quantity of (*S*,*S*)-**2** present in the system (11.95%) for the enantiopure products obtained. The latter finding confirmed that by introducing enantiopure seed to the solution of catalytically equilibrated enantiomers, it was possible to convert the undesired species including the antipode and meso form into (*S*,*S*)-**2** by the action of the CIAT process.

Crystal yield was improved, with up to 86.78% being achieved, by increasing the process time, using a reduced concentration, and applying a polythermal temperature programme which allowed the system to operate closer to equilibrium between the solid and solution phases. Similarly, increases of up to 61.57% where observed in the total quantity of (*S*,*S*)-**2** present in both the solid and solution phases at the end of the process due to the longer process times and wider MSZW at lower concentrations. However, in each of these CIAT runs, and in fact all those operated beyond 90 min, crystallisation of (*S*,*S*)-**2** and *meso*-**2** could not be avoided.

It was shown that this was a result of issues with the catalyst. After approximately 1-2 h, **4** had been completely converted to triphenylphosphine oxide in solution which led to catalytic conversion of the **2** stereoisomers ceasing. Consequently, when the saturated solution was initially seeded, the excess antipode and meso form were converted to (*S*,*S*)-**2** which lowered their concentrations hence they remained within their respective metastable zones and did not spontaneously nucleate which resulted in the ability to obtain enantiopure products for short operation times. At the point where the catalysts had been completely converted to benzaldehyde, the lack of catalytic conversion led to the undesired species becoming increasingly more supersaturated which eventually led to them reaching their metastable limits and thus crystallisation was observed.

Issues were also seen when catalyst **5** was employed in CIAT. In the runs performed for a duration of time in excess of 2 h, the seed crystals that were initially introduced to the system were found to have dissolved with no product being obtained under these conditions, even when the amount of seed was increased to 50 wt% of **5**-rac_{mix}-**2**. Conversely, for process times less than 2 h, solids were recovered; however, the total quantity of (*S*,*S*)-**2** in the system in both the solid and solution phases was seen to decrease. Investigation into the activity of catalyst **5** revealed that, in addition to converting the undesired enantiomers into (*S*,*S*)-**2** which was being removed by crystallisation, each of the stereoisomers was also reacting to form benzaldehyde which led to them eventually being completely consumed. As a result, their solution concentrations were reduced leading to them becoming undersaturated

therefore dissolution of the seed occurred. For the shorter duration runs, this was interrupted before complete dissolution had occurred; however, that which had transferred into solution was converted to the undesired species resulting in a reduction in the (*S*,*S*)-**2** composition being observed.

The attrition-enhanced de-racemisation process (Viedma Ripening) was also attempted using the conglomerate **2** and the racemisation catalysts **4** and **5**. For the reasons discussed above with regards to the performance of the catalysts, no enhancements in optical activity were achieved with no change in the system composition being observed with **4,** and complete dissolution of the solids occurring when **5** was utilised.

9 Future Work

Despite the mixed successes seen during the investigation, CIAT using general purpose racemisation catalysts is sure to become a more utilised method of obtaining single enantiomers from a racemate as the understanding in the respective areas of conglomerate formation and homogeneous racemisation catalysis are progressed. Throughout the course of the study, two factors were found to be a hindrance in achieving a successfully operating CIAT system which are recommended to be the focus of future works:

- The ability to identify suitable candidates for CIAT that form a conglomerate but also have the functionality that allows for racemisation
- The availability of organometallic complexes that:
    - do not require the substrate to have a chiral proton
    - are air stable
    - are capable of efficiently racemising without the need for additives to induce activity which could affect crystallisation
    - have long lasting activity
    - are not consumed during racemisation
    - are selective in that they only induce racemisation and do not catalyse by-product formation
    - are inert to the effects of solvents

During the investigation, the requirement of the conglomerate to possess a chiral proton was perhaps the most significant limitation of the proposed CIAT process. Many examples of racemates that crystallise as conglomerates have been demonstrated in the literature; however, organometallic racemisation is currently constrained to chiral alcohols and amines, with the latter being far less established. This severely restricted the number of conglomerates that could have potentially been used since a wide variety of functionality exists for those that are known. Future work should focus on developing complexes that are functionally more widely applicable to broaden the number of chiral systems that could be potential candidates for CIAT.

For established catalysts that have been shown to be capable of racemising chiral alcohols and amines, efforts should be focussed of increasing performance to give longer activity times, lower by-product formation and solvent tolerance. Furthermore, the vast majority of available organometallics are air sensitive which increases the complexity of operating CIAT since inert atmospheres and degassed solvent must be used. A possible approach to resolving these issues is to take known complexes and trial many different ligands to observe the resultant effects on racemisation performance and applicability.

In addition to the requirement of more robust catalysts, a better understanding of conglomerate formation is required. If conditions could be prescribed that influence conglomerate formation it may be possible to increase the number of racemates that could be used in CIAT. A more realistic short term approach would be to conduct a thorough screening of existing chiral compounds as there are few recent examples. This could also be expanded to altering the molecular functionality of known racemates similarly followed by a structural screening of the configurations that result.

It is known that the formation of salts using achiral agents can significantly increase the probability of conglomerate formation; however, this limits the number of complexes that can be used for racemisation since the acidic or basic process conditions that result from salt dissolution are unsuitable for most racemisation catalysts. Despite this, it is likely that development of this methodology presents the most promising advancement; however, suitably robust catalysts would need to be identified through experimentation.

As of current, development of a successful CIAT system using organometallics is likely due to be determined by the chance of identifying a compatible system of conglomerate and catalyst. In the event that this does occur, the influential conditions discussed in section 7.2.2 in conjunction with the knowledge acquired from existing literature examples of CIAT should be used as a basis for development of a successful process.

10 References

1. Sheldon, R. A. *Chirotechnology: Industrial Synthesis of Optically Active Compounds.* New York: Taylor & Francis, 1993

2. Mislow, K. and J. Siegel. Stereoisomerism and local chirality. *Journal of the American Chemical Society.* 1984, **106**(11), 3319-3328

3. Wagner, K. *Bioinformatics: Amino Acids.*[Online]. 2001. [Accessed March]. Available from: http://www.imb-jena.de/~rake/Bioinformatics_WEB/basics_amino_acids.html

4. Cross, L. and W. KLYNE. REPORT FROM IUPAC COMMISSION ON NOMENCLATURE OF ORGANIC-CHEMISTRY-RULES FOR NOMENCLATURE OF ORGANIC-CHEMISTRY. E. STEREOCHEMISTRY (RECOMMENDATIONS 1974). *Pure and Applied Chemistry.* 1976, **45**(1), 13-30

5. Izumi, T. *Exploring the Origin of Biological Homochirality via Study of Amino Acid Phase Behavior.* Imperial College, 2010

6. Cushny, A. R. and A. R. Peebles. The action of optical isomers II. Hyoscines. *The Journal of physiology.* 1905, **32**(5-6), 501-510

7. Casey, A. F. *Medicinal Chemistry* New York: Wiley International, 1970

8. Daniels, T. and E. Jorgensen. Metabolic changes of drugs and related organic compounds (detoxication). *Textbook of organic, medicinal and pharmaceutical chemistry, 6th edn. Lippincott, Philadelphia.* 1971, **108**

9. Jacques, J., A. Collet and S. H. Wilen. *Enantiomers, racemates, and resolutions.* Wiley, 1981

10. Services, U. S. D. o. H. a. H. *U.S. Food and Drug Administration: Development of New Stereoisomeric Drugs.*[Online]. 1992. [Accessed April]. Available from: http://www.fda.gov/Drugs/GuidanceComplianceRegulatoryInformation/Guidances/ucm122883.htm.

11. Eriksson, T., S. Björkman and P. Höglund. Clinical pharmacology of thalidomide. *European journal of clinical pharmacology.* 2001, **57**(5), 365-376

12. Challener, C. A. *Chiral drugs.* Wiley, 2001

13. de Vries, J. G. and C. J. Elsevier. *Handbook of Homogeneous Hydrogenation: 3 Volumes.* Wiley, 2006

14. Allen, J. V. and J. M. Williams. Dynamic kinetic resolution with enzyme and palladium combinations. *Tetrahedron letters.* 1996, **37**(11), 1859-1862

15. Bäckvall, J.-E. and U. Andreasson. Ruthenium-catalyzed isomerization of allylic alcohols to saturated ketones. *Tetrahedron letters.* 1993, **34**(34), 5459-5462

16. Blacker, A. J., S. Brown, B. Clique, B. Gourlay, C. E. Headley, S. Ingham, D. Ritson, T. Screen, M. J. Stirling and D. Taylor. A Low-Waste Process To Sertraline By Diastereomeric Crystal Resolution and Waste Isomer Racemisation. *Organic Process Research & Development.* 2009, **13**(6), 1370-1378

17. Blacker, A. J., M. J. Stirling and M. I. Page. Catalytic racemisation of chiral amines and application in dynamic kinetic resolution. *Organic Process Research & Development.* 2007, **11**(3), 642-648

18. Hilker, I., G. Rabani, G. K. Verzijl, A. R. Palmans and A. Heise. Chiral polyesters by dynamic kinetic resolution polymerization. *Angewandte Chemie International Edition.* 2006, **45**(13), 2130-2132

19. Kim, M.-J., W.-H. Kim, K. Han, Y. K. Choi and J. Park. Dynamic kinetic resolution of primary amines with a recyclable Pd nanocatalyst for racemization. *Organic letters.* 2007, **9**(6), 1157-1159

20. Reetz, M. T. and K. Schimossek. Lipase-catalyzed dynamic kinetic resolution of chiral amines: use of palladium as the racemization catalyst. *CHIMIA International Journal for Chemistry.* 1996, **50**(12), 668-669

21. Anderson, N. G. Developing processes for crystallization-induced asymmetric transformation. *Organic Process Research & Development.* 2005, **9**(6), 800-813

22. Brands, K. M. and A. J. Davies. Crystallization-induced diastereomer transformations. *Chemical reviews.* 2006, **106**(7), 2711-2733

23. Boyle Jr, W. J., S. Sifniades and J. Van Peppen. Asymmetric transformation of. alpha.-amino-. epsilon.-caprolactam, a lysine precursor. *The Journal of Organic Chemistry.* 1979, **44**(26), 4841-4847

24. Noorduin, W. L., T. Izumi, A. Millemaggi, M. Leeman, H. Meekes, W. J. Van Enckevort, R. M. Kellogg, B. Kaptein, E. Vlieg and D. G. Blackmond. Emergence of a single solid chiral state from a nearly racemic amino acid derivative. *Journal of the American Chemical Society.* 2008, **130**(4), 1158-1159

25. Noorduin, W. L., B. Kaptein, H. Meekes, W. J. van Enckevort, R. M. Kellogg and E. Vlieg. Fast Attrition-Enhanced Deracemization of Naproxen by a Gradual In Situ Feed. *Angewandte Chemie International Edition.* 2009, **48**(25), 4581-4583

26. Noorduin, W. L., H. Meekes, A. A. Bode, W. J. van Enckevort, B. Kaptein, R. M. Kellogg and E. Vlieg. Explanation for the emergence of a single chiral solid state during attrition-enhanced Ostwald ripening: survival of the fittest. *Crystal Growth and Design.* 2008, **8**(5), 1675-1681

27. Noorduin, W. L., H. Meekes, W. J. van Enckevort, A. Millemaggi, M. Leeman, B. Kaptein, R. M. Kellogg and E. Vlieg. Complete Deracemization by Attrition-Enhanced Ostwald Ripening Elucidated. *Angewandte Chemie International Edition.* 2008, **47**(34), 6445-6447

28. Sainz-Díaz, C. I., A. P. Martín-Islán and J. H. Cartwright. Chiral symmetry breaking and polymorphism in 1, 1'-binaphthyl melt crystallization. *The Journal of Physical Chemistry B.* 2005, **109**(40), 18758-18764

29. Shieh, W.-C. and J. A. Carlson. Asymmetric transformation of either enantiomer of narwedine via total spontaneous resolution process, a concise solution to the synthesis of (-)-galanthamine. *The Journal of Organic Chemistry.* 1994, **59**(18), 5463-5465

30. Tsogoeva, S. B., S. Wei, M. Freund and M. Mauksch. Generation of highly enantioenriched crystalline products in reversible asymmetric reactions with racemic or achiral catalysts. *Angewandte Chemie International Edition.* 2009, **48**(3), 590-594

31. Viedma, C. Chiral symmetry breaking during crystallization: complete chiral purity induced by nonlinear autocatalysis and recycling. *Physical review letters.* 2005, **94**(6), 065504

32. Mullin, J. W. *Crystallization.* Butterworth-Heinemann, 2001

33. Rousseau, E. R. W. *Handbook Of Separation Process Technology.* Wiley India, 2009

34. Myerson, A. S. *Handbook of industrial crystallization [electronic resource].* Butterworth-Heinemann Limited, 2002

35. Harker, J. H., J. R. Backhurst and J. F. Richardson. *Chemical Engineering.* Elsevier Science, 2002

36. Volmer, M. Kinetik der phasenbildung. 1939

37. Ting, H. H. and W. L. McCabe. Supersaturation and crystal formation in seeded solutions. *Industrial & Engineering Chemistry.* 1934, **26**(11), 1201-1207

38. Strickland-Constable, R. and R. Mason. Breeding of nuclei. 1963

39. Garside, J. and R. J. Davey. Invited review secondary contact nucleation: kinetics, growth and scale-up. *Chemical Engineering Communications.* 1980, **4**(4-5), 393-424

40. Nyvlt, J., O. Sohnel, M. Matuchova and M. Broul. The kinetics of industrial crystallizationElsevier. *New York.* 1985

41. Hussain, K., G. Thorsen and D. Malthe-Sørenssen. Nucleation and metastability in crystallization of vanillin and ethyl vanillin. *Chemical engineering science.* 2001, **56**(7), 2295-2304

42. Nývlt, J., R. Rychlý, J. Gottfried and J. Wurzelová. Metastable zone-width of some aqueous solutions. *Journal of crystal growth.* 1970, **6**(2), 151-162

43. Liang, K., G. White, D. Wilkinson, L. J. Ford, K. J. Roberts and W. M. Wood. An examination into the effect of stirrer material and agitation rate on the nucleation of L-glutamic acid batch crystallized from supersaturated aqueous solutions. *Crystal growth & design.* 2004, **4**(5), 1039-1044

44. Mullin, J. W. Crystallization and Precipitation. *Ullmann's Encyclopedia of Industrial Chemistry*: Wiley-VCH Verlag GmbH & Co. KGaA, 2000

45. Roberts, K. J. *Crystal Growth. Lecture notes distributed in PEME5303M Pharmaceutical Product Formulation.* University of Leeds: 2009

46. Lorenz, H., J. von Langermann, G. Sadiq, C. C. Seaton, R. J. Davey and A. Seidel-Morgenstern. The Phase Behavior and Crystallization of 2-Chloromandelic Acid: The Crystal Structure of the Pure Enantiomer and

the Behavior of Its Metastable Conglomerate. *Crystal growth & design.* 2011, **11**(5), 1549-1556

47. Roozeboom, H. B. *Löslichkeit und Schmelzpunkt als Kriterien für racemische Verbindungen, pseudoracemische Mischkrystalle und inaktive Konglomerate.* Engelmann, 1899

48. Mitchell, A. G. *Racemic Mixture, Racemic Compound or Pseudoracemate?*[Online]. 1998. [Accessed 29 April]. Available from: http://www.ualberta.ca/~csps/JPPS1(1)/A.Mitchell/racemicview.htm

49. Schröder, I. Über die Abhängigkeit der Löslichkeit eines festen Körpers von seiner Schmelztemperatur. *Z. phys. Chem.* 1893, **11**, 449-465

50. Van Laar, J. Process of the fusion curves of firm alloys and amalgams. *Arch. Neerl.* 1903, **8**, 264-284

51. Coquerel, G. Preferential crystallization. *Novel Optical Resolution Technologies*: Springer, 2007, 1-51

52. Stosch, R., M. M. Welzel, S. Bauerecker and H. Karlcammenga. Simulation of Calorimetric Melting Processes—A Useful Tool for Enantiomeric Purity Determination. *Molecular Crystals and Liquid Crystals.* 1998, **312**(1), 285-295

53. Lorenz, H., D. Sapoundjiev and A. Seidel-Morgenstern. Enantiomeric mandelic acid system melting point phase diagram and solubility in water. *Journal of Chemical & Engineering Data.* 2002, **47**(5), 1280-1284

54. Barros, G., R. Tamagawa, C. Santana and E. Miranda. Ternary phase diagram of ketamine ((R, S)-2-(2-chlorophenyl)-2methylaminocyclohexanone) in ethanol and preliminary studies aiming at Enantioselective Crystallization of S-ketamine. *Brazilian Journal of Chemical Engineering.* 2009, **26**(2), 427-434

55. Weng, N. S. and S. Hu. On chiral space groups and chiral molecules. 2003

56. Kimoto, H., K. Saigo and M. Hasegawa. The potential energy calculation for conglomerate crystals. *Chemistry Letters.* 1990(5), 711-714

57. Sakai, K., Y. Hashimoto, K. Kinbara, K. Saigo, H. Murakami and H. Nohira. Optical resolution of 1-(3-methoxyphenyl) ethylamine with enantiomerically pure mandelic acid, and the crystal structure of less-

soluble diastereomeric salt. *Bulletin of the Chemical Society of Japan.* 1993, **66**(11), 3414-3418

58. Kozma, D., Z. Böcskei, K. Simon and E. Fogassy. Racemic compound formation–conglomerate formation. Part. 1. Structural and thermoanalytical study of hydrogen malonate, hydrogen phthalate and hydrogen succinate of α-phenylethylamine. *Journal of the Chemical Society, Perkin Transactions 2.* 1994(8), 1883-1886

59. Larsen, S. and K. Marthi. Structures of racemic halogen-substituted 3-hydroxy-3-phenylpropionic acids; relations between spontaneously resolved and racemic compounds. *Acta Crystallographica Section B: Structural Science.* 1995, **51**(3), 338-346

60. Böcskei, Z., C. Kassai, K. Simon, E. Fogassy and D. Kozma. Racemic compound formation–conglomerate formation. Part 3. Investigation of the acidic salts of α-phenylethylamine by achiral dicarboxylic acids. Optical resolution by preferential crystallization and a structural study of (R)-α-phenylethylammonium hydrogen itaconate. *Journal of the Chemical Society, Perkin Transactions 2.* 1996(7), 1511-1515

61. Larsen, S. and K. Marthi. Structural and thermodynamic relationships between optically active and racemic compounds. The crystal structures of optically active chloro-and bromo-substituted 3-hydroxy-3-phenylpropionic acids. *Acta Crystallographica Section B: Structural Science.* 1997, **53**(5), 803-811

62. Kinbara, K., Y. Kobayashi and K. Saigo. Systematic study of chiral discrimination upon crystallisation. Part 2.1 Chiral discrimination of 2-arylalkanoic acids by (1R, 2S)-2-amino-1, 2-diphenylethanol. *J. Chem. Soc., Perkin Trans. 2.* 1998(8), 1767-1776

63. Kinbara, K., Y. Kobayashi and K. Saigo. Chiral discrimination of 2-arylalkanoic acids by (1 S, 2 R)-1-aminoindan-2-ol through the formation of a consistent columnar supramolecular hydrogen-bond network. *Journal of the Chemical Society, Perkin Transactions 2.* 2000(1), 111-119

64. Kitoh, S.-i., A. Kubota, K.-K. Kunimoto, A. Kuwae and K. Hanai. Conglomerate formation and crystal structure of 4-phenyl-1, 3-thiazolidin-2-one. *Journal of molecular structure.* 2005, **737**(2), 277-282

65. Kinbara, K., Y. Hashimoto, M. Sukegawa, H. Nohira and K. Saigo. Crystal structures of the salts of chiral primary amines with achiral carboxylic acids: recognition of the commonly-occurring supramolecular assemblies of hydrogen-bond networks and their role in the formation of conglomerates. *Journal of the American Chemical Society.* 1996, **118**(14), 3441-3449

66. Saigo, K., H. Kimoto, H. Nohira, K. Yanagi and M. Hasegawa. Molecular recognition in the formation of conglomerate crystal. The role of cinnamic acid in the conglomerate crystals of 1-phenylethylamine and 1-(4-isopropylphenyl) ethylamine salts. *Bulletin of the Chemical Society of Japan.* 1987, **60**(10), 3655-3658

67. Kinbara, K., A. Kai, Y. Maekawa, Y. Hashimoto, S. Naruse, M. Hasegawa and K. Saigo. Photoisomerization of ammonium α, β-unsaturated carboxylates in the solid state: effect of the hydrogen-bond network on the reactivity. *J. Chem. Soc., Perkin Trans. 2.* 1996(2), 247-253

68. Kinbara, K., Y. Tagawa and K. Saigo. Probability of spontaneously resolvable conglomerates for racemic acid/racemic amine salts predicted on the basis of the results of diastereomeric resolutions. *Tetrahedron: Asymmetry.* 2001, **12**(21), 2927-2930

69. Kinbara, K., K. Sakai, Y. Hashimoto, H. Nohira and K. Saigo. Chiral discrimination upon crystallisation of the diastereomeric salts of 1-arylethylamines with mandelic acid or p-methoxymandelic acid: interpretation of the resolution efficiencies on the basis of the crystal structures. *Journal of the Chemical Society, Perkin Transactions 2.* 1996(12), 2615-2622

70. Brock, C. P., W. B. Schweizer and J. D. Dunitz. On the validity of Wallach's rule: on the density and stability of racemic crystals compared with their chiral counterparts. *Journal of the American Chemical Society.* 1991, **113**(26), 9811-9820

71. Wallach, O. and A. Herbig. Zur Kenntniss der Terpene und der ätherischen Oele. Ueber Phellandren. *Justus Liebigs Annalen der Chemie.* 1895, **287**(3), 371-384

72. Meyerhoffer, W. The Breaks in The Solubility Curves. *The Journal of Physical Chemistry.* 1904, **8**(8), 571-575

73. Izumi, T. and D. G. Blackmond. The double solubility rule holds for racemizing enantiomers. *Chemistry-A European Journal.* 2009, **15**(13), 3065-3068

74. Pasteur, L. Mémoire sur la relation qui peut exister entre la forme cristalline et la composition chimique, et sur la cause de la polarisation rotatoire. *Annales de Chimie et de Physique.* 1848, **25**(6), 442-459

75. Galland, A., V. Dupray, B. Berton, S. Morin-Grognet, M. Sanselme, H. Atmani and G. Coquerel. Spotting conglomerates by second harmonic generation. *Crystal Growth and Design.* 2009, **9**(6), 2713-2718

76. Gernez, M. Separation des tartrates gauches et des tartrates droits, a l'aide des solutions sursaturees. *Compt. rend.* 1866, **63**, 843

77. Duschinsky, R. A case of spontaneous resolution of a racemic compound (histidine mono-hydrochloride). *Journal of the Society of Chemical Industry.* 1934, **53**(1), 10-20

78. Collins, A. N., G. Sheldrake and J. Crosby. *Chirality in industry II: Developments in the commercial manufacture and applications of optically active compounds.* John Wiley & Sons, 1997

79. Alvarez Rodrigo, A., H. Lorenz and A. Seidel-Morgenstern. Online monitoring of preferential crystallization of enantiomers. *Chirality.* 2004, **16**(8), 499-508

80. Elsner, M. P., D. F. Menendez, E. A. Muslera and A. Seidel-Morgenstern. Experimental study and simplified mathematical description of preferential crystallization. *Chirality.* 2005, **17**(S1), S183-S195

81. Courvoisier, L., E. Ndzié, M. Petit, U. Hedtmann, U. Sprengard and G. Coquerel. Influence of the Process on the Mechanisms and the Performances of the Preferential Crystallization: Example with (+/-)-5-(4-Bromophenyl)-5-Methylhydantoin. *Chemistry Letters.* 2001, **30**(4), 364-365

82. Levilain, G. and G. Coquerel. Pitfalls and rewards of preferential crystallization. *CrystEngComm.* 2010, **12**(7), 1983-1992

83. *Stereochemistry of Carbon Compounds.* Tata McGraw-Hill, 1975

84. Kaiser, K. and R. Benner. Hydrolysis-induced racemization of amino acids. *Limnology and Oceanography: Methods.* 2005, **3**(8), 318-325

85. Ebbers, E. J., G. J. Ariaans, J. P. Houbiers, A. Bruggink and B. Zwanenburg. Controlled racemization of optically active organic compounds: prospects for asymmetric transformation. *Tetrahedron.* 1997, **53**(28), 9417-9476

86. Murahashi, S., N. Yoshimura, T. Tsumiyama and T. Kojima. Catalytic alkyl group exchange reaction of primary and secondary amines. *Journal of the American Chemical Society.* 1983, **105**(15), 5002-5011

87. Parvulescu, A., D. De Vos and P. Jacobs. Efficient dynamic kinetic resolution of secondary amines with Pd on alkaline earth salts and a lipase. *Chemical communications.* 2005(42), 5307-5309

88. Pàmies, O., A. H. Éll, J. S. Samec, N. Hermanns and J.-E. Bäckvall. An efficient and mild ruthenium-catalyzed racemization of amines: application to the synthesis of enantiomerically pure amines. *Tetrahedron letters.* 2002, **43**(26), 4699-4702

89. Koh, J. H., H. M. Jeong and J. Park. Efficient catalytic racemization of secondary alcohols. *Tetrahedron letters.* 1998, **39**(31), 5545-5548

90. Huerta, F. F., A. B. Minidis and J.-E. Bäckvall. Racemisation in asymmetric synthesis. Dynamic kinetic resolution and related processes in enzyme and metal catalysis. *Chemical Society Reviews.* 2001, **30**(6), 321-331

91. Blum, Y. and Y. Shvo. Catalytically Reactive Ruthenium Intermediates in the Homogeneous Oxidation of Alcohols to Esters. *Israel Journal of Chemistry.* 1984, **24**(2), 144-148

92. Mays, M. J., M. J. Morris, P. R. Raithby, Y. Shvo and D. Czarkie. X-ray structure, reactivity and catalytic properties of a (cyclopentadienone) ruthenium dimer,[(C4Ph4CO)(CO) 2Ru] 2. *Organometallics.* 1989, **8**(5), 1162-1167

93. Menashe, N. and Y. Shvo. Catalytic disproportionation of aldehydes with ruthenium complexes. *Organometallics.* 1991, **10**(11), 3885-3891

94. Menashe, N., E. Salant and Y. Shvo. Efficient catalytic reduction of ketones with formic acid and ruthenium complexes. *Journal of organometallic chemistry.* 1996, **514**(1), 97-102

95. Larsson, A. L., B. A. Persson and J. E. Bäckvall. Enzymatic Resolution of Alcohols Coupled with Ruthenium-Catalyzed Racemization of the Substrate Alcohol. *Angewandte Chemie International Edition in English.* 1997, **36**(11), 1211-1212

96. Huerta, F. F., Y. S. Laxmi and J.-E. Bäckvall. Dynamic kinetic resolution of α-hydroxy acid esters. *Organic letters.* 2000, **2**(8), 1037-1040

97. Casey, C. P., S. W. Singer, D. R. Powell, R. K. Hayashi and M. Kavana. Hydrogen transfer to carbonyls and imines from a hydroxycyclopentadienyl ruthenium hydride: evidence for concerted hydride and proton transfer. *Journal of the American Chemical Society.* 2001, **123**(6), 1090-1100

98. Csjernyik, G., K. Bogár and J.-E. Bäckvall. New efficient ruthenium catalysts for racemization of alcohols at room temperature. *Tetrahedron letters.* 2004, **45**(36), 6799-6802

99. Kim, W.-H., R. Karvembu and J. Park. Alumina-supported ruthenium catalysts for the racemization of secondary alcohols. *BULLETIN-KOREAN CHEMICAL SOCIETY.* 2004, **25**(6), 931-933

100. Martín-Matute, B., M. Edin, K. Bogár and J. E. Bäckvall. Highly compatible metal and enzyme catalysts for efficient dynamic kinetic resolution of alcohols at ambient temperature. *Angewandte Chemie International Edition.* 2004, **43**(47), 6535-6539

101. Gibbins, E. J., J. L. Irwin, A. G. Livingston, J. C. Muir, D. A. Patterson, C. Roengpithya and P. C. Taylor. An improved protocol for the synthesis and nanofiltration of Kim and Park's aminocyclopentadienyl ruthenium chloride racemisation catalyst. *Synlett.* 2005, **2005**(19), 2993-2995

102. Wuyts, S., K. De Temmerman, D. De Vos and P. Jacobs. Acid zeolites as alcohol racemization catalysts: Screening and application in biphasic dynamic kinetic resolution. *Chemistry-A European Journal.* 2005, **11**(1), 386-397

103. Yamaguchi, K., T. Koike, M. Kotani and M. Matsushita. S, Shinachi, N. Mizuno. *Chem. Eur. J.* 2005, **11**, 6574-6582

104. Zsigmond, Á., A. Kecskeméti, K. Bogár, F. Notheisz and E. Mernyák. Efficient heterogeneous racemization of secondary alcohols: Convenient

synthesis of 17α-estradiol 3-methyl ether. *Catalysis Communications.* 2005, **6**(8), 520-524

105. Fransson, A.-B. L., Y. Xu, K. Leijondahl and J.-E. Bäckvall. Enzymatic resolution, desymmetrization, and dynamic kinetic asymmetric transformation of 1, 3-cycloalkanediols. *The Journal of Organic Chemistry.* 2006, **71**(17), 6309-6316

106. Xi, Q., W. Zhang and X. Zhang. (η< SUP> 5</SUP>-Triphenylindenyl) Ru (CO)< SUB> 2</SUB> Cl: A New Ruthenium Catalyst for the Highly Efficient Racemization of Chiral 1-Phenylethanol at Room Temperature. *Synlett.* 2006, **2006**(06), 945-947

107. Koh, J. H., H. M. Jung, M.-J. Kim and J. Park. Enzymatic resolution of secondary alcohols coupled with ruthenium-catalyzed racemization without hydrogen mediator. *Tetrahedron letters.* 1999, **40**(34), 6281-6284

108. Jung, H. M., J. H. Koh, M.-J. Kim and J. Park. Practical ruthenium/lipase-catalyzed asymmetric transformations of ketones and enol acetates to chiral acetates. *Organic letters.* 2000, **2**(16), 2487-2490

109. Lee, D., E. A. Huh, M.-J. Kim, H. M. Jung, J. H. Koh and J. Park. Dynamic kinetic resolution of allylic alcohols mediated by ruthenium-and lipase-based catalysts. *Organic letters.* 2000, **2**(15), 2377-2379

110. Choi, J. H., Y. K. Choi, Y. H. Kim, E. S. Park, E. J. Kim, M.-J. Kim and J. Park. Aminocyclopentadienyl ruthenium complexes as racemization catalysts for dynamic kinetic resolution of secondary alcohols at ambient temperature. *The Journal of Organic Chemistry.* 2004, **69**(6), 1972-1977

111. Akai, S., K. Tanimoto, Y. Kanao, M. Egi, T. Yamamoto and Y. Kita. A dynamic kinetic resolution of allyl alcohols by the combined use of lipases and [VO (OSiPh3) 3]. *Angewandte Chemie.* 2006, **118**(16), 2654-2657

112. van Nispen, S. F., J. van Buijtenen, J. A. Vekemans, J. Meuldijk and L. A. Hulshof. Efficient dynamic kinetic resolution of secondary alcohols with a novel tetrafluorosuccinato ruthenium complex. *Tetrahedron: Asymmetry.* 2006, **17**(15), 2299-2305

113. Choi, Y. K., J. H. Suh, D. Lee, I. T. Lim, J. Y. Jung and M.-J. Kim. Dynamic kinetic resolution of acyclic allylic acetates using lipase and palladium. *The Journal of Organic Chemistry.* 1999, **64**(22), 8423-8424

114. Martín-Matute, B., M. Edin, K. Bogár, F. B. Kaynak and J.-E. Bäckvall. Combined ruthenium (II) and lipase catalysis for efficient dynamic kinetic resolution of secondary alcohols. Insight into the racemization mechanism. *Journal of the American Chemical Society.* 2005, **127**(24), 8817-8825

115. Borén, L., B. Martín-Matute, Y. Xu, A. Córdova and J. E. Bäckvall. (S)-Selective Kinetic Resolution and Chemoenzymatic Dynamic Kinetic Resolution of Secondary Alcohols. *Chemistry-A European Journal.* 2006, **12**(1), 225-232

116. Dinh, P. M., J. A. Howarth, A. R. Hudnott, J. M. Williams and W. Harris. Catalytic racemisation of alcohols: Applications to enzymatic resolution reactions. *Tetrahedron letters.* 1996, **37**(42), 7623-7626

117. Berkessel, A., M. L. Sebastian-Ibarz and T. N. Müller. Lipase/Aluminum-Catalyzed Dynamic Kinetic Resolution of Secondary Alcohols. *Angewandte Chemie International Edition.* 2006, **45**(39), 6567-6570

118. Persson, B. A., A. L. Larsson, M. Le Ray and J.-E. Bäckvall. Ruthenium- and enzyme-catalyzed dynamic kinetic resolution of secondary alcohols. *Journal of the American Chemical Society.* 1999, **121**(8), 1645-1650

119. Ahn, Y., S.-B. Ko, M.-J. Kim and J. Park. Racemization catalysts for the dynamic kinetic resolution of alcohols and amines. *Coordination Chemistry Reviews.* 2008, **252**(5), 647-658

120. Kim, M.-J., Y. K. Choi, M. Y. Choi, M. J. Kim and J. Park. Lipase/ruthenium-catalyzed dynamic kinetic resolution of hydroxy acids, diols, and hydroxy aldehydes protected with a bulky group. *The Journal of Organic Chemistry.* 2001, **66**(13), 4736-4738

121. Pàmies, O. and J.-E. Bäckvall. Enzymatic kinetic resolution and chemoenzymatic dynamic kinetic resolution of δ-hydroxy esters. An efficient route to chiral δ-lactones. *The Journal of Organic Chemistry.* 2002, **67**(4), 1261-1265

122. Pàmies, O. and J. E. Bäckvall. Efficient Lipase-Catalyzed Kinetic Resolution and Dynamic Kinetic Resolution of β-Hydroxy Nitriles. A Route to Useful Precursors for γ-Amino Alcohols. *Advanced Synthesis & Catalysis.* 2001, **343**(6-7), 726-731

123. Pamies, O. and J.-E. Bäckvall. Dynamic kinetic resolution of β-azido alcohols. An efficient route to chiral aziridines and β-amino alcohols. *The Journal of Organic Chemistry.* 2001, **66**(11), 4022-4025

124. Pàmies, O. and J.-E. Bäckvall. An efficient route to chiral α-and β-hydroxyalkanephosphonates. *The Journal of Organic Chemistry.* 2003, **68**(12), 4815-4818

125. Choi, J. H., Y. H. Kim, S. H. Nam, S. T. Shin, M. J. Kim and J. Park. Aminocyclopentadienyl ruthenium chloride: catalytic racemization and dynamic kinetic resolution of alcohols at ambient temperature. *Angewandte Chemie.* 2002, **114**(13), 2479-2482

126. Ko, S.-B., B. Baburaj, M.-J. Kim and J. Park. Air-Stable Racemization Catalysts for the Dynamic Kinetic Resolution of Secondary Alcohols. *The Journal of Organic Chemistry.* 2007, **72**(18), 6860-6864

127. Hongo, C., S. Yamada and I. Chibata. Asymmetric transformation of N-acetyl-DL-leucine. *Bulletin of the Chemical Society of Japan.* 1981, **54**(11), 3291-3295

128. Hongo, C., S. Yamada and I. Chibata. Asymmetric Transformation of N-Acyl-DL-Amino Acids. *Bull. Chem. Soc. Jpn.* 1981, **54**, 1905-1910

129. Vedejs, E. and Y. Donde. Crystallization-induced asymmetric transformation of a tertiary phosphine. *The Journal of Organic Chemistry.* 2000, **65**(8), 2337-2343

130. Tsubaki, K., M. Miura, H. Morikawa, H. Tanaka, T. Kawabata, T. Furuta, K. Tanaka and K. Fuji. Synthesis of Optically Active Oligonaphthalenes via Second-Order Asymmetric Transformation. *Journal of the American Chemical Society.* 2003, **125**(52), 16200-16201

131. Paulsen, H., C. Graeve and D. Hoppe. This special case of a dynamic kinetic resolution through crystallization is also referred to as ‘asymmetric transformation of the second order.’13.,(a) and (b) For an example see. *Synthesis.* 1996, **1**, 141

132. Reider, P. J., P. Davis, D. L. Hughes and E. J. Grabowski. Crystallization-induced asymmetric transformation: stereospecific synthesis of a potent peripheral CCK antagonist. *The Journal of Organic Chemistry.* 1987, **52**(5), 955-957

133. Viedma, C. Chiral symmetry breaking and complete chiral purity by thermodynamic-kinetic feedback near equilibrium: implications for the origin of biochirality. *Astrobiology.* 2007, **7**(2), 312-319

134. Viedma, C., J. E. Ortiz, T. d. Torres, T. Izumi and D. G. Blackmond. Evolution of solid phase homochirality for a proteinogenic amino acid. *Journal of the American Chemical Society.* 2008, **130**(46), 15274-15275

135. Colter, A. K. and L. M. Clemens. Solvent Effects in the Racemization of 1, 1'-Binaphthyl. A Note on the Influence of Internal Pressure on Reaction Rates1. *The Journal of Physical Chemistry.* 1964, **68**(3), 651-654

136. Kondepudi, D. K., J. Laudadio and K. Asakura. Chiral symmetry breaking in stirred crystallization of 1, 1'-binaphthyl melt. *Journal of the American Chemical Society.* 1999, **121**(7), 1448-1451

137. van der Meijden, M. W., M. Leeman, E. Gelens, W. L. Noorduin, H. Meekes, W. J. van Enckevort, B. Kaptein, E. Vlieg and R. M. Kellogg. Attrition-enhanced deracemization in the synthesis of Clopidogrel-A practical application of a new discovery. *Organic Process Research & Development.* 2009, **13**(6), 1195-1198

138. Wang, X. J., H. Wiehler and C. B. Ching. Physicochemical Properties and the Crystallization Thermodynamics of the Pure Enantiomer and the Racemate for N-Methylephedrine. *Journal of Chemical & Engineering Data.* 2003, **48**(5), 1092-1098

139. Lorenz, H., D. Polenske and A. Seidel-Morgenstern. Application of preferential crystallization to resolve racemic compounds in a hybrid process. *Chirality.* 2006, **18**(10), 828-840

140. Polenske, D., H. Lorenz and A. Seidel-Morgenstern. Potential of different techniques of preferential crystallization for enantioseparation of racemic compound forming systems. *Chirality.* 2009, **21**(8), 728-737

141. Maillard, D., G. Koller, E. Wakaresko and S. Gottburg-Reininger. *Process of isolating enantiomer components from enantiomer mixtures by particle-size-controlled crystallization.* US 20110184169 A1. 2013

142. Shiau, L.-D., K.-F. Liu and P.-H. Huang. Purification of hydrobenzoin enantiomers by stripping crystallization. *Journal of the Taiwan Institute of Chemical Engineers.* 2013, **44**(5), 707-712

143. Collet, A., M. J. Brienne and J. Jacques. Optical resolution by direct crystallization of enantiomer mixtures. *Chemical reviews.* 1980, **80**(3), 215-230

144. Li, X., J. Blacker, I. Houson, X. Wu and J. Xiao. An efficient Ir (III) catalyst for the asymmetric transfer hydrogenation of ketones in neat water. *Synlett.* 2006, **2006**(08), 1155-1160

145. Hückel, W. and F. Mössner. Ein Beitrag zum Problem: Optische Antipoden, Racemat und racemisches Gemisch. Die optischen Antipoden des α-Indanols, ihr Schmelzen und Erstarren im Gemisch und ihr dielektrisches Verhalten in Lösung. *Justus Liebigs Annalen der Chemie.* 1960, **637**(1), 57-72

146. Ikariya, T., S. Hashiguchi, K. Murata and R. Noyori. Preparation of Optically Active (R,R)-Hydrobenzoin from Benzoin or Benzil. *Organic Syntheses*: John Wiley & Sons, Inc., 2003

147. Horeau, A. and J. Guette. Interactions diastereoisomeres d'antipodes en phase liquide. *Tetrahedron.* 1974, **30**(13), 1923-1931

148. Guetté, J., D. Boucherot and A. Horeau. Interactions diastereoisomeres d'enantiomeres en phase liquide-II: Peut-on séparer les antipodes d'un composé chiral par distillation? *Tetrahedron letters.* 1973, **14**(6), 465-468

149. Pennington, W. T., S. Chakraborty, I. C. Paul and D. Curtin. Crystal structures of D-(+)-and meso-hydrobenzoin. Absolute direction of the dipole moment of D-and L-hydrobenzoin in the crystal and correlation with crystal morphology, pyroelectric effect, and absolute configuration. *Journal of the American Chemical Society.* 1988, **110**(19), 6498-6504

150. Staples, R. and A. Spencer. Crystal structure of S, R-(+)-N-methylephedrine, C11H17NO. *Zeitschrift für Kristallographie-New Crystal Structures.* 2005, **220**(3), 437-438

151. Ito, M., M. Hirakawa, A. Osaku and T. Ikariya. Highly Efficient Chemoselective Hydrogenolysis of Epoxides Catalyzed by a (η5-C5 (CH3) 5) Ru Complex Bearing a 2-(Diphenylphosphino) ethylamine Ligand. *Organometallics.* 2003, **22**(21), 4190-4192

152. Fujita, K.-i. and R. Yamaguchi. Cp* Ir complex-catalyzed hydrogen transfer reactions directed toward environmentally benign organic synthesis. *Synlett.* 2005, **2005**(04), 560-571

153. Blacker, J. and C. E. Headley. Dynamic Resolution ofChiral Amine Pharmaceuticals: Turning Waste Isomers into Useful Product. *Green Chemistry in the Pharmaceutical Industry.* 2010

154. Fujita, K. i. and R. Yamaguchi. Catalytic Activity of Cp* Iridium Complexes in Hydrogen Transfer Reactions. *Iridium Complexes in Organic Synthesis.* 2008, 107-143

155. Oro, L. A., M. A. Ciriano, M. Campo, C. Foces-Foces and F. H. Cano. Indenyl complexes of ruthenium (II), crystal structure of [Ru (CO)(PPh3) 2 (η5-C9H7)] ClO4• 1/2CH2Cl2. *Journal of organometallic chemistry.* 1985, **289**(1), 117-131

156. Levenspiel, O. *Chemical reaction engineering.* Wiley, 1972

157. Samec, J. S., J.-E. Bäckvall, P. G. Andersson and P. Brandt. Mechanistic aspects of transition metal-catalyzed hydrogen transfer reactions. *Chemical Society Reviews.* 2006, **35**(3), 237-248

158. Warner, M. C. and J.-E. Bäckvall. Mechanistic Aspects on Cyclopentadienylruthenium Complexes in Catalytic Racemization of Alcohols. *Accounts of chemical research.* 2013, **46**(11), 2545-2555

159. Habib, A., R. S. Tanke, E. M. Holt and R. H. Crabtree. Ring slip in associative reactions of some indenyl-and phenylcyclopentadienyliridium complexes. *Organometallics.* 1989, **8**(5), 1225-1231

160. Warner, M. C., O. Verho and J.-E. Bäckvall. CO dissociation mechanism in racemization of alcohols by a cyclopentadienyl ruthenium dicarbonyl catalyst. *Journal of the American Chemical Society.* 2011, **133**(9), 2820-2823

161. Nyhlén, J., T. Privalov and J. E. Bäckvall. Racemization of Alcohols Catalyzed by [RuCl (CO) 2 (η5-pentaphenylcyclopentadienyl)]—Mechanistic Insights from Theoretical Modeling. *Chemistry-A European Journal.* 2009, **15**(21), 5220-5229

162. Jiang, S. and J. H. ter Horst. Crystal Nucleation Rates from Probability Distributions of Induction Times. *Crystal growth & design.* 2010, **11**(1), 256-261

163. Randolph, A. D. and M. A. Larson. *Theory of particulate processes: analysis and techniques of continuous crystallization.* Academic Press, 1988

11 Appendix

11.1 Equipment and Analytical Techniques

11.1.1 Equipment

Unless stated otherwise, all procedures were carried out in multi-neck heat-resistant glass round bottom flasks equipped, where necessary, with a thermometer, reflux condenser and Argon/N_2 gas supply. Heating and agitation were provided by a digital magnetic stirrer hotplate, with an overhead motor-driven agitator being used for larger scale syntheses.

11.1.2 ^{1}H Nuclear Magnetic Resonance (NMR) Spectroscopy

Structural analysis was performed using proton nuclear magnetic resonance (^{1}H NMR) with a Brucker Avance 500 MHz NMR spectrometer. Samples (~ 1-3 mg) were added to 5 mm diameter borosilicate glass NMR tubes, dissolved in deuterated chloroform ($CDCl_3$), and sealed with a polyethylene cap prior to analysis.

11.1.3 Polarimetry

Optical rotations were determined under ambient conditions (20°C) using a Schmidt + Haensch H532 polarimeter (0.0001° resolution) with an electromagnetic wavelength of 589.44 nm. Samples were prepared by dissolving a known quantity of solid in a prescribed solvent (1-indanol – chloroform c = 2; methylephedrine - methanol c = 5; hydrobenzoin – ethanol c = 2.5) with the resulting solution being added to a 100 mm path length micro tube cell and sealed. The loaded cell was placed in the polarimeter and the absolute rotation recorded after sufficient time had elapsed for the signal to remain stable.

11.1.4 Differential Scanning Calorimetry (DSC)

Melting points and enthalpies of fusion were determined by differential scanning calorimetry (DSC) using a Mettler Toledo DSC820 calorimeter equipped with a

Mettler Toledo TS0801R0 sample robot. Samples of approximately 5 mg were loaded into 40 µl aluminium pans and weighed before and after analysis to ensure decomposition did not occur. The applied heating programme for 1-indanol, methylephedrine and hydrobenzoin consisted of holding the pan temperature for 25 min at 25°C, 40°C and 80°C, and heating at a rate of 2°C min^{-1} to 90°C, 110°C and 170°C respectively.

11.1.5 High Performance Liquid Chromatography (HPLC)

The enantiomeric composition hydrobenzoin was determined by chiral high performance liquid chromatography (HPLC) using an Agilent 1290 Infinity UHPLC. To identity a suitable resolution method a range of different normal phase chiral HPLC columns were trialled with different solvents at ambient temperature using racemic and enantiopure samples. Hydrobenzoin was analysed using a Daicel CHIRALCEL® OD-H chiral column (length = 150 mm, internal diameter = 4.6 mm, particle size = 5 µm), also using a 5 v/v% binary solvent of propan-2-ol in hexane as a mobile phase at a rate of 1 ml min^{-1}, with a DAD wavelength of 210 nm. Peak areas were calibrated using external standards (see section 11.4.1 for HPLC calibration data)

11.1.6 X-ray Diffraction

Powder XRD was performed using a Phillips X'Pert-Pro diffractometer, under ambient conditions, using Cu-Kα radiation without a monochromator, and a generator current and tube current of 40 mA and 40 kV respectively. Samples were ground to a fine powder, paced in an aluminium holder and scanned with a diffraction angle 2θ range of 5-80˚.

Single crystal XRD was performed using a Bruker-Nonius Apex X8 diffractometer equipped with an Apex II CCD detector and using graphite monochromated Mo-Kα radiation from a FR591 rotating anode generator at -123°C. Single crystals of each enantiomer were grown from toluene by firstly dissolving the solid and allowing the solvent to evaporate.

11.1.7 FT-Infra-Red Spectroscopy

FT Infra-red analysis was performed using a Bruker ALPHA spectrometer using powdered samples.

11.2 Materials Preparation

11.2.1 (*R*)- and (*S*)-1-indanol (1) Synthesis

The pure enantiomers of 1-indanol were synthesised individually according to the procedure given by Li *et al* [144], with the intention of obtaining the racemate for analysis by combining equal amounts of the two stereoisomers and recrystallising them from the melt. The reaction proceeds by asymmetric transfer hydrogenation of 1-indanone (C_9H_8O) in neat water using pentamethylcyclopentadienyl iridium dichloride dimer ($[Cp^*IrCl_2]_2$) as a pre-catalyst, and excess sodium formate (HCOONa) as a hydrogen source. To direct the handedness of the resulting enantiomer, the chiral ligand *N*-camphorsulphonyl-1,2-diphenylethylenediamine (CsDPEN) was used with $[Cp^*IrCl_2]_2$ to form the active chiral catalytic species Ir-CsDPEN (0.1 mol%), with the (*R*,*R*,*R*)- and (*S*,*S*,*S*)- forms of Ir-CsDPEN leading to the synthesis of (*R)*-1-indanol and (*S)*-1-indanol respectively, giving yields in excess of 85% (Scheme 11.1). Table 11.1list the materials and quantities used during the procedure for a 10 mmol scale synthesis with the methodology given below.

Table 11.1 Materials used in the synthesis of (*R*)-1-indanol and (*S*)-1-indanol (10 mmol scale)

Material	Molecular weight (g/mol)	Quantity (mmol)	Quantity
1-indanone (C_9H_8O)	132.16	10	1322 mg
Pentamethylcyclopentadienyl iridium dichloride dimer ($[Cp^*IrCl_2]_2$)	796.71	0.005	4 mg
(*R,R,R*) and (*S,S,S*)-*N*-camphorsulphonyl-1,2-diphenylethylenediamine (CsDPEN)	426.20	0.012	5.1 mg
Sodium formate (HCOONa)	68.01	50	3400 mg
Diethyl ether	74.12	76.99	8 ml
Distilled water	18.02	443.27	8 ml
Anhydrous sodium sulphate	142.04		
Petrol (40-60°C)	-	As required	
Hexane	86.18		

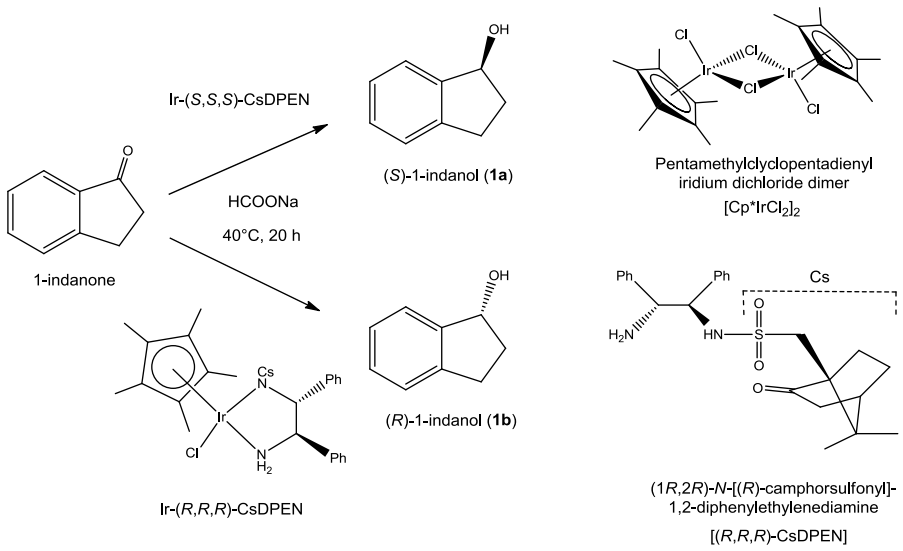

Scheme 11.1 Formation of (*R*)- and (*S*)-1-indanol by asymmetric transfer hydrogenation of 1-indanone in water using $[Cp^*IrCl_2]_2$ and (*R*,*R*,*R*)- / (*S*,*S*,*S*)-CsDPEN as a catalyst (0.1 mol%), and excess HCOONa as a hydrogen source.

*Procedure for (S)-1-indanol (**1a**) synthesis (10 mmol scale)*: To prepare the catalyst, 0.005 mmol (4 mg) of $[Cp^*IrCl_2]_2$ and 0.012 mmol (5.1 mg) of (*S,S,S*)-CsDPEN were added to 8 ml of distilled water in a 25 ml round bottom flask and stirred for 1 hour at 40˚C forming the active chiral species Ir-(*S,S,S*)-CsDPEN. 50 mmol (3.4 g) of HCOONa and 10 mmol (1.322 g) of 1-indanone were then

added to the suspension and left to stir for 20 hours at 40˚C. After allowing the reaction mixture to cool to room temperature the organic phase was extracted three times using 8 ml of diethyl ether and dried using anhydrous sodium sulphate. The solution was then filtered, concentrated and passed through a short silica gel column using a 2:3 mix of petrol and diethyl ether as the eluent. Finally, after evaporating the solvent and drying under vacuum, the crude product was recrystallized from hexane resulting in the formation of very fine white needles (9.2 mmol, 1230 mg).

*Procedure for (R)-1-indanol synthesis (**1b**) (10 mmol scale)*: **1b** was obtained following the same procedure as **1a** using (*R*,*R*,*R*)-CsDPEN instead as a ligand.

Table 11.2 Specific rotation, $[\alpha]_D^{20^\circ C}$, of the synthesised enantiomers of 1-indanol (c = 2 in chloroform)

(*R*)-1-indanol	**(*S*)-1-indanol**
-31.2	30.4

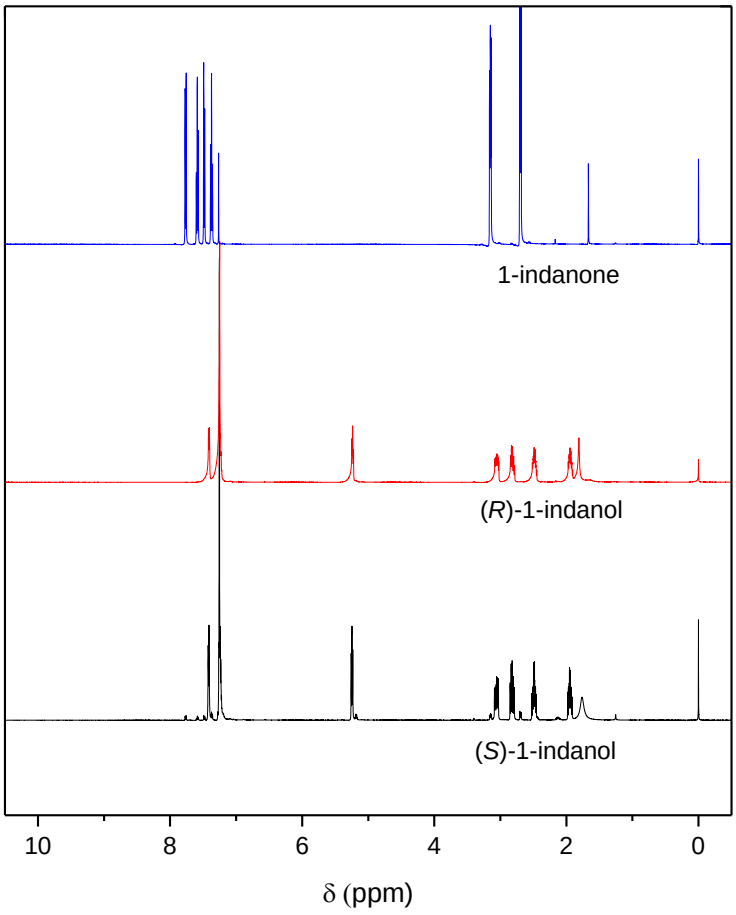

Figure 11.1 ^{1}H NMR (500 MHz, $CDCl_3$): 1-indanone δ 7.76 (d, 1H, J = 7.8 Hz, aryl H), 7.59 (t, 1H, J =7.3 Hz, aryl H), 7.48 (d, 1H, J = 7.8 Hz, aryl H), 7.37 (t, 1H, J =7.3 Hz, aryl H), 3.15 (t, 2H, J = 6.4 Hz, cyclopentyl H), 2.70 (t, 2H, J = 6.4 Hz, cyclopentyl H); (*R*)-1-indanol δ 7.41 (d, 1H, J = 6.4 Hz, aryl H) 7.32-7.22 (m, 3H, aryl H), 5.29-5.21 (m, 1H, OH), 3.17-3.01 (m, 1H, cyclopentyl H), 2.91-2.77 (m, 1H, cyclopentyl H), 2.56-2.43 (m, 1H, cyclopentyl H), 2.03-1.89 (m, 1H, cyclopentyl H), 1.86-1.76 (m, 1H, cyclopentyl H); (*S*)-1-indanol δ 7.42 (d, 1H, J = 6.4 Hz, aryl H) 7.36-7.20 (m, 3H, aryl H), 5.29-5.21 (m, 1H, OH), 3.17-3.01 (m, 1H, cyclopentyl H), 2.91-2.77 (m, 1H, cyclopentyl H), 2.56-2.43 (m, 1H, cyclopentyl H), 2.03-1.89 (m, 1H, cyclopentyl H), 1.86-1.76 (m, 1H, cyclopentyl H).

11.2.2 (*S*,*S*)- and (*R*,*R*)-hydrobenzoin (2)Synthesis

The pure enantiomers of hydrobenzoin were synthesised according to the procedure given by Ikariya *et al* [146], with the intention of obtaining the racemate for analysis by combining equal amounts of the two stereoisomers and recrystallising them from the melt. The reaction proceeds by asymmetric transfer hydrogenation of benzil (diphenylethanedione) without solvent using a molar 1.69:1 mixture of formic acid and triethylamine as a hydrogen source, and the chiral organometallic catalysts RuCl[(1*S*,2*S*)-*N*-*p*-toluenesulfonyl-1,2-diphenylethanediamine](η^6-*p*-cymene) (RuCl[(*S*,*S*)-TsDPEN(η^6-*p*-cymene)]) and its corresponding enantiomer RuCl[(*R*,*R*)-TsDPEN(η^6-*p*-cymene)] (0.1 mol%) to give (*R*,*R*)- and (*S*,*S*)-hydrobenzoin respectively (Scheme 11.2). Table 11.3 lists the materials used during the synthesis with the procedure for a 10 mmol scale synthesis given below.

Table 11.3 Materials used in the synthesis of (*S*,*S*)- and (*R*,*R*)-hydrobenzoin ((*S*,*S*)-**2** and (*R*,*R*)-**2**) (10 mmol scale).

Material	Molecular weight (g/mol)	Quantity (mmol)	Quantity
Benzil	210.23	10	2100 mg
Formic acid	46.03	48.3	1.83 ml
Triethylamine	101.19	28.6	4 ml
Rucl[(*R*,*R*)-TsDEPN(*p*-cymene)] Rucl[(*S*,*S*)-TsDEPN(*p*-cymene)]	636.21	0.01	6.36 mg
Distilled water	18.02	1163	21 ml
Methanol	32.04	259.5	10.5 ml
Propan-2-ol	60.1	27.5	2.1 ml

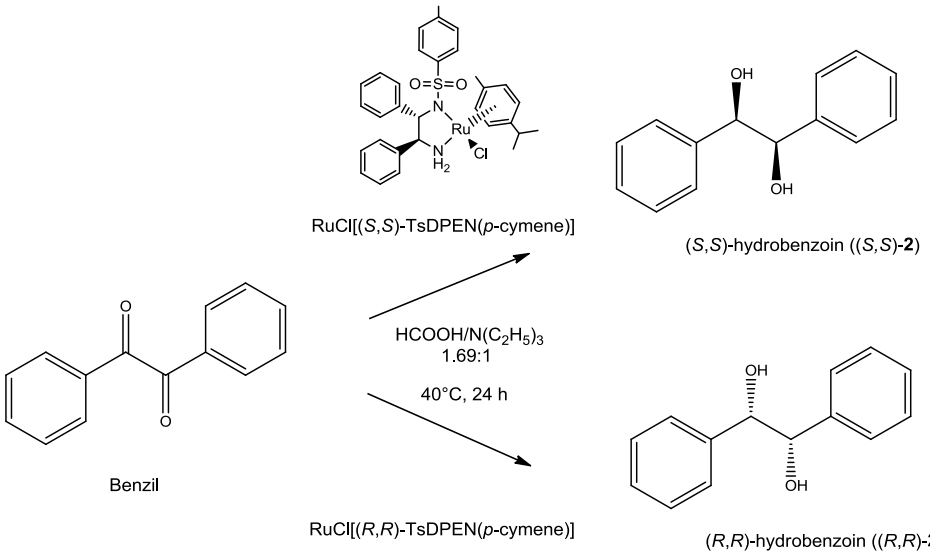

Scheme 11.2 Synthesis of (*S*,*S*)- and (*R*,*R*)-hydrobenzoin ((*S*,*S*)-**2** and (*R*,*R*)-**2**) by asymmetric transfer hydrogenation using RuCl[(*S*,*S*)-TsDPEN(*p*-cymene)] and RuCl[(*R*,*R*)-TsDPEN(*p*-cymene)] as catalysts respectively (0.1 mol%), and a formic acid/triethylamine mixture (1.69:1) as a hydrogen source[146].

*Procedure for (S,S)-hydrobenzoin ((S,*S*)-**2**) synthesis (10 mmol scale)***:** A four-neck round bottom flask equipped with a reflux condenser, thermometer and nitrogen gas supply, was charged with 4 ml of triethylamine (28.6 mmol) and cooled to 4°C in an ice bath. 1.83 ml of formic acid (48.3 mmol) was then added slowly using a dropping funnel ensuring the exothermic process was sufficiently cooled. After allowing the mixture to return to room temperature, 2100 mg benzil (10 mmol) and 6.36 mg RuCl[(*S*,*S*)-TsDPEN[*p*-cymene)] (0.01 mmol) were added and the vessel heated to 40°C. After stirring the reaction for 24 h, the mixture was cooled to 4°C in an ice bath, and 10.5 ml of distilled water added resulting in precipitation of a pale pink solid. This was filtered and washed with a further 10.5 ml of water and dried under vacuum giving a white solid. The crude product was dissolved in 10.5 ml of methanol at 60°C, after which being cooled to -40°C in a propan-2-ol/dry ice bath resulting in the formation of the final crystalline product. This was filtered and washed with 2.1 ml of cold propan-2-ol giving 1.69 g of *(S,*S*)-**2*** as white crystals (78.8% yield).

*Procedure for (R,R)-hydrobenzoin ((R,*R*)-**2**) synthesis (10 mmol scale)*: *(R,*R*)-**2*** was obtained following the same procedure as (*S*,*S*)-hydrobenzoin using instead RuCl[(*R*,*R*)-TsDPEN(*p*-cymene)] as a catalyst.

Table 11.4 Specific rotation, $[\alpha]_D^{20^\circ C}$ (°), of the synthesised enantiomers of hydrobenzoin (c = 2.5 in ethanol).

(*R,R*)-hydrobenzoin	**(*S,S*)-hydrobenzoin**
92.1	-92.7

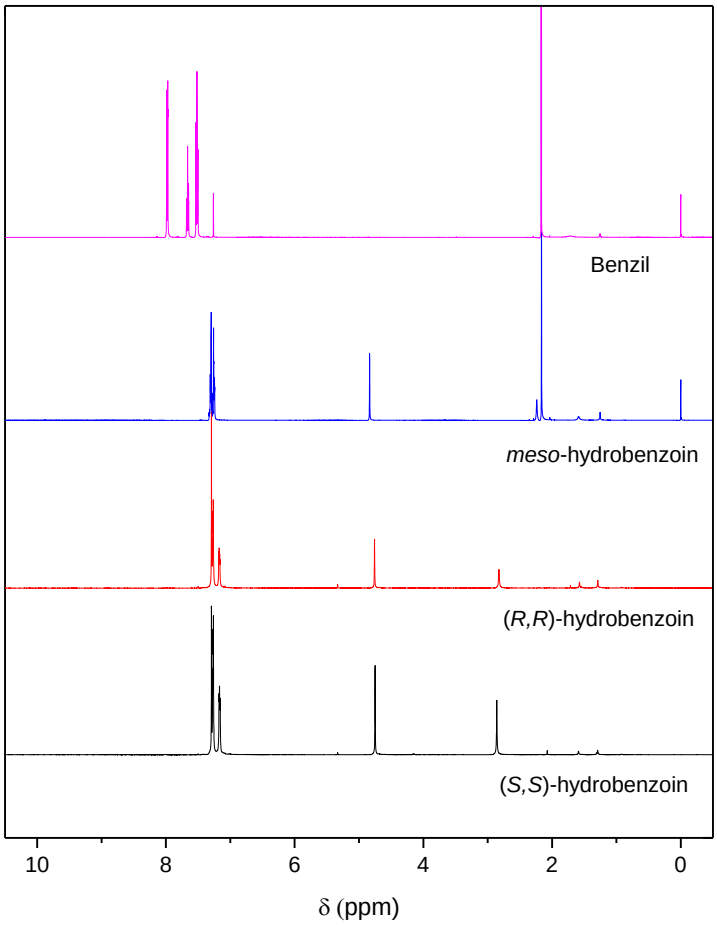

Figure 11.2 ^{1}H NMR (500 MHz, $CDCl_3$): Benzil δ 8.15-7.17 (m, 10H, aryl H); *meso*-hydrobenzoin δ 7.34-7.22 (m, 10H, aryl H), 4.83 (s, 2H, OH), 2.16 (s, 2H, CH); (*R*,*R*)-hydrobenzoin δ 7.32-7.12 (m, 10H, aryl H), 4.76 (s, 2H, OH), 2.83 (s, 2H, CH); (*S*,*S*)-hydrobenzoin δ 7.32-7.12 (m, 10H, aryl H). 4.75 (s, 2H, OH), 2.86 (s, 2H, CH) ((*S*,*S*)-**2** spectra was obtained using the seed crystals synthesised using the recipe described above and prepared for CIAT using the methodology given in 6.3.5.

11.2.3 N-Methylephedrine (3) Preparation

(*R*,*S*)- and (*S*,*R*)-*N*-methylephedrine ((*R*,*S*)-**3** and (*S*,*R*)-**3** respectively) were purchased from Sigma Aldrich (*ee* > 99%) and used directly without further purification.

Table 11.5 Specific rotation, $[\alpha]_D^{20^\circ C}$ (°), of the commercial enantiomers of methylephedrine (c = 5 in methanol).

(*R*,*S*)-*N*-methylephedrine	**(*S*,*R*)-*N*-methylephedrine**
-30.1	29.7

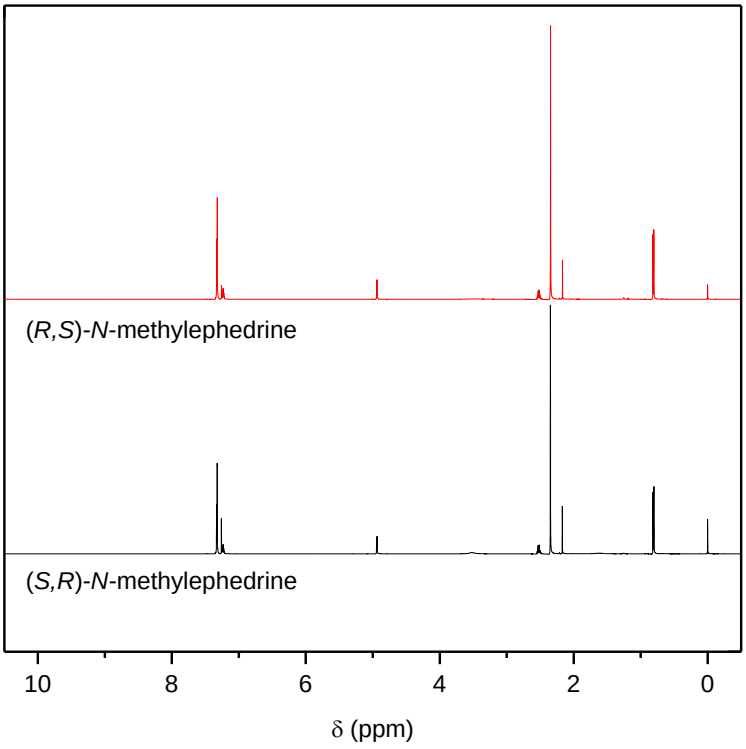

Figure 11.3 ^{1}H NMR (500 MHz, $CDCl_3$): (1*R*,2*S*)-*N*-methylephedrine δ 7.36-7.19 (m, 5H, aryl H), 4.93 (d, 1H, J = 3.7 Hz, OH), 2.56-2.47 (m, 1H, C<u>H</u>(CH_3)), 2.35 (s, 6H, $(CH_3)_2$), 2.17 (s, 1H, C<u>H</u>(OH)), 0.81 (d, 3H, J = 6.42, CH(C<u>H</u>$_3$)); (1*S*,2*R*)-*N*-methylephedrine δ 7.35-7.19 (m, 5H, aryl H), 4.94 (d, 1H, J = 3.7 Hz, OH), 2.54-2.47 (m, 1H, C<u>H</u>(CH_3)), 2.35 (s, 6H, $(CH_3)_2$), 2.17 (s, 1H, C<u>H</u>(OH)), 0.81 (d, 3H, J = 6.4, CH(C<u>H</u>$_3$)).

11.2.4 Chloro(indenyl)-bis-(triphenylphosphine)ruthenium(II) (4) Synthesis

Chloro(indenyl)-bis-(triphenylphosphine)ruthenium(II) ($[RuCl(PPh_3)_2(\eta^5\text{-}C_9H_7)]$) (**4**) was synthesised according to the procedure given by Oro *et al* [155]. The route involves refluxing $[RuCl_2(PPh_3)_3]$ with indene (C_9H_8) and potassium hydroxide, in dry ethanol under a N_2 gas atmosphere (Scheme 11.3). Table 11.6 gives the materials and quantities used during the reaction for a 1.04 mmol scale synthesis with the methodology given below.

Table 11.6 Materials used in the synthesis of $[RuCl(PPh_3)_2(\eta^5\text{-}C_9H_7)]$ (**4**) (1.04 mmol scale)

Material	Molecular weight (g/mol)	Quantity (mmol)	Quantity
$[RuCl_2(PPh_3)_3]$	958.83	1.04	1000 mg
Indene (C_9H_8)	116.16	17.17	2 ml
KOH	56.11	1.04	58.4 mg
Ethanol	-	-	19.3 ml
Dichloromethane	-	-	8 ml
Methanol	-	-	30 ml
Diethyl ether	-	As required	

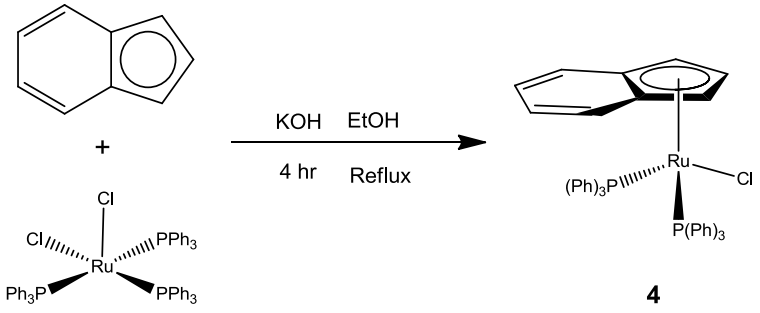

Scheme 11.3 Synthesis of catalyst **4** ($[RuCl(PPh_3)_2(\eta^5\text{-}C_9H_7)]$) by the reaction between indene, $[RuCl_2(PPh_3)_3]$ and potassium hydroxide in ethanol.

*Procedure for catalyst **4** synthesis (1.04 mmol scale):* 1.04 mmol (58.4 mg) of KOH was added to a 50 ml Schlenk flask, evacuated and filled with N_2, after which 9.3 ml of dry ethanol was added to make a 0.11 M solution. This was then rapidly added to a refluxing suspension of $RuCl_2(PPh_3)_3$ (1.04 mmol, 1000 mg) and indene (17.17 mmol, 2 ml) in 10 ml of ethanol, and under N_2, giving a red-brown suspension after 20 min of stirring. After allowing the reaction to

procedure for 4 h, the vessel was left to cool to room temperature and filtered, with the crude product then being extracted with 8 ml of dichloromethane. The extract was filtered leaving a solution to which 30 ml of methanol was added leading to precipitation of a red solid. This was filtered and washed with cold methanol, then diethyl ether, and dried under vacuum to give 614 mg of the final crystalline product (76% yield).

11.2.5 Chlorocarbonyl-triphenylphosphene(1,2,3,4,5-pentaphenylcyclopentadienyl)-ruthenium(II) (5) Synthesis

Chlorocarbonyl-triphenylphosphene(1,2,3,4,5-pentaphenylcyclopentadienyl)-ruthenium(II) ([RuCl(PPh_3)(CO)(η^5-Ph_5C_5)]) (**5**) was synthesised according to the procedure given by Ko *et al* [126]. The reaction involves substituting a carbonyl ligand on the chlorodicarbonyl-(1,2,3,4,5-pentaphenylcyclopentadienyl-ruthenium(II) complex (catalyst **5**) with a triphenylphosphine group, at 25°C under an argon atmosphere (Scheme 11.4). Table 11.7 list the materials and quantities used during the synthesis with the procedure for a 0.5 mmol scale given below.

Table 11.7 Materials used in the synthesis of [RuCl(PPh_3)(CO)(η^5-Ph_5C_5)] (**5**) (0.5 mmol scale)

Material	Molecular weight (g/mol)	Quantity (mmol)	Quantity
[RuCl$(CO)_2$(η^5-Ph_5C_5)]	638.12	0.50	319 mg
Triphenylphosphine	262.29	0.55	144 mg
Trimethylamine *N*-oxide	75.11	1.00	75.1 mg
Dichloromethane	-	-	5.3 ml
Acetonitrile	-	-	2.1 ml
Methanol	-	As required	

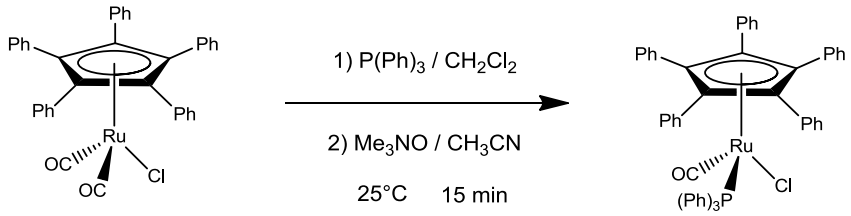

6 **5**

Scheme 11.4 Synthesis of [RuCl(PPh$_3$)(CO)(η^5-Ph$_5$C$_5$)] (**5**) by the substitution of a CO ligand on ([RuCl(CO)$_2$(η^5-Ph$_5$C$_5$)]) (**6**) with triphenylphosphine.

*Procedure for catalyst **5** synthesis (1.04 mmol scale):* 0.5 mmol [RuCl(CO)$_2$(η^5-Ph$_5$C$_5$)] (319 mg) and 0.55 mmol triphenylphosphine (144 mg) was added to a 25 ml Schlenk flask which was evacuated and filled with argon gas. The solids were dissolved in 5.3 ml of dry dichloromethane, then a solution of trimethylamine *N*-oxide (1.00 mmol, 75.1 mg) in 2 ml of dry acetonitrile was added slowly whilst stirring at room temperature. After 15 min the solution was concentrated and chromatographed on silica using a two stage elution of methanol followed by dichloromethane. The resulting solution was again concentrated giving 362 mg of the final solid product (83% yield).

11.3 Appendix C – Single Crystal X-Ray Diffraction and Refinement Data for 1-indanol (1)

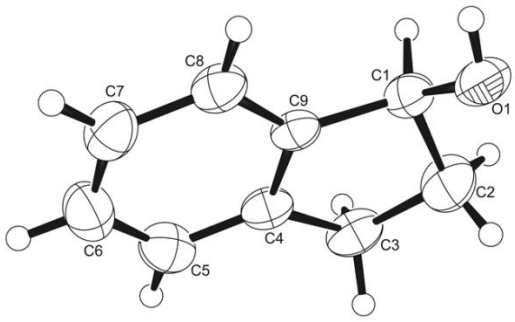

Figure 11.4 (S)-(-)-1-indanol

(±)-1-indanol

The structure was solved by direct methods and refined using SHELXL-97. The racemate crystallises in the body-centred tetragonal space group $I4_1/a$ with 16 molecules in the unit cell. All non-hydrogen atoms were refined anisotropically. All hydrogen atoms could be located in a difference Fourier map but, in the final stages of the refinement, they were placed in calculated positions and refined using a riding model. All Uiso(H) values were constrained to be 1.2 times (1.5 for hydroxyl) Ueq of the parent atom.

(±)-1-indanol Crystallographic Data

Formula	$C_9H_{10}O$	
Formula weight	134.17	
Size	0.26 x 0.14 x 0.12 mm	
Crystal morphology	Colourless prism	
Temperature	150(2) K	
Wavelength	0.71073 Å [Mo-K_a]	
Crystal system	Tetragonal	
Space group	$I4_1/a$	
Unit cell dimensions	a = 20.1935(16) Å	α = 90°
	b = 20.1935(16) Å	β = 90°
	c = 7.6039(7) Å	γ = 90°
Volume	3100.7(4) Å^3	
Z	16	
Density (calculated)	1.15 Mg/m^3	
Absorption coefficient	0.073 mm^{-1}	
F(000)	1152	

Data collection range	$2.02 \leq q \leq 29.22°$
Index ranges	$-27 \leq h \leq 27$, $-27 \leq k \leq 27$, $-10 \leq l \leq 10$
Reflections collected	29038
Independent reflections	2087 [*R*(int) = 0.0542]
Observed reflections	1657 [$I > 2s(I)$]
Absorption correction	multi-scan
Max. and min. transmission	0.9912 and 0.7861
Refinement method	Full
Data / restraints / parameters	2087 / 0 / 92
Goodness of fit	1.046
Final *R* indices [$I > 2s(I)$]	$R_1 = 0.0435$, $wR_2 = 0.1121$
R indices (all data)	$R_1 = 0.0568$, $wR_2 = 0.1225$
Largest diff. peak and hole	0.213 and -0.150e.Å^{-3}

Table 11.8 Interatomic distances (Å) *rac*-1-indanol with s.u.s in parentheses.

O(1)-C(1)	1.4514(14)	C(9)-C(4)	1.4137(15)
C(9)-C(8)	1.4162(15)	C(9)-C(1)	1.5360(15)
C(1)-C(2)	1.5609(16)	C(3)-C(4)	1.5327(16)
C(3)-C(2)	1.551(2)	C(7)-C(8)	1.4098(18)
C(7)-C(6)	1.411(2)	C(4)-C(5)	1.4112(17)
C(5)-C(6)	1.410(2)		

Table 11.9 Angles between interatomic vectors (°) with s.u.s in parentheses

C(4)-C(9)-C(8)	120.91(10)	C(4)-C(9)-C(1)	110.46(9)
C(8)-C(9)-C(1)	128.59(10)	O(1)-C(1)-C(9)	114.92(9)
O(1)-C(1)-C(2)	109.58(10)	C(9)-C(1)-C(2)	103.35(9)
C(4)-C(3)-C(2)	103.88(9)	C(8)-C(7)-C(6)	120.33(11)
C(5)-C(4)-C(9)	120.19(11)	C(5)-C(4)-C(3)	129.13(11)
C(9)-C(4)-C(3)	110.67(10)	C(7)-C(8)-C(9)	118.68(11)
C(6)-C(5)-C(4)	118.84(12)	C(5)-C(6)-C(7)	121.05(12)
C(3)-C(2)-C(1)	106.42(10)		

(*R*)-1-indanol

The structure was solved by direct methods and refined using SHELXL-97. The enantiomer crystallises in the chiral monoclinic space group $P2_1$ with one molecule of C_9 H_{10} O in the asymmetric unit. In the absence of significant anomalous scattering effects, the absolute configuration could not be confirmed from the diffraction data and Friedel pairs were merged. The model was assigned on the basis of the known stereochemistry of the starting material, (*R*) at C1 therefore the absolute configuration was established by the structure determination of a compound containing a chiral reference molecule of known absolute configuration. All non-hydrogen atoms were refined anisotropically. All hydrogen atoms could be located in a difference Fourier map but, in the final stages of the refinement, they were placed in calculated positions and refined using a riding model. All Uiso(H) values were constrained to be 1.2 times (1.5 for hydroxyl) Ueq of the parent atom.

(R)-1-indanol Crystallographic Data

Formula	$C_9H_{10}O$	
Formula weight	134.17	
Size	0.36 x 0.14 x 0.08 mm	
Crystal morphology	Colourless fragment	
Temperature	150(2) K	
Wavelength	0.71073 Å [Mo-K_a]	
Crystal system	Monoclinic	
Space group	$P2_1$	
Unit cell dimensions	a = 7.0645(8) Å	α = 90°
	b = 4.8427(5) Å	β = 95.749(6)°
	c = 11.0135(12) Å	γ = 90°
Volume	374.89(7) $Å^3$	
Z	2	
Density (calculated)	1.189 Mg/m^3	
Absorption coefficient	0.076 mm^{-1}	
F(000)	144	
Data collection range	$1.86 \leq q \leq 29.35°$	
Index ranges	$-9 \leq h \leq 9$, $-6 \leq k \leq 5$, $-15 \leq l \leq 15$	
Reflections collected	8184	
Independent reflections	1142 [R(int) = 0.0494]	

Observed reflections	1085 [I >2s(I)]
Absorption correction	multi-scan
Max. and min. transmission	0.9940 and 0.7373
Refinement method	Full
Data / restraints / parameters	1142 / 1 / 92
Goodness of fit	1.046
Final R indices [I >2s(I)]	R_1 = 0.0347, wR_2 = 0.0924
R indices (all data)	R_1 = 0.0369, wR_2 = 0.0946
Largest diff. peak and hole	0.316 and -0.148e.Å^{-3}

Table 11.10 Interatomic distances (Å) for (*R*)-1-indanol with s.u.s in parentheses.

O(1)-C(1)	1.4529(16)	C(1)-C(9)	1.522(2)
C(1)-C(2)	1.565(2)	C(2)-C(3)	1.561(2)
C(3)-C(4)	1.527(2)	C(4)-C(5)	1.407(2)
C(4)-C(9)	1.4164(18)	C(5)-C(6)	1.408(2)
C(6)-C(7)	1.415(2)	C(7)-C(8)	1.409(2)
C(8)-C(9)	1.411(2)		

Table 11.11 Angles between interatomic vectors (°) with s.u.s in parentheses

O(1)-C(1)-C(9)	110.86(12)	O(1)-C(1)-C(2)	113.53(12)
C(9)-C(1)-C(2)	103.60(12)	C(3)-C(2)-C(1)	106.41(12)
C(4)-C(3)-C(2)	103.73(11)	C(5)-C(4)-C(9)	120.16(13)
C(5)-C(4)-C(3)	129.17(12)	C(9)-C(4)-C(3)	110.65(13)
C(4)-C(5)-C(6)	119.14(13)	C(5)-C(6)-C(7)	120.73(15)
C(8)-C(7)-C(6)	120.30(14)	C(7)-C(8)-C(9)	118.92(12)
C(8)-C(9)-C(4)	120.76(13)	C(8)-C(9)-C(1)	128.10(12)
C(4)-C(9)-C(1)	111.11(12)		

(*S*)-1-indanol

The structure was solved by direct methods and refined using SHELXL-97. The enantiomer crystallises in the chiral monoclinic space group $P2_1$ with one molecule of C_9 H_{10} O in the asymmetric unit. In the absence of significant anomalous scattering effects, the absolute configuration could not be confirmed from the diffraction data and Friedel pairs were merged. The model was assigned on the basis of the known stereochemistry of the starting material, (*S*) at C1 therefore the absolute configuration

was established by the structure determination of a compound containing a chiral reference molecule of known absolute configuration. All non-hydrogen atoms were refined anisotropically. All hydrogen atoms could be located in a difference Fourier map but, in the final stages of the refinement, they were placed in calculated positions and refined using a riding model. All Uiso(H) values were constrained to be 1.2 times (1.5 for hydroxyl) Ueq of the parent atom.

(S)-1-indanol Crystallographic Data

Formula	$C_9H_{10}O$	
Formula weight	134.17	
Size	0.37 x 0.34 x 0.29 mm	
Crystal morphology	Colourless fragment	
Temperature	150(2) K	
Wavelength	0.71073 Å [Mo-K_a]	
Crystal system	Monoclinic	
Space group	$P2_1$	
Unit cell dimensions	a = 7.0460(9) Å	α = 90°
	b = 4.8230(6) Å	β = 95.763(8)°
	c = 10.9731(14) Å	γ = 90°
Volume	371.01(8) Å^3	
Z	2	
Density (calculated)	1.201 Mg/m^3	
Absorption coefficient	0.077 mm^{-1}	
F(000)	144	
Data collection range	$2.91 \leq q \leq 30.32°$	
Index ranges	$-9 \leq h \leq 9$, $-6 \leq k \leq 6$, $-15 \leq l \leq 15$	
Reflections collected	6919	
Independent reflections	1217 [R(int) = 0.0656]	
Observed reflections	1158 [$I > 2s(I)$]	
Absorption correction	multi-scan	
Max. and min. transmission	0.9781 and 0.7333	
Refinement method	Full	
Data / restraints / parameters	1217 / 1 / 92	
Goodness of fit	1.086	
Final R indices [$I > 2s(I)$]	R_1 = 0.0399, wR_2 = 0.1023	
R indices (all data)	R_1 = 0.0417, wR_2 = 0.1039	
Largest diff. peak and hole	0.371 and -0.181e.Å^{-3}	

Table 11.12 Interatomic distances (Å) for (*S*)-1-indanol with s.u.s in parentheses.

O(1)-C(1)	1.4464(16)	C(1)-C(9)	1.517(2)
C(1)-C(2)	1.561(2)	C(2)-C(3)	1.554(2)
C(3)-C(4)	1.523(2)	C(4)-C(5)	1.406(2)
C(4)-C(9)	1.4091(17)	C(5)-C(6)	1.404(2)
C(6)-C(7)	1.408(2)	C(7)-C(8)	1.406(2)
C(8)-C(9)	1.4068(19)		

Table 11.13 Angles between interatomic vectors (°) for (*S*)-1-indanol with s.u.s in parentheses.

O(1)-C(1)-C(9)	110.88(12)	O(1)-C(1)-C(2)	113.66(11)
C(9)-C(1)-C(2)	103.53(12)	C(3)-C(2)-C(1)	106.51(12)
C(4)-C(3)-C(2)	103.68(11)	C(5)-C(4)-C(9)	120.17(12)
C(5)-C(4)-C(3)	129.03(12)	C(9)-C(4)-C(3)	110.79(12)
C(6)-C(5)-C(4)	119.02(13)	C(5)-C(6)-C(7)	120.82(15)
C(8)-C(7)-C(6)	120.33(13)	C(7)-C(8)-C(9)	118.81(12)
C(8)-C(9)-C(4)	120.86(13)	C(8)-C(9)-C(1)	128.01(12)
C(4)-C(9)-C(1)	111.11(12)		

11.4 (*S*,*S*)-hydrobenzoin ((*S*,*S*)-2) Racemisation Raw High Performance Liquid Chromatography (HPLC) Data for Hydrobenzoin

11.4.1 High Performance Liquid Chromatography (HPLC) External Standard Calibration

Benzaldehyde				
Retention Time (min)	**Concentration (mg ml-1)**	**Height (mAU)**	**Area (mAU*min)**	**Relative Area (%)**
9.41	0.5	190.26	76.93	100.00
9.36	1	355.84	189.48	100.00
9.49	1.5	524.75	294.03	100.00
9.50	2	688.68	418.21	100.00

Stilbene				
Retention Time (min)	**Concentration (mg ml-1)**	**Height (mAU)**	**Area (mAU*min)**	**Relative Area (%)**
22.56	0.5	341.30	393.60	100.00
22.44	1	677.04	814.47	100.00
22.48	1.5	969.54	1195.00	100.00
22.44	2	1259.02	1611.95	100.00

Benzil				
Retention Time (min)	**Concentration (mg ml-1)**	**Height (mAU)**	**Area (mAU*min)**	**Relative Area (%)**
23.76	0.5	232.30	274.69	100.00
23.57	1	412.54	482.95	100.00
23.33	1.5	617.58	750.37	100.00
23.28	2	790.14	1024.23	100.00

(*S*,*S*)-hydrobenzoin				
Retention Time (min)	**Concentration (mg ml-1)**	**Height (mAU)**	**Area (mAU*min)**	**Relative Area (%)**
41.42	0.5	78.80	191.17	100.00
41.09	1	139.95	352.60	100.00
40.55	1.5	216.82	564.91	100.00
40.32	2	279.10	743.95	100.00

(*R*,*R)*-hydrobenzoin				
Retention Time (min)	**Concentration (mg ml-1)**	**Height (mAU)**	**Area (mAU*min)**	**Relative Area (%)**
49.36	0.5	69.60	189.69	100.00
48.93	1	136.02	383.79	100.00
48.36	1.5	198.01	567.47	100.00
46.84	2	233.03	670.80	100.00

meso-hydrobenzoin				
Retention Time (min)	**Concentration (mg ml-1)**	**Height (mAU)**	**Area (mAU*min)**	**Relative Area (%)**
63.38	0.5	65.95	236.38	100.00
63.18	1	132.38	478.07	100.00
63.05	1.5	189.00	695.21	100.00
62.93	2	242.98	918.74	100.00

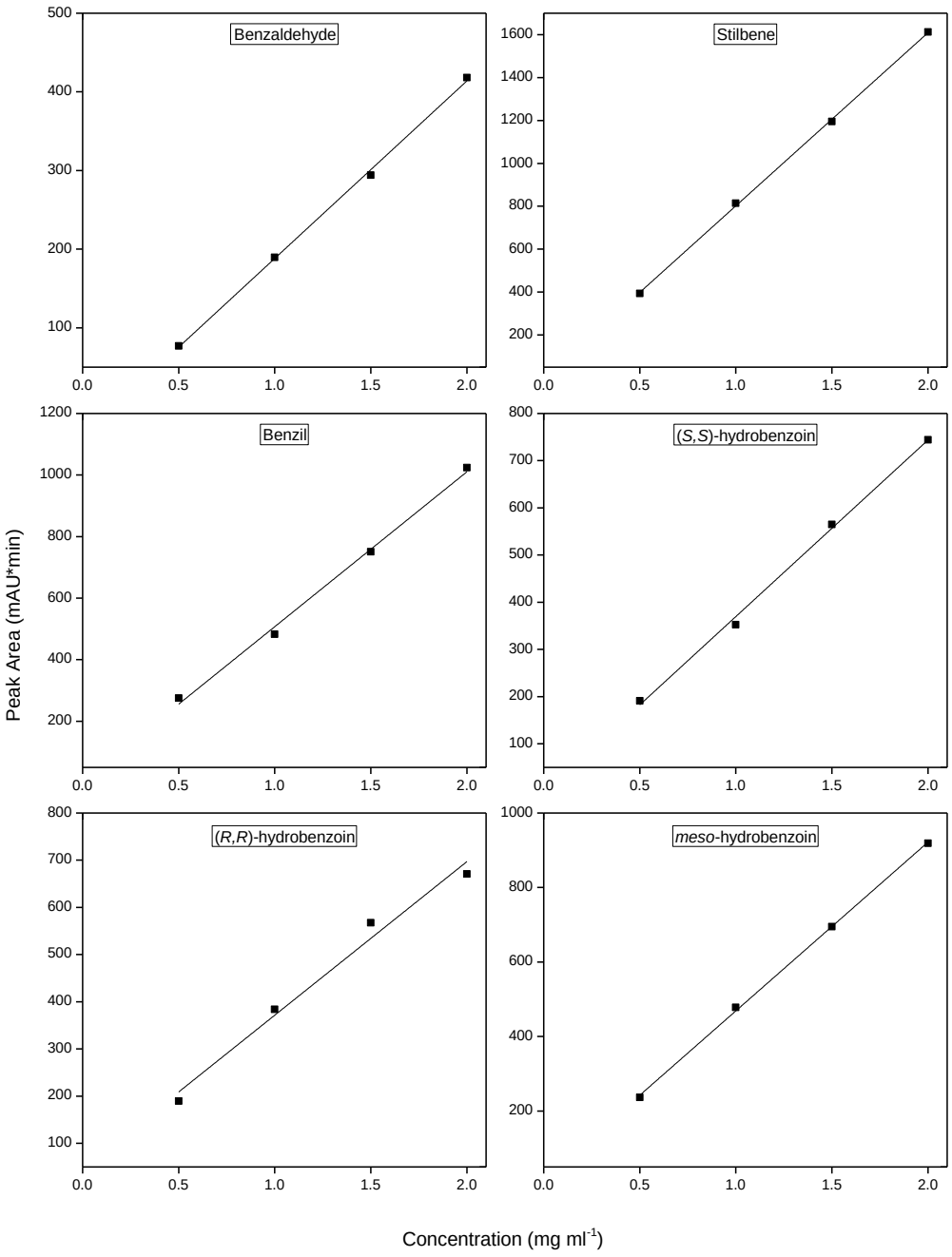

Figure 11.5 High performance liquid chromatography (HPLC) calibration plots of hydrobenzoin and the known components that are formed upon racemisation.

11.4.2 Racemisation by chloro(indenyl)-bis-(triphenylphosphine)ruthenium(II) (4)

Table 11.14 Raw data obtained by HPLC for the racemisation of (*S*,*S*)-**2** in toluene (mol fractions) by complex **4.**

0.117 mol l-1 (*S*,*S*)-**2**, 2 mol% **4**, 60°C						
Component	**Time (min)**					
	0	**2**	**5**	**9**	**15**	**25**
Benzaldehyde	0	0.0053	0.0115	0.0101	0.0131	0.0093
Stilbene	0	0.0050	0.0055	0.0060	0.0055	0.0063
Benzil	0					
(*S*,*S*)-hydrobenzoin	0.117	0.0420	0.0371	0.0372	0.0355	0.0376
(*R*,*R*)-hydrobenzoin	0	0.0368	0.0373	0.0382	0.0366	0.0386
***meso*-hydrobenzoin**	0	0.0276	0.0254	0.0252	0.0259	0.0248

0.117 mol l-1 (*S*,*S*)-**2**, 1 mol% **4**, 60°C						
Component	**Time (min)**					
	0	**2**	**5**	**9**	**15**	**25**
Benzaldehyde	0	0.0013	0.0227	0.0145	0.0139	0.0148
Stilbene	0	0.0036	0.0033	0.0039	0.0036	0.0037
Benzil	0					
(*S*,*S*)-hydrobenzoin	0.117	0.0538	0.0363	0.0391	0.0385	0.0383
(*R*,*R*)-hydrobenzoin	0	0.0329	0.0324	0.0361	0.0361	0.0362
***meso*-hydrobenzoin**	0	0.0250	0.0220	0.0231	0.0246	0.0236

0.117 mol l-1 (*S*,*S*)-**2**, 4 mol% **4**, 60°C						
Component	**Time (min)**					
	0	**2**	**5**	**9**	**15**	**25**
Benzaldehyde	0	0.0373	0.0557	0.0338	0.0559	0.0169
Stilbene	0	0.0110	0.0082	0.0119	0.0030	0.0092
Benzil	0					
(*S*,*S*)-hydrobenzoin	0.117	0.0260	0.0196	0.0260	0.0213	0.0338
(*R*,*R*)-hydrobenzoin	0	0.0266	0.0207	0.0274	0.0223	0.0359
***meso*-hydrobenzoin**	0	0.0158	0.0125	0.0176	0.0142	0.0209

0.117 mol l-1 (*S*,*S*)-**2**, 2 mol% **4**, 50°C						
Component	**Time (min)**					
	0	**2**	**5**	**9**	**15**	**25**
Benzaldehyde	0	0.0140	0.0204	0.0097	0.0083	0.0069
Stilbene	0	0.0054	0.0059	0.0068	0.0057	0.0069
Benzil	0					
(*S*,*S*)-hydrobenzoin	0.117	0.0503	0.0335	0.0367	0.0375	0.0368
(*R*,*R*)-hydrobenzoin	0	0.0231	0.0331	0.0383	0.0397	0.0387
***meso*-hydrobenzoin**	0	0.0239	0.0238	0.0252	0.0256	0.0274

0.117 mol l-1 (*S*,*S*)-**2**, 2 mol% **4**, 70°C						
Component	**Time (min)**					
	0	**2**	**5**	**9**	**15**	**25**
Benzaldehyde	0	0.0156	0.0353	0.0170	0.0059	0.0178
Stilbene	0	0.0065	0.0052	0.0068	0.0064	0.0061
Benzil	0					
(*S*,*S*)-hydrobenzoin	0.117	0.0360	0.0279	0.0337	0.0378	0.0334
(*R*,*R*)-hydrobenzoin	0	0.0351	0.0289	0.0348	0.0399	0.0353
***meso*-hydrobenzoin**	0	0.0234	0.0194	0.0244	0.0266	0.0242

11.4.3 Racemisation by chloro(indenyl)-bis-(triphenylphosphine)ruthenium(II) (5)

Table 11.15 Raw data obtained by HPLC for the racemisation of (*S*,*S*)-**2** in toluene (mol fractions) by complex **5.**

0.117 mol l-1 (*S*,*S*)-**2**, 2 mol% **5** 60°C							
Component	**Time (min)**						
	0	**2**	**5**	**9**	**15**	**25**	**60**
Benzaldehyde	0	0.0096	0.0209	0.0184	0.0217	0.0240	0.0295
Stilbene	0	0.0004	0.0013	0.0020	0.0052	0.0064	0.0091
Benzil	0	0.0002	0.0006	0.0009	0.0027	0.0030	0.0046
(*S*,*S*)-hydrobenzoin	0.117	0.0982	0.0701	0.0562	0.0391	0.0365	0.0299
(*R*,*R*)-hydrobenzoin	0	0.0026	0.0103	0.0236	0.0316	0.0304	0.0262
***meso*-hydrobenzoin**	0	0.0059	0.0134	0.0156	0.0163	0.0164	0.0173

0.117 mol l-1 (*S*,*S*)-**2**, 1 mol% **5**, 60°C							
Component	**Time (min)**						
	0	**2**	**5**	**9**	**15**	**25**	**60**
Benzaldehyde	0.0000	0.0175	0.0168	0.0173	0.0140	0.0110	0.0113
Stilbene	0.0000	0.0002	0.0006	0.0005	0.0009	0.0012	0.0015
Benzil	0.0000	0.0001	0.0004	0.0004	0.0005	0.0007	0.0010
(*S*,*S*)-hydrobenzoin	0.1170	0.0960	0.0884	0.0771	0.0705	0.0608	0.0520
(*R*,*R*)-hydrobenzoin	0.0000	0.0015	0.0041	0.0078	0.0148	0.0264	0.0339
***meso*-hydrobenzoin**	0.0000	0.0013	0.0064	0.0135	0.0160	0.0166	0.0170

0.117 mol l-1 (*S*,*S*)-**2**, 4 mol% **5**, 60°C

Component	Time (min)						
	0	**2**	**5**	**9**	**15**	**25**	**60**
Benzaldehyde	0.0000	0.0511	0.0633	0.0630	0.0679	0.0653	0.0516
Stilbene	0.0000	0.0004	0.0004	0.0010	0.0013	0.0021	0.0031
Benzil	0.0000	0.0003	0.0003	0.0010	0.0013	0.0021	0.0047
(*S*,*S*)-hydrobenzoin	0.1170	0.0566	0.0366	0.0249	0.0199	0.0191	0.0230
(*R*,*R*)-hydrobenzoin	0.0000	0.0027	0.0064	0.0148	0.0159	0.0179	0.0220
***meso*-hydrobenzoin**	0.0000	0.0056	0.0096	0.0120	0.0104	0.0102	0.0123

0.117 mol l-1 (*S*,*S*)-**2**, 2 mol% **5**, 50°C

Component	Time (min)						
	0	**2**	**5**	**9**	**15**	**25**	**60**
Benzaldehyde	0.0000	0.0129	0.0133	0.0183	0.0167	0.0118	0.0528
Stilbene	0.0000	0.0002	0.0005	0.0008	0.0011	0.0023	0.0036
Benzil	0.0000	0.0001	0.0002	0.0004	0.0007	0.0010	0.0022
(*S*,*S*)-hydrobenzoin	0.1170	0.1014	0.0921	0.0753	0.0658	0.0507	0.0241
(*R*,*R*)-hydrobenzoin	0.0000	0.0007	0.0031	0.0070	0.0170	0.0329	0.0210
***meso*-hydrobenzoin**	0.0000	0.0014	0.0074	0.0148	0.0153	0.0179	0.0131

0.117 mol l-1 (*S*,*S*)-**2**, 2 mol% **5**, 70°C

Component	Time (min)						
	0	**2**	**5**	**9**	**15**	**25**	**60**
Benzaldehyde	0.0000	0.0174	0.0120	0.0179	0.0154	0.0165	0.0351
Stilbene	0.0000	0.0010	0.0033	0.0055	0.0077	0.0088	0.0097
Benzil	0.0000	0.0006	0.0021	0.0033	0.0052	0.0042	0.0042
(*S*,*S*)-hydrobenzoin	0.1170	0.0592	0.0420	0.0345	0.0329	0.0314	0.0232
(*R*,*R*)-hydrobenzoin	0.0000	0.0173	0.0363	0.0356	0.0348	0.0337	0.0248
***meso*-hydrobenzoin**	0.0000	0.0212	0.0210	0.0199	0.0206	0.0221	0.0197

11.5 HEL Automate Solubility Raw Data for Chloro(indenyl)-bis-(triphenylphosphine)ruthenium(II) racemisation mixture (4-*rac*$_{mix}$-2) in Toluene

Table 11.16 Crystallisation, T_{Cryst}, and dissolution, T_{Diss}, temperatures for a range of concentrations of **4**-*rac*$_{mix}$-**2** in toluene under a cooling rate of 0.25°C min^{-1}.

	0.25°C/min									
Run	**Measured Temperature (°C)**									
	Concentration (mol l^{-1})									
	0.0014[a]		**0.0035**		**0.0070**		**0.0105**		**0.0140**	
	T_{Cryst}	T_{Diss}	T_{Cryst}	T_{Diss}	T_{Cryst}	T_{Diss}	T_{Cryst}	T_{Diss}	T_{Cryst}	T_{Diss}
1	7.6	24.9	18.6	36.9	35.3	43.9	46.9	-	49.7	55.0
2	7.7	25.3	21.4	35.2	36.3	44.6	45.0	51.1	52.4	56.0
3	7.8	25.3	22.0	-	36.8	44.5	42.0	53.4	46.9	56.7
4	8.1	25.5	27.5	36.1	36.6	45.1	48.1	52.8	-	-
5	7.6	22.1	-	-	-	-	45.7	52.0	-	-
6	7.7	22.1	-	-	-	-	42.9	52.9	-	-
7	7.8	23.7	-	-	-	-	-	-	-	-
8	8.1	25.1	-	-	-	-	-	-	-	-
Av. (°C)	**7.8**	**24.2**	**22.4**	**36.1**	**36.2**	**44.5**	**45.1**	**52.5**	**49.7**	**55.9**
St. Dev. (°C)	**0.2**	**1.3**	**3.2**	**0.7**	**0.6**	**0.4**	**2.1**	**0.8**	**2.3**	**0.7**
St. Error (%)	**0.92**	**1.95**	**7.18**	**1.06**	**0.80**	**0.45**	**1.93**	**0.67**	**2.63**	**0.71**

[a]Data obtained using the Crystal16 system.

Table 11.17 Crystallisation, T_{Cryst}, and dissolution, T_{Diss}, temperatures for a range of concentrations of **4**-*rac*$_{mix}$-**2** in toluene under a cooling rate of 0.5°C min^{-1}.

0. 5°C/min										
Run	**Measured Temperature (°C)**									
	Concentration (mol l^{-1})									
	0.0014[a]		**0.0035**		**0.0070**		**0.0105**		**0.0140**	
	T_{Cryst}	T_{Diss}	T_{Cryst}	T_{Diss}	T_{Cryst}	T_{Diss}	T_{Cryst}	T_{Diss}	T_{Cryst}	T_{Diss}
1	5.4	24.4	18.5	39.4	31.6	49.5	38.5	54.6	45.7	56.9
2	5.5	24.6	19.4	36.7	30.5	48.8	36.5	54.3	49.3	58.9
3	5.7	24.7	21.8	-	35.5	50.9	39.4	55.3	46.0	-
4	6.0	24.8	25.3	38.1	-	48.4	39.6	55.5	47.6	59.4
5	4.5	24.4	-		-	-	-	-	-	-
6	5.4	24.6	-	-	-	-	-	-	-	-
7	5.5	24.7	-	-	-	-	-	-	-	-
8	5.7	24.8	-	-	-	-	-	-	-	-
Av. (°C)	**5.4**	**24.6**	**21.3**	**38.0**	**32.5**	**49.4**	**38.5**	**54.9**	**47.2**	**58.4**
St. Dev. (°C)	**0.4**	**0.1**	**2.6**	**1.1**	**2.1**	**1.0**	**1.2**	**0.5**	**1.5**	**1.1**
St. Error (%)	**0.15**	**0.05**	**1.32**	**0.64**	**1.23**	**0.48**	**0.62**	**0.24**	**0.73**	**0.62**

[a]Data obtained using the Crystal16 system.

Table 11.18 Crystallisation, T_{Cryst}, and dissolution, T_{Diss}, temperatures for a range of concentrations of **4**-*rac*$_{mix}$-**2** in toluene under a cooling rate of 0.75°C min^{-1}.

0. 75°C/min										
Run	**Measured Temperature (°C)**									
	Concentration (mol l^{-1})									
	0.0014[a]		**0.0035**		**0.0070**		**0.0105**		**0.0140**	
	T_{Cryst}	T_{Diss}	T_{Cryst}	T_{Diss}	T_{Cryst}	T_{Diss}	T_{Cryst}	T_{Diss}	T_{Cryst}	T_{Diss}
1	3.2	24.9	18.6	40.5	29.4	-	35.9	56.3	41.0	57.7
2	4.6	25.1	22.7	40.9	29.1	49.8	33.6	56.6	46.0	58.1
3	7.5	25.1	-	40.9	33.3	49.3	36.8	-	42.4	57.8
4	8.1	25.2	20.6	41.3	31.3	51.5	39.4	53.5	-	-
5	1.9	24.9	-	-	30.7	49.7	35.5	54.6	-	-
6	2.8	25.1	-	-	30.3	-	35.5	53.3	-	-
7	1.3	25.1	-	-	-	-	-	-	-	-
8	1.3	25.2	-	-	-	-	-	-	-	-
Av. (°C)	**3.8**	**25.1**	**20.6**	**40.9**	**30.7**	**50.1**	**36.1**	**54.8**	**43.1**	**57.9**
St. Dev. (°C)	**2.5**	**0.1**	**1.7**	**0.3**	**1.4**	**0.9**	**1.8**	**1.4**	**2.1**	**0.2**
St. Error (%)	**0.89**	**0.04**	**0.96**	**0.13**	**0.56**	**0.43**	**0.72**	**0.62**	**1.20**	**0.09**

[a]Data obtained using the Crystal16 system.

Table 11.19 Crystallisation, T_{Cryst}, and dissolution, T_{Diss}, temperatures for a range of concentrations of **4**-*rac*$_{mix}$-**2** in toluene under a cooling rate of 1°C min^{-1}.

1°C/min										
Run	**Measured Temperature (°C)**									
	Concentration (mol l^{-1})									
	0.0014[a]		**0.0035**		**0.0070**		**0.0105**		**0.0140**	
	T_{Cryst}	T_{Diss}	T_{Cryst}	T_{Diss}	T_{Cryst}	T_{Diss}	T_{Cryst}	T_{Diss}	T_{Cryst}	T_{Diss}
1	1.6	25.4	14.5	40.7	-	52.6	33.4	58.4	40.5	61.4
2	2.1	25.4	19.3	40.9	29.9	50.8	33.0	-	41.8	-
3	2.8	25.4	-	41.2	-	49.0	35.7	58.5	41.0	62.0
4	4.5	25.5	16.9	41.4	26.2	50.8	35.3	57.7	39.8	63.2
5	1.6	25.4	-	-	25.4	51.0	-	-	-	-
6	1.6	25.4	-	-	27.5	53.5	-	-	-	-
7	2.1	25.4	-	-	27.1	-	-	-	-	-
8	2.8	25.5	-	-	-	-	-	-	-	-
Av. (°C)	**2.4**	**25.4**	**16.9**	**41.0**	**27.2**	**51.3**	**34.4**	**58.2**	**40.8**	**62.2**
St. Dev. (°C)	**0.9**	**0.1**	**2.0**	**0.3**	**1.5**	**1.4**	**1.1**	**0.4**	**0.7**	**0.7**
St. Error (%)	**0.33**	**0.02**	**1.13**	**0.14**	**0.69**	**0.58**	**0.57**	**0.22**	**0.37**	**0.43**

[a]Data obtained using the Crystal16 system.

11.6 Crystal16 Calibration

Table 11.20 Crystal16 calibration: Measured vessel temperatures for given set temperatures

Block	Set Point							
	20°C				40°C			
	Vessel Number							
	1	2	3	4	1	2	3	4
	Measured Temperature (°C)							
A	19.9	19.9	20	20.1	38.2	38.4	38.2	38.4
	19.9	19.9	20	20.1	38.4	38.5	38.4	38.3
	19.9	19.9	20	20	38.3	38.4	38.3	38.3
B	20	20	20.2	20.1	38.5	38.7	38.4	38.7
	19.9	20	20.2	20.1	38.8	38.9	38.7	38.6
	20	19.9	20.1	20.1	38.7	38.8	38.5	38.6
C	19.9	20	20.2	20	38.5	38.6	38.4	38.4
	20	20	20	20.1	38.6	38.6	38.4	38.4
	19.9	20	20.1	20	38.5	38.6	38.4	38.4
D	20	20	20.3	20.3	38.7	38.9	38.7	38.4
	20.2	20.2	20.4	20.3	38.7	38.9	38.7	38.6
	20.2	20.2	20.3	20.3	38.7	38.9	38.7	38.5

Block	Set Point							
	60°C				80°C			
	Vessel Number							
	1	2	3	4	1	2	3	4
	Measured Temperature (°C)							
A	57.8	58	57.7	57.5	76.3	77.1	77	75.7
	57.8	58	57.8	57.4	76.4	77.1	76.9	75.8
	57.8	58	57.8	57.5	76.4	77.2	76.9	75.7
B	58.5	58.5	58.4	58.2	76.5	77.1	77.4	76.7
	58.3	58.5	58	58.5	76.5	77.2	77.2	76.7
	58.4	58.5	58.2	58.3	76.6	77.3	77.4	76.8
C	58.1	58.2	57.9	58	76.2	76.4	75.9	75.1
	57.8	58.2	57.7	58.3	76.1	76.7	76.1	75.2
	58	58.2	57.8	58.1	76.2	76.5	76	75.1
D	58.5	58.7	57.4	58.2	75.8	77	77.2	76.2
	58.2	58.4	57.8	58.1	75.6	77.1	77.4	76
	58	58.4	58	58.3	75.8	77.2	77.2	76.3

Table 11.21 Crystal16 calibration: Average measured temperatures for a given set temperature

Block A			Block B		
Set Point	**Measured Temperature (°C)**	**Standard Deviation**	**Set Point**	**Measured Temperature (°C)**	**Standard Deviation**
20	19.97	0.07	20	20.05	0.10
40	38.34	0.09	40	38.66	0.14
60	57.76	0.19	60	58.36	0.16
80	76.54	0.55	80	76.95	0.34

Block C			Block D		
Set Point	**Measured Temperature (°C)**	**Standard Deviation**	**Set Point**	**Measured Temperature (°C)**	**Standard Deviation**
20	20.02	0.08	20	20.23	0.12
40	38.48	0.09	40	38.70	0.15
60	58.03	0.18	60	58.17	0.33
80	75.96	0.52	80	76.57	0.65

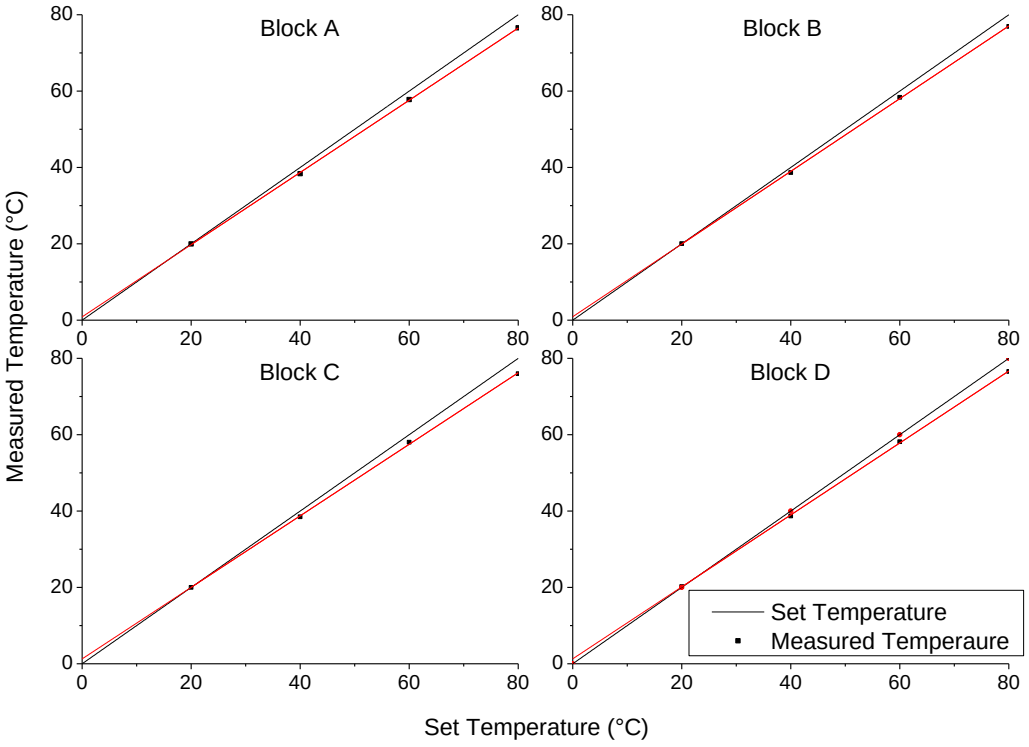

Figure 11.6 Crystal16 calibration: Measured temperature vs. set temperature for each Crystal16 block.

Table 11.22 Calibration equations for Crystal16 blocks

Block	Equation	R^2
A	y=0.94571x+0.86667	0.999
B	y=0.952x+0.90417	0.999
C	y=0.93683x+1.27917	0.999
D	y=0.94246x+1.29167	0.999

11.7 Calibrated Crystal16 Raw Solubility Data

11.7.1 Chlorocarbonyl-triphenylphosphene(1,2,3,4,5-pentaphenylcyclopentadienyl)-ruthenium(II) (5-*rac*$_{mix}$-2) in Toluene

Table 11.23 Measured and calibrated crystallisation, T_{Cryst}, and dissolution, T_{Diss}, temperatures for **5**-*rac*$_{mix}$-**2** in Toluene under a cooling rate of 0.25°C min^{-1}.

0.25°C/min								
Run	**Block A: 0.311 mol l^{-1}**				**Block B: 0.233 mol l^{-1}**			
	Measured T (°C)		**Calibrated T (°C)**		**Measured T (°C)**		**Calibrated T (°C)**	
	T_{Cryst}	T_{Diss}	T_{Cryst}	T_{Diss}	T_{Cryst}	T_{Diss}	T_{Cryst}	T_{Diss}
1	35.6	52.6	34.5	50.6	32.1	48.9	31.5	47.5
2	35.7	52.7	34.6	50.7	32.6	49.1	31.9	47.6
3	36.1	52.9	35.0	50.9	33.2	49.2	32.5	47.7
4	36.7	53.2	35.6	51.2	35.1	49.7	34.3	48.2
5	31.2	52.6	30.4	50.6	24.3	42.4	24.0	41.3
6	35.8	52.7	34.7	50.7	24.5	49.2	24.2	47.7
7	35.9	52.7	34.8	50.7	24.8	49.5	24.5	48.0
8	37.3	53.1	36.1	51.1	32.0	49.7	31.4	48.2
Average (°C)			**34.5**	**50.8**			**29.3**	**47.0**
Standard Deviation (°C)			**1.6**	**0.2**			**4.0**	**2.2**
Standard Error (%)			**0.58**	**0.07**			**1.41**	**0.78**

Run	**Block C: 0.155 mol l^{-1}**				**Block D: 0.078 mol l^{-1}**			
	Measured T (°C)		**Calibrated T (°C)**		**Measured T (°C)**		**Calibrated T (°C)**	
	T_{Cryst}	T_{Diss}	T_{Cryst}	T_{Diss}	T_{Cryst}	T_{Diss}	T_{Cryst}	T_{Diss}
1	26.4	44.7	26.0	43.2	11.0	32.1	11.7	31.5
2	27.2	45	26.8	43.4	13.0	32.6	13.5	32.0
3	27.3	45.5	26.9	43.9	13.8	33.0	14.3	32.4
4	27.5	45.6	27.0	44.0	13.9	33.1	14.4	32.5
5	18.7	44.7	18.8	43.2	7.0	32.8	7.9	32.2
6	19.4	45.2	19.5	43.6	8.3	32.9	9.1	32.3
7	22.0	45.7	21.9	44.1	8.6	33.1	9.4	32.5
8	25.9	45.8	25.5	44.2	8.7	33.2	9.5	32.6
Average (°C)			**24.0**	**43.7**			**11.2**	**32.3**
Standard Deviation (°C)			**3.2**	**0.4**			**2.4**	**0.3**
Standard Error (%)			**4.75**	**0.31**			**7.63**	**0.35**

Table 11.24 Measured and calibrated crystallisation, T_{Cryst}, and dissolution, T_{Diss}, temperatures for **5**-*rac*$_{mix}$-**2** in Toluene under a cooling rate of 0.5°C min^{-1}.

0.5°C/min								
Run	**Block A: 0.311 mol l^{-1}**				**Block B: 0.233 mol l^{-1}**			
	Measured T (°C)		**Calibrated T (°C)**		**Measured T (°C)**		**Calibrated T (°C)**	
	T_{Cryst}	T_{Diss}	T_{Cryst}	T_{Diss}	T_{Cryst}	T_{Diss}	T_{Cryst}	T_{Diss}
1	26.8	52.7	26.2	50.7	24.7	49.3	24.4	47.8
2	28.1	52.79	27.4	50.8	24.9	49.5	24.6	48.0
3	31.9	52.96	31.0	51.0	26.3	49.6	25.9	48.1
4	36.7	53	35.6	51.0	30.3	49.6	29.7	48.1
5	28.6	52.7	27.9	50.7	27.4	49.6	27.0	48.1
6	31.7	52.9	30.8	50.9	28.5	49.6	28.0	48.1
7	32.7	52.9	31.8	50.9	29.2	49.7	28.7	48.2
8	33.07	53.1	32.1	51.1	30.2	49.9	29.7	48.4
Average (°C)			**30.4**	**50.9**			**27.3**	**48.1**
Standard Deviation (°C)			**2.8**	**0.1**			**2.0**	**0.2**
Standard Error (%)			**1.01**	**0.04**			**0.70**	**0.05**

Run	**Block C: 0.155 mol l^{-1}**				**Block D: 0.078 mol l^{-1}**			
	Measured T (°C)		**Calibrated T (°C)**		**Measured T (°C)**		**Calibrated T (°C)**	
	T_{Cryst}	T_{Diss}	T_{Cryst}	T_{Diss}	T_{Cryst}	T_{Diss}	T_{Cryst}	T_{Diss}
1	19.8	45.4	19.8	43.8	8.3	32.3	9.1	31.7
2	21.3	45.5	21.2	43.9	8.6	32.6	9.4	32.0
3	21.6	45.5	21.5	43.9	15	33	15.4	32.4
4	21.6	45.8	21.5	44.2	20	33.1	20.1	32.5
5	19.2	45.2	19.3	43.6	8	32.9	8.8	32.3
6	20.1	45.4	20.1	43.8	10.8	32.9	11.5	32.3
7	20.4	45.7	20.4	44.1	10.8	33.2	11.5	32.6
8	23.7	45.7	23.5	44.1	17.4	33.2	17.7	32.6
Average (°C)			**20.9**	**43.9**			**12.9**	**32.3**
Standard Deviation (°C)			**1.2**	**0.2**			**4.0**	**0.3**
Standard Error (%)			**2.09**	**0.14**			**10.79**	**0.3**

Table 11.25 Measured and calibrated crystallisation, T_{Cryst}, and dissolution, T_{Diss}, temperatures for **5**-*rac*$_{mix}$-**2** in Toluene under a cooling rate of 0.75°C min^{-1}.

0.75°C/min								
Run	**Block A: 0.311 mol l^{-1}**				**Block B: 0.233 mol l^{-1}**			
	Measured T (°C)		**Calibrated T (°C)**		**Measured T (°C)**		**Calibrated T (°C)**	
	T_{Cryst}	T_{Diss}	T_{Cryst}	T_{Diss}	T_{Cryst}	T_{Diss}	T_{Cryst}	T_{Diss}
1	24.1	53	23.7	51.0	23.4	50	23.2	48.5
2	24.4	53.13	23.9	51.1	23.4	50.1	23.2	48.6
3	24.6	53.2	24.1	51.2	24.9	50.1	24.6	48.6
4	24.7	53.3	24.2	51.3	25.4	50.2	25.1	48.7
5	25	53.1	24.5	51.1	22.9	49.7	22.7	48.2
6	25	53.3	24.5	51.3	23.1	49.9	22.9	48.4
7	25.5	53.5	25.0	51.5	23.4	50	23.2	48.5
8	25.5	53.6	25.0	51.6	23.4	50	23.2	48.5
Average (°C)			**24.4**	**51.2**			**23.5**	**48.5**
Standard Deviation (°C)			**0.4**	**0.2**			**0.8**	**0.1**
Standard Error (%)			**0.64**	**0.12**			**1.21**	**0.10**

Run	**Block C: 0.155 mol l^{-1}**				**Block D: 0.078 mol l^{-1}**			
	Measured T (°C)		**Calibrated T (°C)**		**Measured T (°C)**		**Calibrated T (°C)**	
	T_{Cryst}	T_{Diss}	T_{Cryst}	T_{Diss}	T_{Cryst}	T_{Diss}	T_{Cryst}	T_{Diss}
1	17.9	45.9	18.0	44.3	6.5	33.2	7.4	32.6
2	18.4	45.9	18.5	44.3	7.1	33.4	8.0	32.8
3	18.4	46	18.5	44.4	7.1	33.4	8.0	32.8
4	18.8	46	18.9	44.4	7.2	33.5	8.1	32.9
5	17.6	46	17.8	44.4	4.2	33.3	5.3	32.7
6	17.7	46	17.9	44.4	4.4	33.4	5.4	32.8
7	18.3	46	18.4	44.4	4.8	33.5	5.8	32.9
8	18.5	46.1	18.6	44.5	5.9	33.5	6.9	32.9
Average (°C)			**18.3**	**44.4**			**6.9**	**32.8**
Standard Deviation (°C)			**0.4**	**0.1**			**1.1**	**0.1**
Standard Error (%)			**0.71**	**0.04**			**5.77**	**0.10**

Table 11.26 Measured and calibrated crystallisation, T_{Cryst}, and dissolution, T_{Diss}, temperatures for **5**-*rac*$_{mix}$-**2** in Toluene under a cooling rate of 1°C min^{-1}.

1°C/min								
Run	**Block A: 0.311 mol l^{-1}**				**Block B: 0.233 mol l^{-1}**			
	Measured T (°C)		**Calibrated T (°C)**		**Measured T (°C)**		**Calibrated T (°C)**	
	T_{Cryst}	T_{Diss}	T_{Cryst}	T_{Diss}	T_{Cryst}	T_{Diss}	T_{Cryst}	T_{Diss}
1	22.72	53.7	22.4	51.7	21.3	50	21.2	48.5
2	23.6	53.7	23.2	51.7	21.7	50.2	21.6	48.7
3	23.6	54	23.2	51.9	22.1	50.4	21.9	48.9
4	23.89	54.1	23.5	52.0	22.1	50.6	21.9	49.1
5	22.6	53.4	22.2	51.4	18.9	50.2	18.9	48.7
6	23.1	53.5	22.7	51.5	19.8	50.2	19.8	48.7
7	24	53.9	23.6	51.8	20.3	50.6	20.2	49.1
8	24.5	54	24.0	51.9	21	50.8	20.9	49.3
Average (°C)			**23.1**	**51.7**			**20.8**	**48.9**
Standard Deviation (°C)			**0.6**	**0.2**			**1.0**	**0.2**
Standard Error (%)			**0.89**	**0.15**			**1.74**	**0.17**

Run	**Block C: 0.155 mol l^{-1}**				**Block D: 0.078 mol l^{-1}**			
	Measured T (°C)		**Calibrated T (°C)**		**Measured T (°C)**		**Calibrated T (°C)**	
	T_{Cryst}	T_{Diss}	T_{Cryst}	T_{Diss}	T_{Cryst}	T_{Diss}	T_{Cryst}	T_{Diss}
1	13.2	46.2	13.6	44.6	4.2	33.6	5.3	33.0
2	16.1	46.5	16.4	44.8	4.5	33.8	5.5	33.1
3	16.5	46.8	16.7	45.1	6	33.9	6.9	33.2
4	16.6	46.9	16.8	45.2	1.2	33.6	2.4	33.0
5	15.2	46.3	15.5	44.7	2.9	33.7	4.0	33.1
6	15.9	46.5	16.2	44.8	3.5	33.7	4.6	33.1
7	16.4	46.6	16.6	44.9	4.1	33.9	5.2	33.2
8	17	46.8	17.2	45.1	3.7	33.7	4.8	33.1
Average (°C)			**16.1**	**44.9**			**4.8**	**33.1**
Standard Deviation (°C)			**1.1**	**0.2**			**1.2**	**0.1**
Standard Error (%)			**2.31**	**0.17**			**8.86**	**0.11**